Kriging based methods for the structural damage assessment of offshore wind turbines

Quentin Huchet

Université Clermont-Auvergne
École Doctorale des Sciences Pour L'ingénieur

THÈSE

présentée par

Quentin Huchet,
Ingénieur IFMA

En vue d'obtenir le grade de
Docteur d'Université

Spécialité doctorale "Génie Mécanique"

Utilisation des méthodes de Krigeage pour le dimensionnement en fatigue des structures éoliennes posées en mer

Soutenue publiquement le jeudi 13 décembre 2018 à SIGMA Clermont, devant le jury composé de :

Pr. Rodolphe Le Riche	Mines de Saint-Etiennes	Président du Jury
Pr. Joseph Morlier	ISAE-Supaéro, Toulouse	Rapporteur
Pr. Franck Schoefs	Université de Nantes	Rapporteur
Dr. Jean-Marc Bourinet	SIGMA, Clermont-Ferrand	Examinateur
Pr. Nicolas Gayton	SIGMA, Clermont-Ferrand	Directeur de thèse
Dr. Nicolas Relun	EDF R&D, Saclay	Encadrant industriel
Dr. Cécile Mattrand	SIGMA, Clermont-Ferrand	Co-encadrante
Dr. Pierre Beaurepaire	SIGMA, Clermont-Ferrand	Co-encadrant

Université Clermont-Auvergne
Institut Pascal, SIGMA Clermont, UMR CNRS 6602
Campus de Clermont-Ferrand - Les Cézeaux - CS20265 63175 AUBIERE - France

Kriging based methods for the structural damage assessment of offshore wind turbines

A thesis submitted by

Quentin Huchet

in partial fulfillment of the requirements for the degree of doctor of philosophy (Mechanical Engineering)

Defended publicly on ***December 13, 2018*** *in front of a defense committee made up of:*

Pr. Rodolphe Le Riche	Mines de Saint-Etiennes	President of the Jury
Pr. Joseph Morlier	ISAE-Supaéro, Toulouse	Reviewer
Pr. Franck Schoefs	Université de Nantes	Reviewer
Dr. Jean-Marc Bourinet	SIGMA, Clermont-Ferrand	Examiner
Pr. Nicolas Gayton	SIGMA, Clermont-Ferrand	Thesis director
Dr. Nicolas Relun	EDF R&D, Saclay	Industrial advisor
Dr. Cécile Mattrand	SIGMA, Clermont-Ferrand	Co-advisor
Dr. Pierre Beaurepaire	SIGMA, Clermont-Ferrand	Co-advisor

Université Clermont-Auvergne
Institut Pascal, SIGMA Clermont, UMR CNRS 6602
Campus de Clermont-Ferrand - Les Cézeaux - CS20265 63175 AUBIERE - France

EDF Lab Paris Saclay
Boulevard Gaspard Monge - 91120 PALAISEAU - France

This manuscript was typeset with LaTeX-2ϵ (TeX Live 2016) using Math Design as the body font. The source files were edited with TeX Studio 2.12.0 under MacOS Mojave 10.14. Graphical illustrations were produced with Matplotlib 2.0.0 (running on Python 3.7), TikZ and Microsoft PowerPoint®. The bibliography was compiled with BibTeX 0.99d. Each of the simulations were run using Numpy 1.11.3 and Openturns 1.9 packages.

To cite this thesis, please use the following BibTeX entry :

```
@PHDTHESIS{Huchet_PhD_2018,
   author = {Huchet, Q.},
   year = 2018,
   title = {{Kriging based methods for the structural damage assessment of offshore
   wind turbines}},
   school = {Universit\'e Clermont Auvergne}
}
```

AKNOWLEDGEMENT - REMERCIEMENTS

La réalisation de ce projet de thèse est le résultat d'un travail de trois ans qui m'a permis de rencontrer et d'échanger avec beaucoup d'acteurs industriels et universitaires. Je tiens à remercier l'ensemble de ces personnes pour les conseils, le temps et la bienveillance générale que chacun m'a apportés.

Je tiens à adresser mes sincères remerciements aux rapporteurs de ce travail, Franck Shoefs et Joseph Morlier, qui ont accepté de relire l'ensemble de ce document et m'ont permis de défendre cette thèse. La bienveillance et l'intérêt qu'ils ont montrés pour ces travaux m'ont permis d'aborder la difficile épreuve de la soutenance avec optimisme et recul grâce aux retours très constructifs de leurs rapports. Je remercie également Rodolphe Le Riche d'avoir présidé le jury avec intérêt et grâce à qui la séance de questions-réponses fut très intéressante et riche en nouvelles perspectives de développement. J'adresse également mes remerciements à Jean-Marc Bourinet pour son implication dans ce jury de thèse, mais également pour les échanges, moments passés ensemble ainsi que sa présence rassurante lors de ma première conférence internationale (ICOSSAR).

La réussite de ce projet n'aurait pas pu se faire sans la présence indéfectible de l'équipe encadrante de cette thèse. Merci à Nicolas Gayton d'avoir cru en mes compétences en soutenant ma candidature à cette thèse dès la fin de ma scolarité à l'IFMA. Sa bienveillance, son optimisme et son sens de l'organisation m'ont permis de prendre le recul nécessaire afin de surmonter les difficultés d'un tel projet. Je remercie également infiniment mes deux co-encadrants universitaires, Cécile Mattrand et Pierre Beaurepaire pour m'avoir toujours accordé du temps, de la patience et de précieux conseils.

L'implication d'EDF a été indispensable à l'obtention des résultats de cette thèse. Cela a été surtout possible grâce à Nicolas Relun, encadrant industriel du projet. Les trois années passées à ses côtés m'ont à la fois permis d'apprendre énormément, mais aussi de faire évoluer mon sens scientifique. Je le remercie également pour son accueil et son aide lors de mon intégration au sein de l'équipe de recherche. De plus, je remercie l'ensemble des ingénieurs-chercheurs du groupe PRISME (ex. MRI) qui ont suivi de loin ce projet et qui m'ont permis de présenter mes travaux dans des groupes de travail complémentaires. Merci à eux de m'avoir toujours accordé du temps et une aide précieuse pour venir à bout de certaines difficultés de développement.

J'aimerais également adresser mes remerciements aux membres des différents comités de thèse pour leur retours critiques mais néanmoins positifs et l'ensemble des perspectives proposées au cours de ces réunions. Merci à Betrand Iooss d'EDF R&D PRISME, Jérôme Morio et Mathieu Balesdent de l'ONERA et Guillaume Causse de Phimeca.

En tant que doctorant CIFRE, j'ai passé la plupart du temps intégré à l'équipe d'ingénieurs-chercheurs du groupe ERMES (ex. THEMIS) de la R&D d'EDF. Au delà des échanges très riches, je tiens à remercier l'ensemble de mes collègues pour l'atmosphère de travail positif et tous les bons moments passés ensemble. Merci aux "mécanos" du groupe : Elisabeth, Matteo, Pierre, Jean-Baptiste, Anaïs et Jordan. Merci également au reste de l'équipe et spécialement à Jérémy, Nicolas, Anthony, Jalal, Darius et Laurent ! Je tiens également à remercier Catherine et Véronique pour leur soutien logistique omniprésent tout au long de ces trois années.

Au cours de mes déplacements à Clermont-Ferrand, j'ai également été intégré très facilement à l'équipe des doctorants à qui j'adresse mes amitiés sincères et mes remerciements pour les moments passés ensemble dans la "ZAD". De plus, j'aimerais saluer le travail de Jacqueline qui m'a grandement aidé dans les différents parcours administratifs qui ponctuent un tel projet.

Merci à mes "Thésards anonymes", réels compagnons de galère grâce à qui une frustration pouvait devenir un éclat de rire : Vincent, Mathieu C. et Mathieu S., Rudy, Cédric et Adrien. Mes pensées vont également à deux IFMALIENS particulièrement présents lors de mes retours en Auvergne, mais également lors de la soutenance de thèse. Merci à Florian pour son canapé toujours disponible et sa fameuse tartiflette marmiton et à Badr pour les sorties clermontoises improvisées (malgré un emploi du temps "toujours surchargé") !

Pour finir, j'adresse mes remerciements et mon affection particulière à l'ensemble de mon entourage familial et amical qui m'a apporté un soutien indéfectible tout au long de mes études et de ces trois années. La réussite de ce projet est aussi la vôtre et je vous en suis infiniment reconnaissant.

ABSTRACT

The mechanical certification of wind turbine structures is required for the funding of new offshore projects on the French coasts. In order to ensure a maximal safety level of installations, a series of structural analyzes are required by the certification bodies. Amongst all, the damage based computations represent an important numerical effort for EDF. The presented works focus on the applicability and the performances of Kriging metamodels for the estimation of the lifetime cumulated damage of offshore wind turbine structures (AK-DA approach) and the damage based reliability assessment of new designs (AK-MCS/AK-DA coupling).

Keywords: mechanical damage, certification, Kriging metamodels, offshore wind turbines, reliability.

* * *

La certification mécanique des structures éoliennes est indispensable au financement des nouveaux projets posés en mer le long des côtes françaises. Dans le but de garantir une sécurité maximale de ces installations, différentes analyses structurelles sont exigées par les organismes certificateurs. Parmi ces dernières, l'estimation de l'endommagement à durée de vie représente un investissement numérique important pour EDF. Les travaux présentés se focalisent sur les possibilités et performances des métamodèles de Krigeage pour l'estimation efficace de l'endommagement à durée de vie des structures éoliennes posées en mer (méthode AK-DA) et l'analyse de fiabilité en fatigue des conceptions (couplage AK-MCS/AK-DA).

Mots clefs : Endommagement mécanique, certification, métamodèles de Krigeage, éoliennes posées en mer, fiabilité.

LIST OF PUBLICATIONS

French congress

- Q. Huchet, C. Mattrand, P. Beaurepaire, N. Gayton, and N. Relun. Approximation d'intégrales coûteuses par utilisation de métamodèles, application à la certification en fatigue des structures éoliennes. In *Congrès français de mécanique*. AFM, Association Française de Mécanique, 2017a

International congress

- Q. Huchet, C. Mattrand, P. Beaurepaire, N. Gayton, and N. Relun. The help of meta-models or wind turbine certification. In *ICOSSAR 2017*, 2017b

- Q. Huchet, C. Mattrand, P. Beaurepaire, N. Relun, and N. Gayton. Cost effective strategy using kriging surrogates to compute fatigue at multiple locations of a structure: Application to offshore wind turbine certification. In *12th International Fatigue Congress (FATIGUE 2018)*, volume 165, page 17001. EDP Sciences, 2018b

- Q. Huchet, C. Mattrand, P. Beaurepaire, N. Gayton, and N. Relun. A kriging based procedure for the certification of wind turbine structures: application to large scale models. In *54th ESReDA Seminar*, 2018a

International journal

- Q. Huchet, C. Mattrand, P. Beaurepaire, N. Relun, and N. Gayton. Ak-da: An efficient method for the fatigue assessment of wind turbine structures. *Wind Energy*, 2019

TABLE OF CONTENTS

INTRODUCTION

The development of offshore wind energy

In the current context of energy transition which aims at reducing the carbon footprint of modern societies, the industrial actors of electricity production have to play a leading role in the development of innovative and low carbon technologies. From the mid-twentieth and the progressive development of electricity distribution, the global demand has considerably increased both for industrial and domestic uses. Electricity production has become one of the most important social issue and appears as essential in today's world. To respond to the challenge of national growing demand, EDF (Électricité de France, the French historic energy company) had to progressively develop a complex production system which results today in a diversified energy supply, frequently called the "energy mix" and composed of several sources and technologies.

The end of the 20th century marked an awareness of the common thought on the use of fossil energy and its consequences on the global warming. World political decisions fixing goals on greenhouse gas reduction such as the Kyoto agreement in 1997 or more recently the Paris agreements signed in 2015 by 196 countries have accelerated the development of carbon-free technologies for electricity production. To reduce their dependence with regards to nuclear energy, which represents the main share of the production technology and to gradually break free from fossil based electricity production, industrial actors started from the beginning of the 21st century to turn to the development of renewable energy. Amongst all, solar and wind technologies have drastically enhanced their performances because of significant and recent breakthroughs which have resulted in a rapid development of these technologies in the past few years. In France, the share of these renewable technologies has evolved since this period and represent now respectively 1.7 and 4.5% of the energy mix as presented in Table 1.

This development has to be accelerated to meet the objectives of 32% of renewable energies in the global French mix by 2030 (requirement of the energetic transition legislation "*Loi de la transition énergétique pour la croissance verte*", ratified in 2015). Because of its climatic conditions, France offers a great potential for the development of wind energy. As illustrated in Figure 1, this technology has been widely promoted and industrialized worldwide between 2001 and 2017 with a global installed capacity of more than 500000 MW. In France, a

	Share in the energy mix	Production (TWh)
Nuclear	71.6%	379.1
Hydro	10.1%	53.6
Natural Gas	7.7%	40.9
Wind	4.5%	24.0
Solar	1.7%	9.2
Biofuels and waste	1.7%	9.1
Coal	1.8%	9.7
Oil	0.7%	3.8
Other	0.2%	-
Total	100%	529.4 TWh

Table 1: The French energy supply in 2017 (RTE, *Bilan électrique 2017*)

progressive development has led to an installed capacity that reaches 13559 MW in 2017.

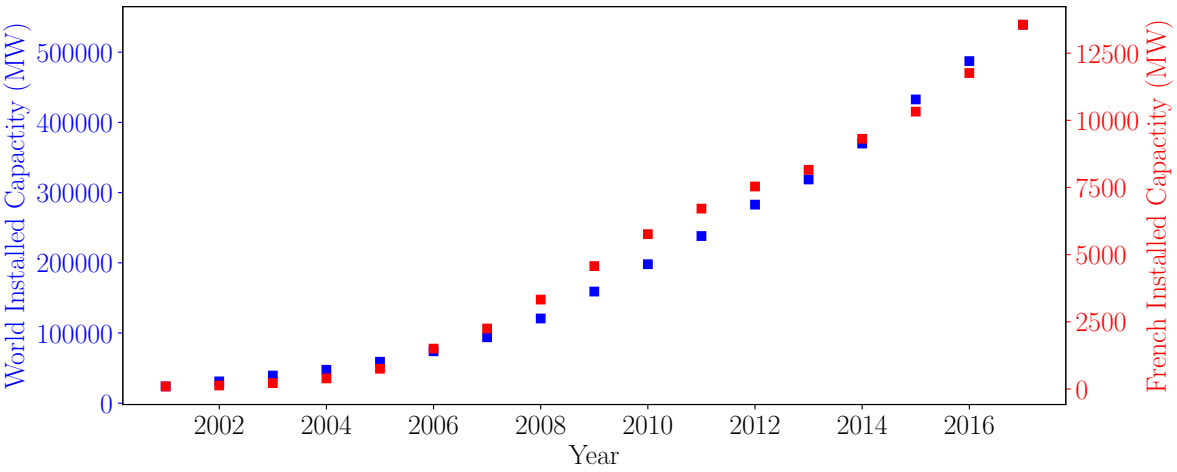

Figure 1: Evolution of the world and French installed capacity of wind power production between 2001 and 2017 (RTE, *Bilan électrique 2017* / GWEC, *Global Wind Report 2017*)

To keep on developing wind energy, France now turns to the sea and the 5800 km of its coasts. Several projects have been signed in the past few years to start the development of offshore production. EDF occupies a major role in the French offshore wind industry with the management of three wind farms to be installed (Saint-Nazaire, Fécamp and Courseulles-sur-Mer).

Compared to the formerly developed onshore installations, wind conditions at the sea present a better production potential with stronger and more constant winds resulting in an increase of the turbines' load factor[1]. Furthermore, offshore installations allow to place more powerful turbines currently reaching nominal capacities of 5 to 8 MW. In the next few years, this capacity is expected to increase with the development of new turbines with nominal capacities of 10 to 12 MW (*e.g.* Vestas V-164-10MW, GE Haliade X). These new structures present uncommon dimensions with total heights of more than 250 meters, turbine weights of several hundreds of thousands tons and total rotor diameters exceeding 200 meters.

[1]The load factor is a numerical quantity which quantifies the production potential. In the context of wind turbine, it is defined by the adimensional ratio between the average power divided by the peak power over a defined period of time.

Industrial problematics of the thesis

To be funded and insured, offshore projects have to be verified with regards to the expected performances and a minimal safety level. This is proceeded by a third party institution, also known as "certification bodies". It relies on the evaluation of the lifetime performances of the entire unit. Considering the mechanical certification, a series of analyses have to be performed to ensure the structural integrity of the proposed design with regards to the loading conditions of installation sites. Because of the high number of cycles the structure has to undergo during its lifetime, a proper estimation of the cumulated damage response of the design has to be performed. To help engineers in the determination of the mechanical responses, an analysis framework as well as a series of requirements are proposed in the certification guidelines. For the particular case of the cumulated damage assessment, the application of the verification framework results in an extensive numerical effort which can be, in certain situation, unaffordable for industrial actors. As a consequence, a first industrial problematic of this thesis concerns the reduction of this numerical effort and is proposed as:

> How to reduce the numerical cost required for damage estimations of the offshore wind turbine structure, although ensuring a sufficient representativeness of the results ?

Furthermore, to limit the simulation investments to the only one required by the certification framework, a systematic approach is used to ensure the structural safety with regards to environmental variabilities and design uncertainties. For each of the proposed designs, a system of conservative safety factors is applied both to overestimate the environmental loading and to underestimate the structural strength with the aim of ensuring a given safety level. This strategy, although expected to be conservative and to ensure an important safety level of the installations, presents the major drawback of resulting to over-designed units. As a consequence, this results in an increase of the industrialization costs which has direct repercussions on the wind energy price. To keep on reducing the cost of offshore wind energy, a reduction of the safety margins can be envisaged under the constraint of a given structural safety. A second industrial problematic is then expressed as:

> How to reduce the safety factors used in the design process of offshore wind turbines while guarantying a given minimal safety level of the installations ?

Content of the thesis

To answer the two problematics stated above, this thesis presents some developments based on the use of Kriging metamodeling. This statistical method allowed to drastically reduce the simulation investment in different industrial applications proposed in the last decades. Kriging metamodeling thus appears particularly well-suited for the considered industrial con-

text of damage estimation based on intensive simulator calls. Also, this method has shown its performances in reliability analyses, which are performed to quantify the failure risk of a design with regards to a defined failure scenario. Developments relative to these two possible uses are presented in this thesis.

Chapter 1 proposes a global introduction to present in details the industrial context of this thesis. In this chapter, a global overview of the certification process is proposed for the validation of the structural strength of wind turbines. For the particular case of structural damage estimation, explanations and illustrations are proposed to identify the related industrial challenges.

Chapter 2 presents the Kriging method which is intensively used in this thesis to respond to the above-mentioned industrial problematics. A formalization of this statistical approach is proposed as well as a presentation of its practical use in the context of numerical code approximation.

Chapter 3 focuses on the developments relative to the reduction of the simulation investments required for the damage assessment of offshore wind turbines with regards to the constraints presented in the certification framework. In this chapter, the Adaptive Kriging for Damage Assessment (AK-DA) method is introduced for such purpose, along with some variants depending on the context of use. All the proposed developments are illustrated on academical and industrial applications.

Chapter 4 presents the early developments of the extension of the AK-DA method for the damage based reliability assessment of offshore wind turbines. In this chapter the management of uncertainties in the design stage is presented and the framework of reliability analysis is introduced. A method named AK-MCS/AK-DA is then proposed to solve the damage based reliability problems. The performances of three methods (Crude Monte Carlo, AK-MCS and AK-MCS/AK-DA) are then compared on an illustrative example to show the potential of the proposed method for further industrial applications.

Finally, the general conclusions and the perspectives of development are presented at the end of this thesis.

CHAPTER 1

MECHANICAL DESIGN AND CERTIFICATION OF OFFSHORE WIND TURBINE STRUCTURES

Contents

To introduce this thesis, this first chapter proposes a global presentation of the industrial context of the project. First, Section 1.1 globally presents wind turbines and the most developed architectures of supporting structures for offshore installations. The certification process is then introduced in Section 1.2 where the requirements for mechanical analyses of wind turbine structures, proposed by certification bodies and based on standards' recommendations, are presented and emphasized. As a continuation, the formalization and the account for the environmental solicitation are presented in Section 1.3. The environmental modeling, proposed in certification guidelines to properly take into account the loading states, and the common practices and requirements for numerical modeling are then explained in Section 1.4. As highlighted in this section, the fatigue-related design load cases proposed in certification represents an important computing investment with regards to damage quantifications and is the focus of this thesis. To introduce this particular analysis, Section 1.5 proposes a detailed description of the induced studies and the numerical chain which is used all over this work. Finally, Section 1.6 proposes a brief literature review of the recently proposed method to cut-off with simulation investments in the context of fatigue estimation of wind turbine structures.

1.1 Introduction to offshore wind energy production

Offshore wind turbines are developed and installed to produce electricity from wind kinetic energy. As a result of a long term evolution, various architectures have been developed but investments rapidly turned to horizontal axis wind turbine (HAWT) equipped of 3 blades rotors in which the turbine is located at the top of a tower and where the rotor shaft is oriented in the same direction as the wind solicitation [Kaldellis and Zafirakis, 2011]. From a global point of view, two parts can be distinguished in the general composition of wind machines: the production components forming the energy transformation chain and the supporting structure. This first section proposes a brief presentation of these two parts to introduce the structure of interest of the project.

1.1.1 Wind turbine and energy conversion components

The production system of horizontal axis wind turbines is located at the top of the structure. Several components form the transformation chain to create electricity from wind loadings as depicted in Figure 1.1. In a first step, the wind kinetic energy is captured by the blades which transform it into rotational energy. The rotor system uses this energy to initialize a rotational movement transferred through the nacelle by the main shaft (low speed shaft). Depending on technological choices, this created movement can either be directly transmitted to a generator or be adapted by means of a gearbox system (mechanical torque and rotational speed).

Blades are typically large spans of evolving shape with a length usually between 50 and 100 meters in offshore installations depending on the machine characteristics. These elements are composed of a structural envelope made of reinforced fiberglass with internal stiffeners such as shear webs. The aerodynamic characteristics are defined to be highly sensitive to

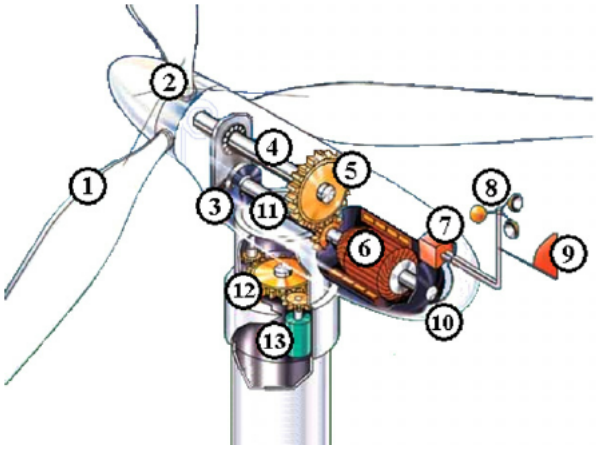

Figure 1.1: Representation of an horizontal axis conversion system with numbering referring to the main components: 1. Blade, 2. Hub, 3. Nacelle, 4-11. Low-speed and high-speed shafts, 5. Gearbox, 6. Generator, 7. Controller, 8. Anemometer, 9. Wind vane, 12-13. Yaw drive and motor [Ciang et al., 2008].

wind and allow to generate mechanical efforts in the perpendicular direction of the wind inflow. For more details, reader can refer to Burton et al. [2011]. As depicted in Figure 1.2, three parts compose the blade. The blade root acts as a connexion component for the fixation of the blade onto the hub. In this sense, this part is of major concern for the transmission of mechanical efforts due to wind loading. The effective part of the blade is the mid-span area which concentrates the most significant share of the energy capture. Finally, the last part is the tip which is located at the end of the blade and designed in order to reduce aerodynamic losses.

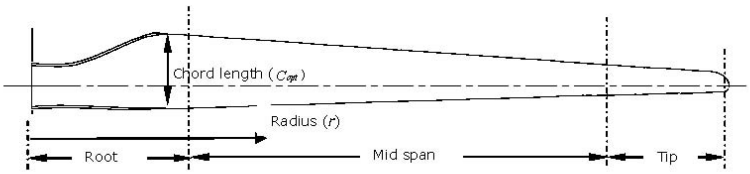

Figure 1.2: Blade composition of an horizontal axis wind turbine [Schubel and Crossley, 2012].

From a global point of view, the aerodynamic behavior of the rotor system is usually qualified by the adimensional ratio between the horizontal wind speed u and the tangential tip speed V_{tip}. This quantity is called the "tip speed ratio" noted λ and introduced as:

$$\lambda = \frac{V_{tip}}{u} = \frac{\Omega r}{u} \tag{1.1}$$

where Ω refers to the structure rotational speed and r to the rotor radius. The conversion potential of a rotor system is qualified by the power coefficient C_p computed from the ratio between the available wind power P_0 and the effective captured power P which is physically dependent of the rotor aerodynamics and so the tip speed ratio λ (Eq. 1.1). Under the hypothesis of horizontal and laminar wind displacement, this coefficient is given as:

$$C_p(\lambda) = \frac{P(\lambda)}{P_0} \quad \text{with} \quad P_0 = \frac{1}{2}\rho A {u_0}^3 \tag{1.2}$$

where ρ is the air density and A the total area swept by the blades. Physically, the entire inflow power can not be transformed by the rotor and the power coefficient C_p is theoretically limited to a certain value known as the "Betz limit" and fixed to 0.59 [Burton et al., 2011]. Furthermore, technological limitations due to rotor system imperfections introduce additional losses depreciating the power coefficient C_p, such as the as tip losses, wake effects, blade shape simplification or drive train efficiency [Schubel and Crossley, 2012].

Once the rotational movement is created by the blades and rotor system, it is transferred to the generator to be transformed into electrical power. Different technologies of generator for offshore wind turbines have been developed since the first installed units, each with their proper operating states so as its pros and cons regarding installation environment [Cheng and Zhu, 2014; Erlich et al., 2012; Islam et al., 2014]. One of the industrial challenges is the optimization of the electrical production with respect to the evolving characteristics of wind. To provide the most effective behavior of the production chain, a real-time adaptation of the generator mechanical input power is implemented into a global and complex control scheme. In this sense, the rotor torque and the rotational speed at generator input are controlled to be as close as possible of the nominal operating state to optimize the energy production. As an illustration, Figure 1.3 depicts the production performances of the reference NREL-5MW wind turbine [Jonkman et al., 2009].

Different domains can be distinguished in the evolution of the production and structural parameters in function of the wind speed u. The production starts for a wind speed of 3 m/s which is called the "cut-in wind speed", noted u_{in} and which represents the minimal condition for the turbine to initialize the blade movement and consequently the shaft rotation. From this start-up regime, the evolution of the wind speed results in an augmentation of the rotational torque and speed until getting closer to their nominal values. During this progressive evolution, the generated power but also the wind-related loads (cumulated rotor thrust) drastically increase as depicted in Figure 1.3a. The machine then reaches its nominal regime regarding the converter capacities (nominal production power of 5MW in the illustrated case) at a wind speed u_{rated}, called the "rated speed". From this point on, the captured power has to be regulated in order to keep on working on the optimal operational state. This feature is technologically ensured by the use of *passive* or *active* regulation methods, also known as "stall" and "pitch" regulations [Hoffmann, 2002]. In the first case, the extracted power is controlled by taking the advantage of the aerodynamic stall characteristics of the blades. Their geometry is subsequently chosen to present stall initialization corresponding to rated wind speed. Although being economical, this technology suffers from the creation of aerodynamic perturbations such as non-laminar flows or vortices which are the sources of important mechanical loads on the whole structure and structural vibrations. As an alternative, the active pitch control permits the modification of the angle of attack of the blades in function of the wind speed. From a practical point of view, this technology uses an actuator to rotate each blades along their principal axis. Therefore, the blade orientation can be adapted to optimize the energy capture from varying winds. As a result, the mechanical solicitations are reduced and the vibrational limitations due to stall regulation are notably decreased. The NREL 5MW is actively regulated as presented in Figure 1.3b which shows the evolution of the pitch angle of the blade in function of the wind speed. From the rated speed u_{rated}, the

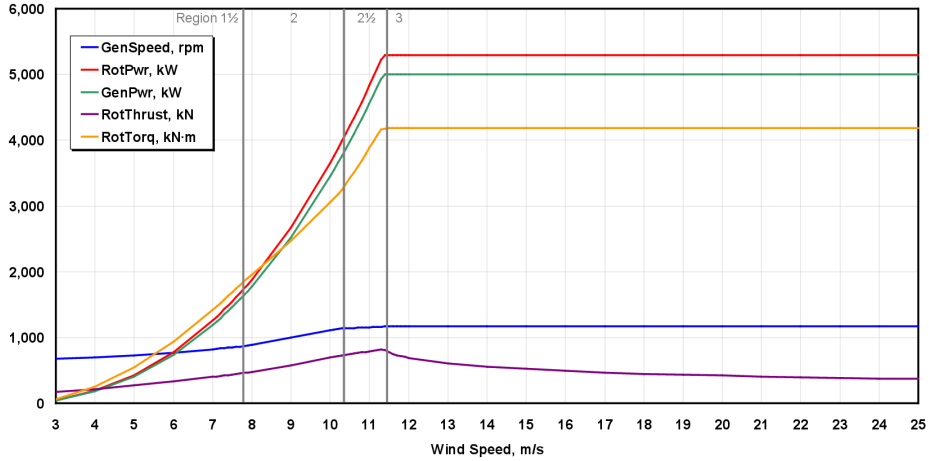

(a) Generator speed, Rotor Power, Generator Power, Rotor Thrust and Torque

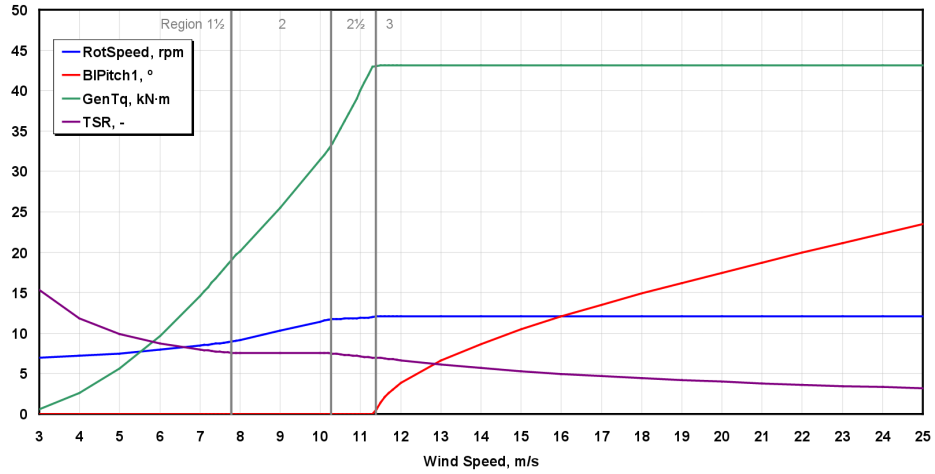

(b) Rotor rotational speed, Blade pitch, Generator torque, Tip speed ratio

Figure 1.3: Evolution of turbine parameters and structural reactions due to the control schemes of the NREL-5-MW [Jonkman et al., 2009].

angle of attack of the blades is modified, passing from an initial pitch angle of 0 degree to an angle of approximatively 25 degrees for important wind speeds (u=25 m/s). This regulation is performed until the "cut-off" wind speed, noted u_{cut}. This speed represents the limit when the turbine is set to a parking or idling state in order to minimize the wind thrust and to guaranty the structural integrity in case of severe winds (extreme natural conditions such as storms).

Production optimization is also achieved by the automatic orientation of the nacelle in the direction of the wind inflow. Measures from sensors (*e.g.* wind vanes or position sensors) allow the controller to compute the optimal nacelle orientation with respect to the wind direction. Rotational adaptations are then ensured by the yaw system composed of a bearing-motor assembly to orientate the nacelle direction.

1.1.2 Supporting structure

The supporting structure permits to install wind turbines within offshore environments. It globally consists of steel or reinforced concrete components linked to the sea soil through a

foundation system. This part aims at stabilizing and fixing the production unit into marine environment with both wind and sea solicitations by maintaining its position and transmitting the cumulated mechanical efforts onto the subsoil of the installation site.

Initially developed in shallow waters, fixed-bottom technologies have been installed in the first offshore wind farms and remain now the most developed alternative. However, the increase of the offshore wind production imposes to enlarge the shore distance for future installation sites to benefit of better production potential. The induced augmentation of the water depth makes the use of fixed-bottom technologies economically unsustainable and first floating designs are now being developed and progressively proposed for industrial deployment [Myhr et al., 2014; Wiser et al., 2016].

The most common substructure systems are the monopiles (Figure 1.4-(b)) and the Gravity Based Foundations (GBF) (Figure 1.4-(a)) which respectively represent about 80% and 10% of the European installed capacity [EWEA, 2015; Oh et al., 2018]. The first technology is based on a foundation composed of an assembly of steel tubular components deeply driven in the sea soil and directly, or through a transition piece, supporting the wind turbine. The simplicity of design makes this technology economically viable for different types of installation sites with water depth up to 40 meters. The structural stability and the rigidity of the bottom part of the structure is here assessed by the mechanical interactions between the foundation, composed of an unique or multiple piles, and the soil mechanical properties. Basically, the monopile can be directly driven into the soil (soft soils such as sand or clay) or after a preliminary drilling operation (for solid calcareous or rock soils) and a grout injection can be installed to enhance mechanical properties of the foundation.

GBF are composed of a massive volume of reinforced concrete stabilizing the structure on the mud-line (*i.e.* the seabed) through its important dead weight. Practically, the installation can be eased by the use of solutions such as the "float and sink" method consisting of modifying the buoyancy characteristics of the substructure in function of the installation advancement: the structure initially presents a floating behavior for the ease of transport and is drawn once positioned in the installation site. As a consequence, the different components can be manufactured and assembled onshore and the entire substructure transported onto the installation site before to be sank filling the hollow cavities with ballast. Site requirements so as cost of production and transportation limit the development of this technology to shallow water up to 15-20 meters.

Other technologies such as those presented in Figure 1.4 can be considered as marginal and are not presented or studied in this project. In case of interest, one can refer to technological descriptions proposed in literature [Butterfield et al., 2005; Miñambres, 2012].

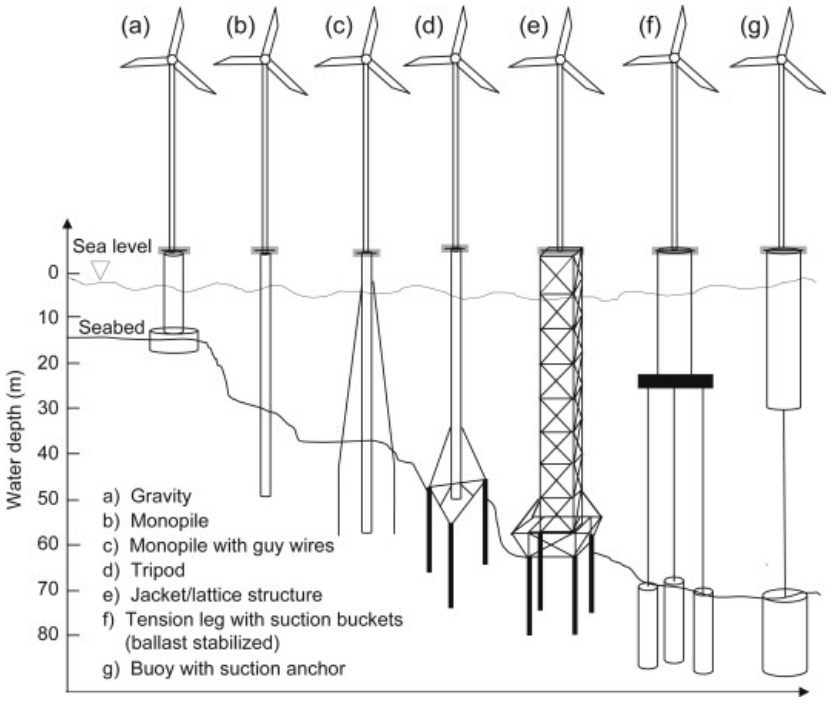

Figure 1.4: Illustration of different types of modern supporting and foundation technologies for offshore wind applications [Arshad and O'Kelly, 2013].

1.2 Standard framework for mechanical certification

The development of offshore wind turbines is an industrial challenge for EDF which acts as the *architect and lead operator* for different projects worldwide. As a consequence, the company proposes assemblies of components (*i.e.* Rotor-nacelle-assembly, tower or substructure) manufactured by different constructors for each of the installation projects. To ensure economical viability of these projects, investors and insurances require the structural designs to be certified. This certification is realized by a third part, known as "certification bodies", and aims at validating the proposed solution regarding minimal expected performances. This control focuses on a various number of characteristics such as the structural strength, the production potential or the installation procedure. General concepts, required performances and analysis constraints are precisely listed and described in standards [IEC, 2005, 2009]. Certification bodies provide "guidelines" [DNV-GL, 2014] to advice and help engineers during the design stage to develop certification granted solutions. In the particular case of mechanical certification and because of the position of EDF in the project organization, the analyses and the certification of the component interfaces is of paramount importance. The certification procedures regarding the control and the validation of the production potential is not under the scope of this thesis which only focuses on the mechanical aspects of the design verification. In the following, a global workflow is proposed focusing on specific notions such as the conceptual situations and the design load cases (DLC), the characterization of installation sites and the management of design safety margins to be considered in order to take into account the procedure uncertainties.

1.2.1 Overview of the mechanical certification procedure

A various number of mechanical requirements are introduced in the certification procedure to guaranty the system performances and minimal safety levels over the entire lifetime of the structure. A design classification is firstly introduced regarding the economical and social consequences of a system failure classifying wind turbines into a normal and a special safety class. Normal safety classes stand for regular designs regarding safety requirements. The wind turbines are classified in function of the wind solicitation states, characterized by the reference wind mean speed u_{ref} (wind mean speed measured over 10 min periods of time [IEC, 2005]) and reference turbulence intensity I_{ref} (expected wind intensity at a height of 15 meters above the sea-level [IEC, 2005]) they can support as presented in Table 1.1. This categorization allows one to consider all the possible types of installation sites and limit the development cost by class-related certification of wind turbine designs. In the case of specific requirements due to local regulation and/or safety considerations, a special safety class S is proposed. Apart the safety margins to consider, the certification work flow remains the same for each of the defined class.

Class		I	II	III	S
u_{ref}	(m/s)	50	42.5	37.5	Site-specific values
A	I_{ref}	0.16			
B	I_{ref}	0.14			
C	I_{ref}	0.12			

Table 1.1: Classification of the wind turbines: the normal safety class is composed of 9 categories going from C-III to A-I and a special safety class S is proposed for specific designs [IEC, 2005].

A systematic approach for the design validation is proposed considering four different limit states, each corresponding to different types of structural reactions over the expected lifetime and for which specific studies have to be performed. Firstly, the *ultimate limit states* (ULS) refer to maximal mechanical reactions of the structure due to environmental solicitations. Those limit states induce mechanical analyses which are performed to estimate the maximal structural reactions and to verify their significance regarding failure modes as the exceeding of material resistance, loss of structural equilibrium (*e.g.* overturning or capsizing) or integrity (*e.g.* buckling). Secondly, the *serviceability limit states* (SLS) regroup the design requirements concerning the production function of the unit (*e.g.* limited nacelle tilt or blade vibration behavior during production) and those linked with the environmental physical reactions of the structure (*e.g.* corrosion due to marine environment or evolution of the structural natural frequencies due to marine growth development). A third category is composed of the *fatigue limit states* (FLS), which deal with damage accumulation due to cyclic loading from varying environmental solicitations and their effects regarding structural aging. To finish, the *accidental limit states* (ALS) are introduced to consider structural reactions due to abnormal or accidental events (*e.g.* extreme wind conditions or boat collisions).

1.2.2 Conceptual situations and design load cases

Within the introduced certification procedure, the lifetime of the structure is assimilated to a series of elementary situations. Each of these are considered to be likely to happen consid-

ering the installation site and are assumed to be independent (no consideration of continuity between them). The proposed procedure is based on the verification of the structural performances either estimated for each of the situations or cumulated over several one. Conceptual situations (CS) are listed as a number of height representing lifetime structural states as depicted in Figure 1.5.

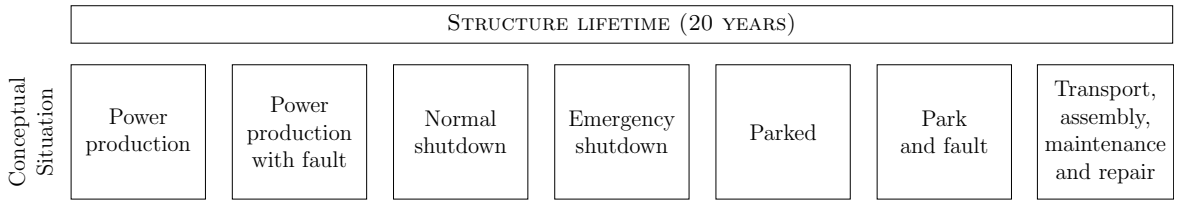

Figure 1.5: Lifetime conceptual situations presented in wind turbine certification procedure.

For each of the conceptual situations, a list of design load cases (DLC) is given corresponding to the complete set of mechanical analyses to be carried out. Each of the DLC is presented as a formal framework regrouping different informations relative to the analysis requirements listed as:

- the *environmental models of solicitations* (*e.g.* Normal Wind Model, Normal Turbulence Model, etc.)
- the *models of variation of the environmental parameters* (directions of wind and wave loadings, range of variations, etc.)
- the *specific conditions* (*e.g.* loss of grid connexion, abnormal behavior of a component, etc.)
- the *type of mechanical analyses to perform* (ULS or FLS for each of the defined cases)

Additionally and depending on the DLC, serviceability limit states or accidental limit states may have to be considered to complete the global analysis of the structural behavior. As an example, the conceptual situation 1 which refers to *normal power production* and the subsequent design load cases are presented in Appendix A. The analysis of the fatigue limit states related design load cases are particularly demanding when validating a design as explained in Section 1.5 and compose the central purpose of this thesis. As a consequence, the rest of the documents focuses on the DLC 1.2 and the other analysis cases will not be discussed or illustrated.

1.2.3 Metocean characterization of installation site

For each of the installation sites, the variations of environmental solicitations have to be carefully addressed to ensure the representativeness of modeling and the relevance of the estimated structural reactions. Metocean data (abbreviation for *meteorology and oceanography*) represent the variation of environmental conditions at the installation site based on descriptive parameters such as the evolution of the mean wind speed at hub height or the significant wave height computed for a defined period of time given by standards. *In situ* measurement campaigns are ordered to determinate the parameter ranges as well as their joint probability

of occurrence. Practically, data can be determined from measurements carried out with wind masts and buoys, with an acquisition time depending on the parameters and the situations to model. Measured series can additionally be completed by generic statistical models to infer the occurrence of rare events which may have not been covered during the acquisition period such as the maximal significant wave height with return period of 50 years.

From a more formal point of view, all the considered environmental parameters can be viewed as n random variables X_i, with $i \in \{1, \dots, n\}$, which can be encompassed in a set of random variables $\boldsymbol{X}$. The metocean characterization aims at determining the joint density probability function $p(\boldsymbol{x})$ where $\boldsymbol{x}$ hereafter denotes a realization of the $\boldsymbol{X}$. The function p thus reads:

$$\text{Prob}\Big(\boldsymbol{X} \in [\boldsymbol{x}, \boldsymbol{x} + \mathrm{d}\boldsymbol{x}]\Big) = p(\boldsymbol{x})\mathrm{d}\boldsymbol{x} \tag{1.3}$$

The characterization of the metocean is critical for the representativeness of the computations proposed in the standards and certification guidelines. One can refer to Stewart et al. [2015] for an illustration of the metocean construction from *in situ* measurements.

1.2.4 Safety factors and design validation

For each of the presented DLCs, the structural reactions obtained from numerical computations (details given in Section 1.4) are supposed to suffer from uncertainties induced by the assumptions of the proposed analysis framework. As a matter of facts, several sources of uncertainties have to be considered as the modeling imprecisions leading to imperfect structural or environmental models (*e.g.* numerical modeling of the structure based on beam elements as introduced in Section 1.5.1 or uncertainties regarding mechanical constants as the Young modulus) or the simplifications induced by the certification framework (*e.g.* discretization of the environmental parameters introduced in the particular case of the fatigue analysis in Section 1.5). To ensure a minimal structural safety level, these uncertainties are considered by the use of *partial safety factors* aiming at integrating all the uncertainty the design scheme may be influenced by. Additionally, these coefficients are determined in function of the importance of the component of interest and the possible structural consequences in case of failure.

A formalization of this is given in standards with the introduction of the design loading effect and resistance notions, namely S_d and R_d. The validation criterion is presented by the "design inequality" to be at least verified as:

$$S_d < R_d \tag{1.4}$$

Partial safety factors on loads

Uncertainties of environmental solicitations are considered in a deterministic way by the use of a loading partial safety factor γ_f which have to be elected depending on the analyzed conceptual situation. Let $\mathcal{M}_s$ be the analysis model adapted to the design load case to be

assessed. The integration of this security factor can be proceeded in two different ways as presented in Figure 1.6 depending the designed component.

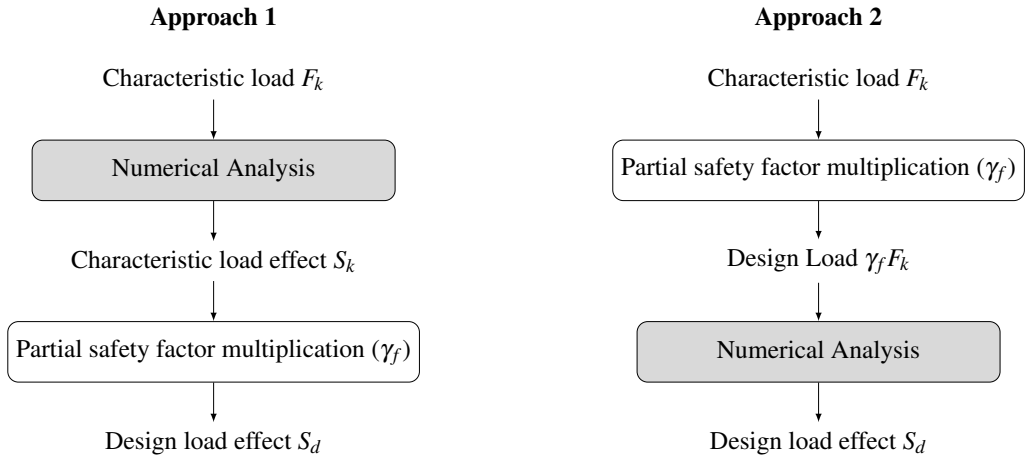

Figure 1.6: Two approaches for the consideration of loading partial safety factor to apply [IEC, 2009].

In the first approach, the characteristic load effect S_k obtained from the structural response due to the characteristic load F_k is increased by the use of the loading partial safety factor γ_f:

$$S_d = \gamma_f S_k = \gamma_f \mathcal{M}_s(F_k) \tag{1.5}$$

This first approach is particularly suitable for the mechanical analysis of component where the dynamic reactions need to be precisely estimated as for the design of tower regarding aerodynamic loading. The second proposed approach aims at integrating the partial safety factor before the mechanical analysis by increasing the characteristic load F_k:

$$S_d = \mathcal{M}_s(\gamma_f F_k) \tag{1.6}$$

Standards indicate to process this second approach when considering non-linearities of model responses as, for example, in case of supporting structure or foundation design. This recommendation is proposed to ensure the conservatism of the estimations of structural reactions.

Partial safety factors on resistance

The strategy used to consider the uncertainties associated with the capacity R_d is similar to the one applied to the load and two different methods are available. The choice of the method to apply depends on the standard of reference and the structural component. In one hand, the partial safety factor can be integrated directly to the value for the material strength f_k. The characteristic value therefore reads:

$$R_d = R_k\Big(\frac{1}{\gamma_m} f_k\Big) \tag{1.7}$$

From a more global point of view, a second proposition is based on the modification of the component capacity value R_k:

$$R_d = \frac{1}{\gamma_m} R_k \tag{1.8}$$

In addition to the global framework proposed in standards and briefly introduced in this section, requirements are presented for the modeling of environmental states and structural responses subsequently. The two next sections aim at giving additional details on the analysis procedure proposed by the standards.

1.3 Offshore environmental solicitations

Wind turbine structures are subjected to complex solicitation states. In the offshore context, the solicitation environment is composed of a variety of excitation sources as illustrated in Figure 1.7 and they have to be carefully considered to ensure the representativeness of numerical simulations required in certification procedures. In the following, the loading environment is described as it is presented in guidelines and usually considered for numerical approaches in mechanical analyses.

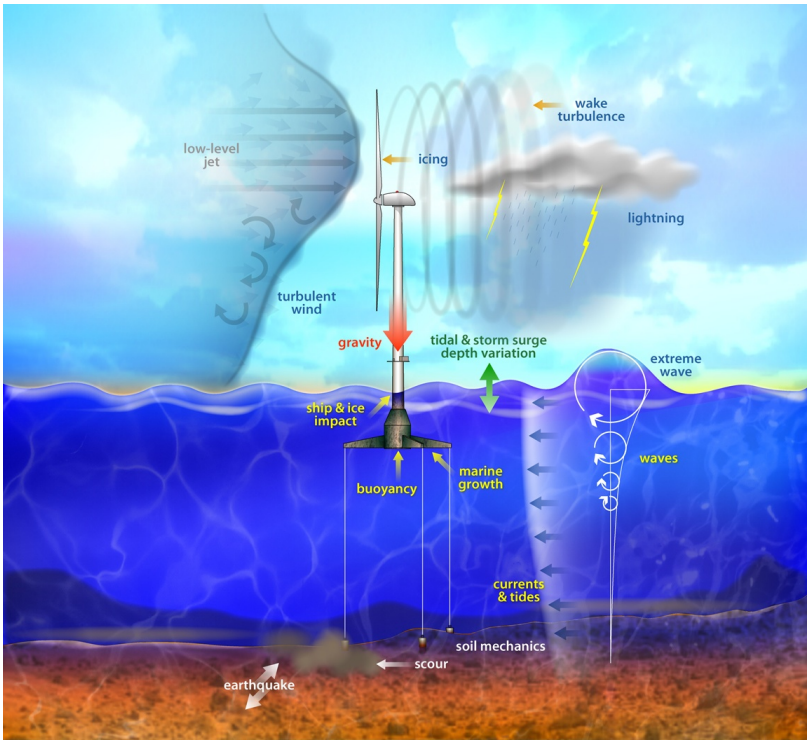

Figure 1.7: Illustration of the environmental loading state of offshore wind turbine [NREL website].

1.3.1 Wind solicitations

The wind acts on the upper part of the structure composed of the rotor nacelle assembly, the tower and possibly the upper part of the substructure. As a consequence, several loading modes have to be considered. Firstly, a rotor thrust is created from the cumulated effort over the rotor area which applies on the top of the tower. Furthermore, a distributed load applies

all along the tower length with possible wind shear effects due to spatial variations of wind loading.

In real situations, wind presents a turbulent characteristic with important variations both spatially (evolutions in the three dimensions) and temporarily. It is common to consider the wind variations as the composition of a long-term and a short-term phenomena. The long-term evolutions are represented by the evolution of the wind mean speed u for a fixed period of time, usually equals to 10 min. This evolution is statistically considered assuming it is the realization of a random variable U distributed on a parameterized Weibull probability density function f_U introduced as:

$$f_U(u) = k\frac{u^{k-1}}{c^k}\exp\Big(-\Big(\frac{u}{c}\Big)^k\Big) \tag{1.9}$$

with c and k, respectively the scale and the shape parameters. This distribution has to be adapted to the installation site by fitting the introduced coefficients to the *in situ* measurements (metocean). This description stands as a reference model used to deduce the global wind evolution (in the three directions and all along the structure height). As an illustration, three different distributions of the wind mean speed are depicted in Figure 1.8a for a fixed coefficient $c = 7m/s$ and multiple values of the shape parameter k.

The variations of the wind speed and as well as the wind direction within a 10-min time period are considered as short-term evolutions and are taken into account by the definition of a turbulence model. The speed variations are considered within the "turbulence intensity" I defined from the standard deviation σ_u of the wind speed during the considered 10-min period of time as:

$$I = \frac{\sigma_u}{u} \tag{1.10}$$

The characterization of the short-term variation of the wind speed is monitored by the use of turbulence spectra which are function, among others, of the wind mean speed u and the turbulence intensity I. The Kaimal and Von Kármán models present turbulence spectra which are extensively used for industrial applications [Burton et al., 2011]. As an illustration, Figure 1.8b presents the Kaimal turbulence spectra for a wind mean speed $u = 12$ m/s.

From this generic description, different models are proposed to represent a particular situation introduced in the design load case definitions, for the turbulence behaviors (*e.g.* normal turbulence model), the wind profile (*e.g.* normal wind profile) or the change in wind direction (*e.g.* extreme direction change). The generation of wind time series is practically performed using random generators parametrized to correspond to the simulated wind state. This generation allows one to obtained wind speed time series on the three spatial directions. An illustration of this aleatory generation is presented in Figure 1.9a and Figure 1.9b which respectively depict the evolution of the horizontal wind mean speed u at hub height and the evolution of the wind direction of solicitation over a period of 600s (10 min).

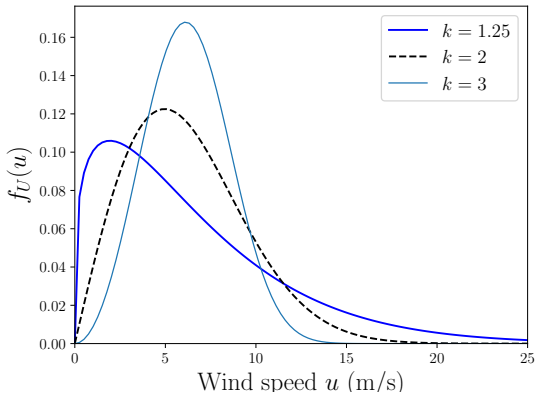

(a) 10-min wind mean speed distribution

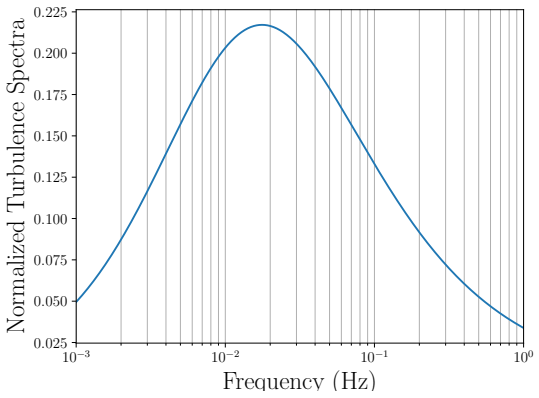

(b) Wind turbulence spectra

Figure 1.8: Illustration of the wind mean statistical distribution (a) and wind turbulence spectra (b) estimated for a wind mean speed $u = 12$ m/s and turbulence intensity factor $I = 0.17$.

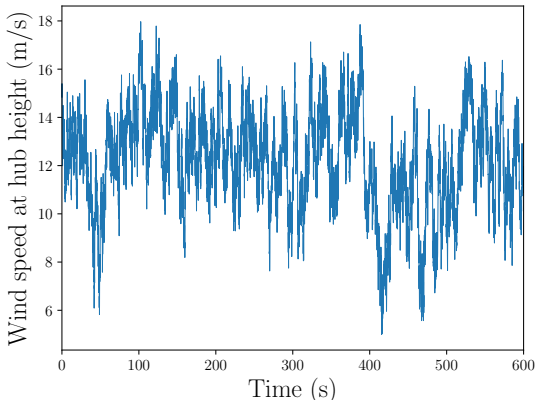

(a) Horizontal wind speed at hub height

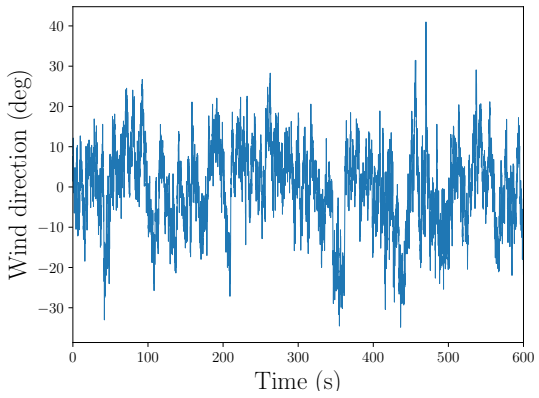

(b) Direction of solicitation

Figure 1.9: Illustration of the random generation of wind history from TurbSim [Jonkman and Kilcher, 2012]. The 10-min wind speed is fixed to 12 m/s with a normal turbulence model (NTM) with intensity factor $I = 0.17$. The wind mean speed at hub height is depicted in (a) and the variation of the wind direction of solicitation is presented in (b).

1.3.2 Sea solicitations

Sea loading are mainly due to waves and current interactions with the submerged part of the structure. The wave evolution can be considered as a long and short term behaviors, similarly to the approach used in the wind model. The wave state is considered as the superposition of elementary functions (sinus functions) and the analysis of its evolution for a defined time period leads one to the elaboration of frequency spectra. In the context of wind turbine analysis, two spectra are widely used to represent the wave information content. The "Pierson-Moskowitz" proposed by Pierson and Moskowitz [1964] and the "Jonswap" spectra presented by Hasselmann et al. [1973]. These latter are parametrized by the spectral peak period t_p and the significant wave height h_s computed for the covered period of time. In the following, each of these sea parameters are assumed to be realizations of random variables respectively noted T_p and H_s. From a practical point of view, standards propose to consider the long term evolutions as one to three hour evolutions, depending on the design load case.

Considering given values for the wave parameters, *i.e.* a fully defined wave spectrum representing the sea state for a long period of time, say three hours, an inverse operation allows

to aleatory generate wave histories by combining a finite number of mono-periodic waves with spectral-representative heights and random phases. As an illustration, Figure 1.10 depicts a wave elevation history of 600 seconds based on a Jonswap spectrum and parametrized by a significant wave height $h_s = 3$ meters and a spectral peak period of $t_p = 10$ seconds.

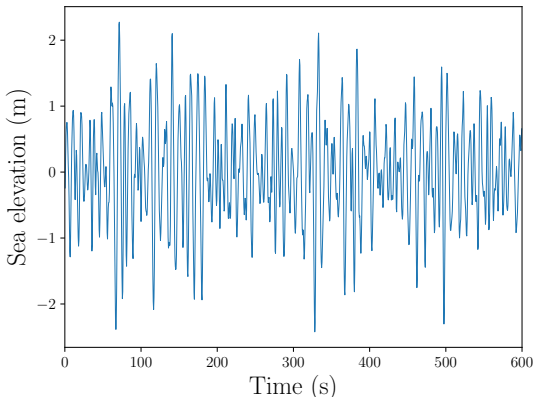

Figure 1.10: sea elevation extracted from an aleatory generation of sea state based on Jonswap spectrum

To summarize, global sea states are defined in standards to model each of the possible situation the structure may have to undergo during its lifetime and the aleatory generation process is adapted to account for particular features of the sea state (*e.g.* normal or extreme wave height, severe or extreme sea states accounting for exceptional situations usually considered likely to happen once every 50 years).

1.3.3 Soil conditions

The composition of the soil and the possible interactions with the foundation system or the substructure are also of primary interest for numerical analyses. In this sense, the structural model has to take into account the mechanical characteristics of the sub-soil (material layers, stiffness characteristics, etc.). It should be noticed that this modeling represents an important challenge in today's research field to determinate the proper characteristics of a material (clay, rock, sand, etc.) but also to characterize the uncertainty of the soil response due to limited measurement campaigns as presented in Dolores Esteban et al. [2015]. In addition, several installation sites are subjected to seismic activity and earthquakes can create mechanical solicitations and the bottom of the structure which have to be analyzed.

1.3.4 Rotor excitation and tower shadow effect

One of the particularity of wind turbines is the presence of a massive rotor at the top of the supporting tower. The mechanical excitation due to the cyclic movements of the blades has to be considered when defining the loading state of the structure. Two domains of excitation defined by the evolution of frequencies, named f_{1P} and f_{3P} can be observed in Figure 1.11. The first one represents the imperfection effects of the rotor equilibrium (mechanical imbalances) and the second one corresponds to the effects of blade passing over the tower ("tower shadow effect"). The structural frequencies of the design have to be excluded from these two areas of cyclic loadings to prevent periodic structural reactions and possible risks for unit

integrity. Three types of structures are then distinguishable regarding the design strategy: the *soft-soft* structures which present a first structural frequency f_0 located between the wind and wave spectra peaks, the *soft-stiff* structures with frequency f_0 between the f_{1P} and f_{3P} (as depicted in Figure 1.11) and finally the *stiff-stiff* designs which present large structural frequencies greater than the f_{3P} frequency.

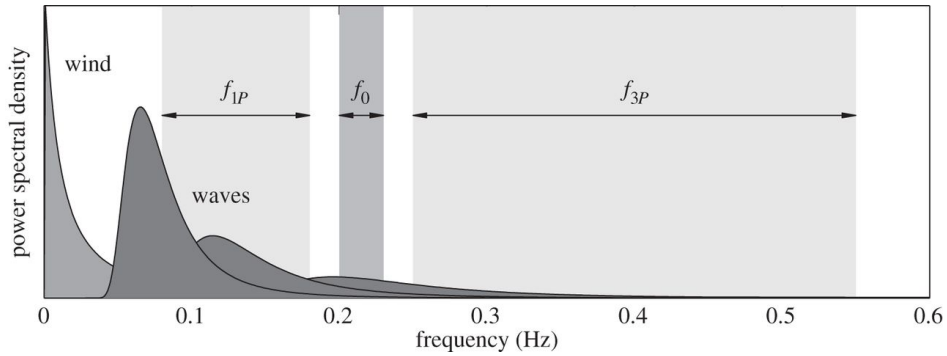

Figure 1.11: Example of solicitation spectra of an offshore wind turbine. More than the wind and wave, rotor cycle loading of frequencies f_{1P} and f_{3P} have important consequences in the structural loading state [Kallehave et al., 2015].

1.3.5 Complementary sources of solicitations

In addition to the points presented here-before, possible temporary solicitations such as lightning or blade icing may be required to be taken into account to represent particular loading states. Furthermore, geometrical evolutions due to natural effects such as corrosion or marine growth are crucial to be considered for the representativity of the simulations and the analyses of aging consequences.

1.4 Numerical modeling of offshore wind turbines

1.4.1 Geometrical simplifications

The geometry of wind turbine structures and the consideration of stress fields, mostly resulting from bending and compression, allow to model the ensemble as a beam with evolving characteristics along its height. As a consequence, elementary approaches based on beam elements with six degrees of freedom are commonly used for dynamic analyses of wind turbine structures. Each of the structural elementary geometries can be considered by adjusting beam element characteristics such as mass or stiffness parameters. The nacelle rotor assembly is considered as a node mass located at the top of the structure. This choice provides reasonable computational times and is particularly easy to implement compared to complete finite element modeling applied to the entire structural details. In the following, soil so as aerodynamic and hydrodynamic load modeling due to external solicitations are briefly introduced.

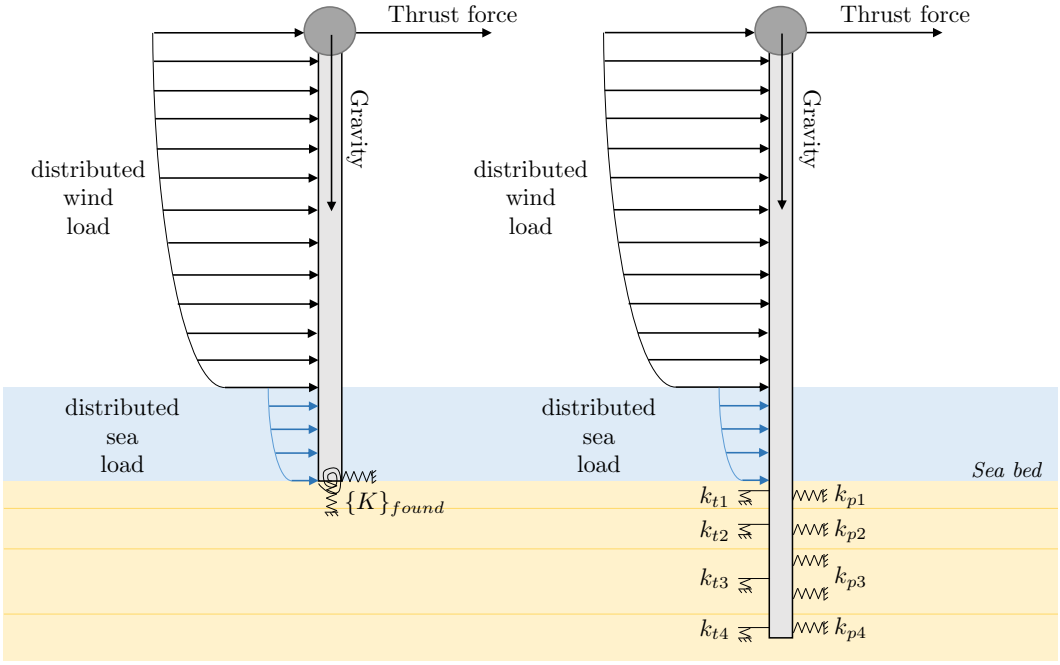

Figure 1.12: 2D beam representations of the wind turbine structure (monopile foundation) with two commonly used soil-structure models: simple stiffness element (left) and "$p-y/t-z$" modeling (right).

1.4.2 Soil modeling

The most simple structural models do not consider the soil-structure interactions and clamp the monopile bottom at the mud-line level. This drastically reduces the structural model complexity but results in lower quality estimations because of the unrepresentative computations of structural frequencies. To provide more representative models, the consideration of these interactions can be done resorting to different modeling methods [Arany et al., 2017; Passon, 2006]. A stiffness element located at the bottom of the structure can be added to represent the soil characteristics. This approach is simple to implement and proposes to sum-up the soil mechanics by means of a single point which mechanical characteristics are viewed as a foundation stiffness represented by the $\{K\}_{found}$ torsor in Figure 1.12 (left hand side). As a drawback, this method does not consider the evolution of the soil mechanical properties due to the presence of different soil layers and only provides a linear approach of the soil-structure interaction.

To enhance the representativeness of the numerical models, more complex approaches have been developed such as the "$p-y$" (lateral displacement) and "$t-z$" (vertical displacement) non-linear representations for monopile components. They are well suited to account for more complex relations but require to adopt iterative resolutions to solve the equilibrium state at each step of the structural dynamic resolution (non linear modeling) and require a comprehensive soil survey to use appropriate stiffness values.

1.4.3 Aerodynamic load computation

Structural responses are strongly influenced by the aerodynamic loads due to the wind-blades interactions. On one hand, interactions cause the rotor thrust which acts on the upper part of the structure. On the other hand, they create an aerodynamic damping along the rotor

axis direction. Together with servo modifications of the aerodynamic characteristics of the rotor system, nowadays integrated in wind turbine systems, their consideration becomes a keystone for representative modeling of wind turbine loading. The use of traditional fluid-structure interactions tools as the Computational Fluid Dynamics (CFD) would lead one to a representative estimation of the rotor thrust but also to an important computational efforts. As an alternative, the wind turbine aerodynamics is usually approximated by the use of the Blade Element Momentum Theory ("BEMT") which combines the "blade element" and the "momentum" theories. In this approach, two assumptions are made: firstly, the aerodynamic interactions between blades are neglected and secondly, the forces are determined only from the lift and drag coefficients [Ingram, 2011].

To briefly introduce this approach, blades are considered as a finite number of elements for which a basic aerodynamic analysis, function of their rotational speed and profile (*e.g.* chord length or twist angle) is performed. The application of the momentum theory allows one to determinate the axial forces δT and torque δQ from the *actuator disc and stream tube* modeling, as presented in Figure 1.13:

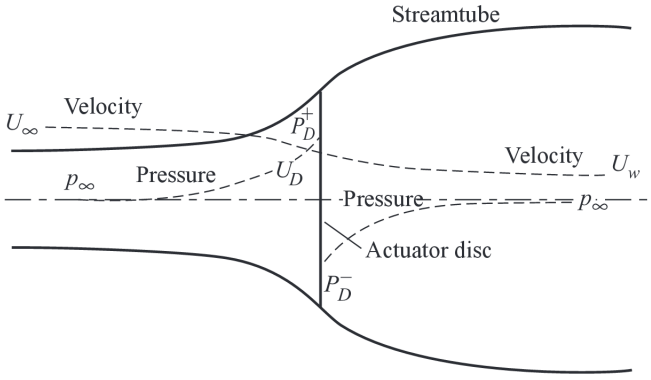

Figure 1.13: Actuator disc and stream tube concept for the blade element theory as depicted in Burton et al. [2011].

$$\delta T = 2\pi r \delta r \rho U_\infty (1-a) 2a U_\infty \tag{1.11}$$

$$\delta Q = 2\pi r \delta r \rho U_\infty (1-a) 2a' r^2 \Omega \tag{1.12}$$

where a and a' are the axial and tangential flow induction factors, r and Ω respectively the blade element radius and rotational speed, U_∞ the inflow wind speed and ρ the air density. By applying the blade element theory based on a geometrical analysis (see Figure 1.14), the quantities δT and δQ can also be calculated from Eq. 1.13 and Eq. 1.14.

$$\delta T = \frac{1}{2}\rho W^2 B c (C_l \cos\phi + C_d \sin\phi)\delta r \tag{1.13}$$

$$\delta Q = \frac{1}{2}\rho W^2 B c r (C_l \sin\phi + C_d \cos\phi)\delta r \tag{1.14}$$

where W is the resultant relative velocity at the blade, B the number of blades, c the profile chord and finally C_l and C_d the lift and drag coefficients of the blade element. By combining

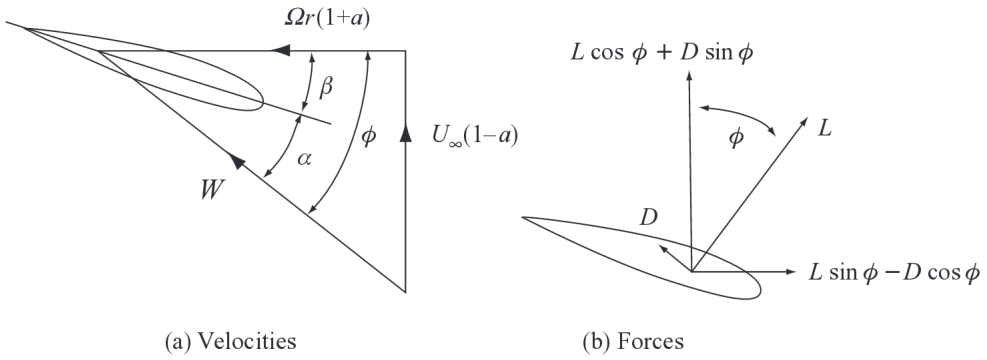

Figure 1.14: Blade element approach as depicted in Burton et al. [2011] where D and L stand for the drag and lift forces.

the proposed formulations, two equations of equilibrium are then developed as:

$$\frac{W^2}{U_\infty^2} B \frac{c}{R} (C_l \cos\phi + C_d \sin\phi) = 8\pi a(1-a)\mu \tag{1.15}$$

$$\frac{W^2}{U_\infty^2} B \frac{c}{R} (C_l \sin\phi + C_d \cos\phi) = 8\pi \lambda \mu^2 a'(1-a) \tag{1.16}$$

with $\mu = r/R$ and λ, the tip speed ratio. It can be observed that these two quantities are not independent and the solving of this formulation for each of the blade elements (coefficients a, a', λ) is only possible by an iterative implementation which can, in certain cases, be the source of important computational efforts. Once the equilibrium is reached and the parameters presented in Eq. 1.15 and Eq. 1.16 are determined, the axial forces and torque can be computed for the entire rotor-blade system by integrating the differential quantities over the blades length. This simplified approach allows one to have an estimation of the wind-rotor system interaction and to compute approximations of the created torque and rotor thrust which directly act on the rotor shaft. For more details, readers can refer to Burton et al. [2011] and Ingram [2011].

1.4.4 Hydrodynamic load computation

To account for hydrodynamic loads, the Morison's equation is used within the formulation of moving body in an oscillatory flow. This approach is semi-empirical and its assumptions concern the geometrical proportions of the substructure regarding the wave length and its diameter-length ratio. For thin structures as monopiles or combined tubular assembles proposed in certain types of jacket substructure, the above-mentioned assumptions are acceptable.

From the displacement of the water which is aleatory generated as presented in Section 1.3.2, the hydrodynamic forces acting on the part of the structure which is under the sea level are given as:

$$F = \rho_s V \dot{u} + \rho C_a V(\dot{u} - \dot{v}) + \frac{1}{2}\rho C_d A(u-v)|u-v| \tag{1.17}$$

where ρ_s is the water density, C_a and C_d are respectively the inertia and drag coefficients, V is the volume of the body u and $\dot{u}$ the flow velocity and acceleration, v and $\dot{v}$ the body velocity and acceleration. Finally A is the cross sectional area of the body. For each of the structural elements under sea loading, the forces at each finite element node can be determined and the finite element model is updated. This equation is commonly considered under the assumption of fixed structure which does not admit any displacement. In this particular case, the structural velocity and the acceleration of the body are assumed to be equal to zero: $v = 0$ and $\dot{v} = 0$.

1.4.5 Simulation requirements and limitations

The structural reactions due to mechanical loads the environmental situation creates have to be estimated by the use of numerical simulators. These latter aim at approximating the real structure behavior with the implementation of a numerical model to estimate the mechanical strength of the design to install and more generally to assess the design load cases listed in the certification guidelines. To ensure the representativeness of the computations engineers have to perform, several requirements guide the choice of the simulation process. First, the simulator have to consider each of the four physics the wind turbine is subjected to:

- aerodynamics: integration of the wind-structure interactions
- hydrodynamics: integration of the sea-structure interactions
- elastic mechanics: consideration of the structural linear deformations
- servo: integration of the production and security control schemes

As a result, multi-physics simulators are required to compute the structural reactions due to environmental loading. Furthermore, two of the presented characteristics induce non-linearities in the simulations. The first one is the aerodynamic damping, created within the interaction between wind and rotor (blades). These interactions are known as "aero-elasticity" interactions and result in double interaction both from the fluid (the air here) to the structure and from the structure to the fluid. Additionally, the servo and more specifically the control of the production induces major changes in the aerodynamic behavior of the turbine (*e.g.* pitch evolution of the blades). These evolutions make the structural solicitation evolving with regards to the wind loading as depicted in Figure 1.3a where the rotor thrust presents a nonlinear evolution with respect to the wind speed.

These nonlinearities are considered in simulation steps by using time computations with relatively small simulation steps. This choice allows engineers to properly simulate the structural responses due to environmental loading. Also, certain design load cases as the DLC 3.1 (estimation of the cumulated fatigue for start-up) require the computation of the transitional structural reactions which is only possible with the implementation of time simulations. The consequences of these requirements mainly concern the numerical investment required for a single simulation. Considering a 600 seconds (10 min) loading history, the only computation of structural reactions is about from a few minutes for simple designs (monopile with rigid foundation) to hours for complex situations (idling floating turbine).

1.5 Practical approach of the fatigue limit state analyses

The fatigue limit state analyses (FLS) presented in standards and certification guidelines are crucial to assess the structural performances regarding the lifetime cumulated reactions of the design. Because of the high number of cycles the supporting components have to face during the unit lifetime, a proper and well guided investigation is mandatory to estimate the cumulated damages at several structural locations of interest. This thesis focuses on the particularly demanding design load case 1.2 for which engineers have to numerically estimate the cumulated damage for the "normal production" conceptual situation (see Appendix A for a more detailed description of the analyses required for this conceptual situation). This quantification is hereafter realized by the use of the global mean damage D, introduced here and being taken as the quantity of interest all along this thesis. To better explain the implemented numerical chain, the computation of this quantity is also explained and illustrated.

1.5.1 Definition of the global mean damage D

Let $\boldsymbol{x} = \{x_1, \dots, x_n\} \in \mathcal{D}_{\boldsymbol{x}}$, be the vector of parameters describing the environmental solicitation state (*e.g.* hub height wind mean speed u, peak period of the wave spectrum t_p, etc.). The global mean cumulated damage D_{t_0} computed over a period of time t_0 at a given structural location is formalized as:

$$D_{t_0} = \int_{\boldsymbol{x} \in \mathcal{D}_{\boldsymbol{x}}} d_{t_0}(\boldsymbol{x})\, p(\boldsymbol{x})\, \mathrm{d}\boldsymbol{x} \tag{1.18}$$

with $d_{t_0}(\boldsymbol{x})$, the estimation of the short term damage due to a given solicitation state of parameters $\boldsymbol{x}$ over a period of time t_0 (*i.e.* a realization of the random vector $\boldsymbol{X}$ introduced in Section 1.2.3) and $p(\boldsymbol{x})$, the joint probability of occurrence of the vector of environmental parameter $\boldsymbol{x}$. For the sake of clarity, the mean damage D_{t_0} and short-term damages d_{t_0} are respectively noted D and d in the following.

The integral form of the quantity of interest D presented in Eq. 1.18 is not computable in practice and an approximation is proposed by the consideration of an environmental regular grid. This latter is composed of n_c combinations of environmental parameters, and the damage quantity of interest is approximated by:

$$D \approx \sum_{i=1}^{n_c} d(\boldsymbol{x}_i)\, p(\boldsymbol{x}_i)\, \Delta = \sum_{i=1}^{n_c} d_i\, p_i\, \Delta \tag{1.19}$$

with Δ the integration unit of the continuous space discretization. This quantity is defined from the discretization δ_i of each domain of variation of environmental parameter i. Considering n environmental parameters, the term Δ therefore reads:

$$\Delta = \delta_1 \times \cdots \times \delta_n \tag{1.20}$$

Certification guidelines indicate the minimal discretization unit to use in the application of Eq. 1.19. The illustrative example presented in Table 1.2 shows the high number of environmental parameter combinations to take into account when only considering a reduced number of environmental parameters (for example, the sea level or the turbulence intensity variability are not considered here). Standards require to only consider the co-directional loadings with equal sea and wind directions of loading. To ensure the representativeness of the simulation and not to miss unexpected structural reactions, the wind and sea directions of loading are commonly considered as independent.

		Illustrative example	
Environmental parameter	Maximal admitted binning δ_i	Domain of Variation	Number of cases
Wind mean speed U	2 m/s	$[3:25]$ m/s	12
Significant wave height H_s	0.5 m	$[0:5]$ m	10
Wave peak period T_p	0.5 s	$[3:10]$ s	14
Wind direction θ_{wind}	30 deg	$[-150:180]$ deg	11
Wave direction θ_{wave}	30 deg	$[-150:180]$ deg	11
	Total number of combinations n_c		203 280

Table 1.2: Maximal admitted binning for simulations provided by the DNV-GL guidelines [DNV-GL, 2014].

1.5.2 Numerical model for the computation of the short term damage d

For each of the n_c combinations of environmental parameters, the structural damage d has to be assessed to estimate the global mean damage presented in Eq. 1.19. This step requires the implementation of a numerical chain which global architecture is presented in Figure 1.15 and described hereafter. To better explain its implementation, the environmental set of parameter $\boldsymbol{x}$ is decomposed into a wind-related and a sea-related sets, respectively noted $\boldsymbol{x}_{wind}$ and $\boldsymbol{x}_{sea}$.

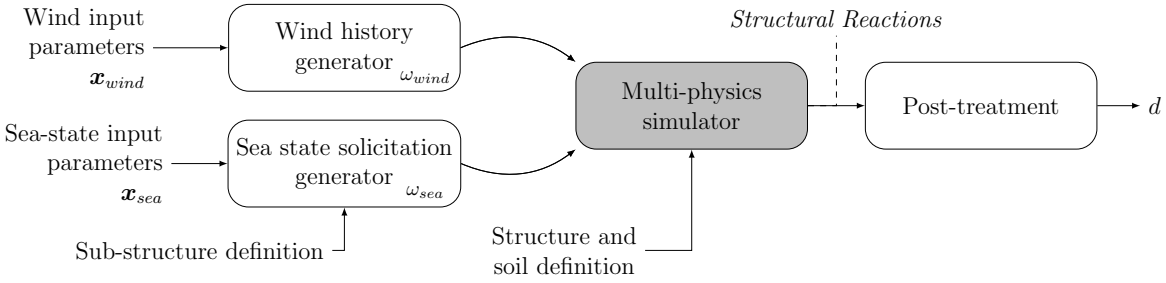

Figure 1.15: Presentation of the numerical chain for the estimation of the short term damage due to a given solicitation state of environmental parameter $\boldsymbol{x} \in \mathcal{D}_{\boldsymbol{x}}$.

The numerical chain is first initialized by the generation of random time histories for environmental loads. For both wind and sea related loading histories, generators are run considering the environmental parameter inputs as the wind mean speed at hub height u, the wind profile evolution or the turbulence spectrum for the wind and significant wave height, the wave spectrum or the current models for sea states. The generation has to be performed with respect to a "Normal Turbulence Model" for the wind history and a "Normal Sea State" model for the sea state generation (see Appendix A).

An infinite number of time series or trajectories can be simulated from the definition of the aforesaid inputs by varying the random seeds, represented in Figure 1.15 by ω_{wind} and ω_{sea}. Certification guidelines recommend to sample several trajectories for each environmental solicitations (wind and sea states). In the case of the design load case 1.2, the fatigue analysis has to be performed with six different generations of 10 min time period or a single 1-hour generation both for wind and sea-state histories. In the case where engineers choose to handle 10-min damage estimations, a more representative 1-hour damage short term damage is computed by summing the six short term damages estimated over a period of time equals to 10 min. Considering the illustrative discretization proposed in Table 1.2, this represents an increase from 203280 to $203280 \times 6 = 1219680$ situations to simulate for a single estimation of the global mean damage D, which is obviously unmanageable for industrial applications. Time simulations are then performed to determinate the structural responses due to the generated environmental solicitations at each of the different locations of interest. Generalized stresses are finally post-processed before the computation of the estimated short term damages d. In the presented work, because of the stress mode of the structure which is mainly composed of traction and compression, the Von Mises equivalent stresses are computed. This recomposing leads to a time evolving signal which can be treated using the rainflow cycle counting method to extract the fatigue cycles.

As a result, a finite number of fatigue cycles are considered and their related damages can be computed by means of the so-called S-N curves provided by the certification guidelines. For each of the considered structural locations, the design geometry as well as the environment (*e.g.* air, sea water with or without cathodic protection) orientate engineers to the most relevant curves to use. This step allows one to obtain the equivalent number of cycles to failure for each extracted fatigue cycles. The cumulated damages d are finally obtained by the use the Miner's cumulative law. Additional details regarding the rainflow counting, S-N approaches and Miner's cumulative law are given in Appendix B.

1.5.3 Illustrative example of the damage estimation

To close this section, an example of damage estimation is presented to illustrate the numerical chain of structural damage computation. The analyzed structure is the NREL 5MW OC3 Monopile with a clamped foundation. This example only considers two variable environmental parameters which are the wind mean speed u and the wind-wave misalignment θ. In the present case, the wind direction of solicitation is fixed to 0° and as a consequence, this parameter is equivalent to the wave direction of solicitation θ_{wave}. The sea-related parameters (t_p and h_s) are considered as fixed in this study and the hydrodynamic loading is composed of regular waves of period 10 seconds and 2-meters significant wave height. Considering a discretization combining 23 wind mean speeds between 3 and 25 m/s and 12 wind-wave misalignments between -150 and 180°, the total number of damage estimations reaches 276 (representing 276 simulation calls). This leads to a discretization unit of $\Delta = 30$ deg m/s (30 deg $\times 1$ m/s). The simulation chain is implemented as presented in Figure 1.15.

For each combinations of environmental parameters, time series of wind and sea-state are aleatory generated. By post-processing the results from the multi-physics simulator, time

series of Von Mises stresses are obtained, as illustrated in Figure 1.16a where the mean speed parameter is fixed to 12 m/s and the misalignment to 0 degree (wind and waves acting on the same direction). The rainflow post-treatment of this particular signal leads to the matrix of fatigue stress cycles represented in Figure 1.16b.

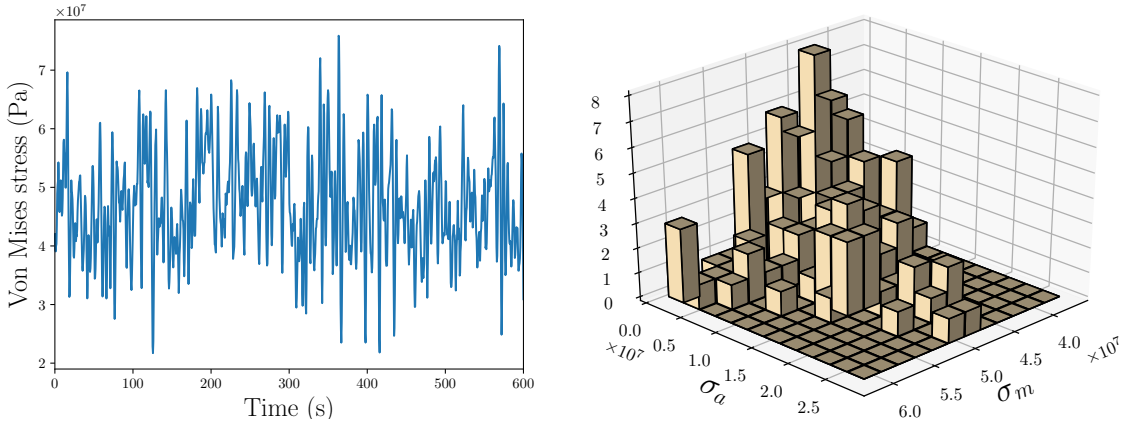

(a) Time signal of the Von Mises stress.

(b) Rainflow cycle decomposition of signal (a).

Figure 1.16: Evolution of the Von Mises stress at the azimuth 0° of the mud-line level of the NREL 5 MW (aleatory loading histories generated with wind mean speed $u = 12m/s$ and misalignment $\theta = 0$ deg) and its rainflow matrix (σ_a and σ_m respectively refer to the stress amplitude and mean).

This procedure is performed for each of the 276 combinations of environmental parameters (only one set of aleatory seeds ω_{wind} and ω_{sea}) and results are plotted in Figure 1.17. The global mean damage D, presented in Eq. 1.19 is then computed as:

$$D = \sum_{i=1}^{n_c=276} d_i \, p_i \, \Delta = 3.81 \times 10^{-13} \tag{1.21}$$

The obtained value is here computed for a 10-min period of time. To respect the certification grid, six simulations of 10-min or a single simulation of 1-hour should have been performed. As a consequence, the global mean damage D is calculated over a period of 1 hour. To get the lifetime cumulated damage due to the conceptual situation of interest (here, the "normal production"), the obtained global mean damage has to be multiplied by the number of hours the structure is expected to be in this conceptual situation. In this thesis, this is not proceeded and all the results are proposed based on 10-min simulations.

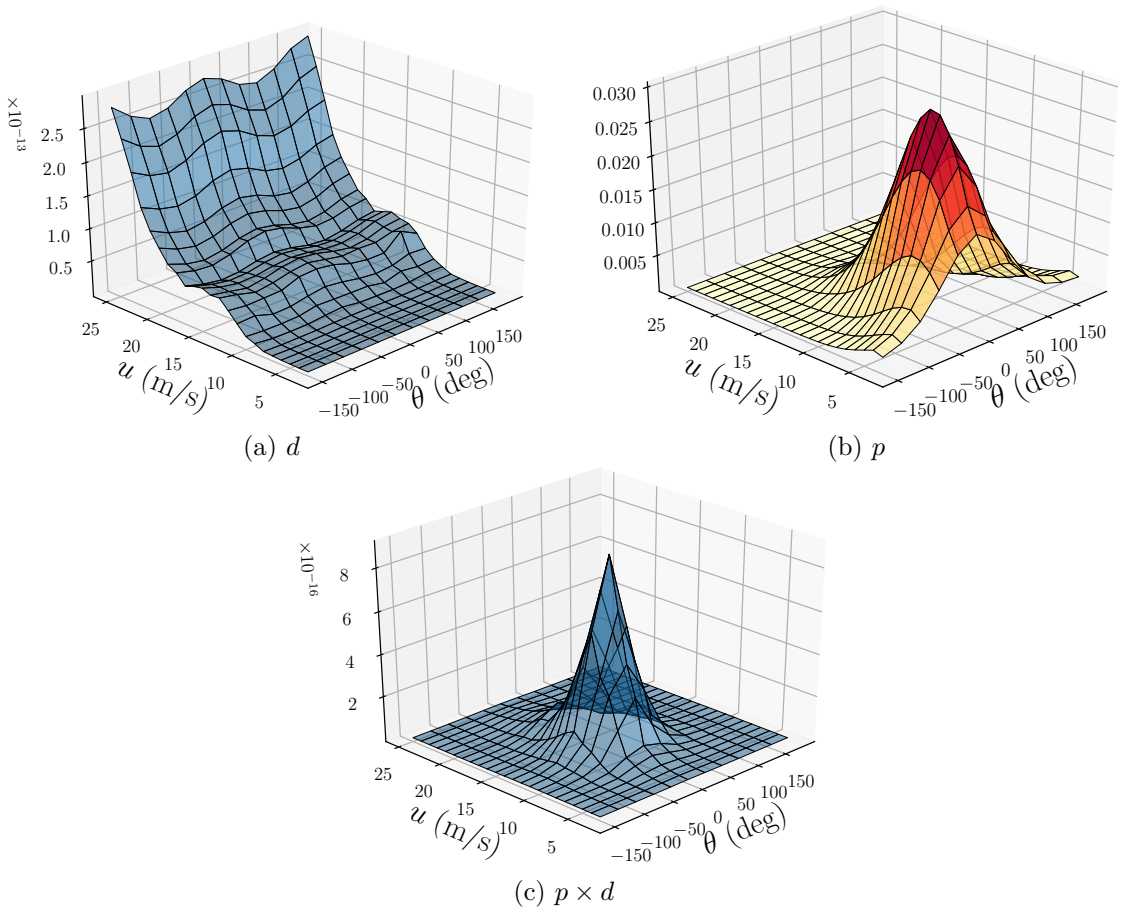

(a) d (b) p

(c) $p \times d$

Figure 1.17: Illustration of the damage d, the considered metocean joint probability p and the quantity $p \times d$ computed the 276 combinations of environmental parameters.

1.6 Industrial limitations and proposed alternatives

This first chapter shows the degree of complexity involved in design and/or certification of wind turbine structures. To have an appropriate representation of the lifetime states of solicitations, the number of simulations is high and can, in certain cases be unmanageable for industrial actors. Focusing on the damage estimation described in DLC 1.2, the representation of loading environment induces a discretization of definition domains of the environmental parameters which can lead to tens of thousands simulation calls for a single estimation of the global cumulated damage D (Eq. 1.19).

Furthermore, for each of the short-term damages d, the simulation requirements make engineers performing multiple demanding time simulations to account for the physical uncertainty of environmental loads (wind and waves). Depending on the considered design and its model definition, a numerical estimation of the short term damage d lasts from minutes (in the case of simple monopile designs) to hours (for complex floating models). The high number of simulations needed and their duration are a limitation industrial actors have to deal with. To tackle this challenge, and to propose less demanding approaches, researchers have proposed several contributions over recent years. From a global point of view, three types of methods can be distinguished:

- **Model reduction approaches** which propose to use simpler and less demanding numerical models to approximate high-fidelity simulators.
- **Reduction of the simulation number** which aims at reducing the number of simulations to perform by only considering the most probable environmental combinations or regrouping them with respect to the short term damage they cause.
- **Regression approaches** which propose to build a regression model of the damage response d from a reduced grid (surrogate model approach).

1.6.1 Model reduction

Model reduction approaches aim at reducing the complexity of numerical models to perform faster simulations and as a consequence, less demanding evaluations of the damage d relative to a defined set of environmental parameters. Practically, it consists in implementing a simpler model that does not consider the full physical modeling but only a part of it resorting to different assumptions. The difficulty of this model reduction method is to keep on considering the non-linearity of the aerodynamic structural responses due to the complexity of rotor behavior as well as the consideration of the aerodynamic damping. Muskulus [2015] presented a comparison of several numerical approaches for the consideration of simpler aerodynamic model to replace complete time analyses. Even though they reduce the computational effort, each of the proposed methods (*e.g.* based on deterministic thrust curve or stochastic response model) has shown a loss of accuracy up to 20% when representing the fatigue loads estimated for a jacket support application.

Spectral approaches have also been investigated in numerous studies in the last decades. Initially proposed by Wirshing and Mohsen Shehata [1977] and widely developed in oil and gas industry, several arrangements and modification have been proposed to enhance their applicabilities (*e.g.* Larsen and Irvine [2015]; Sherratt et al. [2005]). This approach basically consists in computing a frequency transfer function to account for the rotor nacelle assembly behavior. The estimated power spectral density (psd) of the rotor thrust can then be transformed into stress psd for each of the locations of interest by the means of several assumptions regarding the global structural behavior such as the linearity relationship between rotor thrust and structural displacements and an aerodynamic damping model, usually considered as linear. Several methods can be used to estimate the cumulated damages directly from the stress spectra, as the Rayleigh approximation (narrow band spectra) [Rychlik, 1993] or the Dirlick's formula (wide band spectra) [Dirlik, 1985]. Numerous studies have been proposed to use or to compare spectral approaches for wind turbine applications (*e.g.* Tibaldi et al. [2016]; Yeter et al. [2016]). However, Schneider and Senders [2010] explain spectral methods are not well suited for wind turbines by contrast with oil and gas industry, as such approaches can not entirely represent the loading situations because of the induced linearization of load-structural reaction relations. In the context of wind energy and because of the important non-linearity of rotor behavior, these method can not therefore replace time model analyses when estimations need to be accurate. To tackle this limitation, combined approaches hae been proposed. For example, Schløer et al. [2018] use pre-computed aerodynamic loading reactions, based on less demanding onshore model and re-combined them with spectral hydrodynamical com-

putations to estimate offshore wind turbine reactions with enough accuracy and important simulation gains. Schafhirt et al. [2015] propose to use the impulse based sub-structuring to determinate the structural reactions due to a loading history. By massively parallelize the computations with graphical processors, an important speed up is obtained which accurate estimates of the model responses.

1.6.2 Reduction of the number of simulations

The reduction of the number of simulations to perform is also importantly developed in industrial context and different methods have been proposed so far. Practically, this type of methodology does not only aim at reducing the number of simulations but also inferring general informations from partial metocean data. For that purpose, Mittendorf [2009] presents different approaches to estimate the correlation structures between wind and wave solicitations when analyzing wind turbine structural responses based on metocean data. From this statistical relation, environmental parameters can be aggregated with various strategies as the lumping of metocean presented by Kühn [2001], which allows one to regroup simulations by their similarities regarding design fatigue responses. Despite the important reduction of simulation investment, Passon and Branner [2016] underline that traditional lumping based methods do not allow to ensure the same accuracy when several structural locations are analyzed.

1.6.3 Regression methods

The regression approaches aim at approximating the model response d by any type of regression method. The approximation of the damage model response d can therefore be established from the use of a reduced set of model observations. Different choices regarding the regression basis can be done and accurate estimations can be obtained as presented in Zwick and Muskulus [2015]. However, the difficulty of this kind of approach is the *a priori* choice of the regression model as a trade-off between its capability to approximate the damage response surfaces and the cost of its calibration when the model gets more complex (*e.g.* increase of the regression degree for polynomials). Häfele et al. [2017] presented the effect of reducing the number of simulation cases by considering the joint probabilities of occurrence compared to traditional unidirectional wind and wave method and underlined the possibilities of reducing the number of load cases to consider. The proposed application showed accurate results in the approximation of the damage response at several locations of a jacket type structure. Fuglsang et al. [2002] and more recently Stieng and Muskulus [2018] proposed to determinate the most important $p \times d$ contributions (defined in this paper as "severity") from a complete damage computation on a reference structure. The subsequent subset of environmental parameters is then kept to estimate the fatigue design response of similar structures in the same solicitation environment. This proposition shows accurate results in estimating the damage response of the reference NREL 5-MW monopile structure. To conclude, regression and interpolation based methods are also used to reduce the required time of a single estimation of the short term damage d. An estimation of the model response can be computed from the extrapolation of reduced time analyses as presented in Stieng et al. [2015]. The partial infor-

mation provided by this type of method reduces the representativeness of the analyses which is a major limitation when focusing on the damage estimation for the purpose of structural design or certification.

As presented here, the reduction of computational efforts can be achieved with sufficient accuracy for the fatigue quantification of offshore wind turbine structures. Some techniques rely on regression methods, which need a reduced set of simulations whereas other techniques focus on the approximation of the damage quantities by restricting computations only to relevant damage situations. Beside accurate results in diverse applications, the proposed methods are based on either a demanding reference computation or an *a priori* selection of a representative basis of regression functions. In this thesis, an alternative approach is presented based on the Kriging method, also known as Gaussian process regression which, to the author's best knowledge, has never been used for the particular case of damage approximation as it is introduced in this chapter.

1.7 Conclusions

This first chapter introduced the industrial context of the project. During the design stage of offshore wind turbine structures, the certification is required to ensure a minimal safety level and thus the project founding. To guide engineers, certification bodies propose design guidelines based on standards recommendations and which list the minimal requirements the numerical approaches have to fulfill either for the modeling of environmental states or the structural modeling and the related mechanical approaches. Within the proposed procedure, the lifetime of the structure is considered as a series of elementary situations for which a structural state (conceptual situation) or the type of analysis to perform and the environmental model to consider (Design Load Cases). Amongst all the proposed studies, fatigue related design load cases can rapidly represent important numerical investments (*e.g.* DLC 1.2: *fatigue estimation for normal production structural state*). Indeed, to properly represent the possible situations the wind turbine may have to face during this life cycle, each of the possible environmental states have to be analyzed by considering each of the possible combinations of environmental parameters.

A numerical chain is implemented to estimate the cumulated damage relative to each of the proposed combinations of environmental parameters. This latter is based on an aleatory generation of loading history and the computation of the design responses from time structural analyses. The obtained results, recomposed as general Von Mises stresses, are finally decomposed with a rainflow procedure before to deduce the elementary damages by the use of S-N curves proposed in guidelines. From the estimation of the short term damages relative to each of the combination of environmental parameters, a global mean damage can be computed.

Although being complete and ensuring the representativeness of damage estimation, the numerical investments induced by the proposed framework is important and limit the industrial applications. To tackle this, several scientific contributions have been proposed either to reduce the number of simulator calls required for the estimation of the global mean damage or to reduce the simulation time for each of the structural analyses.

Since several decades, metamodeling approaches have been developed and applied in numerous industrial contexts to reduce simulation investments. From all the proposed methodologies, Kriging metamodeling (also known as Gaussian process regression) showed interesting results in the context of numerical model regression. To present this method, the next chapter focuses on the formalization of this statistical approach.

References

L. Arany, S. Bhattacharya, J. Macdonald, and S. J. Hogan. Design of monopiles for offshore wind turbines in 10 steps. *Soil Dynamics and Earthquake Engineering*, 92:126–152, 2017.

M. Arshad and B. C. O'Kelly. Offshore wind-turbine structures: a review. *Proceedings of the Institution of Civil Engineers - Energy*, 166:139–152, 2013.

T. Burton, N. Jenkins, D. Sharpe, and E. Bossanyi. *Wind Energy Handbook, 2nd Edition*. Wiley, 2011.

S. Butterfield, W. Musial, J. Jonkman, and P. Sclavounos. Engineering challenges for floating offshore wind turbines. In *Proceedings of the 2005 Copenhagen Offshore Wind Conference*, 2005.

M. Cheng and Y. Zhu. The state of the art of wind energy conversion systems and technologies: A review. *Energy Conversion and Management*, 88:332 – 347, 2014.

C. C. Ciang, Lee J. R., and H. J. Bang. Structural health monitoring for a wind turbine system: a review of damage detection methods. *Measurement Science and Technology*, 19, 2008.

T. Dirlik. *Application of computers in fatigue analysis*. PhD thesis, University of Warwick, 1985.

DNV-GL. *DNV-OS-J101: Design Of Offshore Wind Turbine Structures*, 2014.

M. Dolores Esteban, J. S. López-Gutiérrez, V. Negro, C. Matutano, F. M. García-Flores, and M. Ángel Millán. Offshore wind foundation design: Some key issues. *Journal of Energy Resources Technology*, 137, 2015.

I. Erlich, F. Shewarega, Feltes C., F. W. Koch, and J. Fortmann. Offshore wind power generation technologies. *Proceedings of the IEEE*, 101(4):891–905, 2012.

EWEA. The european offshore wind industry - key trends and statistics. ewea tech. rep. 23. Technical report, EWEA - European Wind Energy Association, 2015.

P. Fuglsang, C. Bak, J. G. Schepers, B. Bulder, T. T. Cockerill, P. Claiden, A Olesen, and R. van Rossen. Site-specific design optimization of wind turbines. *Wind Energy*, 5:261–279, 2002.

K. Hasselmann, T.P. Barnett, E. Bouws, H. Carlson, D. E Cartwright, K. Enke, Ewind J.A., H. Gienapp, D.E. Hasselman, A. Kruseman, A. Meerburg, P. Müller, D. J. Olbers, K. Richter, W. Sell, and H. Walden. Measurements of wind-wave growth and swell decay during the joint north sea wave project (jonswap). Technical report, Ergnzungsheft zur Deutschen Hydrographischen Zeitschrift Reihe, 1973.

R. Hoffmann. A comparison of control concepts for wind turbines in terms of energy capture. Master's thesis, Darmstadt University of Technology, 2002.

J. Häfele, C. Hübler, C. G. Gebhardt, and R. Rolfes. A comprehensive fatigue load set reduction study for offshore wind turbines with jacket substructures. *Renewable Energy*, 118:99–112, 2017.

IEC. *IEC 61400-1: Wind turbines - Part 1: Design Requirements (Third Edition)*, 2005.

IEC. *IEC 61400-3: Wind turbines - Part 3: Design requirements for offshore wind turbines*, 2009.

G. Ingram. Wind turbine blade analysis using the blade element momentum method - version 1.1. Technical report, Durham University, 2011.

M. R. Islam, Y. Guo, and J. Zhu. A review of offshore wind turbine nacelle: Technical challenges, and research and developmental trends. *Renewable and Sustainable Energy Reviews*, 33:161 – 176, 2014. ISSN 1364-0321.

B. J. Jonkman and L. Kilcher. Turbsim user's guide: Version 1.06.00. Technical report, National Renewable Energy Laboratory, 2012.

J. Jonkman, S. Butterfield, W. Musial, and G. Scott. Definition of a 5-mw reference wind turbine for offshore system development. Technical report, National Renewable Energy Laboratory, 2009.

J. K. Kaldellis and D. Zafirakis. The wind energy (r)evolution: A short review of a long history. *Renewable Energy*, 36:1887–1901, 2011.

D. Kallehave, B. W. Byrne, C. LeBlanc Thilsted, and K. K. Mikkelsen. Optimization of monopiles for offshore wind turbines. *Philosophical Transactions of the Royal Society of London A: Mathematical, Physical and Engineering Sciences*, 373(2035), 2015.

M. Kühn. *Dynamics and design optimisation of offshore wind energy conversion systems.* PhD thesis, Technische Universiteit Delft, 2001.

C. E. Larsen and T. Irvine. A review of spectral methods for variable amplitude fatigue prediction and new results. *Procedia Engineering*, 101:243 – 250, 2015. 3rd International Conference on Material and Component Performance under Variable Amplitude Loading, VAL 2015.

O. Y. Miñambres. Assessment of current offshore wind support structures concepts - challenges and technological requirements by 2020. Master's thesis, Karlshochschule International University, 2012.

K. E Mittendorf. Joint description methods of wind and waves for the design of offshore wind turbines. *Marine Technology Society Journal*, 43(3):23–33, 2009.

M. Muskulus. Simplified rotor load models and fatigue damage estimates for offshore wind turbines. *Phil.Trans. R. Soc. A*, 373, 2015.

A. Myhr, C. Bjerkseter, A. Agotness, and A. T. Nygaard. Levelised cost of energy for offshore floating wind turbines in a life cycle perspective. *Renewable Energy*, 66:714–728, 2014.

K. I. Oh, W. Nam, M. S. Ryu, J. Y. Kim, and B. I. Epureanu. A review of foundations of offshore wind energy convertors: Current status and future perspectives. *Renewable and Sustainable Energy Reviews*, 88:16–36, 2018.

P. Passon. Memorandum - derivation and description of the soil-pile-interaction models, iea-annex xxiii subtask 2. Technical report, University of Stuttgart, 2006.

P. Passon and K. Branner. Condensation of long-term wave climates for the fatigue design of hydrodynamically sensitive offshore wind turbine support structures. *Ships and Offshore Structures*, 11(2):142–166, 2016.

W. J. Jr. Pierson and L. A. Moskowitz. Proposed spectral form for fully developed wind seas based on the similarity theory of s. a. kitaigorodskii. *Journal of Geophysical Research*, 69: 5181–5190, 1964.

I. Rychlik. On the 'narrow-band' approximation for expected fatigue damage. *Prababilistic Engineering Mechanics*, 8:1–4, 1993.

S. Schafhirt, N. Verkaik, Y. Salman, and M. Muskulus. Ultra-fast analysis of offshore wind turbine support structures using impulse based substructuring and massively parallel processors. In *Proceedings of the Twenty-fifth International Ocean and Polar Engineering Conference*, pages 301–308, 2015.

S. Schløer, L. G. Castillo, F. Fejerskov, E Stroescu, and H. Bredmose. A model for quick load analysis for monopile-type offshore wind turbine substructures. *Wind Energy Science*, 3: 57–73, 2018.

J. Schneider and M. Senders. Foundation design: A comparison of oil and gas platforms with offshore wind turbines. *Marine Technology Society Journal*, 2010.

P. J. Schubel and R. J. Crossley. Wind turbine blade design. *Energies*, 5:3425–3449, 2012.

F. Sherratt, N. W. M. Bishop, and T. Dirlik. Predicting fatigue life from frequency domain data. *Engineering integrity*, 18:12 – 16, 2005.

G. M. Stewart, A. Robertson, and M. A. Lackner. The creation of a comprehensive metocean data set for offshore wind turbine simulations. *Wind Energy*, 19:1151–1159, 2015.

L. E. S. Stieng and M. Muskulus. Reducing the number of load cases for fatigue damage assessment of offshore wind turbine support structures by a simple severity-based sampling method (under review). *Wind Energy Science Discussions*, 2018:1–16, 2018. doi: 10.5194/wes-2018-43.

L. E. S. Stieng, R. Hetland, S. Schafhirt, and M. Muskulus. Relative assessment of fatigue loads for offshore wind turbine support structures. *Energy Procedia*, 80:229 – 236, 2015. 12th Deep Sea Offshore Wind R&D Conference, EERA DeepWind'2015.

C. Tibaldi, L. C. Henriksen, M. H. Hansen, and C. Bak. Wind turbine fatigue damage evaluation based on a linear model and a spectral method. *Wind Energy*, 19:1289–1306, 2016.

P. H. Wirshing and A. Mohsen Shehata. Fatigue under wide band random stresses using the rain-flow method. *Journal of Engineering Materials and Technologies*, pages 205–211, 1977.

R. Wiser, K. Jenni, J. Seel, E. Baker, M. Hand, E. Lantz, and A. Smith. Expert elicitation survey on future wind energy costs. *Nature Energy*, 1, 2016.

B. Yeter, Y. Garbatov, and C. Guedes Soares. Evaluation of fatigue damage model predictions for fixed offshore wind turbine support structures. *International Journal of Fatigue*, 87:71 – 80, 2016.

D. Zwick and M. Muskulus. Simplified fatigue load assessment in offshore wind turbine structural analysis. *Wind Energy*, 19(2):265–278, 2015.

CHAPTER 2

KRIGING PREDICTION FOR NUMERICAL CODE APPROXIMATION

Contents

This second chapter is proposed to introduce the Kriging prediction method applied in the context of computer code approximation. This approach, also known as Gaussian process prediction, allows one to compute a response metamodel (*i.e.* a "model of a model") determined from a statistical analysis of a reduced set of observations. This method has been successfully proposed in recent engineering applications and this thesis focuses on the possible benefits it can provide for the reduction of numerical investments during the design and certification stages of wind turbine structures, and more specifically, in the evaluation of the global mean damage D introduced in Chapter 1. As a consequence, the descriptions proposed in this chapter are oriented to this industrial problematic and the possibilities to predict the demanding short term damage d with respect to the certification requirements but with a reduced cost. To get into the subject, Section 2.1 proposes a brief introduction of the metamodel analysis for computer codes by presenting some of the most developed methods of model response predictions. The choice of the Kriging prediction for the approximation of the demanding short term damage quantity d is subsequently motivated. Section 2.2 focuses on the assumptions and the formalization of the Kriging prediction to present readers a sufficient comprehensive description of this numerical tool handled all along this manuscript. To complete this formal description, different points on the practical use of the Kriging prediction such as the design of experiments, the metamodel calibration and validation are described in Section 2.3. To finish, an introduction to iterative Kriging strategies is proposed in Section 2.4 to underline their interests in the context of approximation of unknown model responses.

2.1 Kriging prediction as an effective strategy for numerical code approximation

2.1.1 Introduction to metamodeling analysis

In many engineering fields, models and numerical analyses are widely developed to characterize or to predict unobserved system responses. Despite of the growing capacities of modern computers, these analyses still remain demanding in certain specific cases such as expensive phenomenon characterizations or long-term analyses. In the context of time demanding numerical codes, metamodeling substitutions have been developed to reduce computational investments. In this chapter, a formal example $\mathcal{M}$ of such a model is used and presented as:

$$\begin{aligned} \mathcal{M} : \mathcal{D}_{\boldsymbol{x}} \subset \mathbb{R}^n &\rightarrow \mathcal{D}_y \subset \mathbb{R} \\ \boldsymbol{x} &\rightarrow y(\boldsymbol{x}) \end{aligned} \tag{2.1}$$

where $\boldsymbol{x} \in \mathcal{D}_{\boldsymbol{x}}$ and $y \in \mathcal{D}_y$ respectively denote the *input* vector of dimension n and *output* scalar of the model. Hereafter, the model $\mathcal{M}$ is supposed to represent a computer code considered as a *black-box function*. This assumes that users only manipulate it as an input-output (I/O) relation and have no access to its internal composition (*e.g.* implementation of the code in the case of simulators). Within this approach, the term metamodel gathers all the methodologies which allow one to create a fast and representative approximation of

the demanding model $\mathcal{M}$ based on the partial information coming from a limited number of observations (*i.e.* model evaluations).

In this sense, a metamodel can be seen as a "model of the model" which can be elaborated from a wide panel of methods to fit many types of engineering problems as presented by Chen et al. [2006]. In the field of mechanical engineering, two domains are particularly interested by the use of metamodeling techniques because of the important simulation investments they require: the reliability analysis [Bourinet, 2018; Sudret, 2012] and the design optimization [Ryberg, 2013; Wang and Shan, 2007].

Several methods have been proposed so far to cut off simulation investments and can be distinguished in two main categories: the regression and the classification approaches. Regression metamodeling techniques aim at approximating the model responses over their entire definition domain $\mathcal{D}_{\boldsymbol{x}}$ (global approximations) or over a subspace of interest (local estimations) depending on the objectives of the study in a non-intrusive manner. Different methods are now well defined and commonly used in numerical engineering such as the polynomial response surfaces [Box and Draper, 1987; Khuri and S., 2010], spline regression methods Friedman [1991] or radial basis networks [Hardy, 1971; Regis and Shoemaker, 2005]. They all allow one, from the use of different mathematical tools, to estimate model responses based on the provided partial information of the model behavior. Other types of method propose to statistically analyze the reduced set of model observations with the objective of characterizing the relations between input and output quantities of the partially observed model $\mathcal{M}$ and to determine correlation patterns by introducing dependence structures. Once determined, these latter provide global information to refine the prediction as in the Gaussian process predictions [Rasmussen and Williams, 2006] and its so-called Kriging variance [Krige, 1951; Matheron, 1962; Sacks et al., 1989] which is the scope of this thesis. In the context of uncertainty propagation, polynomial chaos expansion (PCE) has also been widely used. It aims at expanding a random output onto a suitable basis of random variables made of multivariate orthogonal polynomials [Blatman, 2009; Blatman and Sudret, 2010] .

In the context of classification problems, the model responses are required to be classified into a finite number of classes regarding their values (supervised learning). As for the regression methods, different strategies and implementations are available to reduce the relative simulation investments as for example the use of the Artificial Neural Networks (ANN) [Basheer and Hajmeer, 2000; Bilgili et al., 2007] widely developed in artificial intelligence or the Support Vector Machines (SVM) [Bourinet, 2018; Vapnik, 2006] massively implemented in machine learning supervised classification problems.

From a general point of view and to the best of author's knowledge, most metamodel based analyses have a similar flowchart as the one proposed in Figure 2.1. Two main blocks compose the latter: a learning stage (also known as metamodel exploration) based on training and test steps, and a predictive stage (also known as metamodel exploitation). The initial step consists in observing the model behavior by composing an observational set $\{\boldsymbol{\mathcal{X}}_{obs}, \boldsymbol{y}_{obs}\}$ where $\boldsymbol{\mathcal{X}}_{obs}$ is the matrix of input observations of size $n_{obs} \times n$ where n denotes the input dimensions and n_{obs} the number of model observations and $\boldsymbol{y}_{obs}$ is the vector of observed model responses of size n_{obs}.

Several strategies can be adopted to construct this set of model observations based on

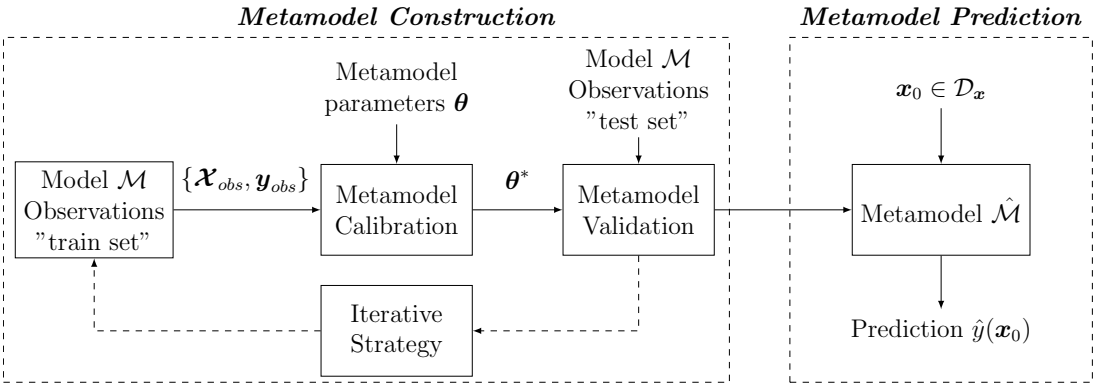

Figure 2.1: Schematic representation of metamodeling construction and prediction.

the consideration of the quantity of interest (*e.g.* local or global quantities) and on expertise. From the information contained in the experiments, a set of parameters regrouped into the vector $\boldsymbol{\theta}$, sometimes called *hyperparameters*, are estimated in order to calibrate a "generic definition" to the particular situation.

A validation procedure is most of the time required to ensure the approximation (which results from the hyper parameters' estimation to a certain extent) is of sufficient quality but also preclude over-fitting phenomenon, i.e. a trade-off between bias and variance is sought. For such a purpose, an extra set of data called test set, which is not used during the training step, usually serves to compute errors between the observations and their predictions during the calibration stage (*i.e.* for model selection). In Kriging interpolation, the calibration of hyper parameters by maximizing a likelihood function may be viewed as an exception. Herein, there is here no systematic quantification of the Kriging metamodel error based on the aforementioned procedure even though the latter remains possible to implement. However, one can rely on the variance of estimation to identify subspaces of input domains which are not enough explained by the metamodel (given a correlation model). Moreover, the over-fitting phenomenon may be no longer concerned if the size of the training set is not too large, as experienced in this work. Details will be given in next sections. If the metamodel lacks in representativeness, the design of experiments is modified or enriched as represented by the iterative loop proposed in Figure 2.1 and stops when the quality in deemed acceptable.

The metamodel can then be used to predict the model response $y(\boldsymbol{x}_0)$ for any non-observed input $\boldsymbol{x}_0 \in \mathcal{D}_{\boldsymbol{x}}$. The functional approximation is hereafter noted $\hat{y}$ and the model response prediction computed as $\hat{y}(\boldsymbol{x}_0)$.

2.1.2 Motivations for resorting to Kriging prediction in the estimation of the short term damage d

Kriging approximations can be designed to show an interpolating character, *i.e.* the metamodel is exact for all of the observed model responses ($\hat{y}(\boldsymbol{x}_{obs}) = y(\boldsymbol{x}_{obs})$). This characteristic is a significant advantage in the context of structural certification of wind turbines. Indeed, the approximation of the damage response d is practically computed from Eq. 1.19 is then not affected by metamodeling errors for the observed inputs. Approximations will only affect the remaining required computations as emphasized later in Chapter 3.

Furthermore, for each of the predictions obtained from the Kriging formalization, a variance of the estimation is provided by the so-called Kriging variance of estimation. This quantity is without a doubt the main advantage of resorting to Kriging metamodeling when a reduced set of observations is available and explain why it is widely used in several industrial applications. It allows to quantify the uncertainty of the metamodel response based on the information contained in the design of experiments. As a matter of fact, users have to keep in mind that this quantity is not a direct quantification of the metamodel error but provides informative indications on areas where the observational informations is not sufficient to provide accurate prediction.

Finally, the practical implementation of the Kriging metamodel is limited to relatively small dimensional problems. The major limitation is the calibration time which can become unmanageable when reaching high dimensional spaces. The introduced industrial case deals with a low number of variables which are composed of the environmental and/or uncertain parameters in this thesis. As a consequence, the total size of the feature domain in which the Kriging metamodel is computed is far below its practical limitations in this thesis.

The rest of this chapter now focuses on a more detailed presentation of the formalization and the practical use of Kriging predictions for the approximation of demanding numerical codes.

2.2 Formalization of the Kriging prediction

In this section, a global presentation of the Kriging prediction is proposed. Focus is made on its underlying assumptions in the context of deterministic numerical code analysis and where the observation set is of limited size as initially presented by Sacks et al. [1989]. This section gives explanations which rely on Dubourg [2011] and Rasmussen and Williams [2006] in which interested readers can find more details and complementary explanations.

2.2.1 The two-stage Gaussian model

Random process prediction methods are based on the assumption that any model response can be considered as the realization of a random process whose characteristics have to be determined. For each of the input vector $\boldsymbol{x} \in \mathcal{D}_{\boldsymbol{x}}$, the true response $y(\boldsymbol{x})$ is then assumed to be a realization of a random variable $Y(\boldsymbol{x}, \omega)$ for which the probability density function is *a priori* unknown. The objective of Kriging lies in determining the parametric distribution of any random variable $Y(\boldsymbol{x}, \omega)$ from a given set of model observations and based on some statistical modeling assumptions. This will then enable one to have an estimation of $y(\boldsymbol{x})$ for any unobserved input $\boldsymbol{x}$.

Stationary Gaussian random processes are generally considered due to their appealing properties, meaning that any subset of vectors $\boldsymbol{Y}_{\boldsymbol{x}}$ follows a multivariate Gaussian distribution fully characterized by its mean vector and covariance matrix. Based on the "universal Kriging" formulation, each random variable $Y_{\boldsymbol{x}_i \in \mathcal{D}_{\boldsymbol{x}}} \equiv Y_i$ is expressed as a sum of a deterministic and stochastic part:

$$Y_i = \sum_{j=0}^{p} f_j(\boldsymbol{x}_i)\beta_j + Z(\boldsymbol{x}_i, \omega) = \boldsymbol{f}_i^T \boldsymbol{\beta} + Z_i \tag{2.2}$$

The deterministic contribution is based on a linear regression of order p calibrated from n_{obs} model observations ($p \leq n_{obs}$). $\boldsymbol{f}_i = \{f_0(\boldsymbol{x}_i), \ldots, f_p(\boldsymbol{x}_i)\}^T$ corresponds to the vector of regressors obtained from the evaluation of the chosen basis of regression for the input $\boldsymbol{x}_i \in \mathcal{D}_{\boldsymbol{x}}$ and $\boldsymbol{\beta} = \{\beta_0, \ldots, \beta_p\}^T$ is the vector of linear weights. This first contribution allows one to capture the global trend of the model response based on the observations. This deterministic approximation is completed by a stochastic component introduced through a stationary Gaussian process Z with zero-mean ($\mathbb{E}[Z(\boldsymbol{x}_i, \omega)] = 0 \ \forall \ \boldsymbol{x}_i \in \mathcal{D}_{\boldsymbol{x}}$) and autocovariance function given as:

$$\mathrm{Cov}[Z_1, Z_2] = \sigma_Z^2 \ r(\boldsymbol{x}_1 - \boldsymbol{x}_2, \boldsymbol{\theta}) \ \text{ for all } \ (\boldsymbol{x}_1, \boldsymbol{x}_2) \in \mathcal{D}_{\boldsymbol{x}} \times \mathcal{D}_{\boldsymbol{x}} \tag{2.3}$$

where σ_Z^2 is the variance of the Gaussian process, r the autocorrelation function which hyperparameters are regrouped into the vector $\boldsymbol{\theta}$.

2.2.2 Model prediction by the "Best Linear Unbiased Predictor"

Considering a non-observed input $\boldsymbol{x}_0 \in \mathcal{D}_{\boldsymbol{x}}$, the probability density function of the random variable Y_0 is directly linked with observations by the Gaussian generic model defined in Eq. 2.2. Given an observational set $\{\boldsymbol{\mathcal{X}}_{obs}, \boldsymbol{y}_{obs}\}$ of size n_{obs}, the probabilistic relation between the unobserved random variable Y_0 and the observed ones, regrouped in the vector $\boldsymbol{Y}_{obs}$, reads:

$$\begin{Bmatrix} Y_0 \\ \boldsymbol{Y}_{obs} \end{Bmatrix} \sim \mathcal{N}_{n_{obs}+1}\Big(\boldsymbol{\mu}, \boldsymbol{\Sigma}\Big) \tag{2.4}$$

where $\mathcal{N}_{n_{obs}+1}$ is the $(n_{obs}+1)$-dimensional Gaussian multivariate distribution. The mean vector $\boldsymbol{\mu}$ and the covariance matrix $\boldsymbol{\Sigma}$ are the unique parameters of this joint probability density function and are introduced as:

$$\boldsymbol{\mu} = \begin{Bmatrix} \mu_0 \\ \boldsymbol{\mu}_{obs} \end{Bmatrix} = \begin{Bmatrix} \boldsymbol{f}_0^T \boldsymbol{\beta} \\ \mathbf{F}\boldsymbol{\beta} \end{Bmatrix} \tag{2.5}$$

$$\boldsymbol{\Sigma} = \sigma_Z^2 \begin{bmatrix} 1 & \boldsymbol{r}_0^T \\ \boldsymbol{r}_0 & \mathbf{R} \end{bmatrix} \tag{2.6}$$

where $\boldsymbol{f}_0$ and $\mathbf{F}$ respectively represent the vector and matrix of regression function evaluated at the unobserved input $\boldsymbol{x}_0$ and at each of the observational set:

$$\boldsymbol{f}_0 = \{f_0(\boldsymbol{x}_0), \ldots, f_p(\boldsymbol{x}_0)\}^T \tag{2.7}$$

$$\mathbf{F} = \begin{bmatrix} f_0(\boldsymbol{x}_1) & \dots & f_p(\boldsymbol{x}_1) \\ \vdots & \ddots & \vdots \\ f_0(\boldsymbol{x}_{n_{obs}}) & \dots & f_p(\boldsymbol{x}_{n_{obs}}) \end{bmatrix} \tag{2.8}$$

$\boldsymbol{r}_0$ is the cross-correlation vector between the unobserved input $\boldsymbol{x}_0$ and each observed values of the design of experiments. $\mathbf{R}$ is the autocorrelation matrix for the observational training set:

$$\boldsymbol{r}_0 = \left\{ r(\boldsymbol{x}_0 - \boldsymbol{x}_1, \boldsymbol{\theta}), \dots, r(\boldsymbol{x}_0 - \boldsymbol{x}_{n_{obs}} \boldsymbol{\theta}) \right\}^T \tag{2.9}$$

$$\mathbf{R} = \begin{bmatrix} 1 & \dots & r(\boldsymbol{x}_1 - \boldsymbol{x}_{n_{obs}}, \boldsymbol{\theta}) \\ \vdots & \ddots & \vdots \\ r(\boldsymbol{x}_{n_{obs}} - \boldsymbol{x}_1, \boldsymbol{\theta}) & \dots & 1 \end{bmatrix} \tag{2.10}$$

Let remind that the objective is to identify the marginal distribution of Y_0 with the view of predicting an estimation of $y_0 \equiv y(\boldsymbol{x}_0)$. Kriging prediction proposes an estimator $\hat{Y}_0$ of the unobserved quantity y_0, called the "Best Linear Unbiased Predictor" (BLUP), which satisfies convenient statistical properties:

- *Linearity*: the predictor is based on a linear combination of the n_{obs} model observations:

$$\hat{Y}_0 = \sum_{i=1}^{n_{obs}} \lambda_i(\boldsymbol{x}_0) Y_i = \boldsymbol{\lambda}_0^T \boldsymbol{Y}_{obs} \tag{2.11}$$

  where $\boldsymbol{\lambda_0}^T = \{\lambda_1(\boldsymbol{x}_0), \dots, \lambda_{n_{obs}}(\boldsymbol{x}_0)\}$ gathers all the weights which have to be determined. Due to the Gaussian assumption, $\hat{Y}_0$ follows a normal distribution.
- *Unbiasedness*: this condition is fulfilled if, for all $\boldsymbol{x}_0 \in \mathcal{D}_{\boldsymbol{x}}$:

$$\mathbb{E}\Big[\hat{Y}_0 - Y_0\Big] = 0 \tag{2.12}$$

- *Minimal variance*: The variance of estimation is minimized by using the mean squared error (MSE):

$$\mathrm{MSE}\Big(\hat{Y}_0\Big) = \mathbb{E}\Big[\Big(\hat{Y}_0 - Y_0\Big)^2\Big] \tag{2.13}$$

The BLUP $\hat{Y}_0$ is obtained by the resolution of the minimization of the vector of weights $\boldsymbol{\lambda}_0$ with regards to Eq. 2.11 and Eq. 2.12. This leads to an optimization problem formalized as:

$$\boldsymbol{\lambda}_0^* = \underset{\boldsymbol{\lambda}_0 \in \mathbb{R}^{n_{obs}}}{\operatorname{argmin}} \ \mathbb{E}\Big[\Big(\hat{Y}_0 - Y_0\Big)^2\Big] \quad w.r.t. \quad \mathbb{E}\Big[\hat{Y}_0 - Y_0\Big] = 0 \tag{2.14}$$

As a result, the vector of optimal regressors $\boldsymbol{\lambda}_0^*$ is given by:

$$\boldsymbol{\lambda}_0^* = \mathbf{R}^{-1} \left(\boldsymbol{r}_0 - \mathbf{F}(\mathbf{F}^T \mathbf{R}^{-1} \mathbf{F})^{-1} (\mathbf{F}^T \mathbf{R}^{-1} \boldsymbol{r}_0 - \boldsymbol{f}_0) \right) \tag{2.15}$$

Details regarding the solution of this optimization problem can be found in [Dubourg, 2011] and are not presented in this thesis. From Eq. 2.15, the parameters of the Gaussian predictor distribution $\hat{Y}_0 \sim \mathcal{N}(\hat{\mu}_0, \hat{\sigma}_0)$ can be expressed as:

$$\hat{\mu}_0 = \boldsymbol{f}_0^T \hat{\boldsymbol{\beta}} + \boldsymbol{r}_0^T \mathbf{R}^{-1}(\boldsymbol{y}_{obs} - \mathbf{F}\hat{\boldsymbol{\beta}}) \tag{2.16}$$

$$\hat{\sigma}_0^2 = \sigma_Z^2\Big(1 - \boldsymbol{r}_0^T \mathbf{R}^{-1}\boldsymbol{r}_0 + \boldsymbol{u}_0^T(\mathbf{F}^T\mathbf{R}^{-1}\mathbf{F})^{-1}\boldsymbol{u}_0\Big) \tag{2.17}$$

where $\boldsymbol{u}_0 = \mathbf{F}^T\mathbf{R}^{-1}\boldsymbol{r}_0^T - \boldsymbol{f}_0$. $\hat{\boldsymbol{\beta}}$ corresponds to the best estimation of the linear weights and reads:

$$\hat{\boldsymbol{\beta}} = (\mathbf{F}^T\mathbf{R}^{-1}\mathbf{F})^{-1}\mathbf{F}^T\mathbf{R}^{-1}\boldsymbol{y}_{obs} \tag{2.18}$$

It is here important to note that he BLUP estimator is interpolant, *i.e.* for all the observed input vectors $\boldsymbol{x}_{obs}$, the mean of the Gaussian predictor $\hat{\mu}(Y_{\boldsymbol{x}_{obs}})$ is equal to the true model response $y(\boldsymbol{x}_{obs})$. For each of the non observed vector $\boldsymbol{x} \in \mathcal{D}_{\boldsymbol{x}}$, the Kriging metamodel $\hat{\mathcal{M}}$ of the original model $\mathcal{M}$ is constructed from the following function:

$$\begin{aligned} \hat{\mathcal{M}} : \mathcal{D}_{\boldsymbol{x}} &\to \mathcal{D}_y \\ \boldsymbol{x} &\to \hat{y}(\boldsymbol{x}) \end{aligned} \tag{2.19}$$

For a given observational set, the variance of estimation $\hat{\sigma}_0^2$ presented in Eq. 2.17 provides an information on the quality of the model information content. Even if it can not be considered as a quantification of the metamodel error, it gives an indication on the confidence one can have in the prediction of the model response. Practically, this quantity is usually handled under the form of confidence intervals as for example the 95% bi-lateral confidence intervals defined, for all $\boldsymbol{x} \in \mathcal{D}_{\boldsymbol{x}}$ by:

$$\hat{y}(\boldsymbol{x}) - 1.96\sigma_0 \leq y(\boldsymbol{x}) \leq \hat{y}(\boldsymbol{x}) + 1.96\sigma_0 \tag{2.20}$$

2.2.3 Assumptions on autocorrelation functions

Autocorrelation function sometimes called kernels, are parametric functions which provide information regarding the statistical dependencies between observations. Most of the time, Kriging theory for computer code analysis uses *stationary* correlation kernels. This characteristic imposes that the kernel is invariant by translation in the domain of analysis $\mathcal{D}_{\boldsymbol{x}}$, *i.e.* it only depends on the shift between the two considered inputs. For all $\boldsymbol{x}_1$ and $\boldsymbol{x}_2 \in \mathcal{D}_{\boldsymbol{x}}$:

$$r(\boldsymbol{x}_1, \boldsymbol{x}_2, \boldsymbol{\theta}) = r(\boldsymbol{x}_1 - \boldsymbol{x}_2, \boldsymbol{\theta}) \tag{2.21}$$

where $\boldsymbol{\theta}$ denotes the autocorrelation parameters of a predefined model. If the autocorrelation is also invariant by rotation, then the stochastic process is said *isotropic*. As a consequence,

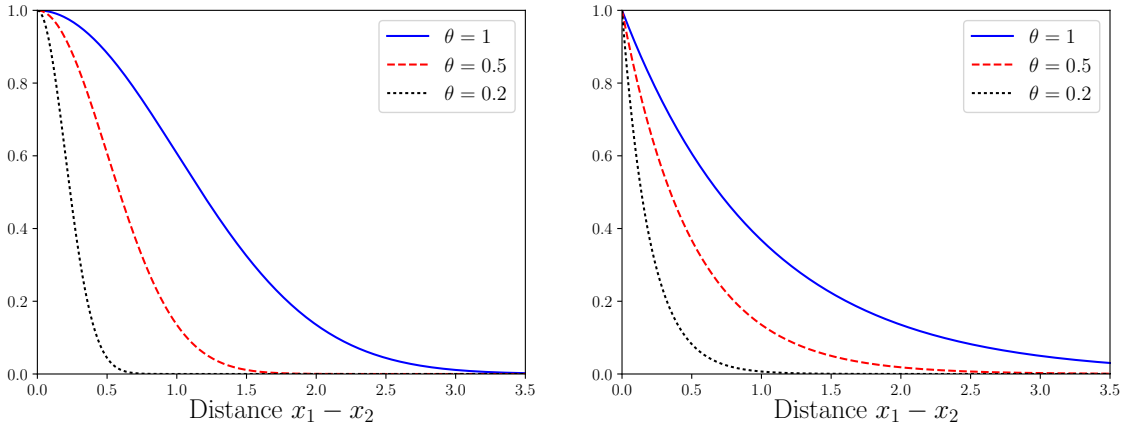

(a) Squared exponential (Eq. 2.24)

(b) Exponential (Eq. 2.25)

Figure 2.2: 1-dimensional illustration of the squared exponential and the exponential autocorrelation models for different values of θ.

the autocorrelation function solely depends on the euclidean distance between the inputs $\boldsymbol{x}_1$ and $\boldsymbol{x}_2 \in \mathcal{D}_{\boldsymbol{x}}$:

$$r(\boldsymbol{x}_1, \boldsymbol{x}_2, \boldsymbol{\theta}) = r(\| \boldsymbol{x}_1 - \boldsymbol{x}_2 \|_2, \boldsymbol{\theta}) \tag{2.22}$$

where $\| \cdot \|_2$ denotes the euclidean distance. If the autocorrelation function is defined by the product of one-dimensional autocorrelation functions r_i ($i \in \{1, \ldots, n\}$), the stochastic process is said *componentwise anisotropic*. For all $\boldsymbol{x}_1$ and $\boldsymbol{x}_2 \in \mathcal{D}_{\boldsymbol{x}}$:

$$r(\boldsymbol{x}_1, \boldsymbol{x}_2, \boldsymbol{\theta}) = \prod_{i=1}^{n} r_i(\boldsymbol{x}_{1,i} - \boldsymbol{x}_{2,i}, \boldsymbol{\theta}_i) \tag{2.23}$$

where n is the dimension of the input vector $\boldsymbol{x}$, $\boldsymbol{x}_{j,i}$ the i-th element of vector $\boldsymbol{x}_j$ and $\boldsymbol{\theta}_i$ corresponds to the correlation parameter set of the i-th dimension. Several correlation functions can be used to parameterize a Gaussian process as presented by Abrahamsen [1997]. For an illustration, the "exponential" and "squared exponential" anisotropic correlation functions are introduced as:

$$\mathrm{r}(\boldsymbol{x}_1, \boldsymbol{x}_2, \boldsymbol{\theta}) = \exp\left(-\frac{1}{2} \sum_{i=1}^{n} \left(\frac{\boldsymbol{x}_{1,i} - \boldsymbol{x}_{2,i}}{\boldsymbol{\theta}_i} \right)^2 \right) \tag{2.24}$$

$$\mathrm{r}(\boldsymbol{x}_1, \boldsymbol{x}_2, \boldsymbol{\theta}) = \exp\left(-\frac{1}{2} \sum_{i=1}^{n} \frac{| \boldsymbol{x}_{1,i} - \boldsymbol{x}_{2,i} |}{\boldsymbol{\theta}_i} \right) \tag{2.25}$$

These two are plotted in 1 dimension in Figure 2.2,for different values of the scale parameter θ.

2.3 Practical use of the Kriging predictor

After having introduced the main assumptions and the generic formalization of the Kriging prediction method, this section proposes a practical illustration of the Kriging implementation by focusing on crucial items: the selection of the design of experiments, the hyperparameter calibration methods given an autocorrelation function and the possible validation procedure for the verification of the metamodel accuracy.

2.3.1 The design of experiments

As presented in the last section, Kriging allows one to predict the model response for an unobserved input, based on given real model observations. As explained in Section 2.2, the computed Kriging approximation depends on the information provided by the model observational set $\{\boldsymbol{\mathcal{X}}_{obs}, \boldsymbol{y}_{obs}\}$ (*i.e.* the design of experiments). The choice of this set is thus crucial and remains an active field of research. The accuracy of the predictions obtained from Kriging metamodel is conditioned by the information inflow from the design of experiments. Discussions on the influence of the design of experiments onto the prediction will be discussed later in the thesis. Depending on the quantity of interest (*e.g.* local or global) and the constraints of the study (*e.g.* deterministic or random variables), several methods have been proposed so far attempting to select effective design of experiments regarding the information it provides. In the context of this thesis, the design of experiments has to be determined in order to provide global information on the model response d over the whole domain of variation $\mathcal{D}_{\boldsymbol{x}}$ of the environmental parameters. Furthermore, one should note the joint probability of occurrence of the environmental parameters is assumed to be known here. Hence, several possibilities are available to construct the design of experiments for the calibration of the Kriging prediction $\hat{y}$ of the function y. Two procedures have been implemented in the sequel: the reduced grid and Latin Hypercube Sampling (LHS).

Deterministic grids

The first method is fully deterministic and based on the use of a geometrical pattern to fill the input domain of definition $\mathcal{D}_{\boldsymbol{x}}$. Considering a reduced number of possibilities for each direction of the input space, a grid can be generated which regularly covers the domain of interest. This method, although being simple to understand and easy to implement enables fast filling of the input space without any *a priori* information. As a drawback, the augmentation of the problem dimensionality leads to an exponential growing of the observational set and thus the computational investment. For an illustration purpose, let considering a two-dimensional domain of definition representing the evolution of parameters x_1 and $x_2 \in [0, 1]$. Space filling by a regular grid composed of 24 points is presented in Figure 2.3a.

LHS aleatory generations

The so-called Latin Hypercube Sampling proposed by McKey et al. [1979] allows aleatory generations of designs of experiments over the input domain of definition with respect to

the probability density functions input parameters. This method presents the advantage of selecting designs of experiments which respect the marginal distributions of each parameter whilst resulting in a slightly better space filling than, for example, a simple Monte Carlo generation does. Let now consider that the parameters x_1 and x_2 are realizations of uniformly distributed random variables X_1 and X_2 which parameters are given as:

$$X_1 \sim \mathcal{U}\Big(0,1\Big) \quad \text{and} \quad X_2 \sim \mathcal{U}\Big(0,1\Big) \tag{2.26}$$

An example of LHS design of experiments composed of 24 points is presented in Figure 2.3b.

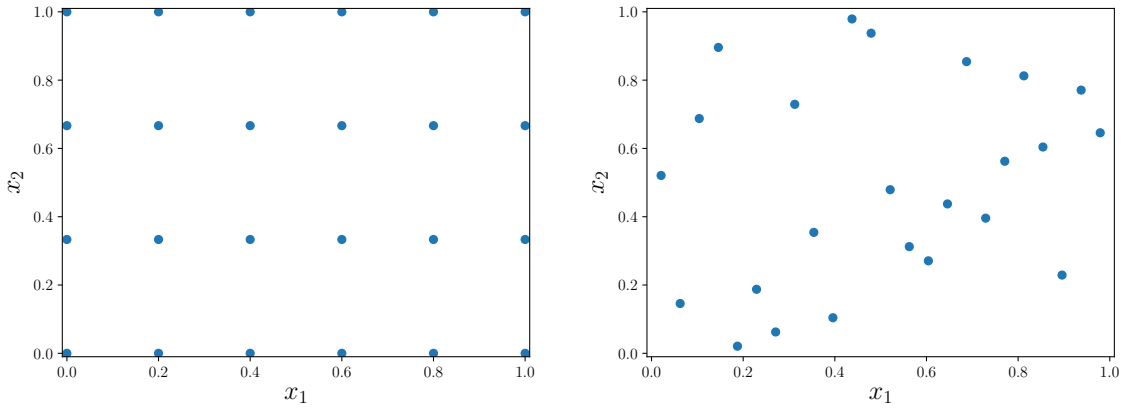

(a) Regular grid ($n = 24$) (b) Latin Hypercube Sampling($n = 24$)

Figure 2.3: Illustration of a regular grid and LHS procedures for the construction of the design of experiments for a two-dimensional domain of definition.

In this thesis, the deterministic grid is used for the estimation of the short term damage prediction d to take advantage of the global covering it allows one and LHS is considered for reliability analyses which are by definition based on the probabilistic description of the uncertain parameters.

2.3.2 Model calibration by maximum likelihood estimation

Once the design of experiments is set, the metamodel has to be calibrated. First, the functional basis $\boldsymbol{f}$ and the type of autocorrelation model r should be specified by the user beforehand and therefore can be viewed as tuning parameters. Their choice can be driven by preliminary studies and/or expert judgment. Then, the hyperparameter vector which gathers the regressive coefficients $\boldsymbol{\beta}$, the Kriging variance σ_Z^2 and the autocorrelation parameters $\boldsymbol{\theta}$ should be estimated from the available design of experiments. In this thesis, the chosen calibration method is the maximum likelihood estimation. This method is, by far, the most developed numerical procedure used in Kriging model calibration. The idea is to maximize the probability to observe the model realizations $\boldsymbol{y}_{obs}$, which is a function of the hyperparameters $\boldsymbol{\theta}$. This latter is called the *likelihood* and is noted $\mathcal{L}$ thereafter. In the particular case of the Kriging approximation and because of the Gaussian assumption, this quantity is computable by:

$$\mathcal{L}(\boldsymbol{y}_{obs}|\boldsymbol{\beta},\sigma_Z^2,\boldsymbol{\theta}) = \frac{1}{\Big((2\pi\sigma_Z^2)^{n_{obs}}\det(\mathbf{R})\Big)^{1/2}}\exp\Big(-\frac{1}{2\sigma_Z^2}\,(\boldsymbol{y}_{obs}-\mathbf{F}\boldsymbol{\beta})^{\mathrm{T}}\mathbf{R}^{-1}(\boldsymbol{y}_{obs}-\mathbf{F}\boldsymbol{\beta})\Big) \quad (2.27)$$

From the optimality conditions of this maximization problem, estimates $\hat{\boldsymbol{\beta}}$ of $\boldsymbol{\beta}$ and $\hat{\sigma}_Z^2$ of σ_Z^2 can be obtained, both solely depending of $\boldsymbol{\theta}$:

$$\hat{\boldsymbol{\beta}}(\boldsymbol{\theta}) = \Big(\mathbf{F}^{\mathrm{T}}\mathbf{R}(\boldsymbol{\theta})^{-1}\mathbf{F}\Big)^{-1}\mathbf{F}^{\mathrm{T}}\mathbf{R}(\boldsymbol{\theta})^{-1}\boldsymbol{y}_{obs} \quad (2.28)$$

$$\hat{\sigma}_Z^2(\boldsymbol{\theta}) = \frac{1}{n_{obs}}\Big(\boldsymbol{y}_{obs}-\mathbf{F}\hat{\boldsymbol{\beta}}(\boldsymbol{\theta})\Big)^{\mathrm{T}}\mathbf{R}(\boldsymbol{\theta})^{-1}(\boldsymbol{y}_{obs}-\mathbf{F}\hat{\boldsymbol{\beta}}(\boldsymbol{\theta})) \quad (2.29)$$

An optimization can then be performed to maximize the likelihood function $\mathcal{L}$ regarding the hyperparameter $\boldsymbol{\theta}$:

$$\boldsymbol{\theta}^* = \underset{\boldsymbol{\theta}\in\mathcal{D}_{\boldsymbol{\theta}}}{\operatorname{argmax}}\ \mathcal{L}(\boldsymbol{\theta}) = \underset{\boldsymbol{\theta}\in\mathcal{D}_{\boldsymbol{\theta}}}{\operatorname{argmin}}\ -\log\mathcal{L}(\boldsymbol{\theta}) \quad (2.30)$$

where $\mathcal{D}_{\boldsymbol{\theta}}$ is the domain of definition for the admitted values of $\boldsymbol{\theta}$ (research domain). By replacing the vector of regressors and the process variance by their optimal values $\hat{\boldsymbol{\beta}}$ and $\hat{\sigma}_Z^2$, the likelihood function reads:

$$-\log\mathcal{L}(\boldsymbol{\theta}) = \frac{n_{obs}}{2}\log(\psi(\boldsymbol{\theta})) + \frac{n_{obs}}{2}(\log(2\pi)+1) \quad (2.31)$$

with $\psi(\boldsymbol{\theta})$, the *reduced likelihood function* which is solely function of $\boldsymbol{\theta}$ is given as:

$$\psi(\boldsymbol{\theta}) = \hat{\sigma}_Z^2(\boldsymbol{\theta})\det(\mathbf{R}(\boldsymbol{\theta}))^{1/n_{obs}} \quad (2.32)$$

In this case, the optimization of the autocorrelation parameters $\boldsymbol{\theta}$ is performed by the only use of the reduced likelihood function and more specifically the reduced log-likelihood function as:

$$\boldsymbol{\theta}^* = \underset{\boldsymbol{\theta}\in\mathcal{D}_{\boldsymbol{\theta}}}{\operatorname{argmin}}\ \log\Big(\psi(\boldsymbol{\theta})\Big) \quad (2.33)$$

By solving the optimization problem proposed in Eq. 2.33 the correlation model is said to be calibrated with regards to the model observations contained in the design of experiments $\{\boldsymbol{\mathcal{X}}_{obs},\boldsymbol{y}_{obs}\}$.

2.3.3 Metamodel validation method

Once the metamodel is calibrated, a validation step can be performed to estimate the approximation accuracy and to judge about the representativeness of the proposed Kriging predictions. As explained before, the Kriging metamodel is commonly trained from the only information provided by the model observations by the maximum likelihood estimation and,

as a consequence, no direct measure of the approximation error is therefore available. However, the quantification of the metamodel error can still be assessed by the implementation of a validation procedure.

These latter consist in splitting the observational set $\{\boldsymbol{\mathcal{X}}_{obs}, \boldsymbol{y}_{obs}\}$ into a training set $\{\boldsymbol{\mathcal{X}}_t, \boldsymbol{y}_t\}$ and a validation set $\{\boldsymbol{\mathcal{X}}_v, \boldsymbol{y}_v\}$ respectively of size $(n_{obs} - n_v)$ and n_v. The metamodel is then calibrated with the training set and its accuracy is tested by comparing the metamodel approximations for each observations of the validation set. Several global scores of quality can be assessed as the mean squared error (MSE) computed as:

$$MSE = \frac{1}{n_v} \sum_{i=1}^{n_v} (y_{v_i} - \hat{y}(\boldsymbol{x}_{v_i}))^2 \tag{2.34}$$

where $\boldsymbol{x}_{v_i}$ and y_{v_i} are respectively the i-th element of $\boldsymbol{\mathcal{X}}_v$ and $\boldsymbol{y}_v$. Reader can here noticed that this quantity may also be used to optimize the Kriging hyperparameters. Complementary, the coefficient of determination $\mathcal{Q}_2$ is widely used to estimate the global quality of a metamodel. Either computable from an independent validation design of experiments or within a cross-validation procedure, it is computed as:

$$\mathcal{Q}_2 = 1 - \frac{\sum_{i=1}^{n_v} \left(y_{v_i} - \hat{y}(\boldsymbol{x}_{v_i})\right)^2}{\sum_{i=1}^{n_v} \left(\bar{\boldsymbol{y}}_v - y_{v_i}\right)^2} \tag{2.35}$$

where $\bar{\boldsymbol{y}}_v$ denotes the mean of the model responses contained in the validation set. $\mathcal{Q}_2$ returns a scalar quantity between 0 and 1 which qualifies the quality of the metamodel by estimating the share of the output uncertainty due to the metamodel and thus, due to the design of experiments and the provided model response information as explained in Iooss et al. [2010].

2.3.4 Illustrative example

After having described the Kriging formalization, its underlying assumptions in Section 2.2 and presented its practical use in this section, a numerical example is here proposed to stress the Kriging approximation. Let consider a one-dimensional function assumed to represent a demanding numerical code (*e.g.* the short term damage d introduced in Chapter 1) and defined for $x \in [0, 10]$ as:

$$y(x) = x \ sin(x) \tag{2.36}$$

An observational set $\{\boldsymbol{\mathcal{X}}_{obs}, \boldsymbol{y}_{obs}\}$, composed of five model calls is randomly selected by a LHS procedure based on an uniform distribution (iso-probability of occurrence). The Kriging metamodel is set with a constant basis of regression ($\boldsymbol{f} = f_0$ in Eq. 2.2) and the "squared exponential" correlation function is selected as presented in Eq. 2.24. An unique scale parameter θ has to be calibrated from the information provided by the five model observations, which is proceeded by the maximum likelihood optimization. The domain of research is chosen as $\mathcal{D}_\theta = [10^{-3}, 10^2]$.

The result of the calibration is presented in Figure 2.4a which depicts the evolution of the reduced log-likelihood function $\log(\psi)$ over the optimization constrain domain $\mathcal{D}_\theta$. The minimum is here detected for a value $\theta^* = 12.53$. By setting the optimal value to the correlation parameter, the metamodel $\hat{\mathcal{M}}$ is computed and the model response is predicted all over the definition domain $\mathcal{D}_x$ as depicted in Figure 2.4b. From the variance of estimation, here noted σ and computed for each input of $\mathcal{D}_x$, the 95% confidence intervals are estimated and illustrated in Figure 2.4b.

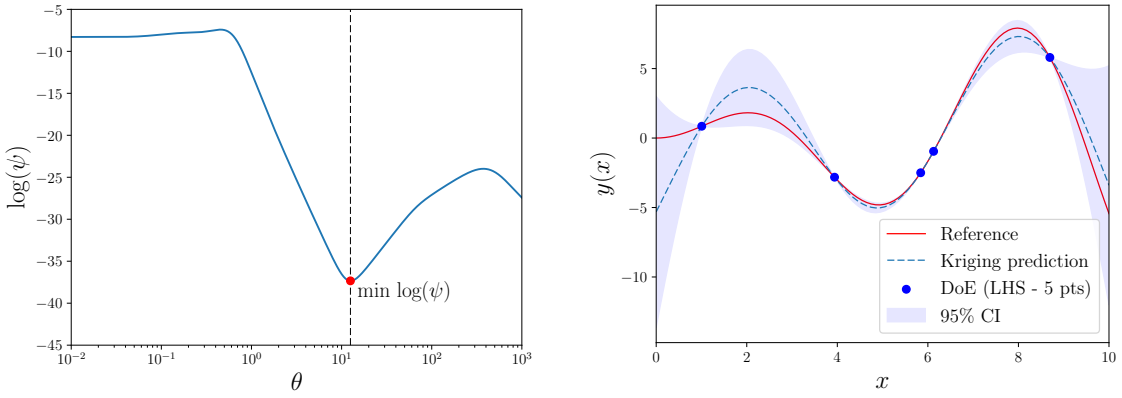

(a) Model calibration (b) Model prediction $\hat{\mathcal{M}}$

Figure 2.4: Illustration of the Kriging model calibration and prediction of the function response $y(x) = x\ sin(x)$ defined for $x \in [0, 10]$ with 5 observations (n_{obs}=5).

As one can observe, the prediction is exact for the five observations composing the design of experiments (*i.e.* the variance of prediction is equal to zero for each of the observed inputs) and the 95% confidence intervals increase as the prediction moves off the observed model responses. This phenomenon is due to the choice of the correlation function which presents a monotone evolution function of the distance between the considered points. It is here recalled that the confidence interval coming directly from the Kriging formulation is only constructed with regards to the model observations and can not be considered as a direct quantification of the metamodel error. As a simple illustration, the metamodel error for the input $x = 10$ is lower than the error $x = 2$ while the 95% confidence interval is larger for $x = 10$ than for $x = 2$. Nevertheless, the evolution of this quantity allows one to inform users of possible "blind areas" where the information is poor (from the point of view of the correlation function) and the metamodel does not have enough information to ensure the confidence on the computed prediction (large confidence intervals).

As explained throughout this chapter, a paradigm in metamodeling research is to find the best trade-off between the exploration and exploitation stages, which most of the time expresses a bias/variance compromise. The selection of the design of experiments plays a major role here and should be objective-oriented. A "static" design of experiments, *i.e.* a non-evolving observational set, may suffer from a lack of flexibility. Iterative Kriging strategies have thus been developed,which propose to sequentially enrich the initial design of experiments with the aim of ensuring the accuracy of the metamodel approximations either on the whole input space or at least over the regions of interest. Section 2.4 introduces this type of architecture to motivate their interest in the analysis of demanding simulation codes and more specifically in the framework of this industrial thesis.

2.4 Iterative Kriging strategies

2.4.1 Motivations and illustrative introduction

The quality and representativeness of Kriging prediction is dependent on the choice of the design of experiments and more precisely to the model response's information it provides. A minimal information inflow relative to the model responses has to be fulfilled to compute representative model predictions. Unfortunately, the lack of knowledge regarding the model behavior does not permit to effectively elect a full informational set of model observations in most of the cases (lack of *a priori*). To this extend and depending on the target quantity of interest one focuses on, diverse adaptive strategies have been developed in the field of metamodeling approaches, refered as active learning strategies.

Considering a set of model observations $\{\boldsymbol{\mathcal{X}}_{obs}, \boldsymbol{y}_{obs}\}$, these methods basically allow one to define a *learning function* which expresses the relevance of observing any given non-observed input with regards to the quantity of interest to approximate. In most of the cases, the *learning function* is derived from the statistical information provided by the calibrated metamodel. By integrating this strategy into an iterative architecture, the initial design of experiments can be sequentially enriched.

As an illustration, the example presented in Section 2.3.4 is resumed. Let consider the user wants the Kriging metamodel to converge over the whole domain of definition $\mathcal{D}_x$. The most simple enrichment strategy is to use the variance of estimation (see Eq. 2.17), here noted σ^2 and provided by the Kriging metamodel, to elect the best input x^* to simulate. This learning optimization is then writable as:

$$x^* = \underset{x \in [0,10]}{\operatorname{argmax}}\ \sigma^2(x) \tag{2.37}$$

For each of the enrichment steps, the elected simulation $y(x^*)$ is performed and added to the observational set before to update the metamodel (calibration procedure). This sequential enrichment is usually performed until a convergence criterion is reached. In the presented example, the metamodel can be assumed as convergent when the maximal coefficient of variation δ defined as:

$$\delta(x) = \frac{\sigma(x)}{|\hat{y}(x)|} \tag{2.38}$$

is small enough, fewer than 10% in this example for all $x \in [0, 10]$(arbitrary choice).

Figure 2.6 illustrates this iterative enrichment, starting from the initial situation presented in Section 2.3.4. The evolutions of the predictions and the variances of estimation for three enrichment steps (only the first, second and fifth enrichments) are depicted. The algorithm proceeds 5 enrichments increasing the initial design of experiments from 5 to 10 observations and reducing the maximal coefficient of variation from 47.15 to 0.072. The evolution of the optimized correlation parameter θ^* with respect to the size of the design of experiments is plotted in Figure 2.5a and the progressive decrease of the maximal coefficient of variation δ

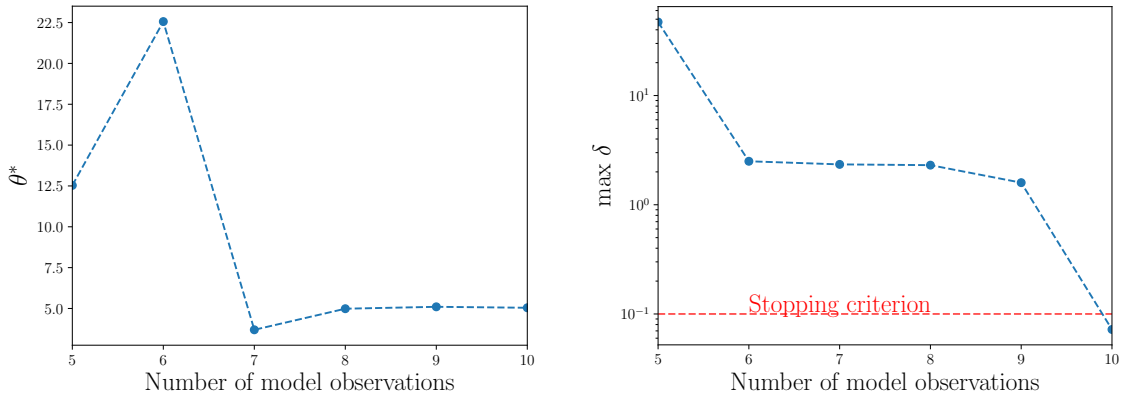

(a) optimized Kriging hyperparameter θ^* (b) max δ

Figure 2.5: Evolution of the optimized Kriging hyperparameter θ^* and the maximal coefficient of variation δ for the 5 enrichments of the proposed iterative application.

is illustrated in Figure 2.5b. As one can see, the evolution of the information contained in the observational set leads to important variations of the optimized correlation parameter. This hyperparameter varies from 12.5 to 22.5 before to reach the final order of magnitude from the second enrichment.

After this general introduction to the adaptive Kriging architectures and the proposed illustration on a simple academical example, the second part of this section presents a short literature review of adaptive kriging strategies developed and used in the fields of optimization and reliability analyses based on demanding computer codes.

2.4.2 Sequential Kriging in reliability and optimization procedures

Important developments have been proposed by the reliability and optimization communities in the field of Kriging based analyses since these domains usually require intensive simulator calls. By resorting to these methods and more specifically to adaptive architectures, they managed to significantly reduce the simulation investments for numerous applications. As a consequence, this short literature review only focuses on these specific domains and more specifically to recent developments that further inspired the developments proposed in this thesis.

From initial papers in the early 90's, engineers have progressively adopted the Kriging formalization to solve their own problems. In the early 2000's, several Kriging based studies have been proposed in the field of shape optimization. Generally speaking, each of these studies can be formulated as the minimization of a cost function $\mathcal{C}$ defined for a set of variables regrouped into the vector $\boldsymbol{x} \in \mathcal{D}_{\boldsymbol{x}}$ as:

$$\boldsymbol{x}^* = \underset{\boldsymbol{x} \in \mathcal{D}_{\boldsymbol{x}}}{\operatorname{argmin}}\ \mathcal{C}(\boldsymbol{x}) \tag{2.39}$$

where $\boldsymbol{x}^*$ here denotes the optimal value of the vector $\boldsymbol{x}$ regarding the problem constraints. For illustration purpose, Simpson et al. [2001] apply Kriging approximation to optimize an aerospike nozzle. Sakata et al. [2003] propose the optimization of a cantilever reinforced beam with three parameters and underline the efficiency and applicability of the Kriging approach

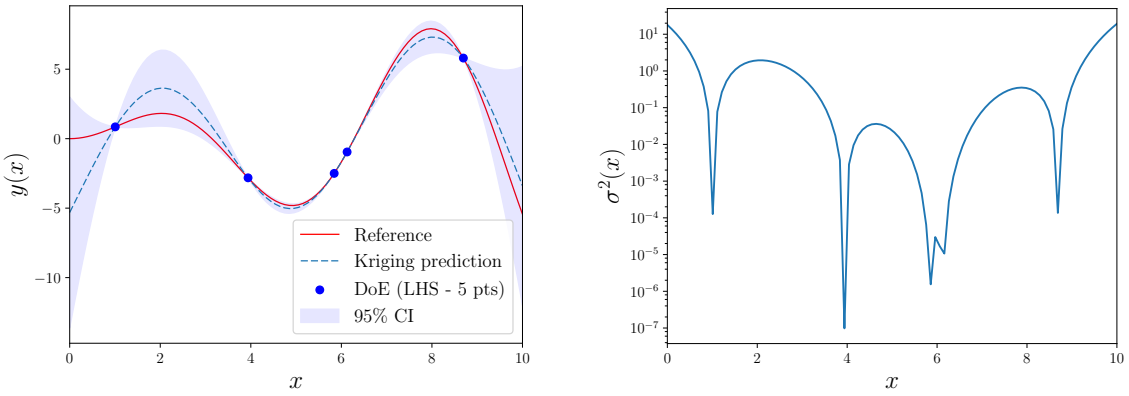

(a) Initial approximation

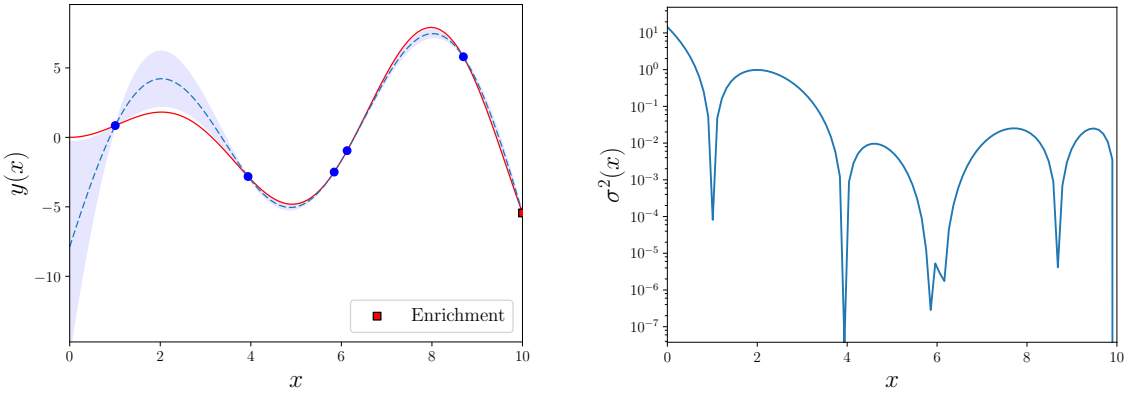

(b) First enrichment

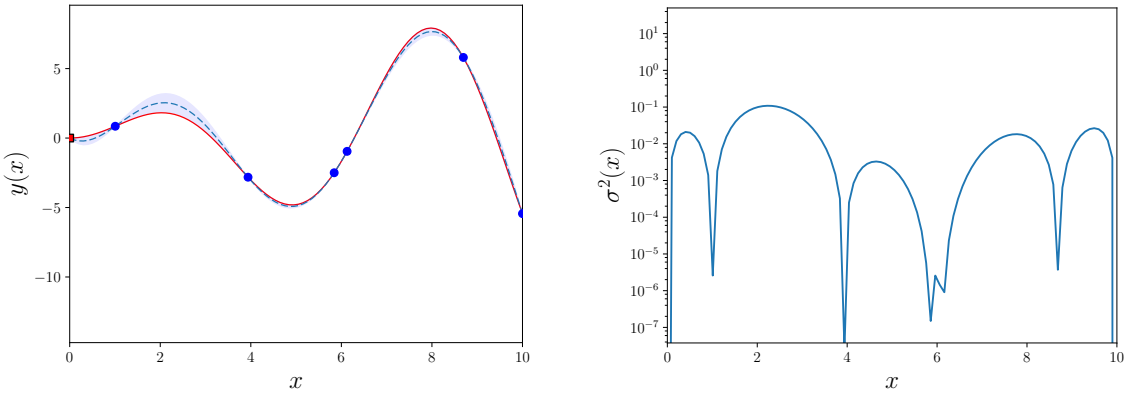

(c) Second enrichment

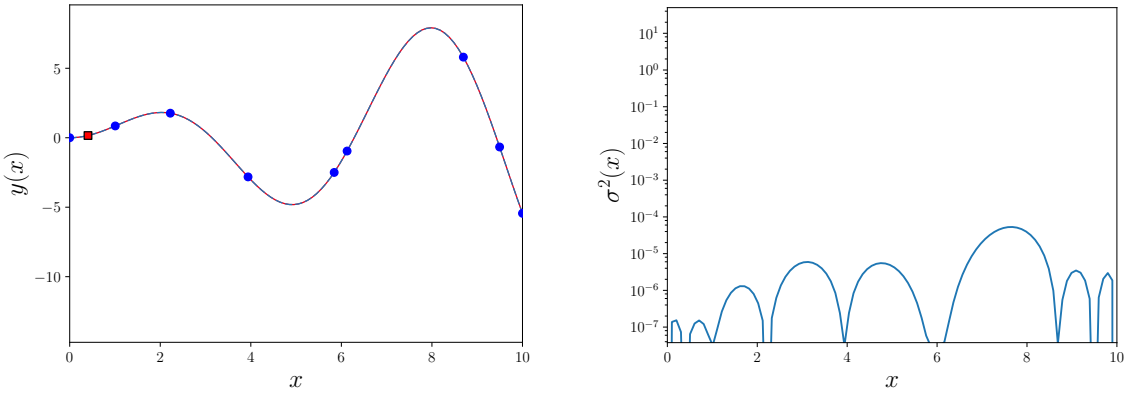

(d) Fifth enrichment

Figure 2.6: Illustration of the iterative enrichment strategy of the design of experiments for $y(x) = x\ sin(x)$ function. The learning quantity is here taken as the variance of estimation σ^2 (depicted on the right side figures) and the enrichment strategy focuses on the input which maximizes this variance.

within the context of structural optimization. Jones et al. [1998] propose the so-called EGO algorithm (Efficient Global Optimization) based on iterative Kriging approximations and the "expected improvement" quantity to provide engineers a global architecture to economically solve optimizations based on demanding numerical codes. In this method, the initial design of experiments is iteratively enriched with respect to the learning criterion defined as:

$$\boldsymbol{x}^* = \underset{\boldsymbol{x}\in\mathcal{D}_{\boldsymbol{x}}}{\operatorname{argmax}}\ \mathbb{E}\Big[I(\boldsymbol{x})\Big] \equiv \underset{\boldsymbol{x}\in\mathcal{D}_{\boldsymbol{x}}}{\operatorname{argmax}}\ \mathbb{E}\Big[\max(\mathcal{C}_{min} - \hat{\mathcal{C}}(\boldsymbol{x}), 0)\Big] \tag{2.40}$$

where I is the improvement function, $\mathcal{C}_{min}$ is the minimal observed value of the cost function and $\hat{\mathcal{C}}$ is the Kriging metamodel of $\mathcal{C}$. As illustrated in the original paper, this method allows to converge to the optimal solution with a reduced computational effort. Other formalizations and enhancements can be found in recent literature for the use of Kriging and adaptive Kriging methodologies in optimization procedures and reader are invited to refer to the literature reviews proposed by Wang and Shan [2007] and Ryberg [2013] for more complete presentations on such a topic.

Numerical reliability analyses also intensively resort to Kriging metamodeling. They aim at classifying the model responses with regards to a threshold value $G_{lim} = 0$ of a *performance function* G which expresses a failure scenario. Considering an ensemble of n random variables $\{X_i, i = 1, \ldots, n\}$ distributed from a joint probability function $f_{X_1,\ldots,X_n}$, these analyses consist in computing the probability P_f or the related reliability index β which can be defined as:

$$P_f = \text{Prob}\Big(G(X_1, \ldots, X_n) \leq 0\Big) \tag{2.41}$$

$$\beta = -\Phi\Big(P_f\Big) \tag{2.42}$$

where Φ is the cumulated density function of the standard Gaussian. Within this formalization, the works proposed by Romero et al. [2004] and Kaymaz [2005] first show the possibilities of using Kriging approximations to estimate the reliability quantities, respectively being the probability of failure P_f and the reliability index β. From then on, general frameworks have been proposed to sequentially construct informative design of experiments. Different strategies have been proposed so far, mostly distinguishable by the learning methodology used to select the next model evaluation with regards to the target quantity of interest. Bichon et al. [2011] proposed the EGRA (Efficient Global Reliability Analysis) architecture that uses the "expected feasibility" which provides information on how likely a considered input $\boldsymbol{x}$ can verify a constrain given as $G(\boldsymbol{x}) = G_{lim}$. This work shows successful reliability application with important reduction in simulator calls by orientating the model observations to the vicinity of the failure domain's limit. Picheny et al. [2011] used a modified "weighted integrated mean square error" which is only defined over input sub-domains where the model responses are at the vicinity of the failure value $\mathcal{G}_{lim}$. An enrichment strategy is then performed to augment the design of experiments with model observations likely to be in this domain of interest. Bect et al. [2012] propose several Kriging based reliability methods which focus on the computation of the volume of excursion of the probability density function of interest. From

this analysis, learning strategies regrouped under the term "Stepwise Uncertainty Reduction" (SUR) have been defined to reduce the uncertainty of the estimations (*e.g.* the probability of failure P_f). Echard et al. [2011] proposed the former "Adaptive Kriging" based method, named AK-MCS, where a learning function U quantifies the probability of each sample of a Monte Carlo population to be misclassified. From then, the AK based method family has rapidly spread with additional works described in a general review proposed by Lelièvre et al. [2018].

To the best of the author's knowledge, adaptive Kriging has been implemented to predict numerical model responses from a local point of view, *i.e.* when solely subspaces of input domains of definition are of interest. The two aforementioned domains of application perform iterative Kriging approximations to sequentially refine the model information response either on the vicinity of the failure domain's boundary (reliability analysis) or on the vicinity of minima of cost functions (optimization). The problematic of this thesis focuses on the approximation of the global mean damage D which is computed from a probability-weighted sum of demanding short term damages d (see Eq. 1.19). As a consequence, the Kriging prediction of this quantity has to be accurate all over its domain of definition or at least, over sub-domains of importance where the product $d \times p$ represents the most important share of the global mean damage sum. For this thesis' objective, the above-mentioned Kriging methods developed for reliability and optimization can not be applied in a straightforward manner. The novelty of this work lies on the development of a proper adaptive method for damage assessment, inspired from previous studies. The architecture proposed by the Adaptive Kriging methods appears here as being advantageous in the extent that the short term damage d has to be estimated over a finite number of points (certification grids). The proposed method is called Adaptive Kriging for Damage Assessment (AK-DA) and slightly differs from reliability approaches because of its global regression character. Iterative Kriging approximations of the demanding quantity d is carried out to sequentially compose an informative design of experiments with the view of proposing a faithful estimation of the mean global damage D. The complete methodology and the results of its application either considering academical or industrial cases of application are presented in Chapter 3.

2.5 Conclusions

In this chapter, Kriging prediction has been introduced in the context of numerical code approximation. This method, also known as Gaussian process prediction, aims at substituting the original model by a metamodel which construct a "model of the model". It is based on a statistical analysis of model observations and the characterization of correlation structures. Comparing with other metamodel techniques, Kriging proposes interesting features with regards to the scientific problematic of this thesis. In the first hand, it is known as being flexible and easily adaptable to a wide range of model responses. Furthermore, the model predictions are interpolating and ensure the exact prediction for observed realizations (design of experiments) which is of prime importance whilst assessing the mean global damage quantity D which should meet the standards' requirements. Finally, the variance of estimation defined for each of the input allows to have an indication on the uncertainty approximation which is appreciable when estimating the confidence one can have to the proposed Kriging predictions. As a consequence, Kriging seems to be a valuable approximation tool to apply in the context of damage analysis of wind turbine structures by reducing the number of computations of the short term damages d.

From a practical point of view, the construction of the Kriging predictor is based on two main steps: the selection of a representative set of observations and the metamodel calibration. The first point is crucial because the approximation is directly based on the information provided by the observational set and therefore the selection of the latter has to be carefully thought with regards to the objective. To ensure the representativeness of the model observations, reliability and optimization analyses based on Kriging have introduced iterative strategies that enable one to sequentially enrich the initial design of experiments depending on the aim of the study (research of a functional minimum, estimation of the probability of failure, etc.). These methods are not directly applicable to the industrial case of the interest here but motivate the development of a new iterative Kriging based method to effectively approximate the global mean damage D. This method, called the Adaptive Kriging for Damage Approximation (AK-DA) and which represent the core this thesis, is presented in the next chapter.

References

P Abrahamsen. A review of gaussian random fields and correlation functions. Technical report, Norwegian Computing Center, Oslo, Norway, 1997.

I. A. Basheer and M. Hajmeer. Artificial neural networks: fundamentals, computing, design, and application. *Journal of Microbiological Methods*, 43(1):3–31, 2000.

J. Bect, D. Ginsbourger, L. Li, V. Picheny, and E. Vazquez. Sequential design of computer experiments for the estimation of a probability of failure. *Statistics and Computing*, 22: 773–793, 2012.

B. J. Bichon, J. M. McFarland, and S. Mahadevan. Efficient surrogate models for reliability analysis of systems with multiple failure modes. *Reliability Engineering and System Safety*, 96:1386–1395, 2011.

M. Bilgili, B. Sahin, and Yasar A. Application of artificial neural networks for the wind speed prediction of target station using reference stations data. *Renewable Energy*, 32(14): 2350–2360, 2007.

G. Blatman. *Adaptive sparse polynomial chaos expansions for uncertainty propagation and sensitivity analysis*. PhD thesis, Université Blaise Pascal, 2009.

G. Blatman and B. Sudret. An adaptive algorithm to build up sparse polynomial chaos expansions for stochastic finite element analysis. *Probabilistic Engineering Mechanics*, 25: 183–197, 2010.

J-M. Bourinet. *Reliability analysis and optimal design under uncertainty - Focus on adaptive surrogate-based approaches*. Habilitation à diriger des recherches, Université Clermont Auvergne, 2018.

G. E. P. Box and N. R. Draper. *Empirical model-building and response surfaces*. Wiley series in probability and mathematical statistics. John Wiley & Sons, 1987.

V. C. P. Chen, K. L. Tsui, R. R. Barton, and M. Meckesheimer. A review on design, modeling and application of computer experiments. *IIE Transactions*, 38:273–291, 2006.

V. Dubourg. *Adaptive surrogate models for reliability analysis and reliability-based design optimization*. PhD thesis, Université Blaise Pascal - Clermont-Ferrand I, 2011.

B. Echard, N. Gayton, and M. Lemaire. AK-MCS: An active learning reliability method combining kriging and monte carlo simulation. *Structural Safety*, 33:145–154, 2011.

J. h. Friedman. Multivariate adaptive regression splines. *Annals of Statistics*, 19:1–67, 1991.

R. L. Hardy. Multiquadric equations of topography and other irregular surfaces. *Journal of Geolophysical Research*, 76(8):1905–1915, 1971.

B. Iooss, L. Boussouf, V. Feuillard, and A. Marrel. Numerical studies of the metamodel fitting and validation processes. *ArXiv e-prints*, 2010.

D. R. Jones, M. Schonlau, and W. J. Welch. Efficient global optimization of expensive black-box functions. *Journal of Global Optimization*, 13:455–492, 1998.

I. Kaymaz. Application of kriging method to structural reliability problems. *Structural Safety*, 27:133–151, 2005.

A. I. Khuri and Mukhopadhyay S. Response surface methodology. *WIREs Comp Stat*, 2: 128–149, 2010.

D. G Krige. A statistical approach to some basic mine valuation problems on the witwatersrand. *Journal of the Southern African Institute of Mining and Metallurgy*, 52:119–139, 1951.

N. Lelièvre, P. Beaurepaire, C. Mattrand, and N. Gayton. AK-MCSi: A kriging-based method to deal with small failure probabilities and time-consuming models. *Structural Safety*, 73: 1–11, 2018.

G. Matheron. *Traité de géostatistique appliquée, Tome I: Mémoires du Bureau de Recherches Géologiques et Miniéres, no. 14*. Editions Technip, Paris, 1962.

M. D. McKey, R. J. Beckman, and W. J. Conover. A comparison of three methods for selecting values of input variables in the analysis of output from a computer code. *Technometrics*, 21:239–245, 1979.

V. Picheny, D. Ginsbourger, Roustant O., R. Hftka, and N-H. Kim. Adaptive designs of experiments for accurate approximation of a target region. *Journal of Mechanical Design*, 132, 2011.

C. E. Rasmussen and C. K. I. Williams. *Gaussian Processes for Machine Learning*. The MIT Press, 2006.

R. G. Regis and C. A. Shoemaker. Constrained global optimization of expensive black box functions using radial basis functions. *Journal of Global Optimization*, 31:153–171, 2005.

V. J. Romero, L. P. Swiler, and A. A. Giunta. Construction of response surfaces based on progressive-lattice-sampling experimental designs with application to uncertainty propagation. *Structural Safety*, 26:201–219, 2004.

A. B. Ryberg. Metamodel-based design optimization - a multidisciplinary approach for automotive structures. Master's thesis, Linköping University - Institute of Technology, 2013.

J. Sacks, Welch W. J., Mitchell T. J., and Wynn H. P. Design and analysis of computer experiments. *Statistical Science*, 4:409–423, 1989.

S. Sakata, F. Ashida, and M. Zako. Structural optimization using kriging approximation. *Computer Methods in Applied Mechanics and Engineering*, 192:923–939, 2003.

T. W. Simpson, T. M. Mauery, J. J. Korte, and F. Mistree. Kriging models for global approximation in simulation-based multidisciplinary design optimization. *AIAA Journal*, 39:2233–2241, 2001.

B. Sudret. Meta-models for structural reliability and uncertainty quantification. In *Fifth Asian-Pacific Symposium on Structural Reliability and its Applications (5APSSRA)*, 2012.

V. Vapnik. *Estimation of Dependences Based on Empirical Data*. Springer, 2006.

G. G. Wang and S. Shan. Review of metamodeling techniques in support of engineering design optimization. *Journal of Mechanical Design*, 129(4):370–380, 2007.

CHAPTER 3

A KRIGING-BASED PROCEDURE FOR THE ESTIMATION OF THE STRUCTURAL DAMAGE (AK-DA)

Contents

This chapter introduces a numerical procedure to estimate the global mean damages D presented in Chapter 1 and required for the certification of offshore wind turbine structures. As explained before, this quantity can become very demanding in function of the considered conceptual situation because of the important number of short term damage d estimations (*e.g.* design load case 1.2). Chapter 2 presents the possibilities offered by the Kriging prediction which allows one to approximate numerical model responses from a reduced number of observations (simulator calls). Based on architectures implemented in iterative Kriging approaches, which are widely developed in the fields of structural optimization or reliability analyses, the proposed method, called *Adaptive Kriging for Damage Assessment* (AK-DA), proposes to compute a prediction of the demanding short-term damage response d from a reduced number of simulations.

In this chapter, a progressive presentation of the AK-DA method is provided. Firstly, Section 3.1 introduces the Kriging estimators implemented within the AK-DA procedure. The architecture of this numerical method and illustrations of its functioning are then presented in Section 3.2. Section 3.3 develops the multi-enrichment extension of the algorithm for its deployment in a context of high performance computing (HPC). Finally, a multi-location implementation is presented in Section 3.4 to depict an extension of the AK-DA procedure for simultaneous estimations of global mean damages cumulated at different structural locations.

3.1 Kriging based estimator of the cumulated damage D

The *Adaptive Kriging for Damage Assessment* (hereafter called AK-DA) is a numerical method which proposes to compute a cost-effective estimation of the global mean damage D introduced in Chapter 1 and being the scope of this thesis. This damage is practically computed for the n_s structural locations of interest from a probability-weighted sum of n_c short term damages d as:

$$D_k = \sum_{i=1}^{n_c} d_k(\boldsymbol{x}_i)\ p(\boldsymbol{x}_i)\ \Delta = \sum_{i=1}^{n_c} d_{k,i}\ p_i\ \Delta \quad \text{with } k \in \{1, \dots, n_s\} \tag{3.1}$$

To ease the notations, the following explanations are given considering a single analysis location ($n_s = 1$). The global mean damage D_k is thus simplified as $D_1 \equiv D$ as well as the short term damages d_1 here denoted by d.

The proposed method is based on the construction of a global mean damage estimator noted $\hat{D}$ and based on the approximation of the short term damages d which represent the computationally demanding quantities. As presented in Chapter 2, Kriging metamodeling can be used to predict demanding quantities based on a finite set of observations (*i.e.* simulator calls). From the direct application of this metamodeling strategy, a prediction $\hat{d}$ can be computed from a reduced set of $n_{obs} < n_c$ observations $\{\boldsymbol{\mathcal{X}}_{obs}, \boldsymbol{d}_{obs}\}$ where $\boldsymbol{\mathcal{X}}_{obs}$ is the observational matrix composed of n_{obs} inputs and $\boldsymbol{d}_{obs}$ regroups their related model responses. From the model information provided by this partial observational set, a Kriging approximation $\hat{d}$ of the demanding short term damage quantity d can be computed for all $\boldsymbol{x} \in \mathcal{D}_{\boldsymbol{x}}$:

$$d(\boldsymbol{x}) \approx \hat{d}(\boldsymbol{x} \mid \{ \boldsymbol{\mathcal{X}}_{obs}, \boldsymbol{d}_{obs} \}) \equiv \hat{d}(\boldsymbol{x}) \tag{3.2}$$

Assuming the representativeness of the design of experiments $\{\boldsymbol{\mathcal{X}}_{obs}, \boldsymbol{d}_{obs}\}$ with respect to the short term damage response, the global mean damage D can be estimated by replacing the short term damage d by its Kriging metamodel $\hat{d}$ in Eq. 3.1. The estimator, hereafter noted $\hat{D}$, thus reads:

$$\hat{D} = \sum_{i=1}^{n_c} \hat{d}(\boldsymbol{x}_i)\ p(\boldsymbol{x}_i)\ \Delta = \sum_{i=1}^{n_c} \hat{d}_i\ p_i\ \Delta \tag{3.3}$$

In this thesis, the probability of occurrence p is considered as fully determined and, as a consequence, is assumed deterministic. Under the assumption of a regular and constant discretization (Δ constant over the input definition space), the variance $\sigma^2_{\hat{D}}$ of the global mean damage estimator $\hat{D}$ can be determined as:

$$\sigma^2_{\hat{D}} = \sum_{i=1}^{n_c} \sum_{j=1}^{n_c} p_i\ p_j\ \mathrm{Cov}(\hat{d}_i, \hat{d}_j)\ \Delta^2 \tag{3.4}$$

The coefficient of variation $\delta_{\hat{D}}$ therefore reads:

$$\delta_{\hat{D}} = \frac{\sigma_{\hat{D}}}{\hat{D}} \tag{3.5}$$

Reader have to keep in mind that for all the n_c computations required by the certification guidelines, n_{obs} simulations are performed from the demanding multiphysics code and due to the valuable property of interpolation of Kriging approximation, $\hat{d}(\boldsymbol{x}_{obs}) = d(\boldsymbol{x}_{obs})$. The Kriging approximation is only considered for the remaining $(n_c - n_{obs})$ unobserved combinations of the certification grid. With respect to the standard requirements, the objective is therefore to keep a small enough number of observations n_{obs} whilst ensuring a limited bias in the estimation of the global mean damage D.

As presented in Chapter 2 and introduced in this section, the Kriging prediction $\hat{d}$ of the demanding quantity d is determined with respect to the information provided by the design of experiments $\{\boldsymbol{\mathcal{X}}_{obs}, \boldsymbol{d}_{obs}\}$. As a matter of fact, the proposed estimators of the short term damage $\hat{d}$ and so the global mean damage $\hat{D}$ are conditioned by the choice of the model response observations. To effectively construct this set of model observations and therefore reduce the risk of high bias (*i.e.* relative error here), this chapter introduces the AK-DA method which allows to iteratively select a reduced but informative design of experiments to calibrate the Kriging metamodel with respect to the quantity of interest D.

3.2 Adaptive Kriging for Damage Assessment (AK-DA)

The AK-DA procedure seeks at proposing engineers an automatic selection of an informative design of experiments to ensure the representativity of the cumulated damage D predictions, presented in Eq. 3.3. From an initial set of model observations $\{\boldsymbol{\mathcal{X}}_0, \boldsymbol{d}_0\}$, an iterative strategy

is performed to progressively enrich the design of experiments with new model observations aiming at reducing the uncertainty of the estimator $\hat{D}$. This sequential construction of the design of experiments is implemented with respect to an adaptive Kriging architecture presented in Figure 3.1.

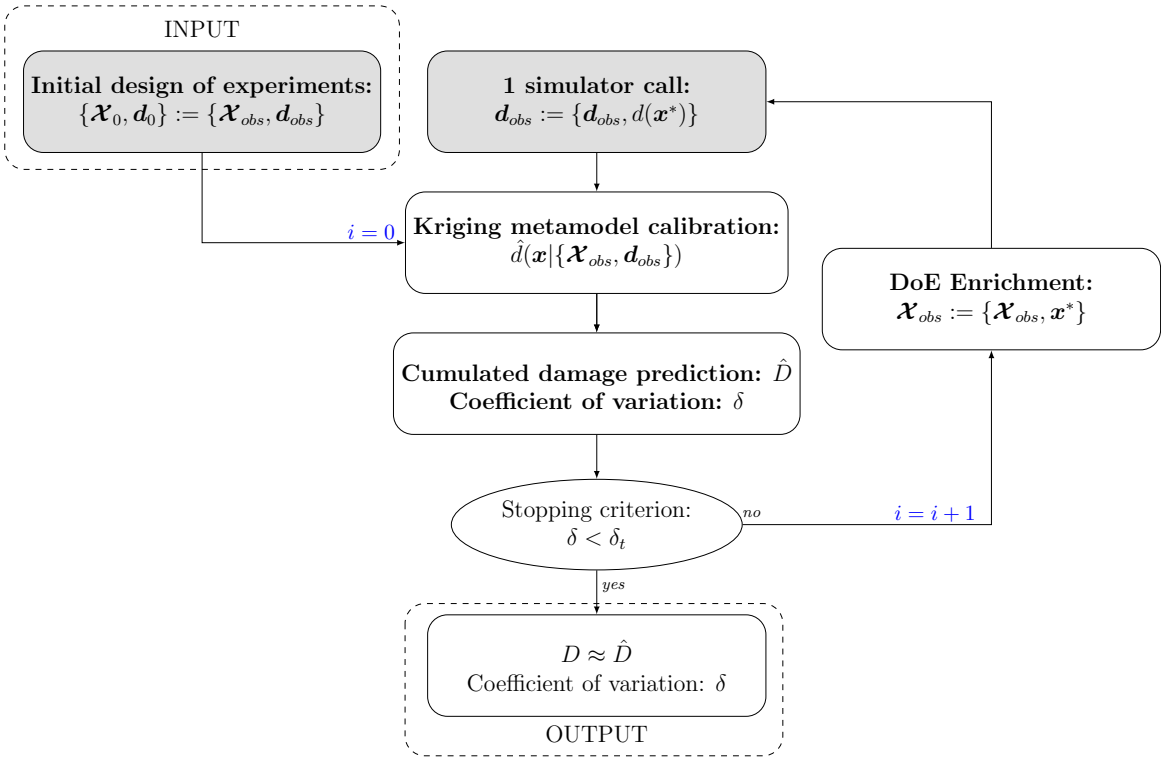

Figure 3.1: Presentation of the AK-DA algorithm.

Four distinctive blocks compose the proposed procedure: the selection of an initial design of experiments, the computation of damage estimators by the calibration of a Kriging metamodel, the enrichment strategy to enhance the representativeness of the design of experiments and the stopping test. Detailed descriptions of these latter are presented in this section to explain the complete implementation of the AK-DA algorithm.

3.2.1 Initial design of experiments

The choice of the design of experiments is a critical issue in metamodeling and is subjective to a certain extent. When adaptive strategies are used, the objective lies in enriching an initial design of experiments of reduced size with elected observations driven by the future use of the metamodel. This goal-oriented selection is expected to reduce the influence of a personal choice of a fully "static" observational set on the quality of the response approximation. The selection of the first design of experiments to initiate an adaptive procedure remains however an open issue and one should note it also affects metamodel results. Together with the choice of the regression basis and autocorrelation model, the selection of the initial design of experiments may be viewed as a user parameter setting of adaptive Kriging metamodeling.

Within the industrial context of this work and more precisely considering the certification process and its requirements, the initial design of experiments, here noted $\{\boldsymbol{\mathcal{X}}_0, \boldsymbol{d}_0\}$, is elected from the grid of environmental combinations proposed by the certification guidelines. To

sufficiently explore the entire domain of definition, it has been here decided to resort to regular grids based on expertise. This choice appears suitable according to the mechanical knowledge of the problem, which is briefly introduced below. Nevertheless, the influence of random initial designs of experiments obtained from LHS (an alternative solution) on Kriging predictions will be briefly discussed on a validation example in Section 3.2.6.

The short term damage response of a wind turbine structure is expected to gradually evolve with respect to the environmental parameters, *i.e.* without sharp peaks or transients. This is practically achieved by means of prior checks when designing the structure. As an example, the computation of the natural frequencies of the structure is performed in the early stage of the design to ensure a minimal risk of damage accumulation due to a superposition of its spectra with the environmental load spectra, as presented in Section 1.3.4. Resonant phenomena should in fact be precluded over the domain of variation of environmental solicitations. Environmental combinations associated with frequencies potentially close to structural frequencies can be added in the regular grid. Then, non-linearities in the aerodynamics behavior of rotor components, and therefore in the evolution of aerodynamic loads, can be deduced from the control scheme of the machine. In particular, three noticeable wind speed values, namely the start-up wind speed u_{in}, the rated wind speed u_{rated} and the cut-off wind speed u_{cut} appear in the evolution of the power due to the servo control and can be considered as "turning points", see section 1.1.1. The information provided by the simulations of short-term damages for these values can then be valuable for the metamodel accuracy and therefore added to the initial design of experiments.

To sum up, initial designs of experiments are here composed of coarse regular grids extended with additional simulations deduced from expertise to be cost-effective. For illustration purpose, Figure 3.2 presents a composite design of experiments as it is used in the implementation of the AK-DA approach introduced in this thesis. Considering two environmental parameters x_1 and x_2, a regular grid (blue circles) is completed by the consideration of extra simulations based on expertise (red squares). For each of the n_0 environmental combinations, the simulator is run to access the model responses d. The initial design of experiments $\{\boldsymbol{\mathcal{X}}_0, \boldsymbol{d}_0\}$ is then obtained and the AK-DA algorithm is initialized.

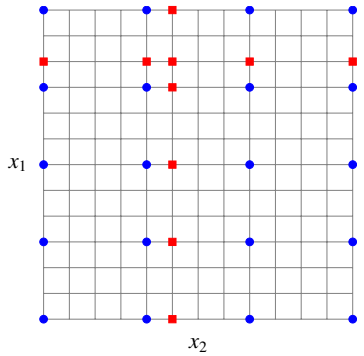

Figure 3.2: Illustration of an AK-DA composite design of experiments used to initialize the algorithm: x_1 and x_2 are two environmental parameters for which 4 values have been set to compose a regular grid (blue points). The expertise points (red points) can be added to integrate informative simulations corresponding to operating points.

3.2.2 Kriging metamodel calibration and prediction

From a given design of experiments $\{\boldsymbol{\mathcal{X}}_{obs}, \boldsymbol{d}_{obs}\}$, a Kriging metamodel of the demanding quantity d is calibrated. This step aims at optimizing the hyperparameter vector $\boldsymbol{\theta}$ knowing the metamodel setting (choice of the autocorrelation function and deterministic trend, see Section 2.2). The resulting optimized vector, noted $\boldsymbol{\theta}^*$, allows one to compute the damage prediction $\hat{d}(\boldsymbol{x})$ for all the environmental parameters $\boldsymbol{x} \in \mathcal{D}_{\boldsymbol{x}}$. An estimator $\hat{D}$ of the global mean damage D is subsequently computed as defined in Eq. 3.3 so as its variance of prediction $\sigma^2_{\hat{D}}$ proposed in Eq. 3.4 and the coefficient of variation $\delta_{\hat{D}}$ defined in Eq. 3.5.

3.2.3 Stopping criterion

The accuracy of the global mean damage estimation is here controlled by the evolution of its coefficient of variation $\delta_{\hat{D}}$ introduced in Eq. 3.5. The quality of the estimation is assumed to be sufficient if the coefficient of variation is lower than a certain value, noted δ_t to be fixed by the user with regards to the required accuracy. However, readers have to keep in mind that this quantity is conditioned by the information provided by the design of experiments. This is not a direct quantification of the estimation error between the unknown value and the predicted one but only an indication of the convergence of the algorithm. The defined criterion is used to stop the algorithm enrichment (defined in Section 3.2.4) with the following control step:

$$\delta_{\hat{D}} < \delta_t \tag{3.6}$$

If this relation is not verified ($\delta_{\hat{D}} \geq \delta_t$), an additional enrichment of the design of experiments is performed. In the contrary case ($\delta_{\hat{D}} < \delta_t$), the enrichment procedure is stopped and the estimation $\hat{D}$ is stored. Additionally and as presented in Chapter 2, confidence intervals can be statistically estimated regarding the true value D. As an example, the two-side 95%-confidence interval can be estimated as:

$$\hat{D} - 1.96\ \sigma_{\hat{D}} \leq D \leq \hat{D} + 1.96\ \sigma_{\hat{D}} \tag{3.7}$$

3.2.4 Enrichment Strategy

To accurately approximate the quantity of interest D for each of the structural locations, an adaptive architecture is implemented. Within this procedure, the approximation $\hat{D}$ is refined by sequentially integrating new model observations in the design of experiments. This learning step focuses on the quantification of the potential inflow of information one call could provide regarding the reduction of the estimating uncertainty, here assessed through its variance of prediction $\sigma^2_{\hat{D}}$. The AK-DA method proposes to elect the additional observation with regards to its capacity to reduce this latter quantity.

To quantify this potential information inflow, the variance $\sigma^2_{\hat{D}}$, given in Eq. 3.4 is decomposed as the sum of n_c *variance contributions* $\mathcal{C}$ as:

$$\sigma^2_{\hat{D}} = \sum_{i=1}^{n_c} \mathcal{C}_i \quad \text{with} \quad \mathcal{C}_i = p_i \sum_{j=1}^{n_c} p_j \ \text{Cov}(\hat{d}_i, \hat{d}_j) \ \Delta^2 \tag{3.8}$$

The contribution $\mathcal{C}_i$ is assumed to quantify the level of the metamodel uncertainty computed for each of the n_c combinations of environmental parameter in the global variance of the estimation $\sigma_{\hat{D}}$. Because of the interpolant characteristic of the implemented predictor (*i.e.* $\hat{d}(\boldsymbol{x}) = d(\boldsymbol{x})$ if $\boldsymbol{x}$ is observed), this contribution drastically decreases for simulated environmental combinations since the preponderant variance term vanishes in the presented sum ($\text{Cov}(\hat{d}_j, \hat{d}_j) = \text{Var}(\hat{d}_j) = 0$ if the model response d_j is observed). As a result, only the cross-covariance terms remain ($\text{Cov}(\hat{d}_j, \hat{d}_j)$ with $i \neq j$). Because of the sign of the cross-covariance which can either be positive or negative depending on the estimated cross evolution of the predictions $\hat{d}$ for two different inputs, the absolute contribution $|\mathcal{C}|$ is considered here.

The environmental parameter with the maximal absolute contribution is assumed to reduce the most the estimator's uncertainty, *i.e.* to provide the most important informational inflow. The learning step is thus formalized as the following optimization problem:

$$\boldsymbol{x}^* = \underset{\boldsymbol{x} \in \mathcal{D}_{\boldsymbol{x}}}{\text{argmax}} \ |\mathcal{C}(\boldsymbol{x})| \tag{3.9}$$

The learning environmental parameter $\boldsymbol{x}^*$ is selected to increase the design of experiments with, and a simulator call is performed to observe the true value $d(\boldsymbol{x}^*)$.

The complete description of the AK-DA algorithm has been now proposed. The rest of this section provides an illustration of its use on an academical one-dimensional example. Then two-dimensional academical examples are introduced to validate the method which is finally applied on two industrial cases.

3.2.5 Illustration on a 1-dimensional case

A first illustration of the AK-DA algorithm is here presented considering the one-dimensional function $d(x) = x + xsin(x)$ for $x \in [0, 10]$. It is assumed here that this quantity represents the evolution of the demanding short term damage d regarding a fictional environmental parameter $x \in [0, 10]$. The probability of occurrence of this latter is computed as a Gaussian distribution with mean parameter $\mu_x = 4$ and standard deviation $\sigma_x = 2$. This example is illustrated in Figure 3.3 where the reference function $d(x)$, the probability of occurrence $p(x)$ and the probability-weighted damage $p(x) \times d(x)$ are depicted for $x \in [0, 10]$.

Because of the relative simplicity of the function to approximate, the cumulated damage D can be easily approached using a thin discretization with a total of 1000 points. This choice leads to a discretization unit equal to $\Delta = 10^{-2}$ and the reference global mean damage is computed as:

$$D = \int_0^{10} p(x)(x + x \ sin(x))\text{d}x \simeq \sum_{i=1}^{n_c=1000} p(x_i) \times (x_i + x_i \ sin(x_i)) \ \Delta = 3.239 \tag{3.10}$$

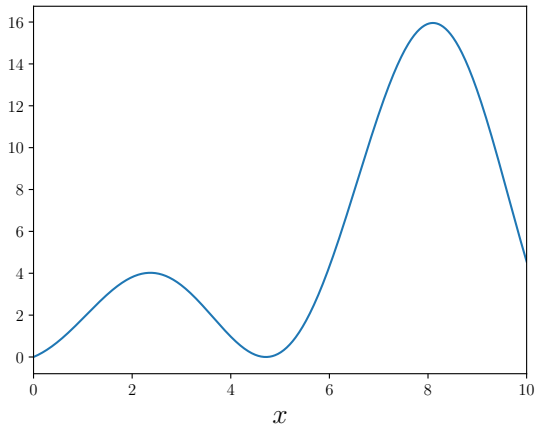

(a) Reference function $d(x)$

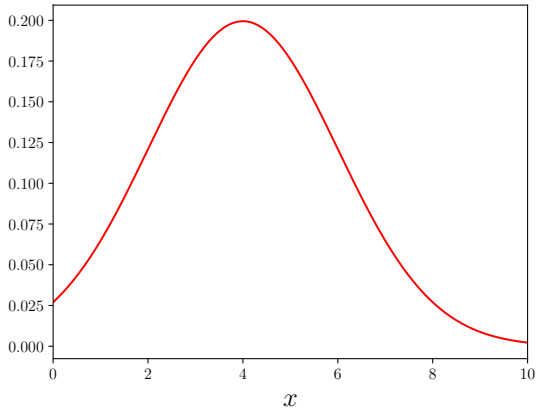

(b) Probability $p(x)$

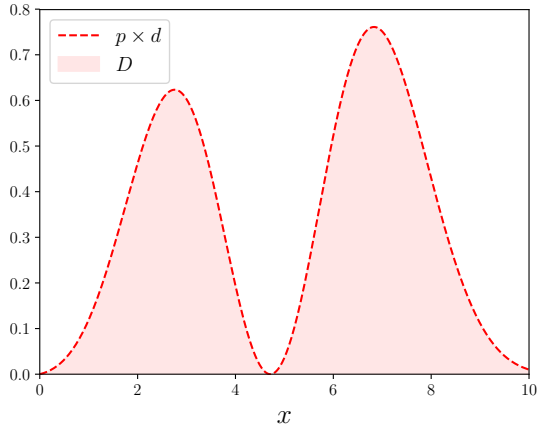

(c) $p(x) \times d(x)$

Figure 3.3: Illustration of the reference quantities of the one-dimensional illustrative example.

The initial design of experiments is here composed of two model observations aleatory chosen by a LHS sampling set on an uniform distribution $\mathcal{U}(0, 10)$. The Kriging metamodel is parameterized with a constant regression basis and a squared exponential covariance function. The AK-DA stopping criterion is arbitrarily set to $\delta_t = 5\%$. Figure 3.4 illustrates the evolution of the AK-DA approximations for the short term damage d (left) and the $p \times d$ quantity (right) for the initial design of experiments and for the next three enrichments required to converge. In addition, the absolute variance contributions $|\mathcal{C}|$ are depicted in Figure 3.5 for each of algorithm iterations. Figure 3.6 shows the evolution of the estimation $\hat{D}$ as well as the evolution of the Kriging parameter θ^* optimized at each step of the algorithm.

The algorithm starts with a design of experiments of reduced size, which is only composed of two model observations. As depicted in Figure 3.4a, the approximation of the damage model response is not accurate because of this lack of information. This remark stands for the approximation of the product $p \times d$ and so the prediction of the quantity of interest which is far below the reference value. The variance contribution computed for this initial design of experiments shows three domains of interest concerning the enrichment possibilities (see Figure 3.5a): two areas for which the $p \times \hat{d}$ product is important (vicinity of $x = 1$ and $x = 4$) and an area where the uncertainty of $\hat{d}$ is important on the unobserved right side of the definition domain. The approximation of $\hat{D}$ still suffers from a lack of information after the first enrichment and the metamodel error is considerably reduced after the second observation

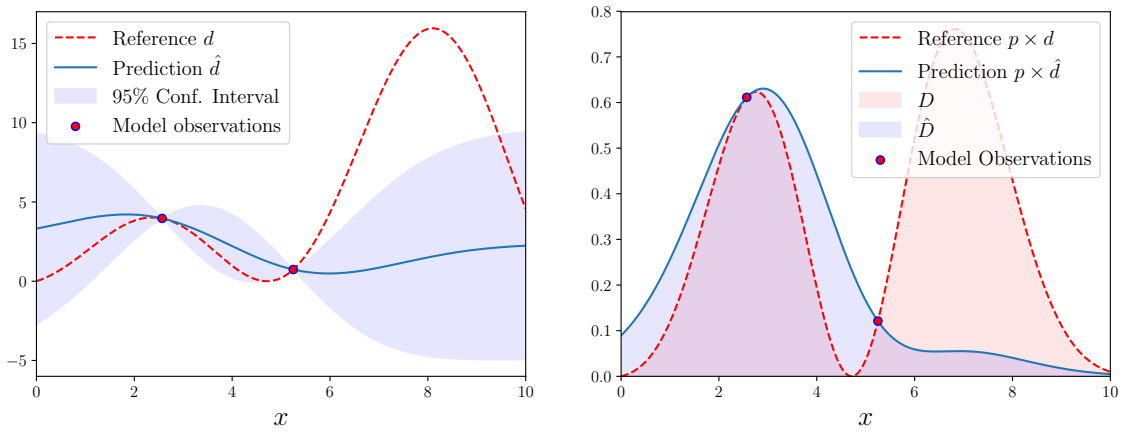

(a) Initialization

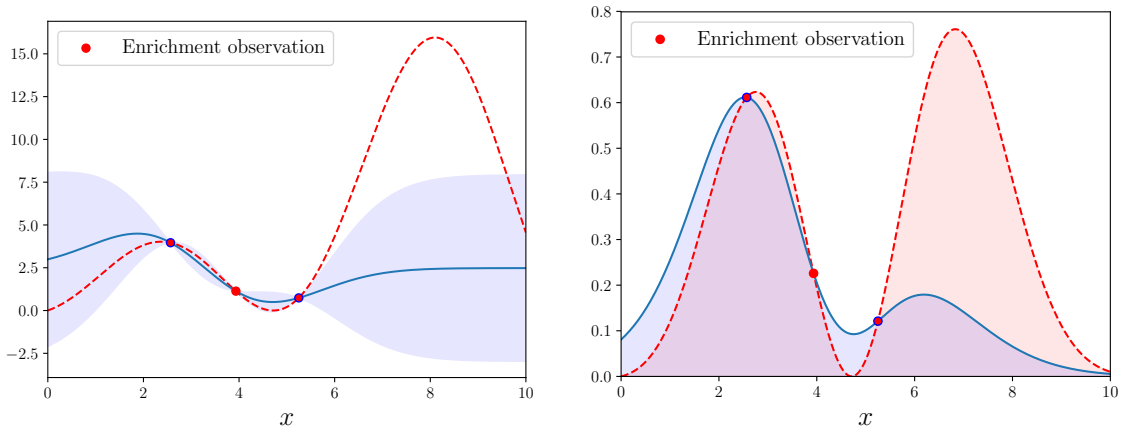

(b) Enrichment 1

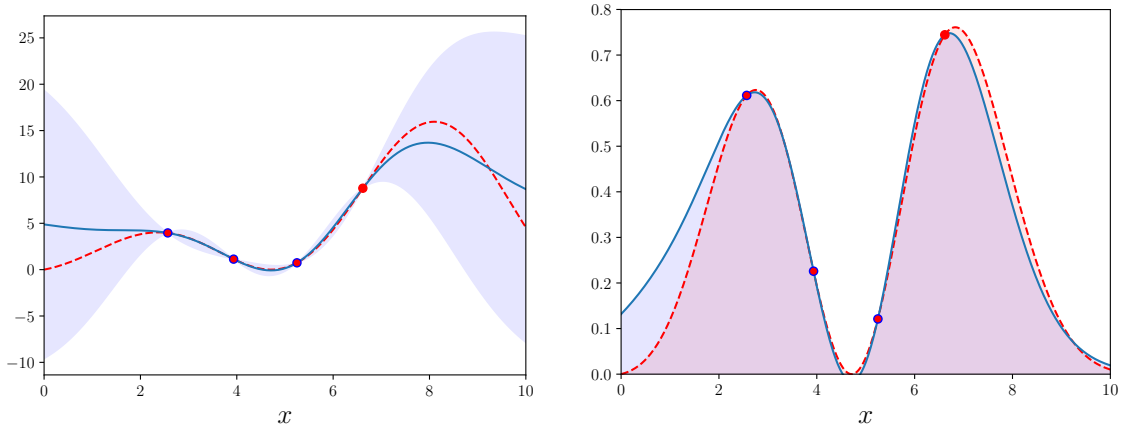

(c) Enrichment 2

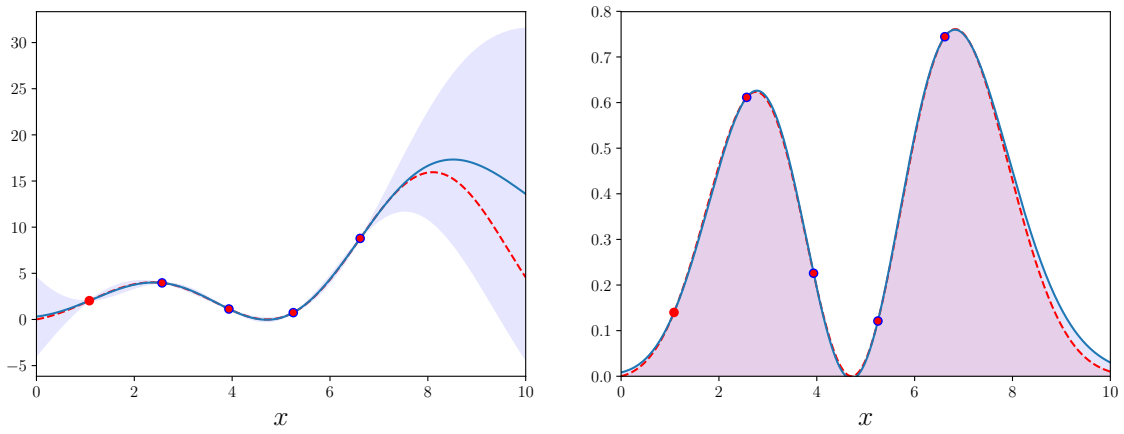

(d) Enrichment 3

Figure 3.4: Evolution of the approximations of the short term damage $\hat{d}$ and the probability-weighted short term damage $p \times \hat{d}$ for the initialization and the three enrichments proposed by the AK-DA method.

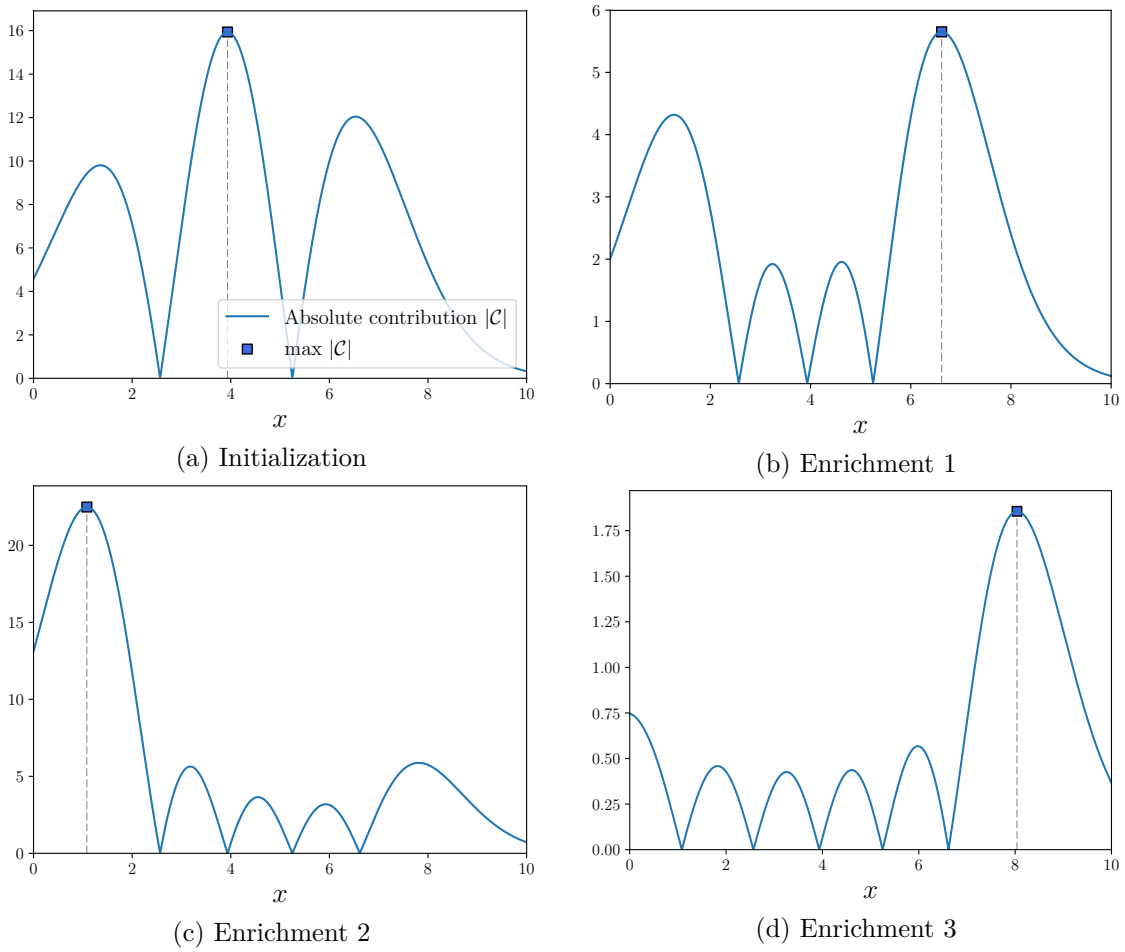

(a) Initialization (b) Enrichment 1

(c) Enrichment 2 (d) Enrichment 3

Figure 3.5: Evolution of the variance contributions for the initialization and the three enrichments proposed by the AK-DA method for the illustrative one-dimensional example.

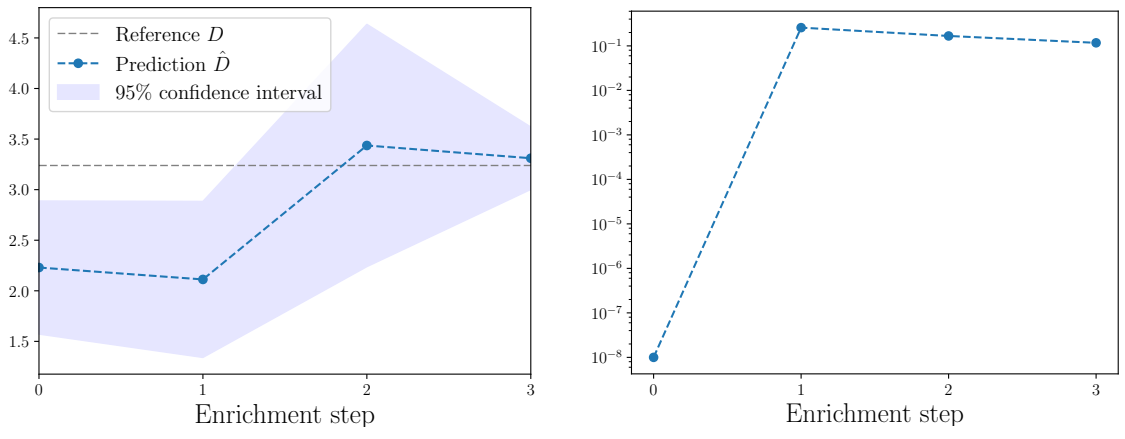

(a) Estimation $\hat{D}$ (b) Kriging hyperparameter θ^*

Figure 3.6: Evolution of the estimation of the global mean damage D (a) and the optimized Kriging hyperparameter θ^* (b) for the initialization and the three enrichments proposed by the AK-DA method for the illustrative one-dimensional example.

enrichment (see Figure 3.6a). This is also observable from Figure 3.6b which depicts the evolution of the optimized Kriging hyperparameter θ^* which reaches its convergence order of magnitude after two iterations of the AK-DA algorithm. From this moment, the metamodel proposes an accurate approximation of the model response and the estimation of the quantity of interest D get closer to the reference value. With a total of four simulator calls, the relative error of the estimation of $\hat{D}$ decreases to 6.10%. helps the metamodel to refine locally with the addition of an observation located on the left side of the definition domain and to reach the stopping criterion with a coefficient of variation $\delta_{hatD} = 4.76\%$. At convergence, the AK-DA algorithm provides an estimation of the global mean damage equals to 3.311 which represents a relative error of 2.22% with respect to the reference value.

This first illustration is here presented to depict the behavior of the AK-DA procedure with a simple one-dimensional example. In the next section, the algorithm is further tested and validated with regards to two-dimensional reference cases.

3.2.6 Two-dimensional validation cases

In the following, the AK-DA procedure is tested with regards to four different validation cases inspired from the industrial context. Two variables x_1 and x_2 are here considered, both assimilated to distinct environmental parameters. Their domains of definition are respectively given by $x_1 \in [1, 20]$ and $x_2 \in [-100, 100]$. A regular discretization introduces 20 possible values for the environmental parameter x_1 and 21 for the parameter x_2. As a consequence, $n_c = 420$ possible combinations of environmental parameters are used to determine the global mean damage D with a discretization unit $\Delta = 10$. The same joint probability density function is assumed for the four examples. This is defined as a non-correlated Gaussian function which exhibits a peak for the environmental combination $\boldsymbol{x} = \{5, 0\}$. This probability function is depicted in Figure 3.7.

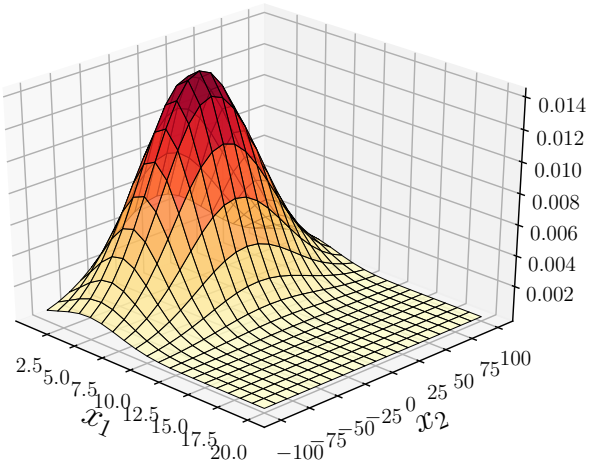

Figure 3.7: Illustration of the probability of occurrence for the parameters x_1 and x_2 defined in the validation test cases.

All along these examples, the AK-DA method is set with a Kriging metamodel computed with constant basis functions and anisotropic "squared exponential" correlation functions. The stopping criterion of the AK-DA procedure is set to $\delta_t = 5\%$ (Eq. 3.6).

The four examples implemented in this test case are named d_1, d_2, d_3 and d_4. Their respective evolutions are depicted in Figure 3.8. The first model (Figure 3.8a) shows a smooth evolution with a peak of response located at $x_1 = 5$ and $x_2 = 0$. The combinations of parameters which lead to this response peak show an important probability of occurrence. This characteristic eases the determination of the global mean damage which expression is presented in Eq. 3.1. To challenge the AK-DA method, three additional examples are considered representing more complex models. In the cases of d_2 and d_3, important damage accumulations appear locally which can be seen as mechanical resonance. Two modes appear in parallel in the test case d_2. The highest values of the damage response are located at the extrema values of the x_2-domain of definition and at $x_1 = 10$ (see Figure 3.8b). The environmental parameters for which this phenomenon is observed have an equal probability of occurrence p and, as a consequence, represent equal importance with regards to the determination of the global mean damage D. The third example (Figure 3.8c) also represents a bi-modal situation but with areas for which the probabilities of occurrence are different. A major peak can be observed for environmental parameters of high probability of occurrence, *i.e.* in the vicinity of $\boldsymbol{x} = \{5, 0\}$. A second and smaller damage accumulation appears for environmental parameters close to $\boldsymbol{x} = \{14, -60\}$ which presents a negligible probability of occurrence. To finish, the fourth example (Figure 3.8d) depicts a model d which is only sensitive to the first environmental parameter x_1.

Reference computations have been performed for each of the proposed test cases to determine the global mean damages D, presented in Table 3.1.

Test case	Reference n_{call}	Reference D (Eq. 3.1)
d_1	440	4.64×10^{-8}
d_2	440	2.55×10^{-8}
d_3	440	2.83×10^{-7}
d_4	440	6.99×10^{-8}

Table 3.1: Reference values of the global mean damages D computed for the four validation test cases.

The point of this validation study is to test the accuracy of the proposed estimation of $\hat{D}$ with regards to the choice of the initial design of experiments and to depict some performances of the AK-DA procedure. A first study focuses on the analysis of the convergence behavior of the proposed method with regards to aleatory generated initial designs of experiments. Subsequently, these results are compared with a deterministic design of experiments to illustrates the pros and the cons of the two proposed approaches.

Random generation of the initial design of experiments

The accuracy of the method here relies on its capacity to propose representative estimations of the demanding global mean damage D. Depending on the initial design of experiments, the method is expected to behave differently and, as a consequence, to compute a global mean damage estimation which varies from one initial observational set to another. To analyze this phenomenon, 30 aleatory generations of initial designs of experiments of size n_0 are performed with $n_0 = \{2, \ldots, 30\}$. To do so, the initial environmental parameters are randomly selected by a LHS procedure. To maximize the covering of the environmental parameters' domain

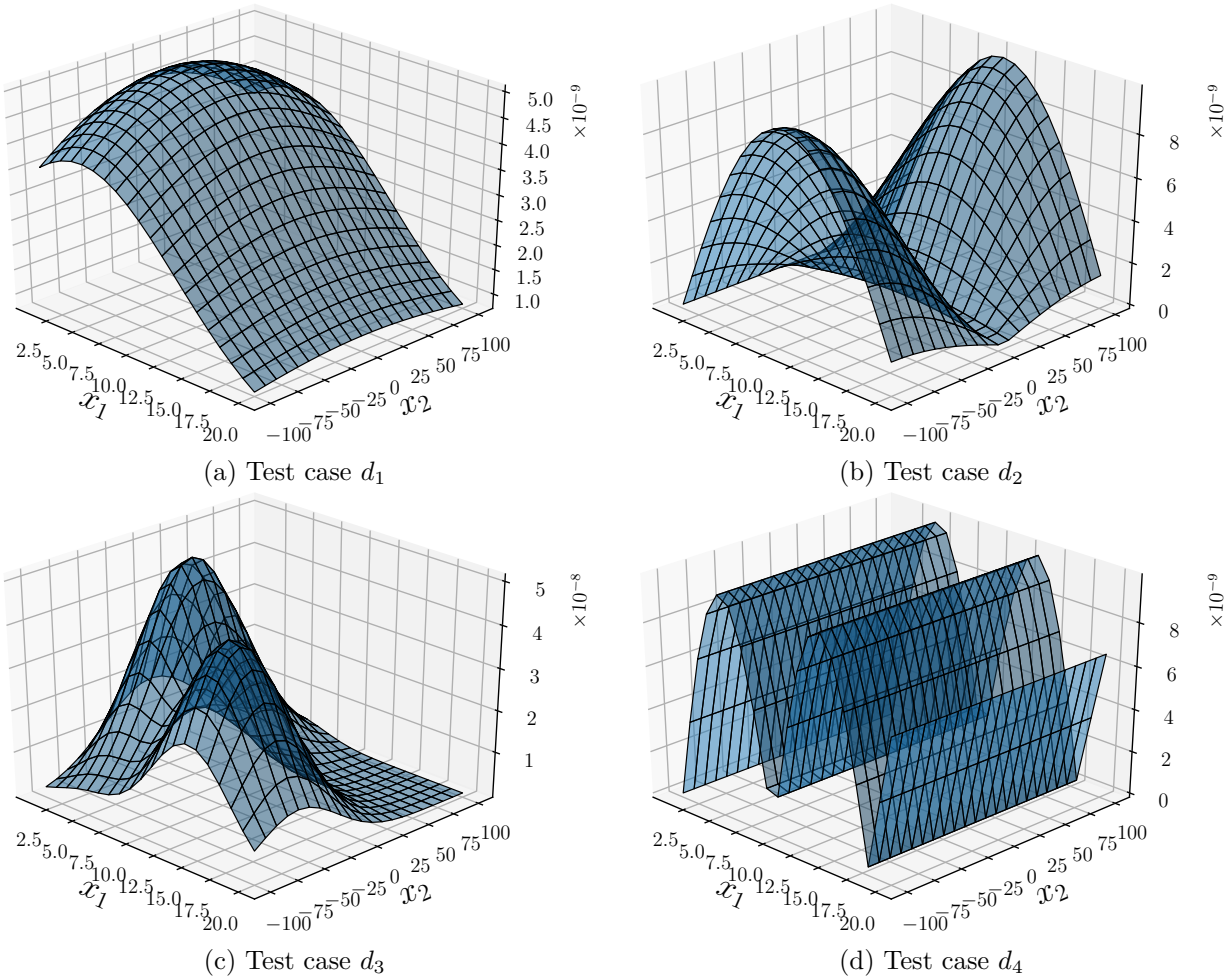

(a) Test case d_1

(b) Test case d_2

(c) Test case d_3

(d) Test case d_4

Figure 3.8: Illustration of the fictional short term damages used for the validation of the method.

of definition, this generation is done from uniform probability density functions, respectively denoted $\mathcal{U}_1$ and $\mathcal{U}_2$ for the parameters x_1 and x_2. These two distributions are parameterized with the lower and upper bounds of the respective domains of definition as:

$$\mathcal{U}_1 = \mathcal{U}\Big(0, 20\Big) \quad \text{and} \quad \mathcal{U}_2 = \mathcal{U}\Big(-100, 100\Big) \tag{3.11}$$

To adapt the result of the LHS to the proposed certification grid, each of the samples is transformed to correspond to the reference elements induced by the discretization of the problem. This step is simply performed by the minimization of the distance between each randomly generated points and the reference ones. By proceeding this way, the aleatory choice of the initial design of experiments, which is assumed to be in accordance with the defined grid in this thesis, is mimicked. For each of the initial sizes n_0, the AK-DA method is performed with the 30 aleatory generated designs of experiments. To characterize the performance of this algorithm, the relative error between the convergence approximations and the real value is computed for each of the AK-DA procedures. The mean, minimal and maximal values so as the standard deviations of these relative errors are presented in Figure 3.9 for each of the sizes n_0 of the initial design of experiments. In addition, the average number of enrichments proposed by the AK-DA method for each of the sizes n_0 is depicted in Figure 3.10.

From a global point of view, the estimator $\hat{D}$ shows a limited mean relative error with respect to the reference values. Depending on the complexity of the studied short term damages, the AK-DA proposes enrichments to better approximate the global mean damage D. The number of AK-DA iterations importantly varies depending on the analyzed case. For simple short term damage responses such as d_1, enrichments are only proposed for small initial designs of experiments with $n_0 \leq 7$. Considering more complex damage models such as d_2 or d_3, the average numbers of iterations are greater and the iterative strategy is performed even for important sizes of the initial design of experiments.

It can be observed that the mean as well as the standard deviation of the relative errors decrease when the size n_0 of the initial design of experiments increases. For each of the depicted situations, the mean relative error is low and rapidly converges into the $\pm 5\%$ relative error interval. This is observed from initial sizes n_0 respectively equal to 2, 13, 12 and 6 for the short term damages d_1, d_2, d_3. At the same time, the standard deviation of the relative errors decreases to reach values between 7.70% (d_3 with $n_0 = 13$) and 11.64% (d_2 with $n_0 = 12$). This underlines the risk related to the use of random generated design of experiments. Even if the computed estimator presents an admissible relative error mean which is not very sensitive to the size n_0, some designs of experiments lead to important relative errors. The d_2 and d_3 validation cases show that even if the mean relative error is contained in the $\pm 5\%$ interval, estimations of the global mean damage can sometimes exhibits important relative errors. As an example, within the 30 aleatory generated designs of experiments used for the test case d_2 with $n_0 = 13$, the maximal relative error reaches -45%. This is explained by the information provided by the first design of experiments. For complex short term damage responses, this latter has to provide enough information regarding the global model response to ensure an accurate convergence of the AK-DA algorithm. To tackle this, regular grids combined

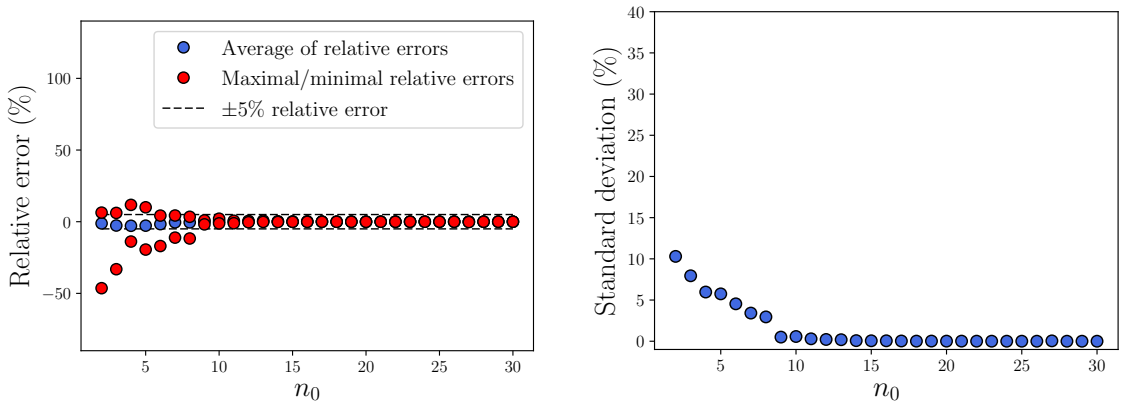

(a) Test Case d_1

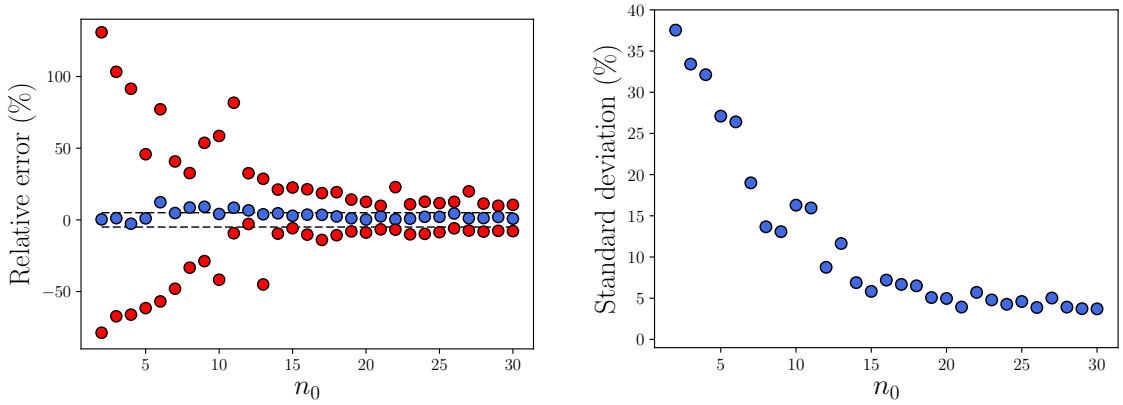

(b) Test Case d_2

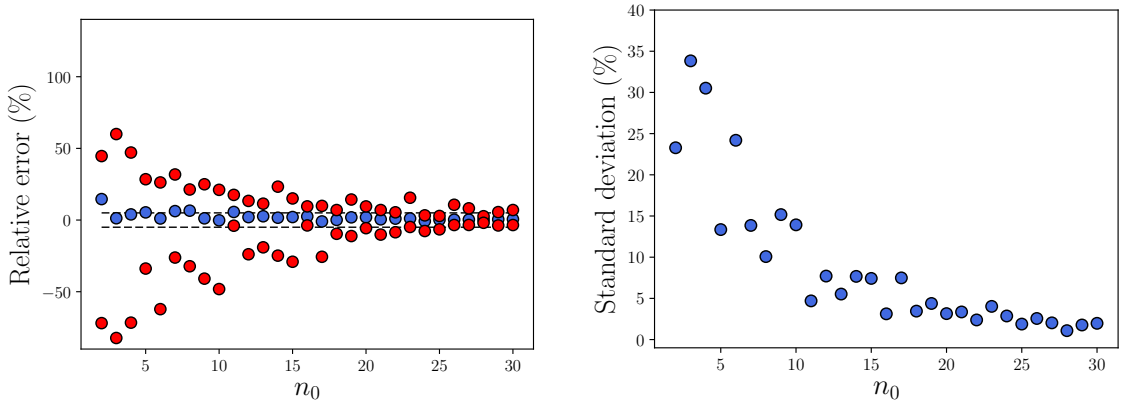

(c) Test Case d_3

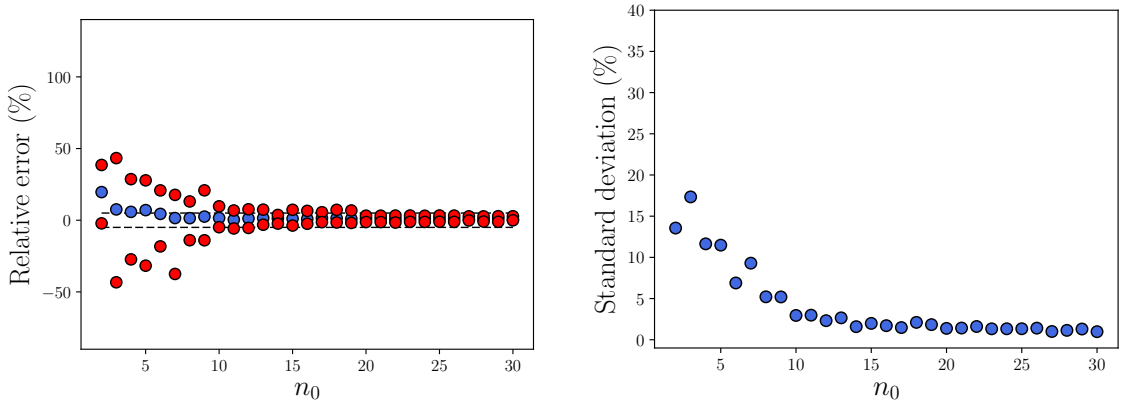

(d) Test Case d_4

Figure 3.9: Evolution of the relative error (left) of the global mean damage estimation with regards to aleatory generated designs of experiments ($n_0 = \{2, \ldots, 30\}$).

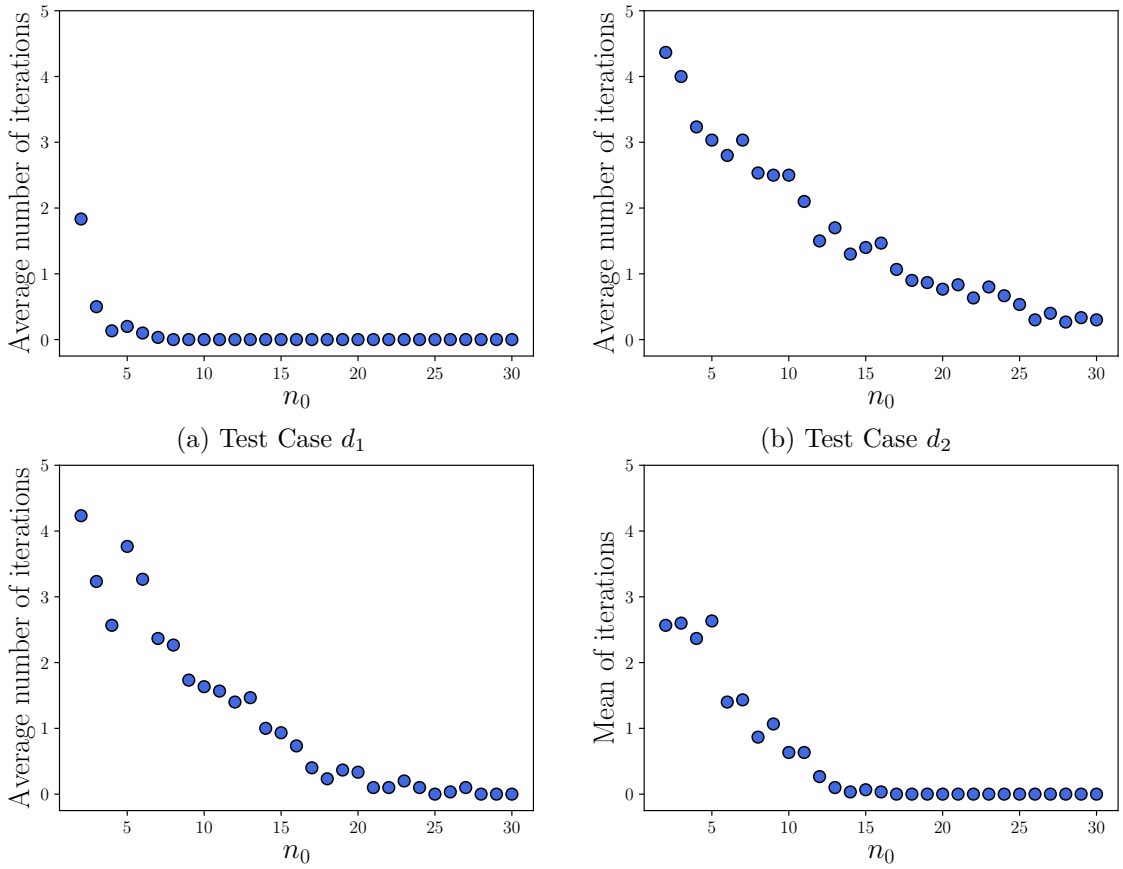

(a) Test Case d_1 (b) Test Case d_2

(c) Test Case d_3 (d) Test Case d_4

Figure 3.10: Mean of the iteration numbers provided by the AK-DA method for the different sizes n_0 of the initial design of experiments.

with expertise can be used to provide the AK-DA method a sufficiently representative initial designs of experiments.

Regular grid combined with expertise

As presented in the description of the method, a possible way to elaborate the initial design of experiments is the choice of a deterministic grid of reduced size with regards to the certification's one. This proposition is motivated by the fact that a sufficient global characterization of the short term damage response is necessary for the AK-DA method to compute accurate estimations of the global mean damage. Furthermore, *a priori* knowledge regarding the evolutions of the general shape of the short term damage response can be either deduced from expertise and physical considerations or by means of cost effective strategies (*e.g.* the spectral analysis, briefly introduced in Section 1.6.1 but not presented in details in this thesis).

Considering the four validation examples presented in this section, a regular grid composed of 9 environmental parameters is used. This initial design of experiments regroups all the possible combinations obtained by considering three values both for the x_1 and x_2 environmental parameters. For each, the lower and the upper bounds of the definition domain is used as well as the mean value. As a consequence, this initial grid is here defined for $x_1 = \{1, 10, 20\}$ and $x_2 = \{-100, 0, 100\}$. The AK-DA algorithm is initialized with this grid and the estimations of $\hat{D}$ are compared with the ones obtained with aleatory generations

	d_1	d_2	d_3	d_4
	random initial designs of experiments			
mean of relative error (%)	0.03	9.13	1.19	2.54
maximal relative error (%)	1.87	53.74	40.88	20.84
mean of n_{iter}	0	2.5	1.74	1.07
	regular grid initial designs of experiments			
relative error (%)	-1.5%	0.78%	15%	-1.6%
n_{iter}	0	5	2	3

Table 3.2: Performances of the AK-DA procedure for aleatory generated designs of experiments (30 generations) and the proposed regular grid ($n_0 = 9$)

composed of $n_0 = 9$ (here directly obtained from the previous study). These results of this comparison are presented in Table 3.2.

It can be observed that the reduced grid which is here proposed allows to correctly initialize the AK-DA algorithm which results in an accurate estimation of the global mean damages for the validation test cases d_1, d_2 and d_4 with relative errors between -1.6 and 0.78%. Compared to aleatory generations of the design of experiments, these results are comparable to relative errors means presented in Table 3.2. Figure 3.11a, Figure 3.11b and Figure 3.11d depict both the Kriging approximations of the short term damages d_1, d_2 and d_4 at convergence as well as the enrichments strategy proposed by the AK-DA method. For each of these three examples, the Kriging metamodels of the short term damages present a satisfying accuracy for environmental parameters which exhibit an important probability of occurrence. For the first validation case, the stopping criterion of the AK-DA method is reached from the initial design of experiments. As a consequence, no enrichments are proposed by the AK-DA method. For the validation cases d_2 and d_4, the enrichments are all located on the environmental parameter subsets for which the quantity $p \times d$ is high. Readers can notice that for the validation cases d_1, d_2 and d_4, the Kriging metamodels of the short term damages has not to be accurate over the domain of definition of the environmental parameters. In the particular case of d_4, the proposed approximation is only accurate for environmental parameters which exhibit important $p \times d$ values. This is sufficient for the approximations of the global mean damages to be accurate.

Contrary to the test cases d_1, d_2 and d_4, the application of the AK-DA method with the proposed reduced initial design of experiments leads to a relative error of 15% in the approximation of the global mean damage D_3. Even though this relative error is far below the maximal relative error of 40.88 % proposed by the aleatory generated design of experiments, this accuracy could be not sufficient for industrial application. As illustrated in Figure 3.11c, the Kriging metamodel of the short term damage d_3 is not accurate for environmental combination of parameters that exhibit an important probability of occurrence. As a matter of fact, the accumulation peak located for low values of x_1 and for $x_2 \approx 0$ is not correctly determined in the x_2 direction with a larger dispersion compared to the reference surface (depicted in Figure 3.8c). The two enrichments well focus on the peak of the $p \times d_3$ response but does not allow to globally refine the Kriging approximation of the short term damage. To better estimate the global mean damage D_3, two alternatives are possible: the augmentation of the size of the grid composing the initial design of experiments or an adaptation of the

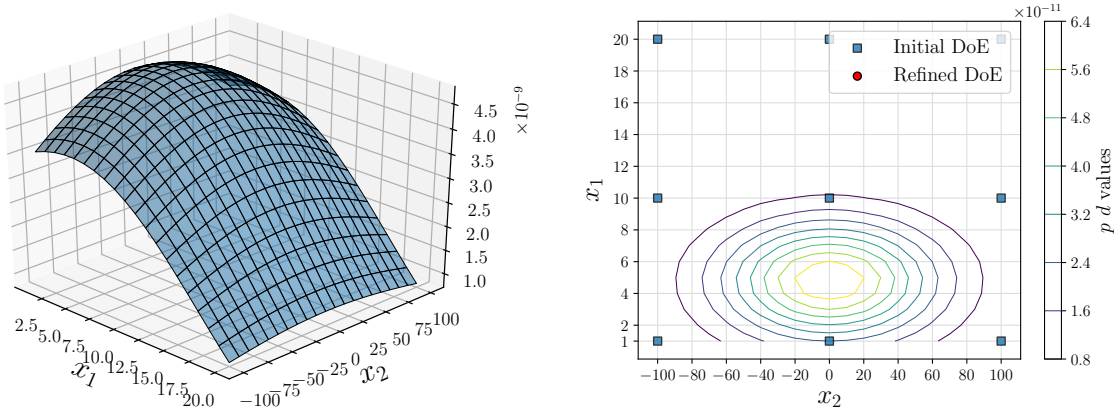

(a) Test Case d_1

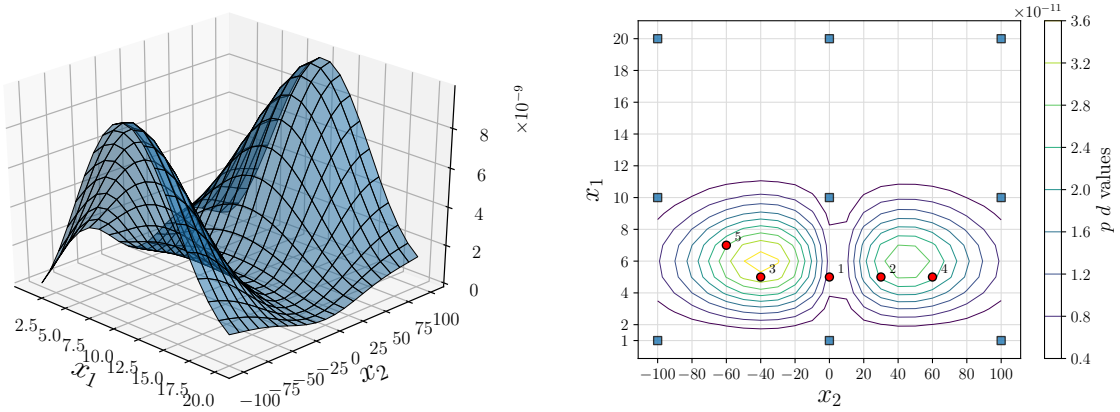

(b) Test Case d_2

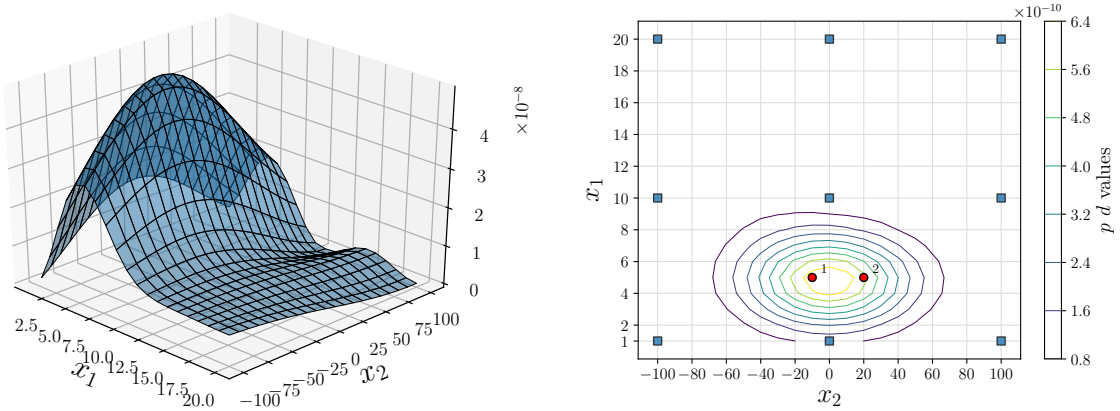

(c) Test Case d_3

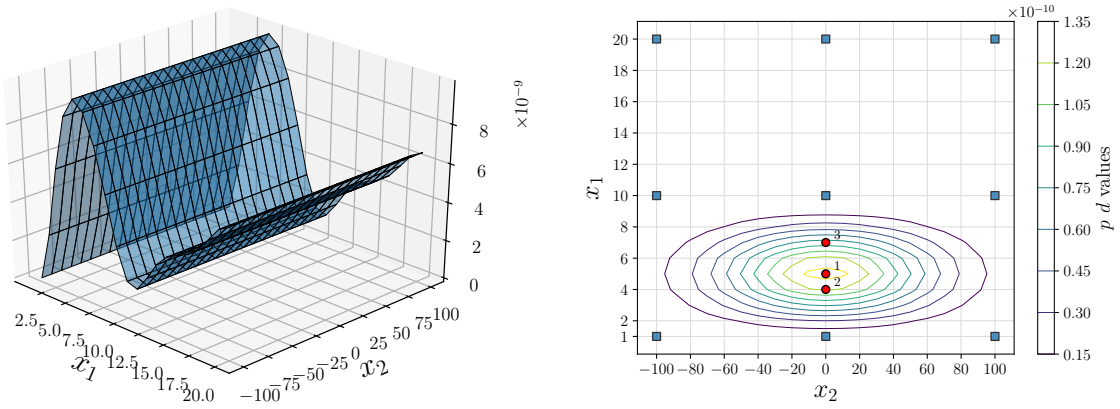

(d) Test Case d_4

Figure 3.11: Illustration of the Kriging approximation of the short term damages at convergence (left) and the enrichment strategy (right) of the AK-DA method with the reduced grid composed of size $n_0 = 9$.

proposed initial grid to better capture the global trend of the short term damage. This latter is possible by the integration of *a priori* knowledge regarding the evolution of the short term damage. As previously said, this can be done based on based on physical considerations or by the means of cost-effective strategies such as spectral approaches. As an example, by

The performances of the AK-DA methodology on the four introduced validation cases show its applicability potential. For each of the presented tests, the method allows to enrich an initial design of experiments with informative simulations to reduce the uncertainty relative to the computed estimator $\hat{D}$. As presented in Figure 3.11, the iterative procedure focuses on the election of environmental parameters which exhibit an important $p \times d$ response. This behavior eases the approximation of the global mean damage, refining the Kriging approximation of the short term damage on areas of interest, defined for environmental parameters for which the $p \times d$ quantity is important. In the rest of the definition domain, the metamodel is not required to be accurate which results in an important reduction of the simulation investment. To compute representative approximations of the global mean damages, the AK-DA method requires an informative initial design of experiments which globally represents the evolution of the short term damage (at least for the environmental parameters which present high $p \times d$ responses). In the case of aleatory generation of the initial design of experiments, an important risks of non representativeness of the approximation exist as shown in this study and should not be used to the author point of view. The proposed alternative is the composition of regular grids which allow to better capture the global trend of the short term damage responses and as a consequence to enhance the approximations provided by the AK-DA algorithm. In the rest of this chapter, regular grids are implemented to elaborate the initial designs of experiments.

3.2.7 Industrial application

This section depicts the performances of the AK-DA procedure applied for industrial examples. The considered design load case is the DLC 1.2 quantifying the cumulated damage D for the "normal production" conceptual situation. This illustration focuses on the reference offshore wind turbine NREL 5MW OC3 with monopile substructure as presented in Jonkman et al. [2009] and the metocean are inspired from Stewart et al. [2015].

In the following, two applications are proposed based on the environmental description presented in Figure 3.12. The first case is a simplified two-dimensional study which only considers the evolution of the wind mean speed u and the wind-wave misalignment θ. The second illustration is a more challenging four-dimensional example created by the integration of the wave significant height h_s and the spectral peak period t_p. In the rest of the section, any set of environmental parameter is presented as either $\boldsymbol{x} = \{u, \theta\} \in \mathcal{D}_{\boldsymbol{x}}$ (two-dimensional example) or $\boldsymbol{x} = \{u, \theta, h_s, t_p\} \in \mathcal{D}_{\boldsymbol{x}}$ (four-dimensional example) with:

$$\mathcal{D}_{\boldsymbol{x}} = \mathcal{D}_u \times \mathcal{D}_\theta \text{ or } \mathcal{D}_{\boldsymbol{x}} = \mathcal{D}_u \times \mathcal{D}_\theta \times \mathcal{D}_{h_s} \times \mathcal{D}_{t_p} \tag{3.12}$$

and where $\mathcal{D}_u$,$\mathcal{D}_\theta$, $\mathcal{D}_{h_s}$ and $\mathcal{D}_{t_p}$ represent the discretized domains of definition for each of the environmental parameters.

The work-flow implemented to compute the short term damages d for any set of environmental parameters is as introduced in Section 1.5. The aleatory generations of wind time histories are performed with the TurbSim model [Jonkman and Kilcher, 2012] set with a "normal turbulence model" (NTM) based on a Von Karman spectrum and a turbulence intensity of 14%. Sea conditions are set with a water depth of 20 meters and a Jonswap spectrum is used to aleatory generate waves in the four-dimensional example. The hydrodynamic loadings as well as the structural reactions are computed with an EDF internally developed code (equivalent to NREL's FAST [Jonkman and Buhl, 2005]). To reduce the simulation costs required for the computation of the reference values, only one seed is used and the short term damages are estimated over a period of time of 10 min. In the presented examples, soil-structure interactions are not taken into account in the numerical model and the substructure is assumed to be clamped onto an infinitely rigid soil.

The presented examples focus on the analysis of the mudline Az-0 structural location which is introduced in Figure 3.12. Thus, the post-processing of the structural reactions is composed of the computation of the Von Mises stresses at this structural location. A decomposition of the Von Mises signal into fatigue cycles is computed with the use of a rainflow procedure. The S-N curves are extracted from DNV-GL guidelines and account for weld in tubular joints in seawater with cathodic protection (Curve T proposed in DNV-GL's guidelines [DNV-GL, 2014]). Finally, the Palmgren-Miner law is used to estimate the cumulated damage due to the environmental loading and as a result, the short term damage d. For more details about this implementation, readers are invited to refer to Appendix B. A complete simulator call for the considered example lasts approximately 145 seconds.

The calibration of the metamodel is achieved by the use of a CMA-ES procedure [Hansen, 2016]. The latter is an evolutionary approach particularly used for non-linear and/or non convex optimizations. Because of the error risk in the optimization result inherent to evolutionary approaches (local minima convergence), a multi-start architecture is here implemented. The elected best estimator $\boldsymbol{\theta}^*$ is the optimization result which maximizes the likelihood function. Five starts are implemented for the optimization of the hyperparameters relative to the initialization of the AK-DA procedure (*i.e.* calibration of the first metamodel $\hat{d}$ with respect to the initial design of experiments) to minimize the risk of error. For each of the enrichment steps, the optimization of the hyperparameters of the Kriging metamodels are initialized with the optimal value obtained from the previous iteration and from an additional one which is aleatory generated.

Simplified two-dimensional industrial case

This first example is a simplified situation of damage estimation with two evolving environmental parameters: the wind mean speed at hub height u and the wind-wave misalignment θ. The rest of the presented parameters (h_s and t_p) are not considered and the hydrodynamic loading is based on regular wave solicitations (sinusoidal form) with a height of 2 meters and a period of 10 seconds (outside the resonant frequency of the analyzed structure which is approximately equal to 5 seconds). The discretization of environmental parameters is depicted in Table 3.3. This situation leads to a total number of simulations to perform equal to $n_c = 276$. From the chosen discretization, the integration step Δ is computed as:

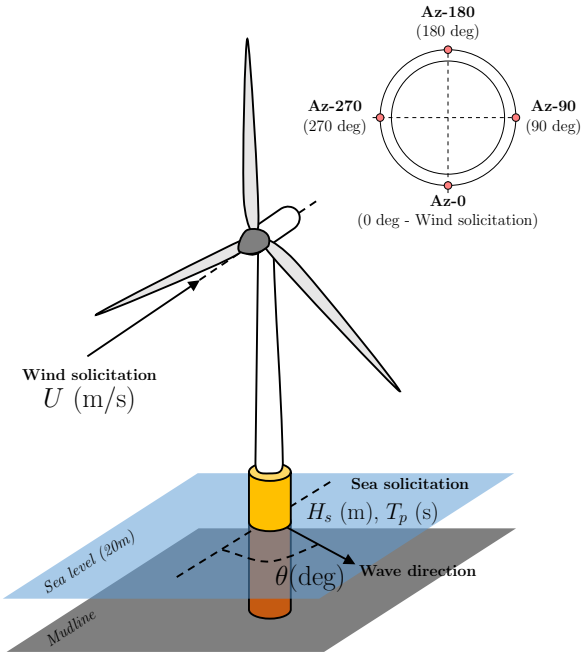

Figure 3.12: Illustration of the NREL 5-MW wind turbine (OC3 monopile) with four environmental parameters: the wind mean speed at hub height u, the wind-sea solicitation misalignment θ, the significant wave height h_s and spectral peak period t_p.

$$\Delta = \delta_u \times \delta_\theta = 1 \text{ m/s } \times 30 \text{ deg } = 30 \text{ m deg/s} \tag{3.13}$$

Parameter	Domain of variation	Discretization δ	Number of cases	Initial grid
u	$[3, 25]$ m/s	1 m/s	23	$\{3, 11, 20, 25\}$ m/s
θ	$[-150, 180]$ deg	30 deg	12	$\{-150, -90, 0, 90, 180\}$ deg
	Number n_c of combinations		276	$n_0 = 20$

Table 3.3: Discretization of the environmental parameter domains considered for the two-dimensional example.

Even in this simplified configuration which only deals with two variable environmental parameters, a single estimation of the global mean damage D requires an important simulation investments, approximately equals to 11 hours using a single core computer. In the present case, the 276 reference computations have been performed for the purpose of validation of AK-DA by the use of distributed simulations over 50 CPUs. As a result, the reference value of the global mean damage D is given as:

$$D = \sum_{i=1}^{n_c=276} d(\boldsymbol{x}_i)\, p(\boldsymbol{x}_i)\, \Delta = 3.81 \times 10^{-13} \tag{3.14}$$

The reference surfaces of the model damage responses d, the probability of occurrence p and the product $p \times d$ are presented in Figure 3.13. The model response is non-linear and the calibration of a metamodel using a coarse grid (*i.e.* with a reduced number of observations) is a difficult task. Firstly, Figure 3.13a evinces a sinusoidal variation in the wind-wave misalignment direction because of the design symmetries. It also depicts a plateau from a

wind speed from about 11 m/s (rated wind speed) to approximately 20 m/s. This is due to the servo reaction of the turbine since it adapts the rotor aerodynamic characteristics and subsequently the acting rotor thrust at the top of the tower. The product $p \times d$ shows an area of interest in Figure 3.13c which concentrates the most important part of the damage D information (which is defined as the sum of the $p \times d$ quantity estimated on the grid of environmental combinations).

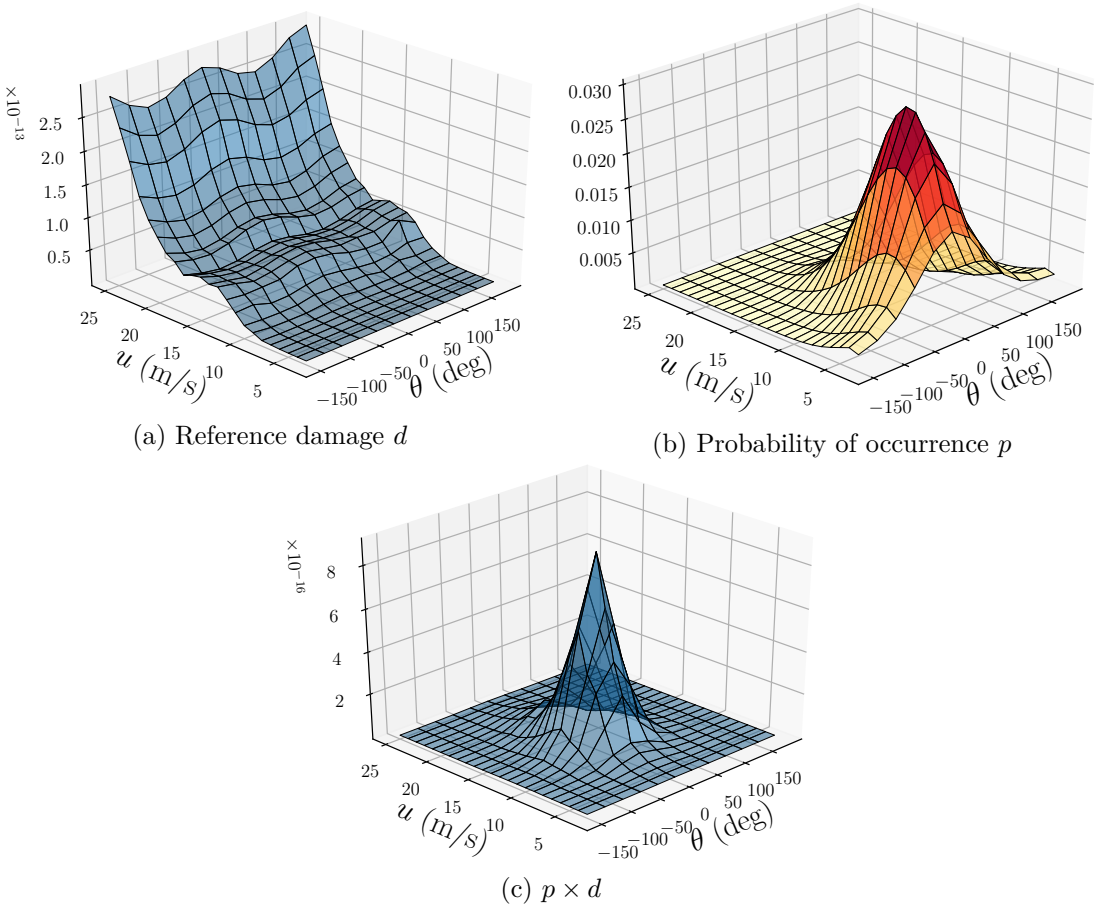

(a) Reference damage d

(b) Probability of occurrence p

(c) $p \times d$

Figure 3.13: Representation of the reference short term damage response d, the probability of occurrence p of the environmental parameters and the probability-weighted damage surface $p \times d$ for the two-dimensional industrial application

The AK-DA procedure is here initialized with a first design of experiments composed of 20 simulations calls located on a reduced grid constructed with 4 wind mean speeds and five wind-wave misalignments as presented in Table 3.3. These samples are selected such as they globally cover the domain of environmental parameters. In addition, expertise have been added to this design of experiments by forcing the initial simulations to provide informational inflow relative to the damage plateau, globally located between $u = 11$ (rated speed) and $u = 20$. The Kriging metamodel is set with a deterministic quadratic basis function and an anisotropic squared exponential correlation function. The enrichment stopping criterion is fixed to $\delta_t = 5\%$.

The initial design of experiments and the AK-DA proposed enrichments are presented in Figure 3.14a. It is observed that the enrichment focuses on the area where the product $p \times d$ is high (enrichments 1 and 3) or where the probability of occurrence is high (enrichments 2, 4 and 5). The increase of model response's information is notable with the evolution of the Kriging

parameters $\boldsymbol{\theta}^*$ depicted in Figure 3.14b. The evolution of these latter shows the progressive information inflow relative to the model response d due to the sequential enrichments. It appears here that the initial design of experiments well captures the model behavior along the misalignment direction θ as the related Kriging hyperparameter shows a quasi constant evolution with the increase of the size of the observational set. This is explained by the initial values taken to fill the first design of experiments with, composed of 5 misalignments over a total of 12 in the complete grid. The Kriging hyperparameter optimized for the misalignment direction presents an initial value far lower than at convergence. The first enrichment allows the metamodel to better capture the damage response d with an enrichment located in the area of high $p \times d$ values (see Figure 3.14a).

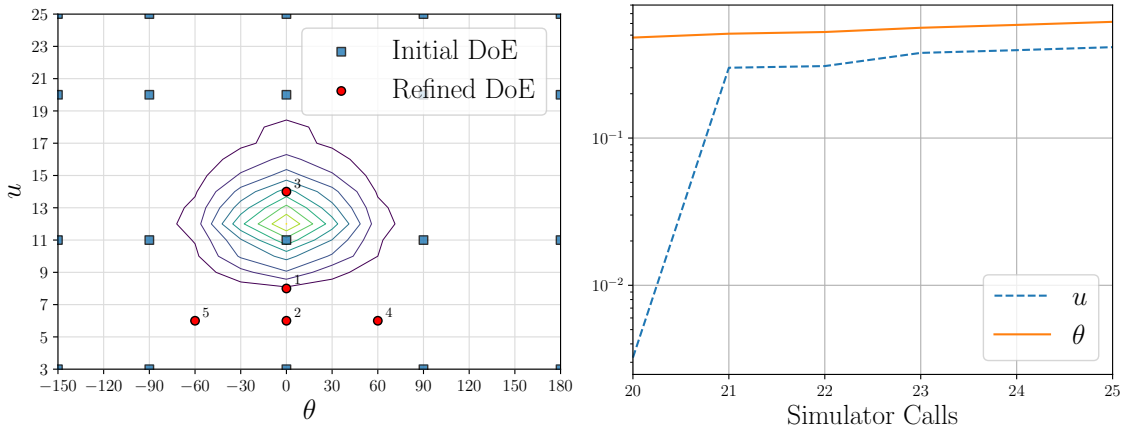

(a) Design of Experiments

(b) Kriging hyperparameters $\boldsymbol{\theta}^*$

Figure 3.14: Illustration of the enrichment procedure of the AK-DA algorithm for the simplified two-dimensional industrial case. The numbering in (a) indicates the enrichment number where the simulation has been integrated in the observational set.

The convergence of the damage estimation of $\hat{D}$ is depicted in Figure 3.15a and the evolution of its coefficient of variation $\delta_{\hat{D}}$ is illustrated in Figure 3.15b. The AK-DA method converges after 5 enrichments ($\delta_{\hat{D}} = 4.49\%$ after the calibration of the metamodel with a total of 25 model observations). The estimation $\hat{D}$ of the global mean damage D is computed as:

$$\hat{D} = \sum_{i=1}^{n_c=276} \hat{d}(\boldsymbol{x}_i)\ p(\boldsymbol{x}_i)\ \Delta = 3.70 \times 10^{-13} \tag{3.15}$$

The relative error is equal to -2.9% with respect to the reference value computed in Eq. 3.14 with a total number of 25 simulator calls which represents a simulator gain of 11.04 with regards to the 276 reference computations. This first industrial illustration shows relevant results on a simplified two-dimensional case. The global behavior of the algorithm has been described all along this example to propose readers a comprehensive illustration of the AK-DA method and more specifically its enrichment strategy. A challenging four-dimensional example is presented in the following to show the potential industrial applicability of the AK-DA procedure.

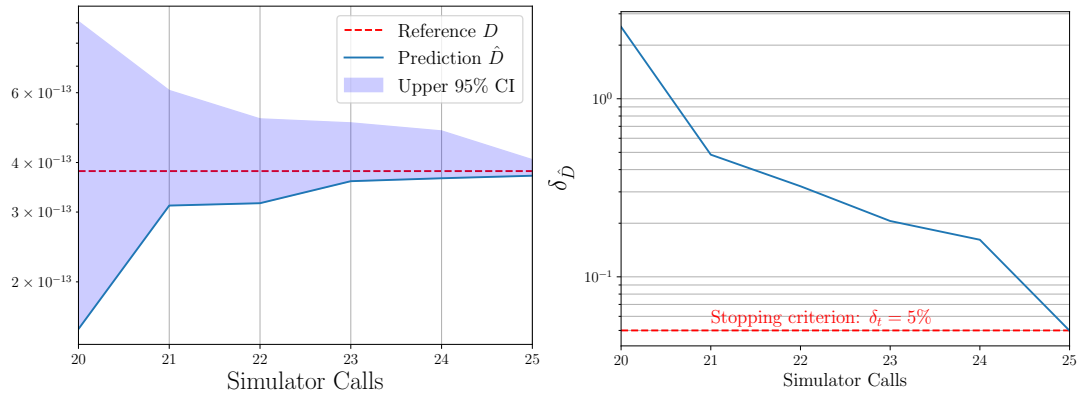

(a) Estimator $\hat{D}$ (b) Coefficient of variation $\delta_{\hat{D}}$

Figure 3.15: Illustration of the convergence behavior of the estimator $\hat{D}$ of the two-dimensional industrial case.

Four-dimensional industrial case

The second example presents a more challenging case dealing with four environmental parameters. In addition to the two parameters of the first illustration u and θ, the wave significant height h_s and the peak spectral period t_p of the Jonswap spectrum are added in the study. Even though the proposed study is performed with the NREL 5MW Monopile, which is a fictional structure of reference, the choice of these four proposed environmental parameters is common in this industrial framework. The discretization of the domains of the four parameters is presented in Table 3.4. The increase of the number of combinations leads to combinatory explosion which makes a reference computation very demanding. To reduce this latter, the parameter θ is here assumed to vary only on a reduced domain of definition between -60 and 60 degrees.

Parameter	Domain of variation	Discretization	Number of cases	Initial grid
u	$[3, 25]$ m/s	1 m/s	23	{3,11,20,25} m/s
θ	$[-60, 60]$ deg	30 deg	5	{-60,-30,0,30,60} deg
t_p	$[5, 15]$ s	1 s	11	{5,8,12,15} s
h_s	$[0.5, 4]$ m	0.5 m	8	{0.5,1.5,2.5,4} m
	Number n_c of combinations		10 120	$n_0 = 320$

Table 3.4: Discretization of the environmental parameters u, θ, h_s and t_p for the four-dimensional illustration of the AK-DA procedure.

The total number of environmental combinations to consider is equal to 10120, each corresponding to a simulator call of about 145 seconds. A reference value of the global mean damage D has been computed using a high performance computing for the purpose of validation and leads to:

$$D = \sum_{i=1}^{n_c=10120} d(\boldsymbol{x}_i)\ p(\boldsymbol{x}_i)\ \Delta = 8.475 \times 10^{-8} \tag{3.16}$$

The Kriging metamodel's parameters remain the same as the two-dimensional example (*i.e.* a quadratic deterministic function with anisotropic squared exponential correlation) and the initial design of experiments is composed of 320 model observations. In this case, the

proposed initial grid is created to provide a global covering of the environmental parameter definition space. As for the two-dimensional industrial illustration, each of the values of the misalignment θ are integrated to the grid and the values for the wind mean speed are the same as previously presented. The two other parameters, namely the spectral peak period t_p and the significant wave height h_s, are regularly discretized.

The convergence of the estimation $\hat{D}$ is depicted in Figure 3.16a. As for the two-dimensional example, it shows a progressive evolution to the reference value D. Once the AK-DA procedure is initialized, the design of experiments is iteratively enriched. The initial prediction, only computed from the 320 initial model observations, is equal to 3.26×10^{-7} which is far greater than the reference estimation. Step by step, the design of experiments is enriched and the estimation progressively converges to the reference value. The evolution of the coefficient of variation $\delta_{\hat{D}}$ is depicted in Figure 3.16b and shows an effective behavior of the strategy of enrichment with a progressive decrease of $\delta_{\hat{D}}$. As a matter of fact, the choice of the learning procedure has been motivated by the iterative reduction of the variance of estimation and thus of its coefficient of variation which is well described in the presented example. As for the two-dimensional example, the evolution of the Kriging hyperparameters regrouped in $\boldsymbol{\theta}^*$ and presented in Figure 3.16c shows the evolution of the metamodel response's information. Each of these parameters present small evolutions after each enrichments of the design of experiments. Moreover, this depicts a progressive knowledge inflow of the model responses. The misalignment related parameter is quasi-constant in this example. This is explained by the important amount of information initially provided to the metamodel by the complete screening of its possibilities (the initial grid is composed of the 5 misalignment values). After 65 enrichments, the coefficient of variation $\delta_{\hat{D}}$ of the estimator $\hat{D}$ reaches the convergence criterion of 5% (see Figure 3.16b). The computation of the estimation $\hat{D}$ is proceeded as:

$$\hat{D} = \sum_{i=1}^{n_c=10120} \hat{d}(\boldsymbol{x}_i)\ p(\boldsymbol{x}_i)\ \Delta = 8.260 \times 10^{-8} \tag{3.17}$$

This results is accurate with a relative error of -2.54% with regards to the reference value presented in Eq. 3.16. In terms of numerical investment, the reduction is important with a total number of 385 simulation calls (observation of the true function d) composed of the 320 elements of the initial grid and 65 enrichments provided by the AK-DA procedure. This results as a numerical gain in simulator calls of approximately 26 (in terms of ratio).

The presented results is balanced by the computation time required for the calibration and the enrichment steps which can not be neglected with regards to the simulator call duration. Indeed, two main steps of the AK-DA algorithm require important computational investments: the calibration of the Kriging hyperparameters and the computation of the variance contribution $\mathcal{C}$ for each of the n_c environmental parameters. The estimation of the variance contributions requires the evaluation of the entire autocovariance matrix of size $n_c \times n_c$. In the presented example, this leads to more than 100 000 000 elements. As an illustration, the evolution of the post-processing duration defined from the end of the simulator call to the selection of the next enrichment simulation to perform is depicted in Figure 3.16d. It is observed that each post-processing step lasts from 45 to 70 seconds

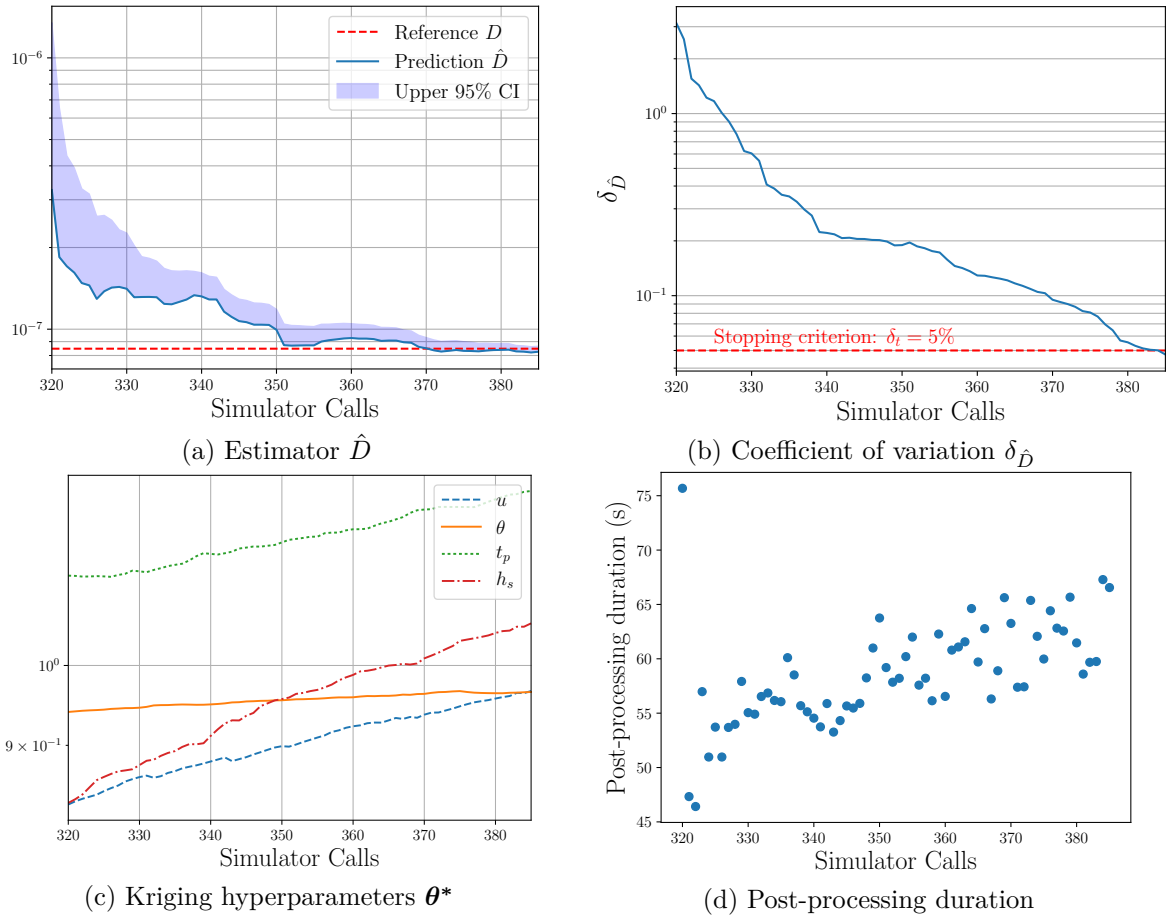

(a) Estimator $\hat{D}$

(b) Coefficient of variation $\delta_{\hat{D}}$

(c) Kriging hyperparameters $\boldsymbol{\theta}^*$

(d) Post-processing duration

Figure 3.16: Results of the AK-DA procedure applied to the estimation of the cumulated damage D for the 4-dimensional illustration.

(excepted the initial post-processing which last approximately 75 seconds because of the five runs of the CMA-ES optimization procedure). Furthermore, the duration globally increases as the size of the observational set increases. Compared to the 145 seconds required for a simulator call d, this order of magnitude represents a long duration which can not be neglected when practically deploying the AK-DA method.

In this section, the Adaptive Kriging for Damage Assessment has been introduced, described and discussed on different examples to show readers its industrial interest and the potential reduction in numerical investment it can provide. Based on an initial design of experiments of reduced size which choice is of prime importance (see Section 3.2.1 and Section 3.2.6), this procedure iteratively enriches the observational set with the aim of reducing the uncertainty in the estimation $\hat{D}$ of the quantity of interest D. Its direct application, either on academical and industrial examples, shows an important reduction of the computational effort by significantly decreasing the number of short term damage computations whilst accurately estimating the global mean damage D. Even though the performances of the proposed method are fruitful (gain in simulator calls of 26 with a relative error of -2.54% compared to the reference value in the four-dimensional example), the duration of the post processing can not be neglected. To keep on reducing the computational effort, the next section presents an alternative architecture which allows one to consider several simulations at each enrichment step of the design of experiments. The multi enrichment strategy is proposed to reduce the

AK-DA iterations and so the post-processing investment.

3.3 Multi-enrichment strategy for parallel computing

To keep on reducing the simulation costs of the damage estimation computed by the AK-DA method, this section presents a multi-enrichment strategy which aims at allowing one to iteratively augment the design of experiments with several model observations at the same time. The motivations of this extension are firstly described before introducing the "area of influence" approach proposed in this thesis. To finish, an illustrative case is presented to highlight the performances of this multi-enrichment strategy for industrial applications.

3.3.1 Motivation for multi-enrichment in the context of parallel computing

The former version of the AK-DA methodology, which is presented in this chapter, proposes an iterative architecture which enriches the initial design of experiments with additional model observations elected from the learning criterion based on the variance contribution. This methodology shows interesting results with noteworthy reductions of numerical investments by drastically reducing the number of short term damage d simulator calls in industrial examples, as presented in Section 3.2.7. The proposed method only elects one environmental parameter combination at a time for the enrichment of the design of experiments which limits the computational gains this method could industrially provide.

Modern computers are now composed of several CPUs which allow engineers to perform multiple independent simulations at the same time. Simultaneously, high performance computing devices (HPC) permit the massive distribution of simulations over hundreds of centralized CPUs. In this thesis, the use of these computational possibilities are encouraged by the independence of the short term damages d computations. Hence, whereas a single d model response is observed at each enrichment steps as proposed in the former AK-DA architecture, several short term damages can be computed simultaneously.

Multiple advantages of this parallel computing are to be expected. First, each of enrichment of the design of experiments is expected to be more informative and, as a result, the number of iterations is expected to decrease. Readers have to keep in mind that the calibration of the metamodel $\hat{d}$ which is performed after each enrichment can be demanding when the dimension of the problem increases. Hence, the reduction of the number of enrichments (equals to the number of metamodels to calibrate) is a significant source of numerical investment reduction. Also, the increase of the information quantity provided by each of the model observational should somewhat regularize the convergence of the estimation, *i.e.* the latter should have a more monotonous behavior.

The choice of the proposed multi-enrichment strategy has been motivated by the goal of selecting sets of enrichments which maximize the model response information. As an alternative to the so-called k-means clustering approach proposed in several studies (see *e.g.* Lelièvre et al. [2018]; Schöbi et al. [2016]), this section proposes to perform this selection from

the analysis of the correlation between environmental parameters directly provided by the Kriging metamodel calibration. This approach is subsequently named "area of influence".

3.3.2 Area of influence for multi-enrichment strategy

The idea of the proposed strategy is to take advantage of the knowledge of the correlation matrix provided by Kriging. The objective is to select a set of enrichments which maximizes the information inflow. The multi-enrichment procedure is based on the assumption that an enrichment set of observations is optimal if each of its model observations is weakly correlated with the other observations of the aforementioned set. More formally, let $\boldsymbol{\mathcal{X}}_e = \{\boldsymbol{x}_1^*, \dots, \boldsymbol{x}_{n_e}^*\}$ be an enrichment set composed of n_e combinations of environmental parameters at a given iteration in the adaptive procedure. The information inflow is assumed to be maximal if the absolute cross correlations between the enrichment inputs are sufficiently small. Setting a "restriction parameter" $r_0 \in [0, 1]$ which quantifies the tolerated cross-correlation, two distinct inputs $\boldsymbol{x}_1$ and $\boldsymbol{x}_2 \in \mathcal{D}_{\boldsymbol{x}}$ should provide weak correlation in the model responses if:

$$|r\Big(\hat{d}(\boldsymbol{x}_1), \hat{d}(\boldsymbol{x}_2)\Big)| \leq r_0 \tag{3.18}$$

The greater r_0 is, the less restrictive the method results with decreasing the admitted *area of influence* of each inputs. This assumption does not guarantee the independence of the model observations proposed by the enrichment design of experiments but reduces the risk of redundant information according to the proposed learning criterion. Informative sets of enrichments can in fact be iteratively constructed based on the information of the absolute variance contribution $|\mathcal{C}|$ of the AK-DA algorithm.

Practically, the first simulation $\boldsymbol{x}_1^*$ is chosen by maximizing the absolute contribution quantity as performed for the single enrichment strategy presented so far. This is performed on a domain of research $\mathcal{D}_1$ initially equals to the domain of definition of the environmental parameters $\mathcal{D}_{\boldsymbol{x}}$:

$$\boldsymbol{x}_1^* = \underset{\boldsymbol{x} \in \mathcal{D}_1}{\operatorname{argmax}} \, |\mathcal{C}(\boldsymbol{x})| \tag{3.19}$$

Once the first learning simulation is elected, the new domain of research is restricted to environmental combinations with a small cross-correlation with the first learning point $\boldsymbol{x}_1^*$ and given a value r_0. The second domain of research, here noted $\mathcal{D}_2$ is deduced:

$$\mathcal{D}_2 = \Big\{\boldsymbol{x} \in \mathcal{D}_1 \text{ such as } |r(\boldsymbol{x}_1^*, \boldsymbol{x})| \leq r_0)\Big\} \tag{3.20}$$

The second model observation $\boldsymbol{x}_2^*$ to be included in the enriched design of experiments with, is elected by the optimization of the absolute variance contribution over the restricted domain of research $\mathcal{D}_2$ as proceeded for the first point (Eq. 3.19). Iteratively, a set of enrichment observations $\boldsymbol{\mathcal{X}}_e = \{\boldsymbol{x}_1^*, \dots, \boldsymbol{x}_{n_e}^*\}$ is constructed until either its size n_e exceeds a given limit enrichment size n_e or the complete domain of definition is influenced by the environmental parameters contained in the enrichment set of experiments ($\mathcal{D}_i = \emptyset$). The complete and formal

presentation of the multi-enrichment procedure implemented here is presented in Algorithm 1. Once this set of enrichments is built, the short term damage values $d(\boldsymbol{x})$ for all $\boldsymbol{x} \in \boldsymbol{\mathcal{X}}_e$ are computed in parallel with multi-CPU devices.

Algorithm 1 *Area of influence* for multi-enrichment strategy for the AK-DA algorithm

Parameterization: Defined a correlation threshold r_0
Initialization: $i = 1$, $\mathcal{D}_1 = \mathcal{D}_{\boldsymbol{x}}$, $\boldsymbol{\mathcal{X}}_e = \{\}$
while ($i < n_e$ or $\mathcal{D}_i \neq \emptyset$) **do**
Selection of the i-th enrichment observation with the optimization of the absolute variance contribution:

$$\boldsymbol{x}_i^* = \underset{\boldsymbol{x} \in \mathcal{D}_i}{\operatorname{argmax}} \, |\mathcal{C}(\boldsymbol{x})|$$

Research of the environmental parameters of $\mathcal{D}_i$ not under the influence (in the correlation sense) of $\boldsymbol{x}_i^*$ and definition of the $i+1$-th domain of research $\mathcal{D}_{i+1}$:

$$\mathcal{D}_{i+1} = \left\{ \boldsymbol{x} \in \mathcal{D}_i \text{ such as } |r(\boldsymbol{x}_i^*, \boldsymbol{x})| \leq r_0 \right\}$$

Storing of the i-th learning point: $\boldsymbol{\mathcal{X}}_e := \{\boldsymbol{\mathcal{X}}_e; \boldsymbol{x}_i^*\}$
$i = i + 1$
end while

As an illustrative example, this strategy is performed for the one-dimensional example presented in Section 3.2.5. The absolute variance contribution computed after the first enrichment and depicted in Figure 3.4 (right hand figure) is here used to show the behavior of the proposed multi-enrichment strategy. The targeted size of the set of simultaneous enrichments is here assumed to be $n_e = 5$. The results of the method for different values of the restriction parameter r_0 (0.9, 0.5, 0.3 and 0.1) is presented in Figure 3.17. For the four depicted situations, each of the selected enrichment inputs is represented by a colored square and the absolute variance contribution computed for influenced inputs are colored in the same manner.

In the first situation (Figure 3.17a), the restriction parameter r_0 is large and equal to 0.9. This configuration results in a reduction of the influence distance and allows one to iteratively construct a set of enrichments composed of 5 observations. One should note that by choosing this restriction parameter, the entire input space is not covered and a subset approximately defined from $x \approx 2$ to $x \approx 4.5$ is not "under influence" of any selected enrichment simulations. By reducing the parameter r_0, the influence distance increases and the domain of definition $\mathcal{D}_{\boldsymbol{x}}$ can be entirely covered in terms of selected inputs' influence. The choice of a restriction parameter equal to 0.5, 0.3 and 0.1 respectively leads to a selection of 4, 3 and 2 enrichment inputs to be computed simultaneously. As a conclusion, the choice of the parameter r_0 is crucial to have a trade-off between optimal coverage regarding the dependencies of model responses and computational capacity, here represented by the number of possible parallel simulations n_e.

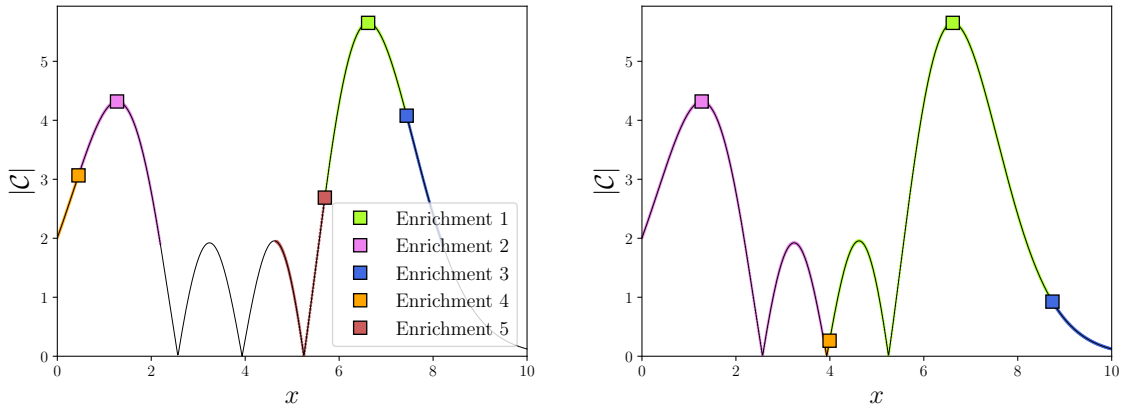

(a) $r_0 = 0.9$ (b) $r_0 = 0.5$

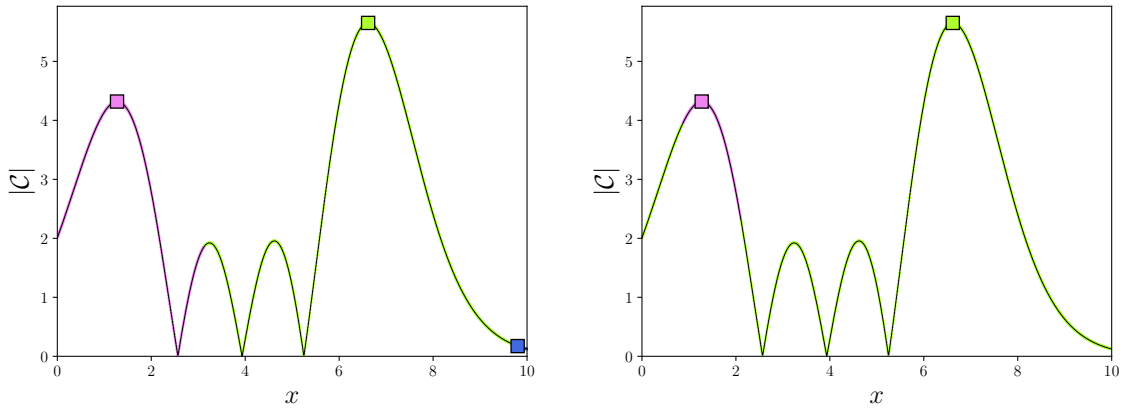

(c) $r_0 = 0.3$ (d) $r_0 = 0.1$

Figure 3.17: Illustration of the multi-enrichment procedure based on the influence reduction.

3.3.3 Illustration of the performances on the four-dimensional industrial example

To illustrate the performances of the multi-enrichment strategy introduced in this section, a comparative study is proposed in the following. Hereafter, the four-dimensional case presented in Section 3.2.7 is performed with the AK-DA procedure implemented with a varying enrichment size n_e from 1 (results previously obtained in Section 3.2.7) to 8. For each analysis, the same initial design of experiments is considered. It corresponds to the initial design of experiments used when implementing the adaptive Kriging procedure based on single enrichment. The Kriging parameterization remains unchanged. The enrichment selection is here performed with a restriction parameter r_0 equals to 0.1. At convergence, the number of AK-DA iterations n_{iter} and the number of simulator calls, *i.e.* the number of model observations n_{obs}, are used to compare the performances of the algorithm. The results of the proposed simulations are summarized in Table 3.5. For validation purpose, the relative error ("Rel. Error") is computed from the reference value D and its estimation $\hat{D}$ as before.

An obvious remark is the reduction of the number of iterations n_{iter} when increasing the number of simultaneous enrichments per iteration n_e. For each of studied cases, the maximal size of the enrichment vector has been reached and as a direct consequence, the total number of simulator calls n_{obs} increases when comparing with $n_e = 1$. This is due to the selection of non optimal observations with respect to the variance contribution criterion. The maximal reduction in terms of number of iteration is obtained for $n_e = 8$. This leads to a convergence of

Enrichment size	n_{iter}	n_{obs}	$\hat{D}$	Rel. Error
1	65	$320 + 65 = 385$	8.260×10^{-8}	-2.54%
2	34	388	8.283×10^{-8}	-2.27%
3	22	386	8.362×10^{-8}	-2.54%
4	17	388	8.535×10^{-8}	0.71%
5	14	390	8.356×10^{-8}	-1.41%
6	12	392	8.298×10^{-8}	-2.09%
7	11	397	8.269×10^{-8}	-2.43%
8	9	392	8.515×10^{-8}	-0.70%

Table 3.5: Consideration of the multiple enrichment strategy within the AK-DA procedure.

the AK-DA algorithm after only 9 iterations and a total number of simulator calls $n_{obs} = 392$. In all the presented situations, the multi-enrichment strategy leads to comparable accuracy when analyzing the global mean damage estimation. The absolute relative errors are between 0.70 and 2.54% which is comparable to the absolute relative error of the single enrichment strategy equals to 2.54%.

As explained before, the implementation of the proposed multi-enrichment strategy aims at reducing the total duration of the estimation procedure by decreasing the number of iterations n_{iter} the AK-DA algorithm requires to converge. The idea is to select vectors of enrichments which maximize the information inflow to efficiently calibrate the Kriging metamodel of the short term damage d with regards to the quantity of interest D. To have an indication of the efficiency of the influence area method, the iteration speed-up is computed for each of the situations studied in this example, it is here defined as:

$$\text{speed-up}(n_e) = \frac{n_{iter}(n_e = 1)}{n_{iter}(n_e)} \tag{3.21}$$

This quantity provides to a certain extent an information regarding the relevance of the selected vectors of enrichments in the sense of the iteration gain they provide. A non informative selection of the sets of simultaneous enrichments would lead to a small reduction of the total number of iterations and a speed-up close to 1. On the contrary, an optimal selection would linearly decrease the number of iterations with a factor equal to the size of the enrichment set n_e. As a consequence, the defined speed-up would be close to n_e. The evolution of the iteration number n_{iter} and the related speed-up are depicted with respect to the evolving size n_e of the enrichment sets in Figure 3.18.

Figure 3.18a shows that the efficiency of the proposed method, when a number $n_e \leq 4$ is chosen, is optimal with reduction of the number of iterations proportional to the size of the enrichment designs of experiments. For these values, the computed speed-up presented in Figure 3.18b shows the efficiency of the method with gains in terms of the ratio of number of iterations close to the optimal speed-up represented by the black dashed line. For these sizes of enrichment vectors, the information is well extracted from the absolute variance contribution learning function and the number of redundancies can be neglected. When considering an higher enrichment size, it can be observed that the efficiency of the method decreases with a stabilization of the number of iterations required for the AK-DA method to converge between 9 ($n_e = 8$) and 14 ($n_e = 5$). As a consequence, the speed-up is not as

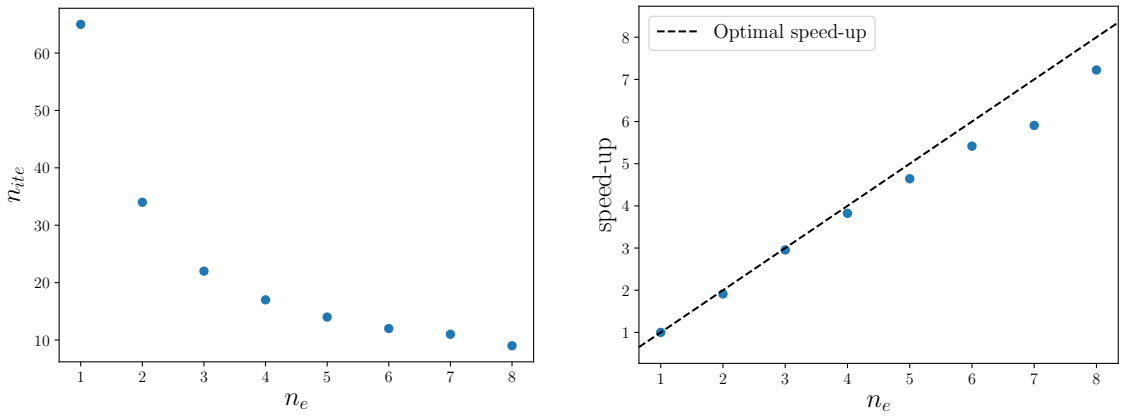

(a) n_{ite} (b) speed up

Figure 3.18: Illustration of the evolution of the required number of iterations n_{ite} of the AK-DA procedure to reach the convergence and the related iterative speed-up for the different sizes n_e of the enrichment sets.

close to the optimal value as previously presented for a smaller enrichment size ($n_e \leq 4$). By increasing a bit too much the number of simultaneous simulations, the risk is to select environmental combinations which do not bring a valuable contribution in terms of reduction of the coefficient of variation $\delta_{\hat{D}}$. This may be explained by the reduction of the adaptability of the algorithm which selects an increasing number of simulations based on the same learning function and without being updated. For each of the enrichments, the algorithm perform less informative simulations which present redundancies with regards to the informational inflow. For each size n_e of the set of experiments, the convergence curves of the estimation of $\hat{D}$ are presented in Figure 3.19. It can be observed that the use of the multi-enrichment strategy allows one to regularize the convergence of the estimation of the quantity of interest.

As a conclusion, this section presents an extension of the AK-DA method to consider several enrichment simulations at the same time. This development is mainly motivated by the increasing computation capacities engineers now possess with the possibility of simulation distribution over several computers. The idea lies also in reducing the number of iterations associated with the AK-DA procedure. As a matter of fact, each of the enrichment step requires the calibration of a Kriging metamodel to approximate the complete short term damage response d and to compute the absolute variance contribution based on the evaluation of the complete Kriging autocovariance matrix which can be demanding. By implementing the area of influence method for multiple enrichments, users can iteratively add sets of enrichments with a reduced cost by directly using the results of the Kriging metamodel calibration obtained at a given iteration, and more precisely the estimated correlation between model approximations. The performances of this strategy result in fruitful iteration gains with regards to a reference single enrichment strategy by proposing informative and low correlated simulations to perform. To finish this chapter, an implementation of the AK-DA algorithm for the simultaneous analysis of multiple structural locations is presented in Section 3.4.

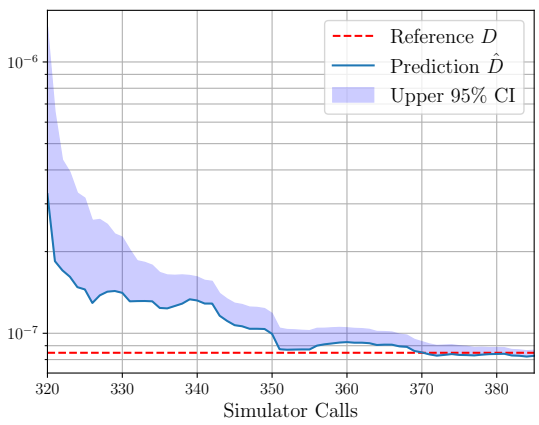

(a) $n_e = 1$

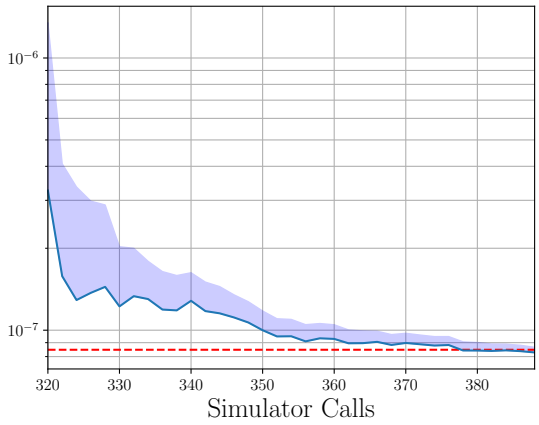

(b) $n_e = 2$

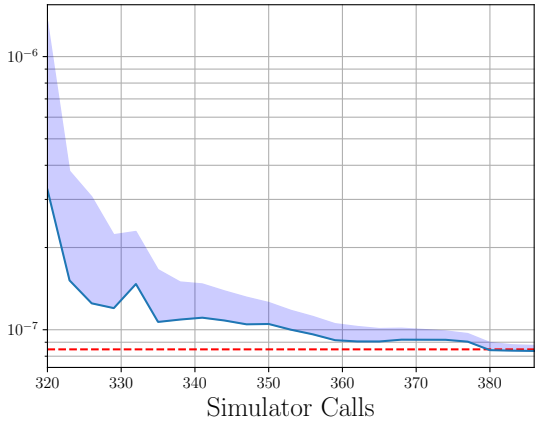

(c) $n_e = 3$

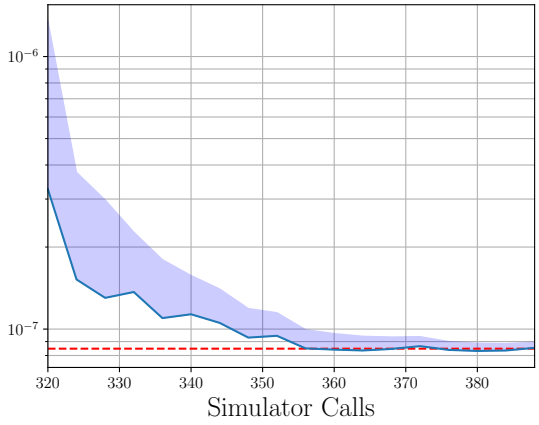

(d) $n_e = 4$

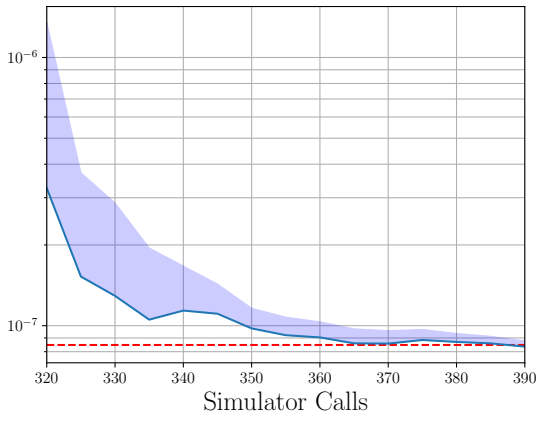

(e) $n_e = 5$

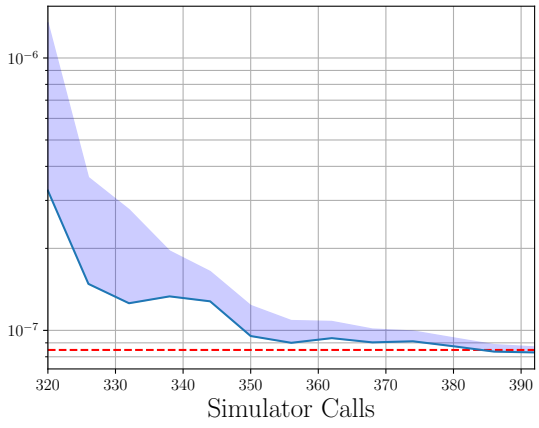

(f) $n_e = 6$

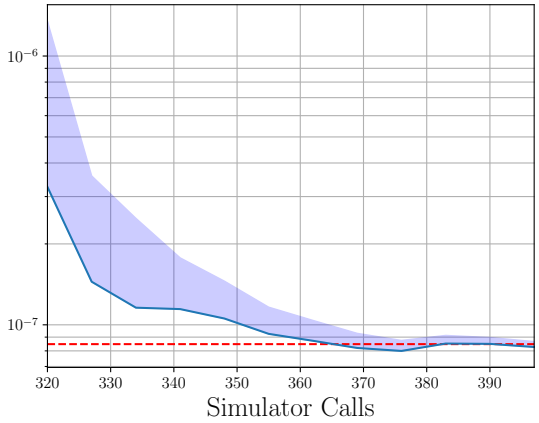

(g) $n_e = 7$

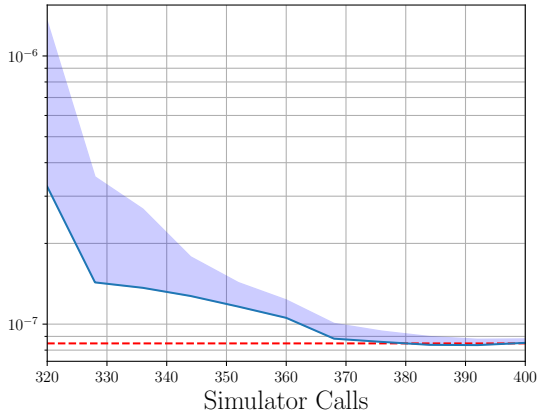

(h) $n_e = 8$

Figure 3.19: Convergence of the global mean damage estimator $\hat{D}$ for different size of the set of simultaneous enrichments.

3.4 Multiple structural location analysis with the AK-DA algorithm

So far, the AK-DA procedure has been implemented and illustrated in the particular case of single location analyses to propose reader a comprehensive description of its principle. As a result, the previous implementations focus on the estimation of a single global mean damage D. As initially introduced in Section 3.1, several locations of interest may have to be analyzed and thus a series of global mean damages D_k with $k \in \{1, \dots, n_s\}$ have to be computed. The first obvious solution is to perform independent AK-DA analyses, *i.e.* to run the AK-DA algorithm sequentially (one location at a time). However, it can not be optimal since each simulated environmental result in the computation of Von Mises stresses at any location of the structure. From this, the determination of the short term damages for each of the location of interest only requires a negligible investment. This section therefore describes an approach for using the AK-DA procedure for the simultaneous estimations of several global mean damages in an efficient manner. In the following, the global architecture of the proposed algorithm is firstly described. To better explain its implementation, the piloting location strategy is then described and the adaptations of the enrichment steps as well as the modification of the stopping criterion are explained. To finish, an illustration of the performances of the proposed method is presented focusing on the four-dimensional industrial case introduced in this chapter.

3.4.1 Global presentation of the multiple structural location analysis

The proposed extension is a generalization of the AK-DA procedure initially introduced for the prediction of the global mean damage D in the particular case of a single structural location analysis ($n_s = 1$). The algorithm is extended to the simultaneous predictions for different structural locations (*i.e.* $n_s > 1$) by computing n_s Kriging predictions of the short term damages d_i, with all the metamodels calibrated on the same environmental inputs $\boldsymbol{\mathcal{X}}_{obs}$ of the design of experiments $\{\boldsymbol{\mathcal{X}}_{obs}, \boldsymbol{d}_{i,obs}\}$ with $i \in \{1, \dots, n_s\}$. The numerical chain presented in Section 1.5 allows to simultaneously compute the short term damages at n_s structural locations for a given input (global simulation of the structural reactions and parallel post-processing for each of the locations of interest). This methodology is designed to globally approximate each of the global mean damage quantity D_k at the same time. The implementation strategy is proposed in Figure 3.20. As the former AK-DA version implemented for the analysis of a single structural location, this methodology is based on a sequential enrichment of a design of experiments $\{\boldsymbol{\mathcal{X}}_{obs}, \boldsymbol{d}_{k,obs}\}$. At each steps, n_s Kriging metamodels are calibrated with respect to their design of experiments from which the estimations of $\hat{D}_k$ are computed.

Compared to the single enrichment version, this methodology differs with a slightly more complex enrichment based on the analysis of "piloting locations" and described in Section 3.4.2. To be adapted to the global approach, the stopping criterion is also modified as described in Section 3.4.3.

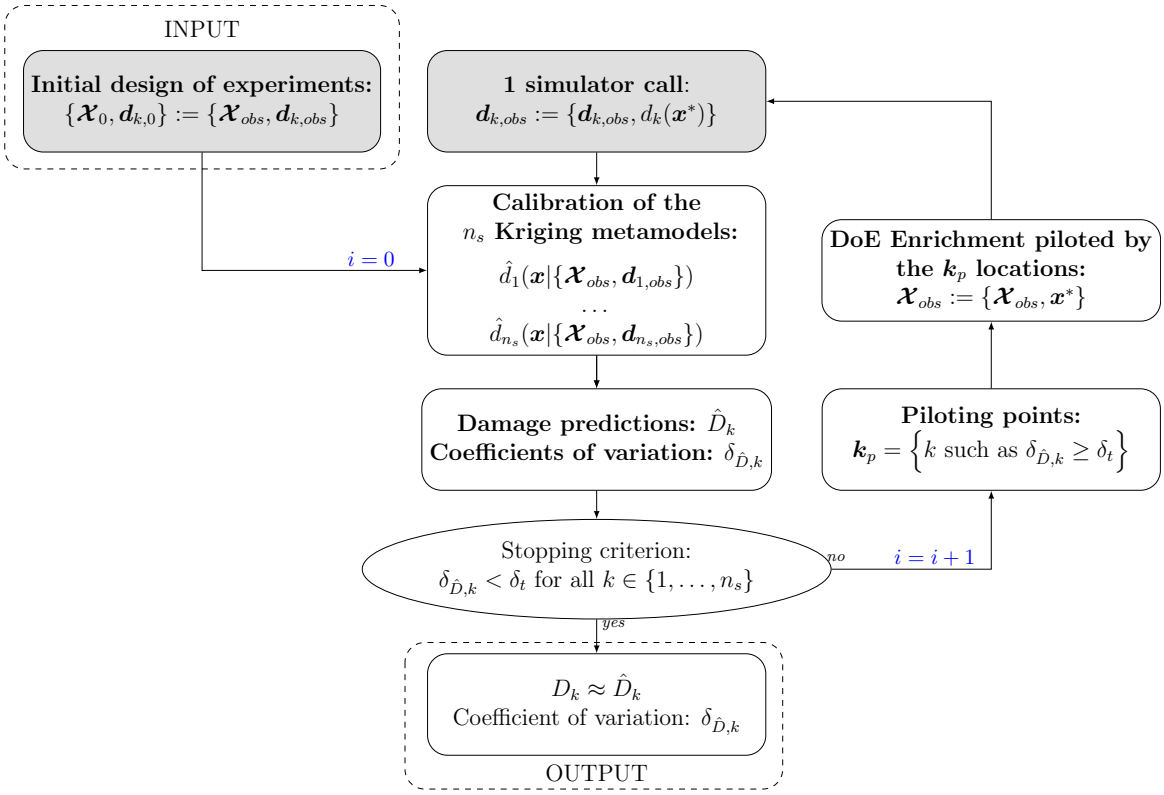

Figure 3.20: Presentation of the multi-location extension of the AK-DA algorithm.

3.4.2 Piloting location enrichment strategy

For each iterations of the AK-DA procedure here implemented for the simultaneous analysis of multiple structural locations, the enrichment strategy only focuses on the locations k for which the estimator $\hat{D}_k$ presents an elevated coefficient of variation. In this section, the coefficients of variation of each of the estimators $\hat{D}_k$ are noted $\delta_{\hat{D},k}$. In the case where an estimator $\hat{D}_k$ presents an important uncertainty, *i.e.* $\delta_{\hat{D},k} \geq \delta_t$, the related structural location is considered as a "piloting location" and is used for the enrichment strategy. The indices of the piloting locations are regrouped in a piloting index vector noted $\boldsymbol{k}_p$ of size n_p which is defined as:

$$\boldsymbol{k}_p = \left\{k \in \{1, \ldots, n_s\} \text{ such as } \delta_{\hat{D},k} \geq \delta_t\right\} \tag{3.22}$$

From the selection of these piloting points, the enrichment strategy aims at selecting the most valuable simulation (or set of simultaneous simulations as presented in Section 3.3) which reduces the most the variances of piloting point's estimators $\hat{D}_{\boldsymbol{k}_p}$. Normalized absolute contributions, hereafter noted $|\bar{\mathcal{C}}|$, are used to quantify the global variance reduction a simulation can provide with regards to the n_p piloting locations. This quantity then verifies:

$$\sum_{i=1}^{n_c} |\bar{\mathcal{C}}_k(\boldsymbol{x}_i)| = 1 \tag{3.23}$$

for each of the piloting locations, *i.e.* for all $k \in \boldsymbol{k}_p$. The enrichment procedure uses this absolute contribution to elect the simulation to perfom relying on the enrichment procedure

described as:

$$\boldsymbol{x}^* = \underset{\boldsymbol{x}\in\mathcal{D}_{\boldsymbol{x}}}{\operatorname{argmax}} \sum_{k=1}^{n_s} \mathbb{1}_{\boldsymbol{k}_p} |\bar{\mathcal{C}}_k(\boldsymbol{x})| \tag{3.24}$$

where $\mathbb{1}_{\boldsymbol{k}_p}$ is the indicator function, equals to 1 if the index is contained in the vector of piloting indices $\boldsymbol{k}_p$ and 0 elsewhere. By implementing this enrichment strategy, each of the structural locations for which the estimator $\hat{D}_k$ presents an high coefficient of variation $\delta_{\hat{D},k}$ is equally treated.

3.4.3 Adaptation of the stopping criterion

Comparing to the former version of the AK-DA algorithm, several structural locations are treated simultaneously. The enrichment strategy is performed until each of the coefficients of variation $\delta_{\hat{D},k}$ of estimators $\hat{D}_k$ becomes smaller than a threshold value δ_t. For all $k \in \{1,\ldots,n_s\}$, the stopping condition then reads:

$$\delta_{\hat{D},k} < \delta_t \tag{3.25}$$

3.4.4 Illustration on the four-dimensional industrial application

The performance of this method is presented through the four-dimensional industrial example introduced in this chapter. The evolution of the environmental parameters remain the same as well as the work-flow implemented to obtain the short term damage estimation d for a given combination of environmental parameters $\boldsymbol{x} \in \mathcal{D}_{\boldsymbol{x}}$. A number of $n_s = 4$ structural locations is here considered on the monopile mud-line: the Az-0, Az-90, Az-180 and Az-270 respectively located at the monopile periphery for azimuths equal to 0, 90, 180 and 270 degrees (see Figure 3.12). The reference values of the global mean damages D_k with $k \in \{1,\ldots,n_s\}$ is computed with the help of distributed simulations. Two approaches are compared: the independent approach which consists in the independent assessment of the four AK-DA estimations of D_k and the introduced more global approach. In both cases, a multi-enrichment procedure with $n_e = 4$ is implemented to speed up the AK-DA convergence and reduce the post processing simulation investments.

The results obtained from the independent approach are proposed in Table 3.6. For each of the considered structural locations, the number of simulator calls varies from 388 (mud-line Az-0) to 428 (mud-line Az-180) with respectively 17 and 27 iterations before convergence. The relative errors of the global mean damages D_k regarding their reference values are all less than 5% which demonstrates again the capability of the AK-DA procedure to effectively approximate the quantity of interest in different situations. The total number of simulator calls for each of the analyses reaches 1624 composed of 563 distinct simulations.

The implementation of the proposed approach has been done and the performances regarding accuracy of predictions and total number of calls and iterations are presented in Table 3.7. At convergence, the relative error of the estimations are comparable with the

Structural location	Simulator calls	AK-DA iterations	$\hat{D}$	D	Relative error
Mud-line Az-0	$320 + 17 \times 4 = 388$	17	8.55×10^{-8}	8.48×10^{-8}	0.83%
Mud-line Az-90	$320 + 22 \times 4 = 408$	22	1.38×10^{-9}	1.39×10^{-9}	−0.72%
Mud-line Az-180	$320 + 27 \times 4 = 428$	27	3.57×10^{-8}	3.41×10^{-8}	4.7%
Mud-line Az-270	$320 + 20 \times 4 = 400$	20	1.39×10^{-9}	1.39×10^{-9}	0%
Total	1624 (563 distinct)	86			

Table 3.6: Results of the independent AK-DA multi-location analysis.

independent simulations presented before with an absolute maximum of 3.60% (Mud-line Az-90).

Structural location	Simulator calls	AK-DA iterations	$\hat{D}$	D	Relative error
Mud-line Az-0	444	31	8.40×10^{-8}	8.48×10^{-8}	−0.94%
Mud-line Az-90			1.34×10^{-9}	1.39×10^{-8}	−3.60%
Mud-line Az-180			3.42×10^{-8}	3.41×10^{-8}	0.29%
Mud-line Az-270			1.38×10^{-8}	1.39×10^{-8}	−0.72%

Table 3.7: Results of the global AK-DA multi-location analysis.

Focusing on the number of iterations n_{ite} and the related number of simulator calls n_{obs}, this approach displays a more efficient behavior with a total of 31 iterations corresponding to 444 simulator calls in total. Compared to the independent computations, this represents a sigificant gain regarding the number of iterations of 2.7, which represents an important reduction of the computational investment by dividing by 2.7 the number of Kriging metamodels to calibrate. The reduction of the simulation calls here represents approximately 20% with respect to the independent implementation. For the global method proposed in this section, the convergence of the estimators are presented in Figure 3.21 and the evolution of the piloting points of the algorithm is depicted in Figure 3.22. In this latter figure, for each of the algorithm iterations, points indicate if the structural location is considered or not in the piloting locations. It can be observed that the strategy well orientates the enrichements and only focuses on the structural locations for which the uncertainty is important. In this example, the first estimation to converge is the one related with the Az-0 location which is not considered after 388 simulator calls (even if its coefficient of variation is checked after each of the metamodel updatings). From this point, only the three other structural points are considered as piloting locations. The estimation of the global mean damage at the Az-90 location converges after 432 simulator calls. Finally the two last structural points are considered as piloting location until the stopping criterion is reached (444 simulator calls).

To sum up, this last section introduced a possible implementation of the AK-DA methodology for the simultaneous estimation of several mean global damages D_k corresponding to n_s structural locations ($k \in \{1, \ldots, n_s\}$). Compared to n_s independent AK-DA strategy, this architecture allows one to reduce the global numerical cost by drastically reducing the number of demanding iterations.

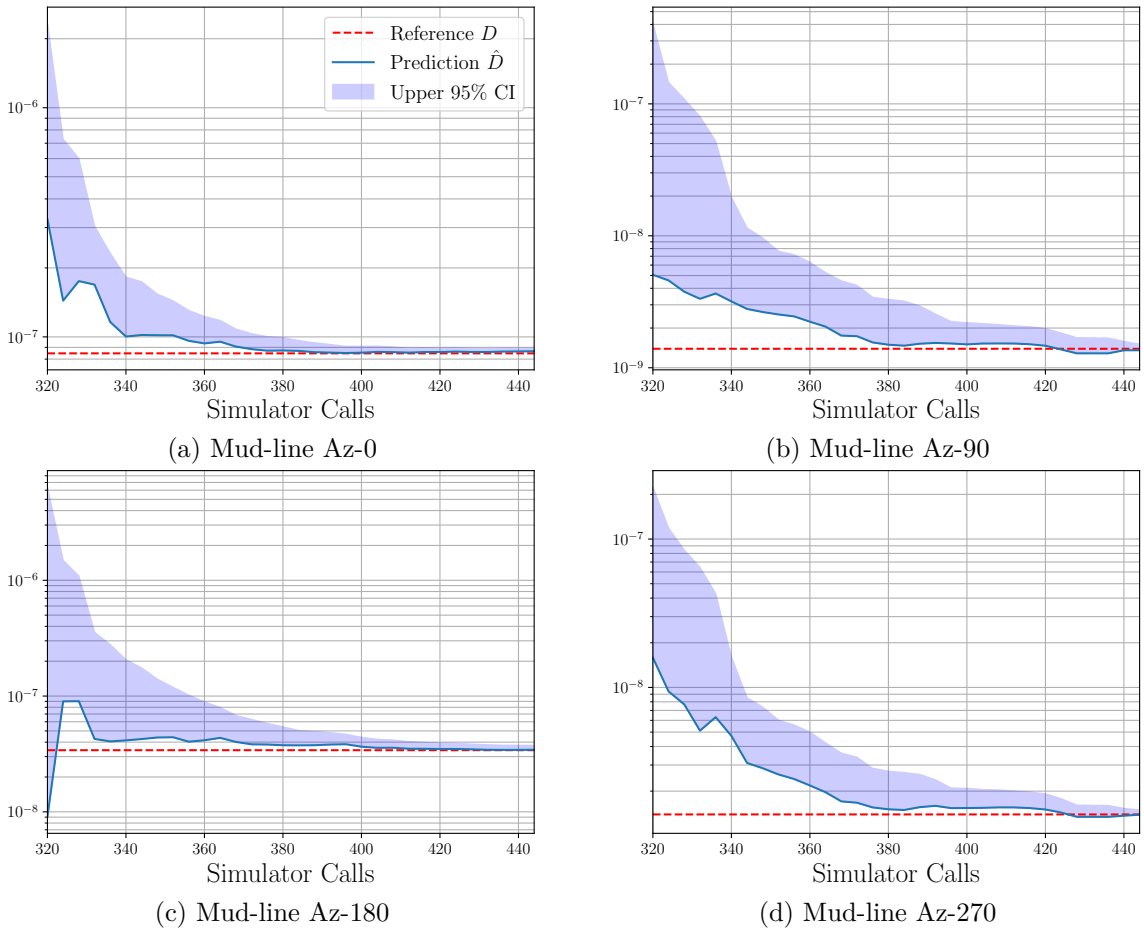

(a) Mud-line Az-0 (b) Mud-line Az-90

(c) Mud-line Az-180 (d) Mud-line Az-270

Figure 3.21: Convergence curves of the four estimations $\hat{D}_k$ with the implementation of the global multi-location approach.

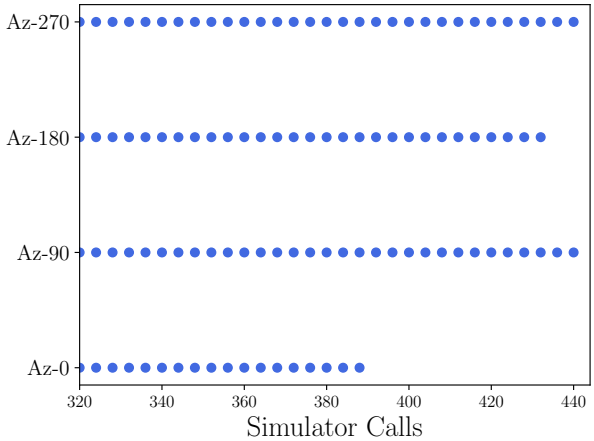

Figure 3.22: Evolution of the piloting points for the four-dimensional multi-location analysis implemented with the multi-location AK-DA approach.

3.5 Conclusions

This third chapter introduces the Adaptive Kriging for Damage Assessment (AK-DA) methodology developed to reduce the simulation investments required for the fatigue analyses as proposed by certification guidelines. The fatigue analysis, which is based on the computation of the global mean damage D for a series of structural locations, implies a large number of simulator calls. In fact, one should estimate demanding short term damages d for a large number of combinations of environmental parameters, as introduced in Chapter 1. The proposed procedure here aims at reducing the number of simulator calls by resorting to Kriging predictions calibrated on a reduced set of model observations d. Kriging enables one to easily compute a prediction of $\hat{d}$ for the short term damage d for each of the combinations of environmental parameters. By considering this approximation in the definition of the global mean damage D, an estimator $\hat{D}$ can be deduced.

As presented in Chapter 2, the choice of the model observations used to calibrate the Kriging metamodels is of major concern regarding the quality of the approximation. As a consequence, the choice of the short term damage d observations is crucial to ensure the representativeness of the approximation $\hat{d}$ and subsequently of the estimation of $\hat{D}$. Inspired by the recent works proposed in numerical optimization and reliability fields, the AK-DA procedure has been elaborated from an automatic and progressive enrichment of the design of experiments (*i.e.* short term damage observations). An Adaptive Kriging (AK) architecture focuses on the reduction of the uncertainty inherent to the estimation of the global mean damage D.

To sequentially enrich the initial design of experiments, the novel approach is proposed focusing on the reduction of the variance of estimation $\sigma^2_{\hat{D}}$. The *absolute variance contribution* learning function, quantifies the consequences of computing each of the non-observed short term damages on the uncertainty of the global mean damage estimation $\hat{D}$. By sequentially enriching the set of model observations with simulations for which the absolute variance contribution is high, a final informative design of experiments can be created and the estimations provided by $\hat{D}$ can be refined. Once the uncertainty over the estimation of $\hat{D}$ is sufficiently reduced, the AK-DA procedure stops. A major concern of the procedure lies on its initialization and more specifically on the choice of the initial design of experiments. A study based on four test cases is proposed in this chapter to illustrate the variations of the bias and variance characteristics of the estimator $\hat{D}$. Two possibilities are underlined to reduce the risk of error of the AK-DA method: the aleatory generation composed of a sufficient number of observations to ensure the accuracy of the approach and the regular grid combined with expertise which presents industrial advantages.

Different examples showed the performance of the proposed method with significant reduction of the simulation investments in the case of industrial examples. The direct application of the AK-DA method on a challenging four-dimensional case results in an important reduction of the simulator calls (385 short term damage estimations compared the 10120 for the reference computation) for an accurate estimation of $\hat{D}$ with a relative error of -2.54% compared to the reference value D. However, the calibration of the Kriging metamodel and the computation of the absolute variance contribution learning function lead to a demanding

post-processing step after each enrichment iteration which can not be neglected with regards to the simulation duration.

To reduce the number of AK-DA iterations, a multi-enrichment strategy has been introduced and presented in this section. Contrary to the single enrichment of the initial design of experiments with a single simulation per iteration, this approach called *influence area* aims at selecting a vector of enrichments to increase the informational inflow at each iteration. This latter choice is proceeded by the analysis of the statistical correlations between model responses estimated by the Kriging approximation. By iteratively selecting sets of simultaneous enrichments with high absolute variance contributions and low cross correlations, redundancies in terms of model observations can be reduced as they provide similar information. A comparison between the single enrichment AK-DA procedure and its multi-enrichment extension has been proposed for the four-dimensional example. The vectors of enrichment allow one to reduce significantly the number of iterations the AK-DA procedure needs to converge (passing from 65 using the strategy with a single enrichment per iterations to 9 with the consideration of 8 simulations in parallel).

Finally, an extension of the AK-DA method have presented which enables one to consider several structural locations at the same time. This method has been compared with the approach which relies on independent approximations to illustrate its interest and performances. Comparable accuracy are obtained when estimating the global mean damages and the simulation effort is overall reduced, either considering the number of simulation calls or number of iterations.

References

DNV-GL. *DNV-OS-J101: Design Of Offshore Wind Turbine Structures*, 2014.

N. Hansen. The CMA evolution strategy: A tutorial. *CoRR*, abs/1604.00772, 2016.

Q. Huchet, C. Mattrand, P. Beaurepaire, N. Gayton, and N. Relun. The help of metamodels or wind turbine certification. In *ICOSSAR 2017*, Vienne, Austria, 2017.

B. J. Jonkman and L. Kilcher. Turbsim user's guide: Version 1.06.00. Technical report, National Renewable Energy Laboratory, 2012.

J. Jonkman, S. Butterfield, and G. Scott. Definition of a 5-mw reference wind turbine for offshore system development. Technical report, National Renewable Energy Laboratory, 2009.

J. M. Jonkman and M. L. Buhl. Fast user's guide. Technical report, National Renewable Energy Laboratory, 2005.

N. Lelièvre, P. Beaurepaire, C. Mattrand, and N. Gayton. AK-MCSi: A kriging-based method to deal with small failure probabilities and time-consuming models. *Structural Safety*, 73: 1–11, 2018.

R. Schöbi, B. Sudret, and S. Marelly. Rare event estimation using polynomial-chaos-kriging. *American Society of Civil Engineers*, 2016.

G. M. Stewart, A. Robertson, and M. A. Lackner. The creation of a comprehensive metocean data set for offshore wind turbine simulations. *Wind Energy*, 19:1151–1159, 2015.

CHAPTER 4

TOWARDS DAMAGE RELIABILITY ASSESSMENT

Contents

As presented in the previous chapters, standards and certification guidelines provide engineers a properly defined framework to numerically estimate the structural reactions and to verify the mechanical performances of a proposed design with regards to a series of criteria. In the particular case of cumulated damage estimation, requirements on structural and environmental modeling are specified to ensure the representativeness of the computations with respect to the real structural behavior. The modeling of the structure has been so far considered as perfect and not suffering from any source of uncertainty or modeling errors. Practically, this assumption does not hold and numerical representations can be impacted by different sources of uncertainty. This chapter proposes to introduce the industrial issue of the uncertainty management during the design stage of wind turbine structures. An extension of the AK-DA is then suggested in order to consider aleatory variations of environmental characteristics within a proper reliability analysis.

Section 4.1 introduces the reliability analysis in the context of offshore wind turbine. This section proposes to highlight the industrial challenges and the potential gains this kind of analysis can provide whilst seeking a trade-off between cost reduction and structural safety. A formalization of the structural reliability problem is then proposed in Section 4.2. Two simulation based methods, namely the Crude Monte Carlo and AK-MCS, are then described and illustrated on a simple test case to depict the numerical investment required for this type of study. Finally, the extension of the AK-DA method (AK-MCS/AK-DA) for the reliability assessment is presented in Section 4.3. The performances of the proposed method are finally compared with the two aforesaid approaches on the illustrative numerical example.

4.1 Reliability analyses in the context of offshore wind turbine design

4.1.1 Sources of uncertainty at the design stage

During the design and/or the certification of wind turbines, engineers use numerical models to estimate the structural reactions of designs of interest to perform the different verification analyses, listed in guidelines and partially described in Chapter 1. To ensure the representativeness of the simulations, the parameterization of the structural model is a major concern. The beam element model, presented in Chapter 1, thus has to be perfectly adapted to the structure of interest. This operation is done by the calibration of a series of model parameters such as the stiffness and mass characteristics, which are defined for each of the involved structural elements. In practice, these values are commonly assumed to be deterministic and determined from the nominal description of the design to represent. In reality, sources of uncertainty should be taken into account because of their influence on the simulation results (*e.g.* Luengo et al. [2019]; Negro et al. [2014]). In the present work, uncertainties are only considered for the soil-structure interactions. This structural modeling is a sensitive point for wind turbine operators because such a lack of representativeness can have a considerable impact on the modeled structural reactions (modification of the structural frequencies, variation of the structural bottom displacements, etc.). A categorization of these sources has been proposed in Sørensen and Toft [2010] in the case of structural analysis of wind turbine

structures and is presented as:

- **Physical uncertainty** which deals with the natural randomness of physical quantities (*e.g.* the aleatory evolution of the wind speed along the structural length and over a given period of time).
- **Measurement uncertainty** resulting from the imperfectness of measurements (*e.g.* impossibility to perfectly measure structural dimensions such as the pile thickness).
- **Statistical uncertainty** due to the limited sizes of samples which are used to characterize the statistics or probabilistic models (*e.g.* characterization of the soil mechanics from a limit number of samples).
- **Model uncertainty** which deals with the possible lack of representativeness of the implemented modeling (*e.g.* the wind aleatory generation or representation of sea-states with the use of the Morison's equations).

As presented, the physical uncertainty regroups the natural randomness of physical phenomena. In the context of offshore wind energy, several structural loadings are created from natural effects such as wind or waves. Within the proposed certification framework, the environmental inputs (*e.g.* the wind mean speed u or the peak spectral period of the sea-state t_p) are considered as deterministic. The fluctuations of the environmental loads over time are considered for a given loading state (*e.g.* given a fixed set of environmental parameters $\boldsymbol{x} \in \mathcal{D}_{\boldsymbol{x}}$) by sampling random processes. As an example, the estimation of the 10-min short term damage response of the structure is repeated six times for each of the environmental set of parameters $\boldsymbol{x}$ in the design load case 1.2 (estimation of the cumulated damage for "normal production" conceptual situation). By summing the 10-min damages, a more representative 1-hour cumulated short term damage is finally assessed. In this chapter, the 1-hour damage computed for a given environmental combination is assumed to be deterministic, *i.e.* not affected by uncertainty even though certainly not true in practice, and the related physical uncertainties are not considered here.

The model uncertainty is also of major concern. As an example, two models for the soil-structure interactions have been introduced in Chapter 1. The choice of this soil or foundation model has to be carefully selected with regards to the simulation to perform because of the sensitivity of the structural behavior [Aasen et al., 2017; Andersen et al., 2018]).

Considering a given model, assumed to be perfectly representative of the structural behavior of the soil-foundation interactions (*i.e.* no model uncertainty), one of the major industrial difficulty is the characterization of the soil mechanics. Because of the related costs of in situ measurements (core drilling), the soil is only characterized with a limited set of samples. A statistical uncertainty is then present and has to be properly determined. This chapter focuses on this type of uncertainty.

4.1.2 Illustrative example: consequences of variations of soil characteristics in damage estimation

To illustrate the importance of the uncertainty consideration in the field of offshore wind turbine a simple example is proposed. Let consider a simplified modeling of the soil-structure interaction implemented using a stiffness node at the bottom of the structure (Aasen et al. [2017]) as depicted in Figure 4.1. In this representation, only the rotational and lateral stiffnesses are considered for the directions $\vec{x}$ and $\vec{y}$.

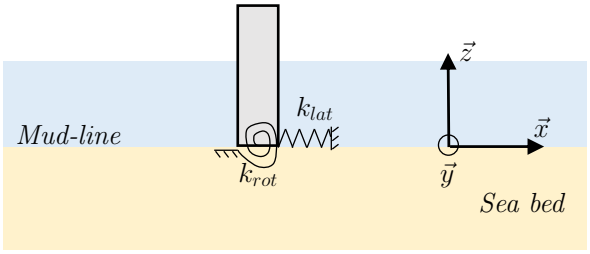

Figure 4.1: Representation of the soil-structure modeling by simple stiffness node added at the bottom of the structure (mud-line level).

Different relations between the rotational and lateral stiffnesses can be adopted depending on the situation to model (see Arany et al. [2017]). In the presented case, a simple relation is assumed as $k_{rot} = 100 \times k_{lat}$, where k_{rot} denotes the rotational stiffness and k_{lat} the lateral stiffness. As a consequence, only the rotational stiffness k_{rot} can be considered to be uncertain. A random variable K is here introduced. It is assumed to be normally distributed with a mean value $\mu_K = 2.6 \times 10^{11}$ N/m (stiff clay) and a low coefficient of variation $\delta_K = 10\%$ arbitrarily chosen.

One hundred realizations of the stiffness parameter K have been used to compute the structural reactions as well as the short terms damages d at the Az-0 point of the structure presented in Chapter 3. The environmental grid is partially considered: six values of the significant wave heights h_s and thirteen values of the spectral peak periods t_p have been selected. The wind mean speed is fixed to $u = 13$ m/s and no misalignments are considered between wind and sea loadings ($\theta = 0$ deg). For illustration purpose, three damage responses are plotted in Figure 4.2. It is observed that the evolution of the stiffness parameter results in a modification of the short term damage response. The peak located at $h_s \approx 5$ m and $t_p = 5$ s, which represents a structural resonance phenomenon ($f_0 \approx 5$ s for the considered structure), varies from approximately 8 ($k_{rot} = 3.25 \times 10^{11}$ depicted in Figure 4.2a) to 10×10^{-6} ($k_{rot} = 2.11 \times 10^{11}$ depicted in Figure 4.2a).

For each of the environmental combinations used in this example, a probability of occurrence is extracted from the global metocean data used in this thesis. The evolution of this probability is represented in Figure 4.3a. The computation of the global mean damages $D(k_{rot})$, for each of the realizations of K, is depicted in Figure 4.3b. It is observed that the quantity of interest decreases from approximatively 3.75 to 3.40×10^{-11}. This represents a maximal variation of approximately 10% between the minimal and maximal computations.

This simple example shows the interest of considering the uncertainty relative to the characterization of the soil mechanics. By modifying a single value of the model parameters,

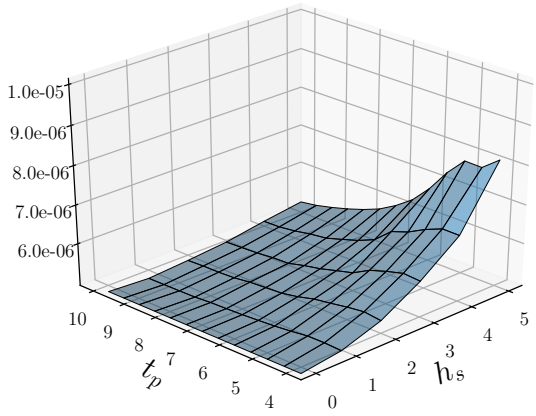

(a) $k_{rot} = 3.25 \times 10^{11}$

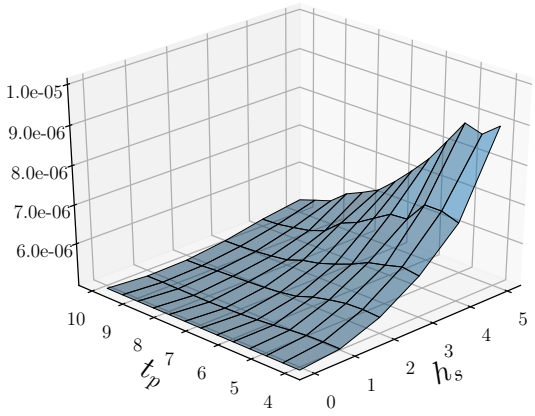

(b) $k_{rot} = 2.61 \times 10^{11}$

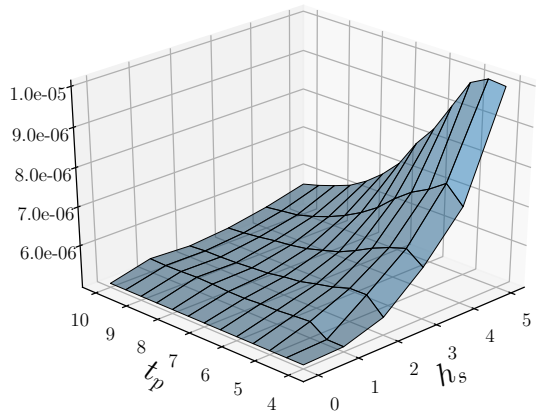

(c) $k_{rot} = 2.11 \times 10^{11}$

Figure 4.2: Illustration of the short-term damage d estimated at the az-0 structural location for a grid composed of 6 significant wave heights h_s and 13 spectral peak periods t_p ($u = 13$ m/s and $\theta = 0$ deg). Three different values of the reference soil stiffness parameter k_{rot} are considered in (a), (b) and (c).

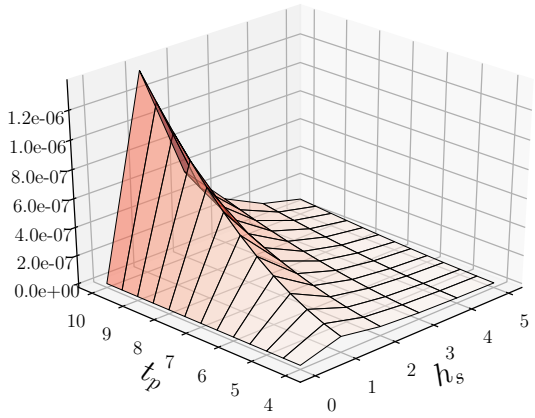

(a) Evolution of the probability of occurrence $p(t_p, h_s|u = 13, \theta = 0)$

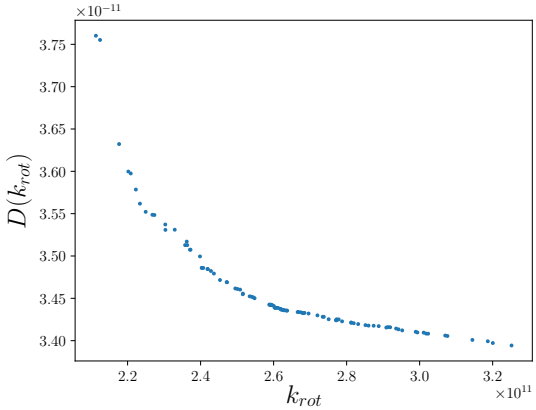

(b) Damages $D(k_{rot})$

Figure 4.3: Evolution of the probability of occurrence p considered in the illustrative example (a) and evolution of the global mean damage for an aleatory generation of 100 k_{rot} (b).

the short term damage d is modified as well as the global mean damage D. To ensure a maximal safety of the installations, these variations have to be properly considered in the design stage. For interested readers, a complete study has been proposed for example by Fontana et al. [2015] which focused on the consequences of structural and foundation damping variations on cumulated damages (variation of 47 to 69% of the cumulated damage at mud-line Az-0 location depending on the chosen damping coefficients).

4.1.3 Motivations for damage reliability analyses

The management of uncertainties is industrially achieved by the use of safety factors which are supposed to globally account for all the sources of uncertainty in the design stage of wind turbine structures. This method aims at over-evaluating the structural reactions obtained from numerical simulations to ensure a given structural safety level with regards to potential variations of the modeling parameters. This may result in conservative structural designs (even though the degree of conservatism is not quantified in practice) and subsequently in an increase of the economical investment of new projects. This latter directly impacts the production cost of wind energy and as a consequence, the reduction of these safety factors should be appealing to reduce global costs.

Hence, the overall objective would be to propose a suitable strategy to fit the safety factors to the design situation by determining an optimal trade-off between installation safety (with regards to mechanical collapsing) and the production cost of wind turbine structures. In other words, the inherent problematic lies on the possibility to reduce safety factors while guarantying a minimal safety level of the installations given the design situation.

Reliability analyses aim at estimating the occurrence of a failure when uncertainties are considered. A failure criterion (corresponding to a failure scenario) is defined depending on the study and is function of the random variables of the problem. A probability of failure can be assessed and used to adapt the safety factors to the designed situation.

The rest of this chapter focuses on the reliability analysis of structures which are designed in fatigue (by means of the global mean damage D) and only the randomness in the soil mechanics is here considered.

4.2 Formalization of the structural damage reliability analysis

This section introduces the formalization of damage based reliability analyses. This thesis focuses on the "Stress-Strength" approach (also known as capacity-demand formalization). In the following, $\boldsymbol{\zeta} = \{\zeta_1, \ldots, n_{\boldsymbol{\zeta}}\} \in \mathcal{D}_{\boldsymbol{\zeta}}$ is considered to represent a set of $n_{\boldsymbol{\zeta}}$ uncertain parameters. These parameters can be assimilated to calibration values for the numerical model to represent the studied situation (*e.g.* soil stiffness and damping coefficients of the soil-structure interface). For the sake of tractable notations, $\boldsymbol{\zeta}$ either stands for the random variable or its realization in the following. The joint probability function of these random variables is assumed to be known and is noted in the following $f_{\boldsymbol{\zeta}}$.

4.2.1 The Resistance-Stress Approach

Consider a mechanical system $\{\mathcal{S}\}$ which presents, for a defined type of stress (demand) of order s (*e.g.* a mechanical stress, damage or displacement), a certain strength (capacity) r. The failure of the mechanical system is assumed to occur if the stress s is greater or equal to the strength r for a given failure scenario. Let now consider that the stress and the resistance quantities are expressed in terms of the set of uncertain parameters $\boldsymbol{\zeta} \in \mathcal{D}_{\boldsymbol{\zeta}}$. As a consequence, the strength and stress quantities becomes random variables, respectively noted R and S in the following. To analyze the performance of the system $\{\mathcal{S}\}$, the computation of a probability of failure P_f is commonly done from a performance performance function G which is introduced to express a given failure scenario:

$$G(\boldsymbol{\zeta}) = R(\boldsymbol{\zeta}) - S(\boldsymbol{\zeta}) \tag{4.1}$$

Negative values of G (*i.e.* $G(\boldsymbol{\zeta}) \leq 0$) characterize the failure domain and positive values (*i.e.* $G(\boldsymbol{\zeta}) > 0$) lead to $\boldsymbol{\zeta}$ values which are located in the safe domain. The frontier in between (*i.e.* $G(\boldsymbol{\zeta}) = 0$) is often called the limit-state function. The probability of failure P_f is defined by the probability that a sample $\boldsymbol{\zeta}$ belongs to the failure domain. It can be expressed in terms of variables R and S as:

$$P_f = \text{prob}\Big(R(\boldsymbol{\zeta}) - S(\boldsymbol{\zeta}) \leq 0\Big) = \int\int_{r-s\leq 0} f_{R,S}(r,s)\ \mathrm{d}r\mathrm{d}s \tag{4.2}$$

where $f_{R,S}(r,s)$ here represents the joint probability density function of the two random variables R and S. Within the industrial context, it is most of the time impossible to compute this integral exactly and this leads the scientific community to propose appropriate methods to estimate the probability of failure P_f.

In the framework of this thesis, the global mean damage corresponds to the probability-weighted sum of short term damages $d(\boldsymbol{x})$, which are computed for each of the given environmental combination $\boldsymbol{x} \in \mathcal{D}_{\boldsymbol{x}}$. If uncertainties such as those observed in soil properties affect the short term damages, then the resulting global mean damage is random and can be expressed as:

$$D(\boldsymbol{\zeta}) = \sum_{i=1}^{n_c} p(\boldsymbol{x}_i)\ d(\boldsymbol{x}_i, \boldsymbol{\zeta})\ \Delta \tag{4.3}$$

where $d(\boldsymbol{x}, \boldsymbol{\zeta})$ denotes the short term damage. It is a function of a given environmental combination $\boldsymbol{x}$, which should be viewed as an index by comparison with the definition of a random process, and a random a random vector $\boldsymbol{\zeta}$. The latter encompasses all involved random variables. The failure is supposed to occur when the global mean damage D exceeds a predefined threshold value D_t which leads to write the performance function as:

$$G(\boldsymbol{\zeta}) = D_t - D(\boldsymbol{\zeta}) \tag{4.4}$$

Then, the probability of failure P_f reads:

$$P_f = \text{prob}\Big(D_t - D(\boldsymbol{\zeta}) \leq 0\Big) = \int_{D_t - D(\boldsymbol{\zeta}) \leq 0} f_{\boldsymbol{\zeta}}(\boldsymbol{\zeta}) \mathrm{d}\boldsymbol{\zeta} \tag{4.5}$$

4.2.2 Industrial limitations for the computation of the probability of failure

Within the proposed formalization (see Eq. 4.3 to Eq. 4.5), the direct computation of the probability of failure P_f may be not industrially feasible. This limitation comes from the impossibility to formally determine the failure domain, *i.e.* the realizations $\boldsymbol{\zeta}$ for which the performance function $G(\boldsymbol{\zeta}) \leq 0$. To tackle this, several methods are developed in reliability analysis to evaluate an estimation $\hat{P}_f$ of the probability of failure P_f. These methods can roughly be classified in two groups: the approximation methods and simulation approaches.

The first introduced class of methods aims at approximating the limit state function ($G(\boldsymbol{\zeta}) = 0$) at the most probable point of failure. Within this kind of methodology, the FORM and SORM are two popular approximations, widely deployed for industrial application which respectively propose to approximate the limit state function by a first or a second order function (*i.e.* linear or quadratic functions).

Simulation approaches rely on the direct evaluation of the performance function G for different random realizations of the parameter $\boldsymbol{\zeta}$. The most natural method is the so-called Monte Carlo strategy which is based on an easy-to-implement procedure described in Section 4.2.3. Its main advantage is the possibility to compute an estimator $\hat{P}_f$ of the probability of failure P_f for which a coefficient of variation $\delta_{\hat{P}_f}$ is available. As a drawback, the implementation of this method usually requires an important number of simulator calls to reach an admissible precision, *i.e.* a low coefficient of variation. In this sense, this method is not suited for industrial application which deal with demanding simulator calls as in the present case. Based on the Monte Carlo principle, other simulation methods have been proposed to reduce the estimator coefficient of variation and so the number of simulator calls as the importance sampling or the subset simulations. Interested reader can refer to Lemaire [2013] for a complete description of the numerical methods for probability of failure estimations.

The above-mentioned reliability methods are confronted to three main limitations for industrial applications (Lelièvre [2018]). Firstly, the evaluation of low probabilities of failure (usually considered for an order of magnitude equals to 10^{-4}) is a difficult task due to the practical difficulty to numerically access the failure domain. This difficulty is furthermore increased when the problems involve a great number of random variables and results in an explosion of the number of simulator calls to perform (the curse of dimensionality). Finally, industrial applications of reliability based analyses may, in certain cases, be based on demanding simulator calls which induces a massive if not unfeasible numerical investment. To develop these kind of structural analyses, the reliability community have progressively proposed more effective methods based on metamodeling. In these latter, the performance function is approximated based on a reduced number of simulator calls (Bourinet [2018]; Lelièvre et al. [2018]; Sudret [2007]).

In the particular context of structural reliability analysis of wind turbines, [Jiang et al., 2017] recently proposed a review of the state-of-the-art applications both for onshore and

offshore applications. In this paper, authors address a complete overview of the most used methods. For structural reliability of monopile assembles for offshore installation, this study underlines the importance of using representative numerical models to properly consider the complex structural reactions and their consequences on reliability assessments.

This thesis focused so far on the use of the Kriging metamodeling technique for which a formalization is presented in Chapter 2. Subsequently, Chapter 3 introduces the use of this metamodel for the cost-effective estimation of the global mean damage D within the AK-DA method. As a natural choice, the AK-MCS method is used in this thesis. The possibilities to couple this latter with the proposed developments are discussed in this chapter. Before presenting the proposed method in Section 4.3, the Crude Monte Carlo and the AK-MCS approaches are presented and illustrated in Section 4.2.3.

4.2.3 Crude Monte Carlo and AK-MCS methods

In this section, two simulation based methods are presented: the so-called Crude Monte Carlo (CMC) and the Adaptive Kriging for Monte Carlo Simulation (AK-MCS). For the sake of illustration and to discuss about the possible applicability of these methods within the industrial context of interest, a two-dimensional fictional example is used in this section.

Crude Monte Carlo simulation

Crude Monte Carlo (CMC) simulations are based on intensive model evaluations and aim at proposing an estimator $\hat{P}_f$ of the probability of failure by classifying each of the obtained model responses with regards to the structural limit state $G(\boldsymbol{\zeta}) = 0$. An indicator function $\mathbb{1}_{G(\boldsymbol{\zeta})\leq 0}$ is therefore introduced for each of the n_{MC} simulations such as:

$$\mathbb{1}_{G(\boldsymbol{\zeta})\leq 0} = \begin{cases} 1 \text{ if } G(\boldsymbol{\zeta}) \leq 0 \\ 0 \text{ if } G(\boldsymbol{\zeta}) > 0 \end{cases} \tag{4.6}$$

The integral function defined for the computation of the probability of failure presented in Eq. 4.2 can be transformed by the use of this indicator function as:

$$P_f = \int_{\mathcal{D}_{\boldsymbol{\zeta}}} \mathbb{1}_{G(\boldsymbol{\zeta})\leq 0} \, f_{\boldsymbol{\zeta}}(\boldsymbol{\zeta}) \, \mathrm{d}\boldsymbol{\zeta} = \mathbb{E}[\mathbb{1}_{G(\boldsymbol{\zeta})\leq 0}] \tag{4.7}$$

The Monte Carlo estimation $\hat{P}_f$ of the probability of failure P_f is computed as:

$$\hat{P}_f = \frac{1}{n_{MC}} \sum_{i=1}^{n_{MC}} \mathbb{1}_{G(\boldsymbol{\zeta}_i)\leq 0} \tag{4.8}$$

where $\boldsymbol{\zeta}_i$ denotes the i-th sample $\boldsymbol{\zeta}$ of the Monte Carlo population of size n_{MC}. The coefficient of variation of $\hat{P}_f$ has to be determined to ensure the representativeness of this estimation and can be computed as:

$$\delta_{\hat{P}_f} = \sqrt{\frac{1 - \hat{P}_f}{n_{MC}\hat{P}_f}} \tag{4.9}$$

To reach small coefficients of variation, this method requires an important number n_{MC} of simulator calls. To reach a probability of failure of order of magnitude 10^{-N} with a coefficient of variation of 10%, the number of simulations is around $n_{MC} \approx 10^{N+2}$, which is unaffordable when considering demanding models. In the context of this thesis, the direct use of the Crude Monte Carlo method would indubitably lead to an unmanageable number of global mean damage estimations. As an illustration, if the probability of failure is about 10^{-3}, the application of this approach would lead to hundreds of thousands global mean damage estimations. For each of the estimation, reader have to keep in mind that n_c short term damage estimations have to be performed.

To reduce the numerical investment required by the Crude Monte Carlo simulation, the Adaptive Kriging based method for Monte Carlo Simulation (AK-MCS) has been proposed and is described in the following section.

Adaptive Kriging for Monte Carlo Simulation (AK-MCS)

The AK-MCS method is proposed by Echard et al. [2011]. It aims at reducing the computational cost of reliability analyses when expensive-to-evaluate performance functions are involved. The global idea is to approximate the performance function G with the help of an adaptive Kriging strategy. The metamodel $\hat{G}$ is used in place of G to evaluate the Monte Carlo simulations.

In short, this method can be described as follows. An initial Monte Carlo population $\mathcal{P}$ of size n_{MC} is randomly generated based on the joint probability density function $f_{\boldsymbol{\zeta}}$ of the random variables ζ_i ($i \in \{1, \ldots, n_{\boldsymbol{\zeta}}\}$). A reduced subset of realizations is used to generate a first set of model observations (*i.e.* initial design of experiments) which is considered to calibrate a first Kriging metamodel $\hat{G}_0$ of the performance function G. An initial estimation $\hat{P}_{f_0}$ of the probability of failure P_f is computed with the help of the Monte Carlo estimator presented in Eq. 4.10 as:

$$\hat{P}_{f_0} = \frac{1}{n_{MC}} \sum_{i=1}^{n_{MC}} \mathbb{1}_{\hat{G}_0(\boldsymbol{\zeta}_i) \leq 0} \tag{4.10}$$

The initial design of experiments is enriched focusing on the risk of misclassification of the entire Monte Carlo population with respect to the approximated performance function $\hat{G}_0$. The enrichment criterion quantifies this risk by computed the learning function U defined, for this initial step, as:

$$U_0(\boldsymbol{\zeta}) = \frac{|\hat{G}_0(\boldsymbol{\zeta})|}{\sigma_{\hat{G}_0}(\boldsymbol{\zeta})} \tag{4.11}$$

where $\sigma^2_{\hat{G}_0}(\boldsymbol{\zeta})$ represents the variance of estimation provided by the Kriging metamodel and estimated for the entire Monte Carlo population. The realization $\boldsymbol{\zeta}$ which has the highest

risk to be misclassified, *i.e.* the minimal value U_0, is added to the design of experiments. By noting this latter $\boldsymbol{\zeta}^*$, the enrichment procedure is formalized as an optimization problem which reads:

$$\boldsymbol{\zeta}^* = \underset{\boldsymbol{\zeta} \in \mathcal{P}}{\operatorname{argmin}}\ U_0(\boldsymbol{\zeta}) \tag{4.12}$$

Once the sample $\boldsymbol{\zeta}^*$ is found, the design of experiments is enriched by running a simulator call at $\boldsymbol{\zeta}^*$ (observation of $G(\boldsymbol{\zeta}^*)$) and a new metamodel $\hat{G}_1$ is calibrated. This sequential enrichment is performed until a convergence criterion is reached, defined as:

$$\min_{\boldsymbol{\zeta} \in \mathcal{P}} U_i(\boldsymbol{\zeta}) > 2 \tag{4.13}$$

where i is the index of the enrichment step. If this criterion is reached, the Monte Carlo coefficient of variation $\delta_{\hat{P}_f}$ of the estimation $\hat{P}_f \equiv \hat{P}_{f_i}$ is computed as proposed in Eq. 4.9 to ensure the representativeness of the results. If this coefficient is not admissible, *i.e.* $\delta_{\hat{P}_f} > \delta_t$, a new Monte Carlo population is aleatory generated and the algorithm goes back to the enrichment step. The total number of simulator calls before convergence is subsequently named $n_{\text{AK-MCS}}$.

In the following part, the two presented methods are illustrated on an academical example inspired from the problematic considered in this thesis.

4.2.4 Illustrative example

To illustrate the reliability analysis of a structural component, the two above-mentioned methods are performed and compared considering a simplified structural wind turbine design for which a reliability analysis of the damage response is required. This example deals with one environmental parameter and one random variable which are considered to be the only inputs of the short-term damage d estimation. As presented before, this quantity is computed from the implementation of a numerical chain whose inputs are the environmental parameters. To mimic a wind turbine certification problem, a variable $x \in [10, 20]$ is assimilated to an environmental parameter as, for instance, the wind mean speed or the wind-wave misalignment and discretized within $n_c = 11$ possible values. To compute the estimation of the global mean damage D, the probability of occurrence $p(x)$ is here assumed Gaussian with a mean value $\mu_x = 12$ and a standard deviation $\sigma_x = 1$. This probability distribution is depicted in Figure 4.4a.

Let us now assume that the structural response d is influenced by an uncertain parameter normally distributed $\zeta \sim \mathcal{N}(\mu_\zeta = 15, \sigma_\zeta = 1)$, which is represented in Figure 4.4b. This modeling represents the situation where a study parameter is not exactly known because presenting a certain variability (*e.g.* the mechanical characteristics of the soil as illustrated in Section 4.1.2). For the purpose of illustration, the short-term damage $d(x, \zeta)$ is here modeled as a Gaussian surface parameterized with a varying mean $\mu_d = \zeta$ and a standard deviation $\sigma_d = 1$:

$$d(x,\zeta) = \frac{1}{\sqrt{2\pi}} \exp\Big(-\frac{1}{2}\,(x-\zeta)^2 \Big) \tag{4.14}$$

The evolution of this short-term damage is illustrated in Figure 3.13a for different values of the parameters between 10 and 20. For a given set of parameter x, the aleatory evolution of the parameter ζ results in a possible variation of the global mean damage D which can be described as a random variable. This phenomenon is illustrated in Figure 4.5b where a reference computation has been done by using Eq. 4.15 to depict the evolution of the global mean damage $D(\zeta)$ with regards to the uncertain parameter ζ:

$$D(\zeta) = \sum_{i=1}^{n_c} p(x)\; d(x,\zeta)\; \Delta \tag{4.15}$$

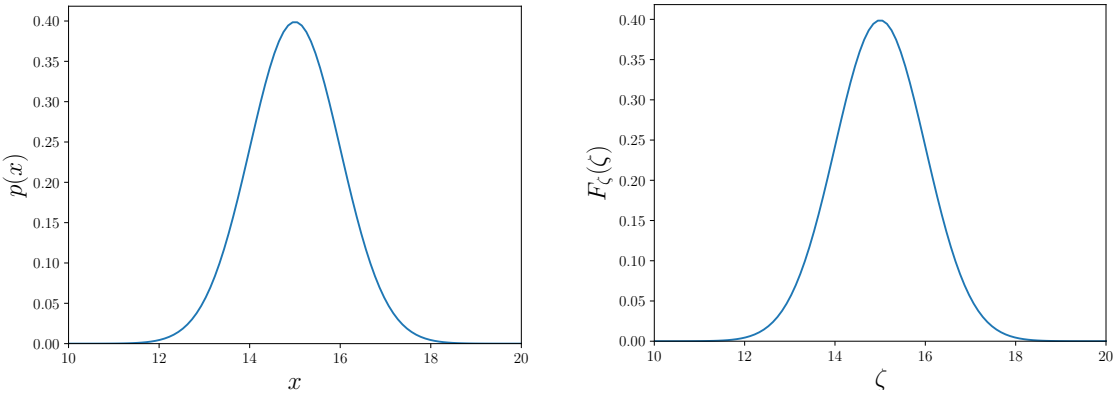

(a) Environmental parameter x (b) Uncertain parameter ζ

Figure 4.4: Illustration of the probability of occurrence p of the deterministic parameter x and probability density function F_ζ of the uncertain parameter ζ.

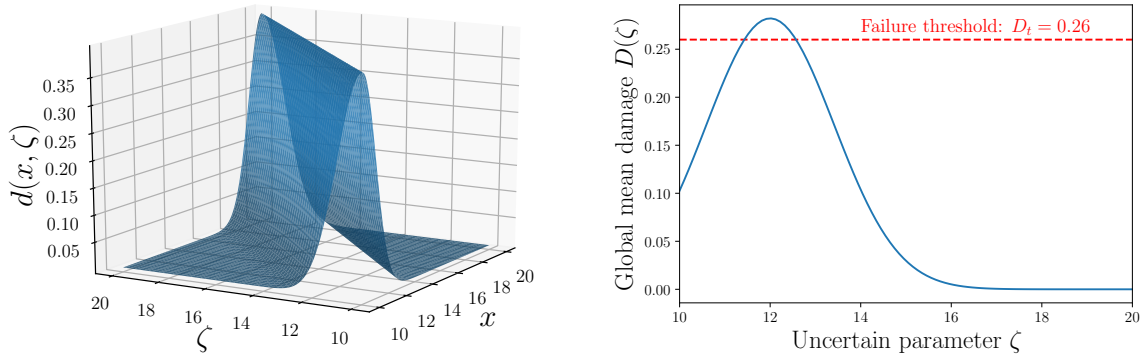

(a) Short-term damage d (b) Global mean damage D

Figure 4.5: Illustration of the short term damage d considered in the illustrative example and the related evolution of the global mean damage $D(\zeta)$ with $\zeta \in [10, 20]$.

The objective of this illustrative example is to assess the probability of failure P_f for the scenario in which the global damage response D exceeds a failure threshold here equals to $D_t = 0.26$:

$$P_f = \text{Prob}\Big(D_t - D(\zeta) \leq 0 \Big) \tag{4.16}$$

According to the formalization proposed in this chapter, the performance function G is expressed as:

$$G(\zeta) = D_t - D(\zeta) \tag{4.17}$$

Firstly, a Crude Monte Carlo (CMC) procedure is implemented to solve this problem. A population of n_{MC} realizations of ζ is sampled according to the probability density function f_ζ of the random variable ζ. For each of the values ζ, the short-term damages are computed for all values of the environmental parameter x and finally the global mean damage $D(\zeta)$ is estimated by the formula presented in Eq. 4.15. For each of the estimations of the global mean damage D, $n_c = 11$ simulator calls of the short term damage d need to be performed. The convergence criterion is based on a coefficient of variation of the estimated probability of occurrence equals to 5%. The estimated probability $\hat{P}_f$ is computed as 7.73×10^{-3}. The evolution of the estimation as well as its two-side 95% confidence interval are presented in Figure 4.6a. In total, $n_{MC} = 51345$ simulators calls (*i.e.* estimations of the the global mean damage $D(\zeta)$) are performed before the convergence of the algorithm. In total, the quantity d is here estimated $n_c \times n_{MC} = 564795$ times.

Following that, the AK-MCS procedure is applied on the same population of ζ as used for the CMC simulation. The Kriging metamodel is set with a quadratic basis and the correlation model is chosen here as the "squared exponential". The initial set of observations is composed of 5 computations of the global mean damage D. Each $D(\zeta)$ is estimated with a value of ζ aleatory selected. A LHS is carried out based on the distribution of the random variable ζ. In this case, a total of three enrichments are required for the algorithm to converge. The evolution of the approximation $\hat{G}$ for the different steps of the algorithm are depicted in Figure 4.7. The algorithm proposes an estimation of the probability of failure equal to 7.73×10^{-3} which perfectly agrees the estimation provided by the CMC procedure (*i.e.* the entire Monte Carlo population is well classified with respect to the failure domain). The advantage of this method is that the simulation effort mainly focuses on the determination of the limit-state function (*i.e.* $G(\zeta) = 0$). Reader can observe that the enrichments are proposed in the vicinity of $\hat{G}(\zeta) = 0$ because of the learning strategy based on the U function. In the rest of the definition domain, no enrichments are proposed if the risk of misclassification is low and even if the Kriging variance of estimation $\sigma^2_{\hat{G}}$ is important. In the presented example, the algorithm stopped despite the variance of prediction $\sigma^2_{\hat{G}}$ is still important for ζ values between 17 and 19 (see Figure 4.7d). A total of $n_c \times n_{\text{AK-MCS}} = 88$ evaluations of the function d is required in this example to compute an accurate estimator $\hat{P}_f$ ($\delta_{\hat{P}_f} = 4.99$). In comparison with the CMC algorithm, the AK-MCS presents important post-processing time. In this example, the entire duration of this latter is 37 seconds which is negligible with regards to the reduction of the computational effort provided by this technique.

To sum up, this simple example shows the behavior of the CMC simulation and AK-MCS method for the numerical computation of the probability of failure P_f. This illustrates the demanding numerical investment required by Crude Monte Carlo algorithm which needs more than 5×10^4 estimations of the global mean damage D to reach a coefficient of variation of 5%. Within the industrial context described in this thesis, this strategy can not be reasonably

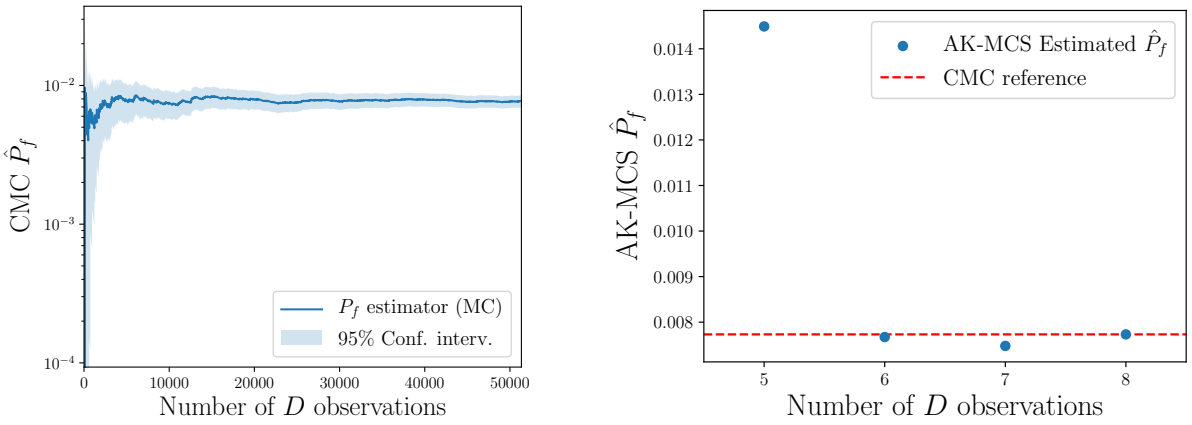

(a) Crude Monte Carlo (b) AK-MCS

Figure 4.6: Evolution of the estimations of the probability of failure P_f obtained with the Crude Monte Carlo and the AK-MCS methods.

applied. The AK-MCS procedure leads to a drastic reduction of the numerical efforts for the estimation of the probability of failure in this simple example. The application of this method in industrial situations therefore appears appealing. However, for each of the observations of vector $\boldsymbol{\zeta}$, a complete damage computation would still be required (needing n_c evaluations of short term damages). To tackle this, an adaptation of the AK-MCS algorithm is proposed in the following section to consider estimations provided by the AK-DA algorithm proposed in Chapter 3.

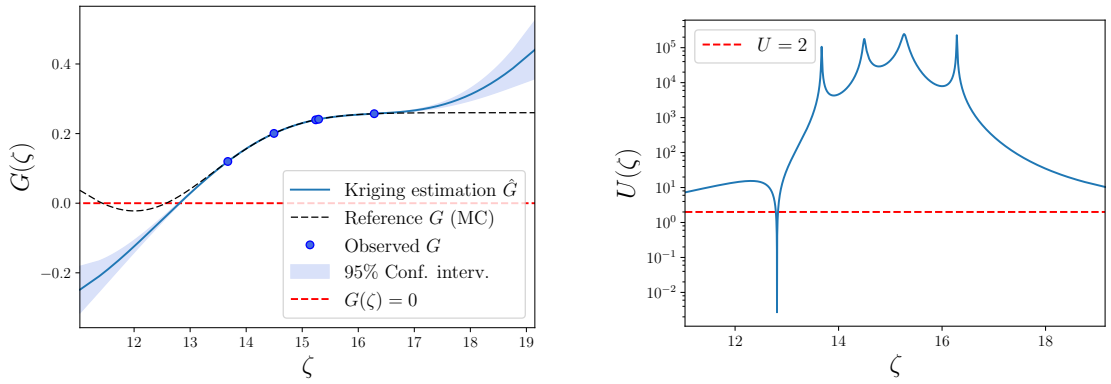

(a) Initialization

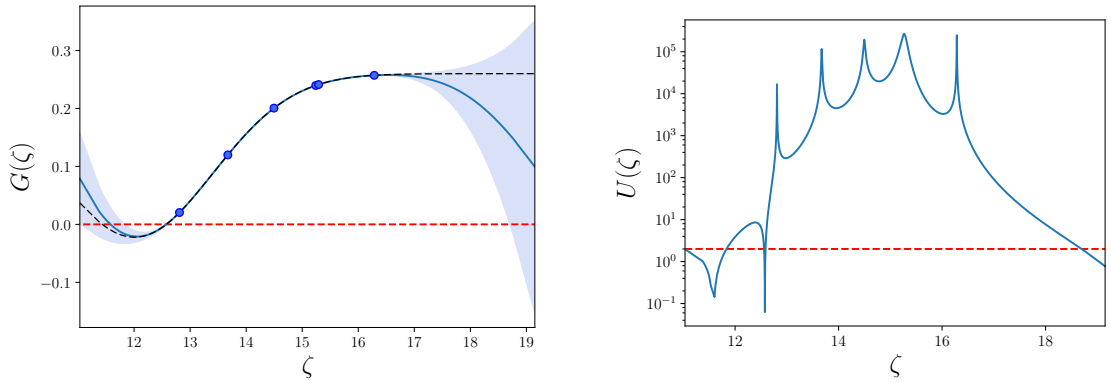

(b) Iteration 1

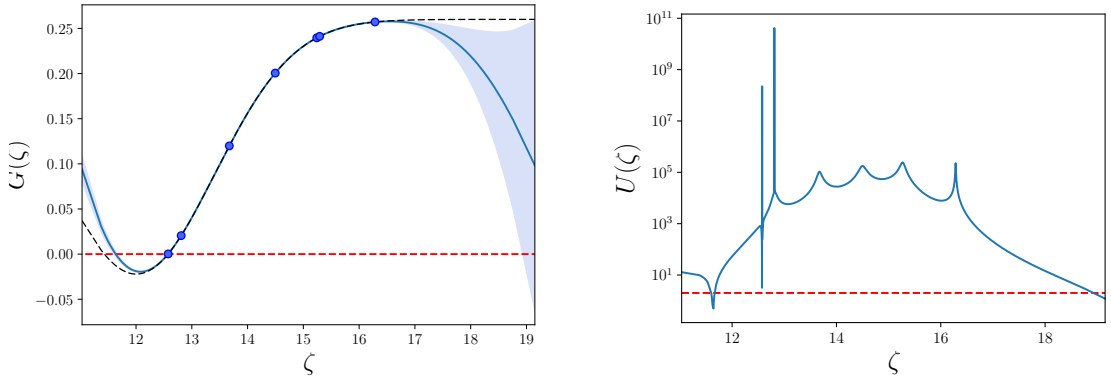

(c) Iteration 2

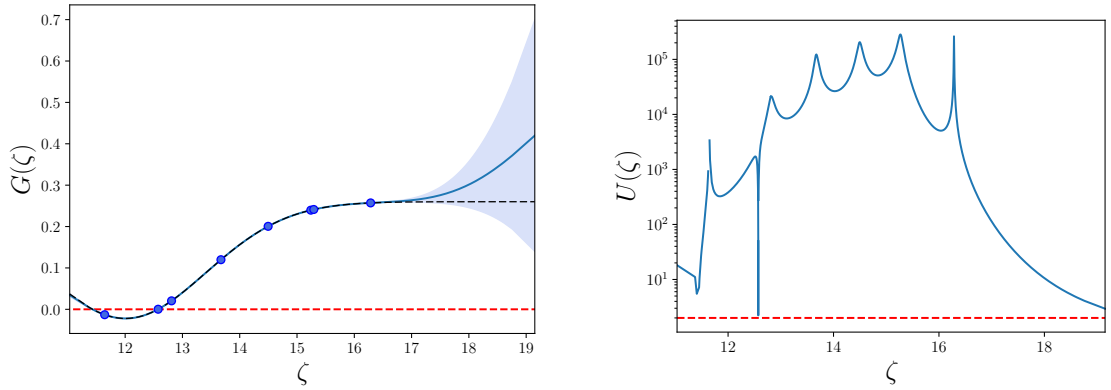

(d) Iteration 3

Figure 4.7: Illustration of the enrichments of the AK-MCS methodology for the illustrative example.

4.3 Coupling of the AK-MCS and AK-DA strategies

Reliability of a wind turbine design with regards to its cumulated damage response is not easy to investigate because of the required number of simulations. In the specific context of the damage analysis of offshore wind turbines, a single estimation of the global mean damage D involves a great number n_c of short term damage estimations as pointed out in Chapter 1. As a consequence, the direct use of the reliability methods introduced in this chapter would rapidly lead to an unmanageable simulation investment. The Crude Monte Carlo technique relies on the complete damage estimation of a large number of samples. In this case, the total number of short term damage simulator calls reaches $n_{MC} \times n_c$ (with n_{MC}, the size of the Monte Carlo population and n_c, the number of environmental combinations) which is practically unfeasible. The implementation of the AK-MCS method allows one to drastically decrease this number as illustrated in Section 4.2.4. In its former version, this methodology would make the reliability analysis less demanding in the context of damage estimation of wind turbines. It may be directly performed for some simple cases (*e.g.* low number of uncertain parameters $n_{\boldsymbol{\zeta}}$ or combinations n_c) by resorting to high performance computing (distribution of the computations). However, when a high number n_c of environmental combinations and/or several random variables are considered, applying AK-MCS in its former version would rapidly become impossible. In fact, for each realization $\boldsymbol{\zeta}$ of the design of experiments of the AK-MCS method, a complete damage design should be required, involving n_c computations of the short term damage d.

The development of the AK-DA method presented in Chapter 3 allows one to compute a sufficiently accurate estimation $\hat{D}$ of the global mean damage D based on a reduced set of model observations. As a consequence, coupling the AK-MCS method with the estimation strategy proposed by the AK-DA procedure can enable one to keep on reducing the simulation costs of the reliability analysis. The proposed approach is not directly applicable and the former version of the AK-MCS algorithm has to be slightly modified for such a purpose. In the following, the modifications of the AK-MCS architecture are presented by introducing an augmented input space in Section 4.3.1, a modification of the learning strategy in Section 4.3.2 and a modification of the stopping criterion in Section 4.3.3. Finally, the modified AK-MCS algorithm is presented in Section 4.3.4.

4.3.1 Augmented input space

The initial version of AK-MCS calibrates a Kriging metamodel in the definition space $\mathcal{D}_{\boldsymbol{x}}$ of the uncertain parameters $\boldsymbol{\zeta}$. However, the short term damages depends both on the random variables $\boldsymbol{\zeta}$ and the environmental parameters $\boldsymbol{x}$. Hence, the idea lies in resorting to an unique Kriging metamodel. This choice is here relevant because physical considerations allow one to consider smooth evolutions of the short term damage evolution with regards to the uncertain parameters. As proposed in different studies, the use of augmented spaces enable to better consider the global evolution of the model responses both determined from the design variables (or index such as time) and uncertain parameters. This has been successfully applied in different studies such as those in the framework of Reliability-Based Design Optimization

(RBDO) (*e.g.* [Dubourg et al., 2011; Taflanidis and Beck, 2008; Zhang et al., 2017]). In time dependent reliability analyses with sufficiently smooth evolutions of the performance function with respect to time, the SILK method has also been proposed by Hu and Mahadevan [2016] relying on the calibration of a Kriging metamodel in an augmented space (composed of the time and the random variables of the problem).

This framework is here used to approximate the short term damage d in order to reduce the numerical efforts. By proceeding this way, the information inflow relative to a simulator call can be used to refine the approximation $\hat{d}$ over the augmented space. This latter is thereafter noted $\mathcal{D}_{\boldsymbol{x},\boldsymbol{\zeta}}$ and composed both of the environmental parameter domain $\mathcal{D}_{\boldsymbol{x}}$ and the uncertain parameter domain $\mathcal{D}_{\boldsymbol{\zeta}}$.

The estimation of the global mean damage D is then computed over the entire Monte Carlo population. For each samples $\boldsymbol{\zeta}$, the AK-DA estimator $\hat{D}(\boldsymbol{\zeta})$ can be written as:

$$\hat{D}(\boldsymbol{\zeta}) = \sum_{i=1}^{n_c} p(\boldsymbol{x}_i)\ \hat{d}(\boldsymbol{x}_i, \boldsymbol{\zeta})\ \Delta \tag{4.18}$$

The variance of the estimation can also be computed as proposed in the AK-DA procedure for each samples of the uncertain parameter. The variance of estimation $\sigma^2_{\hat{D}}(\boldsymbol{\zeta})$ then reads:

$$\sigma^2_{\hat{D}}(\boldsymbol{\zeta}) = \sum_{i=1}^{n_c}\sum_{j=1}^{n_c} p(\boldsymbol{x}_i)\ p(\boldsymbol{x}_j)\ \mathrm{Cov}\Big(\hat{d}(\boldsymbol{x}_i, \boldsymbol{\zeta}), \hat{d}(\boldsymbol{x}_j, \boldsymbol{\zeta})\Big) \tag{4.19}$$

An approximation $\hat{G}$ of the performance function G is finally computed in the uncertain parameter space $\mathcal{D}_{\boldsymbol{\zeta}}$ from the estimator $\hat{D}$ presented in Eq. 4.18 as follows:

$$\hat{G}(\boldsymbol{\zeta}) = D_t - \hat{D}(\boldsymbol{\zeta}) \tag{4.20}$$

4.3.2 Adaptation of the learning criterion

Within the introduced augmented space architecture presented in Section 4.3.1, the direct use of the AK-MCS learning function U does not suit. For each of the samples $\boldsymbol{\zeta}$, the global damage is not perfectly known and solely an estimator $\hat{D}$ is computed with a finite variance $\sigma^2_{\hat{D}}$. In its former definition, the AK-MCS learning optimization would indubitably lead to a loss of performance. By sequentially enriching $\boldsymbol{\zeta}$ value from the Monte Carlo population $\mathcal{P}$ until the estimation of the global mean damage converges, the entire grid of environmental combinations would be computed for each $\boldsymbol{x} \in \mathcal{D}_{\boldsymbol{x}}$ leading to a variance of estimation $\sigma^2_{\hat{D}}(\boldsymbol{\zeta})$ equal to zero. To select the point to enrich the design of experiments with, the following procedure is rather implemented to be more efficient in terms of number of calls. It relies on the use of the AK-DA algorithm.

The main idea is to first select the enrichment value $\boldsymbol{\zeta}^*$ to enrich by means of the U learning function (AK-MCS procedure) and then estimate $\hat{D}(\boldsymbol{\zeta}^*)$ by resorting to the AK-DA algorithm. The variance of estimation $\sigma^2_{\hat{D}}(\boldsymbol{\zeta})$ is no longer equal to zero due to the approximation coming from the use of the AK-DA estimator. Then this should be considered in the new criterion. This is simply implemented by only considering candidates of the Monte

Carlo population for which the estimator $\hat{D}$ has a coefficient of variation $\delta_{\hat{D}}$ greater than a given value δ_t. As a consequence, the optimal uncertain parameter $\boldsymbol{\zeta}^*$ is here chosen as:

$$\boldsymbol{\zeta}^* = \underset{\substack{\boldsymbol{\zeta}\in\mathcal{P} \\ \delta_{\hat{D}(\boldsymbol{\zeta})}>\delta_t}}{\operatorname{argmin}}\ U(\boldsymbol{\zeta}) \tag{4.21}$$

Once the sample $\boldsymbol{\zeta}^*$ is selected, the AK-DA enrichment procedure is performed on the grid of environmental parameters to elect the combination of environmental parameters $\boldsymbol{x}$ which has the highest absolute variance contribution $|\mathcal{C}_{\boldsymbol{\zeta}^*}|$ with regards to the variance of estimation $\sigma^2_{\hat{D}}(\boldsymbol{\zeta}^*)$. To do so, the variance contribution is computed as:

$$\mathcal{C}_{\boldsymbol{\zeta}^*}(\boldsymbol{x}) = p(\boldsymbol{x})\sum_{i=1}^{n_c} p(\boldsymbol{x}_i)\mathrm{Cov}\Big(\hat{d}(\boldsymbol{x},\boldsymbol{\zeta}^*),\hat{d}(\boldsymbol{x}_i,\boldsymbol{\zeta}^*)\Big) \tag{4.22}$$

The enrichment vector of environmental parameter $\boldsymbol{x}^*$ is selected in the environmental parameter space $\mathcal{D}_{\boldsymbol{x}}$ by applying the AK-DA optimization:

$$\boldsymbol{x}^* = \underset{\boldsymbol{x}\in\mathcal{D}_{\boldsymbol{x}}}{\operatorname{argmax}}\ |\mathcal{C}_{\boldsymbol{\zeta}^*}(\boldsymbol{x})| \tag{4.23}$$

By forming an augmented learning vector $\{\boldsymbol{x}^*,\boldsymbol{\zeta}^*\}$ defined in the definition space $\mathcal{D}_{\boldsymbol{x},\boldsymbol{\zeta}}$, a single new short term damage $d(\boldsymbol{x}^*,\boldsymbol{\zeta}^*)$ is assessed and the augmented Kriging metamodel $\hat{d}$ can be updated.

4.3.3 Adaptation of the stopping criterion

The stopping criterion is modified to accept uncertain estimators of the global mean damages $\hat{D}(\boldsymbol{\zeta})$ which are estimated on the entire Monte Carlo population and reads:

$$\min_{\substack{\boldsymbol{\zeta}\in\mathcal{P} \\ \delta_{\hat{D}(\boldsymbol{\zeta})}>\delta_t}} U(\boldsymbol{\zeta}) > 2 \tag{4.24}$$

4.3.4 Formalization of the proposed AK-MCS/AK-DA algorithm

The summary of the coupled AK-MCS/AK-DA algorithm is detailed below. This algorithm is described step by step with a special emphasis laid on the adaptations presented in this section.

1. **Initialization of the algorithm:**

   (a) **Generation of the Monte Carlo population $\mathcal{P}$:** An initial population of size n_{MC} is aleatory generated in the uncertain parameter design space $\mathcal{D}_{\boldsymbol{\zeta}}$.

   (b) **Composition of the initial design of experiments:** The initial design of experiments is created in the augmented space $\mathcal{D}_{\boldsymbol{x},\boldsymbol{\zeta}}$ combining an aleatory selection of points of the Monte Carlo population $\mathcal{P}$ and randomly selected points of the

grid of environmental parameters. The initial size of the design of experiments is denoted n_0.

(c) **Simulator calls**: The short term damage $d(\boldsymbol{x}, \boldsymbol{\zeta})$ is computed for each of the n_0 points of the initial design of experiments.

(d) **Calibration of a Kriging metamodel $\hat{d}$:** In the augmented space $\mathcal{D}_{\boldsymbol{x},\boldsymbol{\zeta}}$, a Kriging metamodel $\hat{d}$ of the short term damage d is calibrated with regards to the initial simulator calls.

(e) **Global mean damage estimation and computation of the performance function:** A projected estimation of the global mean damage is performed in the uncertain parameter space $\mathcal{D}_{\boldsymbol{\zeta}}$:

$$\hat{D}(\boldsymbol{\zeta}) = \sum_{i=1}^{n_c} p(\boldsymbol{x}_i)\ \hat{d}(\boldsymbol{x}_i, \boldsymbol{\zeta})\ \Delta \tag{4.25}$$

The variance of estimation is computed as:

$$\sigma^2_{\hat{D}}(\boldsymbol{\zeta}) = \sum_{i=1}^{n_c}\sum_{j=1}^{n_c} p(\boldsymbol{x}_i)\ p(\boldsymbol{x}_j)\ \mathrm{Cov}\Big(\hat{d}(\boldsymbol{x}_i, \boldsymbol{\zeta}), \hat{d}(\boldsymbol{x}_j, \boldsymbol{\zeta})\Big) \tag{4.26}$$

The approximated performance function $\hat{G}$ defined in the uncertain parameter space $\mathcal{D}_{\boldsymbol{\zeta}}$ is computed as:

$$\hat{G}(\boldsymbol{\zeta}) = D_t - \hat{D}(\boldsymbol{\zeta}) \tag{4.27}$$

(f) **Estimation of the probability of failure:**
The Monte Carlo estimator $\hat{P}_f$ of the probability of failure P_f is computed as well as its coefficient of variation $\delta_{\hat{P}_f}$.

2. **Enrichment strategy:**

(a) **Selection of the enrichment point:** The U-learning function is computed for each of the samples $\boldsymbol{\zeta}$ of the Monte Carlo population $\mathcal{P}$. An enrichment value $\boldsymbol{\zeta}^*$ of the uncertain parameter vector $\boldsymbol{\zeta}$ is selected by solving a first optimization problem in the uncertain parameter definition space $\mathcal{D}_{\boldsymbol{\zeta}}$ by the modified AK-MCS enrichment strategy:

$$\boldsymbol{\zeta}^* = \underset{\substack{\boldsymbol{\zeta}\in\mathcal{P} \\ \delta_{\hat{D}(\boldsymbol{\zeta})}>\delta_t}}{\operatorname{argmin}}\ U(\boldsymbol{\zeta}) \tag{4.28}$$

Given the enrichment vector $\boldsymbol{\zeta}^*$, the variance contribution $\mathcal{C}_{\boldsymbol{\zeta}^*}$ is computed for each $\boldsymbol{x} \in \mathcal{D}_{\boldsymbol{x}}$ as:

$$\mathcal{C}_{\boldsymbol{\zeta}^*}(\boldsymbol{x}) = p(\boldsymbol{x}) \sum_{i=1}^{n_c} p(\boldsymbol{x}_i) \mathrm{Cov}\Big(\hat{d}(\boldsymbol{x}, \boldsymbol{\zeta}^*), \hat{d}(\boldsymbol{x}_i, \boldsymbol{\zeta}^*)\Big) \tag{4.29}$$

The enrichment vector of environmental parameter $\boldsymbol{x}^*$ is selected in the environmental parameter space $\mathcal{D}_{\boldsymbol{x}}$ by applying the AK-DA optimization:

$$\boldsymbol{x}^* = \underset{\boldsymbol{x}\in\mathcal{D}_{\boldsymbol{x}}}{\operatorname{argmax}} \, |\mathcal{C}_{\boldsymbol{\zeta}^*}(\boldsymbol{x})| \tag{4.30}$$

(b) **Simulator call**: The short term damage $d(\boldsymbol{x}^*, \boldsymbol{\zeta}^*)$ is computed for the enrichment vector $\{\boldsymbol{x}^*, \boldsymbol{\zeta}^*\}$.

(c) **Calibration of a Kriging metamodel $\hat{d}$:** Same as 1.(d).

(d) **Global mean damage estimation and computation of the performance function:** Same as 1.(e).

(e) **Estimation of the probability of failure:** Same as 1.(f).

3. **Stopping condition**:
The modified stopping criterion is checked:

$$\min_{\substack{\boldsymbol{\zeta}\in\mathcal{P} \\ \delta_{\hat{D}(\boldsymbol{\zeta})}>\delta_t}} U(\boldsymbol{\zeta}) > 2 \tag{4.31}$$

If the stopping criterion is verified, the coefficient of variation of the probability of failure $\delta_{\hat{P}_f}$ is checked. If this coefficient is low enough (inferior to a limit fixed by the user), the algorithm is stopped. In the contrary case, a new population $\mathcal{P}'$ is aleatory generated. The algorithm goes back to 2.(a). with an updated Monte Carlo population $\mathcal{P} := \mathcal{P} + \mathcal{P}'$.

4.3.5 Illustration of the method

To illustrate the proposed coupling between the AK-MCS reliability method and the damage estimation procedure AK-DA, the numerical example proposed in Section 4.7 is resumed. The Monte Carlo population to classify is the same as the CMC method (i.e. $n_{MC} = 51345$). The initial design of experiments of size $n_0 = 55$ points is randomly generated in the augmented space $\mathcal{D}_{\boldsymbol{x},\boldsymbol{\zeta}}$ (same initial investment as the AK-MCS strategy). This step is done by the use of a LHS procedure. To better cover the augmented space, this generation is set by implementing an uniform distribution both for the environmental parameter and the uncertain parameter. In the environmental parameter direction, the uniform distribution is simply parameterized by the minimal and maximal values of the certification grid. In this case, the uniform density function is chosen as $\mathcal{U}(10, 20)$. For the second parameter, *i.e.* the uncertain parameter ζ, the uniform distribution is parameterized as $\mathcal{U}(\mu_\zeta - 3\sigma, \mu_\zeta + 3\sigma)$. This arbitrary choice allows to approximately cover the entire possible domain of realization of the random parameter. The initial set of environmental parameters is then transformed for the initial values of environmental parameters to correspond to the defined grid composed of $n_c = 11$ distinct points. This is proceeded by a minimization of the $\mathcal{L}_2$ distance between the aleatory generated points and the reference grid. Regarding the coefficient of variation of estimators $\hat{D}(\zeta)$, the threshold is here fixed to $\delta_t = 0.01$. In this example, the algorithm is used to classify the same Monte Carlo population as aleatory generated in Section 4.7 and no aleatory regenerations is implemented ($\mathcal{P}'$ in step 3 of the AK-MCS/AK-DA algorithm presented in Section 4.3.4).

From this initial design of experiments, $n_0 = 55$ simulator calls are performed to compute

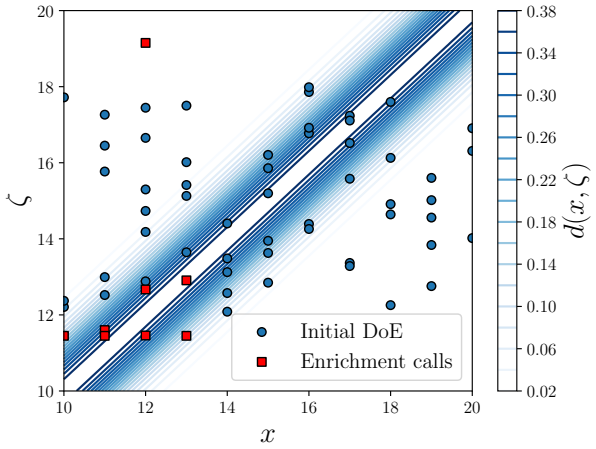

Figure 4.8: Illustration of the initial design of experiments and the enrichments proposed by the AK-MCS/AK-DA for the illustrative example.

the short term damage d in the augmented space $\mathcal{D}_{\boldsymbol{x},\boldsymbol{\zeta}}$. The algorithm is then initialized and the enrichment starts.

To converge, a total of 8 enrichments are required. The estimation of the probability of failure is equal to $\hat{P}_f = 8.7 \times 10^{-3}$ with a coefficient of variation equal to $\delta_{\hat{P}_f} = 4.70\%$. The total number of simulator calls is equal to $n_0 + 8 = 63$. The enrichment proposed by this coupling method is depicted in Figure 4.8 which shows the initial design of experiments and the enrichment points in the augmented space $\mathcal{D}_{\boldsymbol{x},\boldsymbol{\zeta}}$. As it can be observed, the main part of the 8 enrichment points are located in a zone close to the failure domain (in the vicinity of $\zeta = 12$, see Figure 4.8). Furthermore, the AK-DA strategy allows to select enrichment values of environmental parameters x which exhibit an important $p \times d$ value and so significant values for the estimation of the global mean damage. The expected reduction in terms of number of simulations of this coupling is verified on this simple example.

For the sake of illustration of the evolution of the approximated function $\hat{G}$, Figure 4.7 depicts the initialization and 7 iterations of the algorithm. As it can be observed, each of the enrichments does not permit to entirely reduce the uncertainty regarding the global mean damage estimator $\hat{D}$. This phenomena is particularly visible in Figure 4.9c where a residual variance of estimation is still present after the enrichment. The algorithm progressively enriches the initial design of experiments with new observations of the short term damage d. In the iterations 3, 5, 6 and 7, the same uncertain parameter ζ^* is selected by the modified AK-MCS algorithm. For this parameter, four AK-DA enrichments are necessary to sufficiently reduce the coefficient of variation of the estimator $\hat{D}(\zeta^*)$. As shown in Figure 4.8, each of these four observations are associated with the highest $p \times d$ environmental parameters. Once the failure domain is determined (*i.e.* the coefficients of variation of the estimators $\hat{D}$ are small enough in the vicinity of uncertain parameters which lead to failure), the last iteration focuses on the right side of the definition domain. With only one additional observation of the short term damage model d, the coefficient of variation of the estimators $\hat{D}$ computed for high values of ζ drastically decreases and the stopping criterion is verified (Eq. 4.24).

The main drawback of the proposed method is the post-processing time. As implemented in this example, a cumulated duration of 694 seconds is required in this example which represents about 1 min and 25 seconds for each iteration. This time is important and has to

be considered in the performances of the AK-MCS/AK-DA method. Furthermore, this post-processing duration is expected to increase in function of two parameters: the size of the Monte Carlo population (equal to the number of estimators $\hat{D}$ to compute) and the number of environmental parameters as well as the chosen environmental discretization (which determines the size of the autocovariance matrix to compute for the AK-DA enrichment).

To sum up the study of this illustrative case, the performances of the CMC, AK-MCS and AK-MCS/AK-DA for the considered illustrative example are regrouped in Table 4.1.

	$\hat{P}_f$	$\delta_{\hat{P}_f}$	n_D	n_d	Post-processing time
CMC	7.73×10^{-3}	4.99%	51345	594795	-
AK-MCS	7.73×10^{-3}	4.99%	8	88	37 s
AK-MCS/AK-DA	8.7×10^{-3}	4.70%	-	$55 + 8 = 63$	694 s

Table 4.1: Summary of the performances of the three proposed methods for the illustrative reliability analysis. n_D and n_d respectively refer to the number of computations of the global mean damage D and the short term damage d.

As a conclusion, the proposed method dealing with a coupling of the AK-MCS and the AK-DA is validated for this simple illustrative example. Within the proposed study, the initial set of short term damage estimations is composed of $n_0 = 55$ points. At convergence, the proposed method computes an estimation of the failure probability which presents a relative error of 12.5% on average with the estimators provided by the CMC and AK-MCS methods. For each of the enrichments, the algorithm does not compute all the short term damages for each the entire environmental grid contrary to the AK-MCS procedure. Alternatively, it only selects optimal environmental parameter x^* in the sense of the AK-DA optimization. This procedure restricts the simulator calls to the only environmental parameters which present an important $p \times d$ quantity. The evolution of the approximated performance function for different iteration steps shows that this enrichment strategy is sufficient to reduce the error for each of the "partially observed" global mean damages.

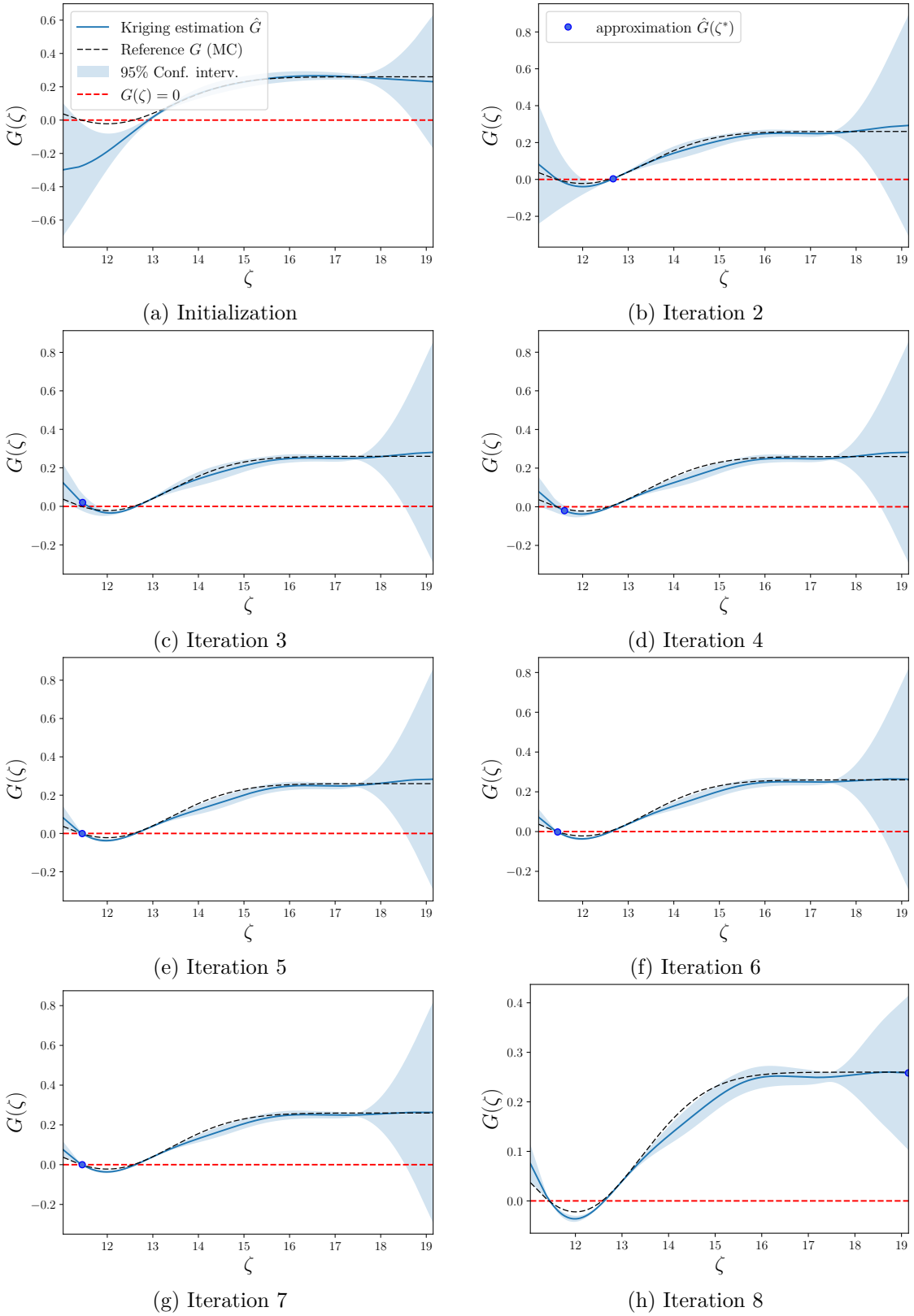

(a) Initialization (b) Iteration 2

(c) Iteration 3 (d) Iteration 4

(e) Iteration 5 (f) Iteration 6

(g) Iteration 7 (h) Iteration 8

Figure 4.9: Illustration of the evolution of the prediction $\hat{G}$ obtained with the implementation of the AK-MCS/AK-DA coupled method for the initialization and 7 different iterations.

4.4 Conclusions

In this last chapter, the context of reliability analysis of wind turbine structures is introduced. A possible traditional approach considers the impact of uncertainty on estimated mechanical reactions by the use of conservative safety factors. This method has shown its performance in today's industrial context but exhibits a major drawback. The choice of the safety factors to adopt is based on standard's recommendations and most of the time estimated from expertise to minimize the systematic risk inherent to any kind of designing situations. As a result, the certified structures are usually over-designed whilst maintaining an acceptable level of safety, even though not quantified in practice.

To reduce the cost of wind energy, an appealing solution is to resort to complete assessments of reliability analyses. These latter often rely on the probabilistic modeling of all the sources of uncertainty which can have an impact on the determination of the structural reactions to estimate. Then, the assessment of the failure probability with respect to a given failure scenario is computed to provide engineers with information regarding the reliability of the proposed design. In this sense and depending on the analyzed structural response, a policy of calibration of safety factors can be deployed. In this chapter, the commonly used Stress-Strength approach has been presented. In this industrial context, complex and costly-to-evaluate simulators are involved and efficient reliability methods should therefore be considered to compute the probability of failure.

After a brief introduction to reliability methods, the Crude Monte Carlo (CMC) and the Adaptive Kriging for Damage Assessment (AK-MCS) have been presented with more details. For illustration purpose, a simple illustrative test case has been proposed and allowed one to compare their performances. This example represents a very simplified situation of structural damage assessment based on a single environmental parameter. In addition, an uncertain parameter is introduced for which the probability density function is known. The modeling of the short term damage response d has been proposed to represent a situation where the value of the uncertain parameter influences the response. The implementation of the two proposed simulation methods clearly underlined the numerical efforts required for such an analysis. For the defined failure scenario, the Crude Monte Carlo approach leads to $n_{MC} = 51345$ estimations of the global mean damage D (*i.e.* 594795 evaluation of the short term damage d) to estimate a probability of failure of $P_f = 7.73 \times 10^{-3}$. By considering that a single estimation of the global mean damage is a challenging task for engineers, these results underline the impossibility of industrial deployment of this method. The AK-MCS approach, based on an adaptive construction of a Kriging metamodel $\hat{G}$ of the performance function G, leads to an accurate estimation of the probability of failure with a drastically reduced simulation investment. In this case, the algorithm only requires a total of 8 simulations to converge, *i.e.* 88 estimations of the short term damage.

To keep on reducing the numerical efforts of damage based reliability analyses, an adaptation of the AK-MCS is proposed. In the former version of AK-MCS, for each of the selected observational points (*i.e.* realization of random variables) a complete computation of the global mean damage is required. Usually it implies a high number of short term damage estimations reaching tens of thousand simulator calls for complete environmental descriptions.

The AK-DA procedure for the estimation of the global mean damages based on a reduced number of simulator calls has therefore been integrated to the AK-MCS architecture. Several changes are required to implement the proposed method for damage reliability assessment. Firstly, the Kriging metamodel calibration is performed in an augmented space defined as the Cartesian product between the space associated with the environmental parameters $\mathcal{D}_{\boldsymbol{x}}$ and the physical space associated with the set of random variables $\mathcal{D}_{\boldsymbol{\varsigma}}$. This choice appears justified since the short term damage response in such a space is expected to evolve smoothly, *i.e.* without the presence of noise. Secondly, the enrichment strategy (based on the U-learning function) has been modified to integrate the selection of the best point to simulate for the AK-DA procedure. Finally, the stopping criterion has been slightly modified to consider the approximations of the global mean damages at the enriched point (non-interpolant character).

The validation of this method has been proposed for the presented simplified example. This analyses has shown the adaptability of the proposed method within the reliability analysis framework described in this chapter. This chapter proposes a single illustration of the proposed coupling between the AK-MCS method and the AK-DA enrichment procedure introduced in this thesis. These preliminary results shows the adaptability of the proposed method with regards to the industrial context with an estimation of the probability of failure which can be considered as accurate with an average error of 12.5 % compared to the reference value obtained using a Crude Monte Carlo procedure. Compared to the direct use of the AK-MCS algorithm, a reduction of the number of simulations is obtained, since convergence is reached for a total of 63 simulator calls, compared to the 88 calls required with the former version of AK-MCS. The major drawback of this procedure is the post-processing time which represents, in this particular case, a total duration of about 700 seconds. This has to be kept in mind for the future applications of the proposed algorithm. The presented results are preliminary illustrations and the AK-MCS/AK-DA has to be further investigated. Firstly, a study on the robustness of the algorithm with regards to the choice of the initial design of experiments have to be performed. Secondly, the method has to be tested for more complex examples dealing with smaller probability of failure (more important Monte Carlo population) and short term damages defined with several environmental parameters.

References

S. Aasen, A. M. Page, K. S. Skau, and T. A. Nygaard. Effect of foundation modelling on the fatigue lifetime of a monopile-based offshore wind turbine. *Wind Energy Science*, 2: 361–376, 2017.

L. V. Andersen, T. L. Andersen, and L. Manuel. Model uncertainties for soil-structure interaction in offshore wind turbine monopile foundations. *Journal of Marine Science and Engineering*, 6, 2018.

Laszlo Arany, S. Bhattacharya, John Macdonald, and S.J. Hogan. Design of monopiles for offshore wind turbines in 10 steps. *Soil Dynamics and Earthquake Engineering*, 92:126 – 152, 2017.

J-M. Bourinet. *Reliability analysis and optimal design under uncertainty - Focus on adaptive surrogate-based approaches.* Habilitation à diriger des recherches, Université Clermont Auvergne, 2018.

V. Dubourg, B. Sudret, and J. M. Bourinet. Reliability-based design optimization using kriging surrogates and subset simulation. *Structural and Multidisciplinary Optimization*, 44(5):673–690, 2011.

B. Echard, N. Gayton, and M. Lemaire. Ak-mcs: An active learning reliability method combining kriging and monte carlo simulation. *Structural Safety*, 33(2):145 – 154, 2011.

C. M. Fontana, W. Carswell, S. R. Arwade, D. J. DeGroot, and A. T. Myers. Sensitivity of the dynamic response of monopile-supported offshore wind turbines to structural and foundation damping. *WIND ENGINEERING*, 39:609–628, 2015.

Z. Hu and S. Mahadevan. A single-loop kriging (silk) surrogate modeling for time-dependent reliability analysis. *Journal of Mechanical Design*, 138, 2016. doi: 10.1115/1.4033428.

Z. Jiang, W. Hu, W. Dong, Z. Gao, and Z. Ren. Structural reliability analysis of wind turbines: A review. *Energies*, 10, 2017.

N. Lelièvre, P. Beaurepaire, C. Mattrand, and N. Gayton. AK-MCSi: A kriging-based method to deal with small failure probabilities and time-consuming models. *Structural Safety*, 73: 1–11, 2018.

N. Lelièvre. *Développement des méthodes AK pour l'analyse de fiabilité. Focus sur les événements rares et la grande dimension.* PhD thesis, Université Clermont-Auvergne, 2018.

Maurice Lemaire. *Structural reliability.* John Wiley & Sons, 2013.

J. Luengo, V. Negro, J. García-Barba, J-S. López-Gutiérrez, and M. Dolores Esteban. New detected uncertainties in the design of foundations for offshore wind turbines. *Renewable Energy*, 131:667 – 677, 2019.

V. Negro, J-S. López-Gutiérrez, M. D. Esteban, and C. Matutano. Uncertainties in the design of support structures and foundations for offshore wind turbines. *Renewable Energy*, 63: 125–132, 2014.

J. D. Sørensen and H. S. Toft. Probabilistic design of wind turbines. *Energies*, 3:241–257, 2010.

B. Sudret. *Uncertainty propagation and sensitivity analysis in mechanical models Contributions to structural reliability and stochastic spectral methods*. Habilitation à diriger des recherches (HDR), Univ. Blaise Pascal - Clermont II, France, 2007.

A.A. Taflanidis and J.L. Beck. Stochastic subset optimization for optimal reliability problems. *Probabilistic Engineering Mechanics*, 23(2):324 – 338, 2008. 5th International Conference on Computational Stochastic Mechanics.

J. Zhang, A.A. Taflanidis Taflanidis, and J. C. Medina. Sequential approximate optimization for design under uncertainty problems utilizing kriging metamodeling in augmented input space. *Computer Methods in Applied Mechanics and Engineering*, 315:369 – 395, 2017.

THESIS CONCLUSIONS AND PERSPECTIVES OF DEVELOPMENT

As presented all along this thesis, the development of offshore wind is a challenging task for engineers and industrial actors. To enhance the production capacities and to maximize the electricity production, the size of offshore turbines has to be necessarily much more important than for traditional onshore installations. To resist the offshore loading conditions and to hold the production components (regrouped in the rotor-nacelle assembly), supporting structures have to be carefully designed to ensure a maximal safety of installations with regards to risks of mechanical collapsing. To guarantee the project development and to secure the related investments, each of the proposed designs has to be certified regarding its mechanical behavior and its capacity to resist within the installation site. Of all the structural verifications to perform and because of the high number of cycles the structures undergo during their lifetimes, the analyses of mechanical fatigue of supporting structures have to be carefully carried out. To help engineers on the determination of cumulated damage responses, certification bodies propose a properly defined framework, listing a series of requirements to ensure the representativeness of numerical simulations. The industrial application of the certification guidelines results in an important simulation effort for the estimation of the fatigue related structural response for a given design. As presented in Chapter 1, this investment is firstly due to the involved number of simulations to perform. For industrial applications dealing with a complete description of the natural environment, tens of thousands simulations have to be performed for a single estimation of the cumulated damage over a given life cycle (*e.g.* the design load case 1.2 which focuses on the determination of the cumulated damage for the "normal production" conceptual situation and which has been the scope of this thesis). Secondly, for each of the simulations, the consideration of nonlinearities of the structural responses, mainly due to the production servo control and aerodynamic damping induced by the rotor-blades assembly, has to be carefully addressed. Certification bodies then require the use of time demanding simulations for each of the proposed fatigue assessments. As a consequence, damage estimations of offshore wind turbines is today a challenge for industrial companies for which a single damage assessment represents several hundreds of hours of simulation.

This thesis focuses on the use of Kriging metamodels and more precisely on adaptive

Kriging approaches for the reduction of the simulation investments for structural fatigue analyses. The formalization of the industrial problematic introduces two quantities of interest. The short term damage d stands for the cumulated structural damage defined over a fixed period of time and for each of the combination of environmental parameters, which is assumed to represent a given loading situation. From the knowledge of this structural response and by the access to the probability of occurrence of each combinations of environmental parameters, a global mean damage D is then computed. This latter quantity represents in this thesis the quantity of interest.

General conclusions of the proposed work

The Kriging metamodel based methods aim at computing approximations of demanding numerical codes based on a reduced set of observations. By the statistical assumptions which are described in Chapter 2, this technique is particularly popular because of its advantages of being non parametric and interpolant. Furthermore, for each of the numerical predictions, a variance of estimation can be easily computed, providing information about the statistical uncertainty of predicted responses. This technique is widely developed in the context of numerical optimization and reliability analyses, which usually require a high number of simulator calls. To better approximate the quantities of interest which is costly to evaluate, these communities have developed iterative strategies based on a sequential enrichment of the model observations. The proposed methods have been successfully applied in the last 20 years for complex engineering problems. Because of the formalization introduced in this thesis regarding the quantity of interest D, computed from a finite number of short term damages d, a specific Adaptive Kriging strategy has been chosen for the purpose of this thesis problematic.

In Chapter 3, the possibilities to use the Kriging prediction for the reduction of the numerical investments required for the estimation of the global mean damage have been investigated. An estimator $\hat{D}$ of the quantity of interest D is introduced, computed from a Kriging predictor $\hat{d}$ of the demanding short term damage function d. Afterwards, the Adaptive Kriging for Damage Assessment (AK-DA) method is presented. This procedure proposes to use adaptive Kriging procedures to sequentially compose a reduced but informative set of short term damage observations d to effectively approximate the global mean damage D. An adaptation of the Adaptive Kriging based methods had to be thought to correspond to the formalization used in this thesis. To iteratively enhance the global mean damage D prediction, a learning strategy based on the reduction of its variance of estimation is proposed. The sequential enrichment aims at extending an initial design of experiments with short term damage estimations for which the Kriging variance of prediction participates the most to the global variance of the predictor $\hat{D}$. This is done by the computation of the "variance contribution" terms defined for each of the combinations of environmental parameters. The application of this method, both for illustrative and industrial cases shows a noteworthy reduction of the simulation efforts required for the estimation of the cumulated damage response of structural designs. To test the method with regards to a challenging application inspired from industrial example, a test case based on the NREL 5MW Monopile design

is used all along the thesis. The considered environmental parameters are the wind mean speed at hub height, the wind-wave misalignment and the spectral peak period and significant height of waves. In the presented example, a single estimation of the global mean damage D is assumed to require 10120 simulator calls of the short term damage model d. The application of the AK-DA method on this challenging four-dimensional test case leads to a convergence after a total number of estimations of the short term damages equal to 385 with a total of 65 iterations of the AK-DA method and an absolute relative error below 5% for the estimation provided by $\hat{D}$ with regards to the reference value D.

Even though the number of simulator calls is drastically reduced, the post-processing duration required for the method to calibrate a Kriging metamodel and to select a new simulation to perform can not be neglected and may in certain cases represent an important time. To this extent and because of the independence of the short term damage computations, the possibilities of multi-enrichment strategies have been analyzed to reduce the number of AK-DA iterations to convergence. For such a purpose, the "influence area" methodology is proposed to select a set of enrichments which maximizes the information inflow of the metamodel based on the analysis of the correlation parameters directly provided by the calibration of the Kriging approximation. The implementation of this method leads to a reduction of the number of enrichment steps provided by the AK-DA algorithm and globally contributes to the reduction of the method's execution time. As a comparison with the single enrichment strategy initially used for the four-dimensional example, the convergence has been reached with only 9 iterations for a set of enrichments composed of 8 model observations. This significant reduction has been obtained with the same accuracy regarding the single enrichment strategy.

Finally, an extension of the AK-DA method for the simultaneous estimation of global mean damages D for multiple structural locations is presented. This last development underlines the potential of the method to be industrially used by promoting a global implementation. Four structural locations have been analyzed simultaneously with a total of 444 estimations of the short term damages d and a number of AK-DA iterations equals to 31.

In Chapter 4, an introduction to damage based reliability analysis is proposed. Design uncertainties have been integrated in the definition of the short term damage model to mimic the design situations in which model parameters can not be accurately determined. The objective of this development is to investigate the possibilities of using the AK-DA method within the framework of a properly defined reliability analysis. In the first hand, the difficulties related to this type of analysis have been highlighted for the particular context of damage based analysis of wind turbine structures. In the second hand, a method based on the coupling between the AK-MCS algorithm and the AK-DA procedure has been introduced and formalized. The first results of this development are presented with regards to an illustrative example inspired from industrial applications and the applicability of such a method is demonstrated.

Perspectives of development

This PhD project has allowed to initialize a research theme at EDF based on the use of metamodeling analyses to reduce simulation costs related to mechanical verifications of wind turbine structures. To further expand the developments proposed in this thesis, several perspectives can be addressed.

Perspectives for the AK-DA method

The AK-DA method has been developed during this project with the constraint to be industrially applicable. As mentioned several times throughout this manuscript, the Kriging metamodel has been used with two possible set-ups. The basis of regression has been arbitrarily chosen as constant for the illustrative examples and quadratic for the industrial applications. Any study has been addressed beforehand to properly analyze the pros and cons of choosing one over another. To better understand the AK-DA behavior, this kind of analysis should be properly done, for example, by comparing the benefits of the different basis of regression with regards to AK-DA performances. Additionally, the choice of the autocorrelation function has always been the anisotropic squared exponential model because of the smoothness of the metamodel it provides. As for the choice of the regression basis, a complete study should be carried out to quantify the advantages of setting the Kriging metamodel with this correlation function, in terms of accuracy regarding the estimation of $\hat{D}$ and the reduction potential, and to turn to other correlation structures in case they provide better results.

The "influence area" method proposed for the consideration of multi-enrichment strategies in the AK-DA algorithm still needs to be further developed. This method has been proposed to benefit from the correlation information provided by the calibration of the Kriging metamodel. This procedure should be compared in terms of performance with traditional k-means clustering techniques used in several studies for multi-enrichment strategies. Secondly, the former version of the "influence area" method presented in this thesis relies on the use of two parameters which are the parameter r_0 (the restriction parameter that defines the admitted cross correlation between enrichment sets of observation) and the required size n_e of the enrichment set. As illustrated in Chapter 3, the choice of the r_0 value is not easy and can lead in certain cases to not respect the specified number of environmental combinations to consider (small r_0 lead to large restrictions in the research domain and possibly to an early covering of the entire definition domain). A possible enhancement would rely on the implementation of an optimization procedure aiming at automatically selecting the better value for this parameter with regards to the computational capacity. In this case, user would only have to specify the number of possible simultaneous simulations and would be sure to get an enrichment set of environmental combinations equals to its specification. From the user point of view, this would also facilitate the global setting of the method by reducing the tuning parameters to a single parameter, namely the number n_e of possible simultaneous calls of the simulator.

The AK-DA algorithm has been presented for illustrative and industrial example where a single aleatory seed is used. As a consequence, the short term damages are only evaluated

over a period of time equals to 10 min. This has been done to ease the first developments by reducing the number of simulations to perform for the computation of reference values. However, the method still has to be validated in the particular case where six aleatory generations are used to determine the short term damage (or when single 1-hour damages are computed) as required by the certification bodies. From a more global point of view, a potential extension of the proposed method would be the direct consideration of the uncertainty of the short term damage response due to the physical uncertainty of the environmental loadings. Indeed, for the DLC 1.2, certification bodies require the use of 6 aleatory generations for each of the short term damage computations. By integrated this variability directly in the Kriging metamodel (*e.g.* by the use of stochastic Kriging set with nugget's effect), a more global approach could be developed. The global mean damage and more specifically its computed variance of estimation could include the potential variation of this latter due to physical uncertainty of environmental loadings.

This finish with the perspectives relative to the AK-DA algorithm, a study can be planned to test its performance for other damage based design load cases. This thesis has focused on the design load 1.2 which aims at estimating the cumulated damage at several structural locations for the conceptual situation "normal production". Other conceptual situations present damage based design load cases which need massive simulation investments to be fulfilled. For an example, the methodology could be tested for the design load case 6.4 which is basically the same study as 1.2 but with a parked or idling turbine (no production).

Perspectives for the damage based reliability assessment (AK-MCS/AK-DA)

The second part of this thesis which deals with damage based reliability analyses of offshore wind turbines is still at its early development. Chapter 4 introduces a possible extension of the AK-DA method in the demanding context of reliability assessment. Even though the first results are promising, the perspectives of developments are numerous before its applicability can be properly validated in an industrial context. Firstly, a complete analysis of the method performances has to be done to test the robustness of the algorithm, by only considering the proposed simplified example. Different types of initial design of experiments could be proposed and compared to the LHS performed in the augmented space which is depicted in this thesis.

Secondly, the performance of the algorithm has to be tested with more complex examples. The presented illustration is only two-dimensional and composed of a single environmental parameter and a single uncertain parameter. More representative test cases should be used to clearly determine the limits of the algorithm. For such a purpose, one could increase the number of environmental parameters, the number of uncertain parameters and finally both the number of environmental parameter and uncertain parameters. By implemented different test case, a limit could be determined in terms of order of magnitude which can be accurately estimated with a reasonable processing time.

The processing time for the algorithm to complete an entire enrichment (calibration of the Kriging metamodel, computation of the estimations of $\hat{D}$ so as the variance of estimation $\sigma^2_{\hat{D}}$ for the entire Monte Carlo population) seems to be a limitation for the direct application of

the proposed algorithm. In this sense, future developments should focus on the possibilities to reduce the duration required for each of the enrichment steps.

APPENDIX A

DESIGN LOAD CASES FOR NORMAL PRODUCTION

Design situation	DLC	Wind Condition	Waves	Wind and wave directionality	Sea currents	Water level	Types of analysis	Partial safety factors
Power production	1.1	Normal Turbulence Model (NTM) $u_{in} < u < u_{out}$	Normal Sea State (NSS) $h_s = \mathbb{E}[H_s, U]$	Codirectional in one direction	Normal Current Model (NCM)	Mean Sea Level (MSL)	ULS	N=1.25
	1.2	Normal Turbulence Model (NTM) $u_{in} < u < u_{out}$	NSS Joint prob. distribution of H_s, T_p and U	Codirectional in multiple direction	No current	Normal Water Level Range (NWLR) or $\geq$ Mean Sea Level (MSL)	FLS	*
	1.3	Extreme Turbulence Model (ETM) $u_{in} < u < u_{out}$	NSS $h_s = \mathbb{E}[H_s, U]$	Codirectional in one direction	Normal Current Model (NCM)	Mean Sea Level (MSL)	ULS	N
	1.4	Extreme Coherent Gust with Direction Change (ECD) $u = u_r - 2, u_r, u_r + 2$	NSS (or NWH) $h_s = \mathbb{E}[H_s, U]$	Misaligned, wind direction change	Normal Current Model (NCM)	Mean Sea Level (MSL)	ULS	N
	1.5	Extreme Wind Shear (EWS) $u_{in} < u < u_{out}$	NSS (or NWH) $h_s = \mathbb{E}[H_s, U]$	Codirectional in one direction	Normal Current Model (NCM)	Mean Sea Level (MSL)	ULS	N
	1.6a	Normal Turbulence Model (NTM) $u_{in} < u < u_{out}$	Severe Sea State (SSS) $H_s = H_{sss}$	Codirectional in one direction	Normal Current Model (NCM)	Normal Water Level Range (NWLR)	ULS	N
	1.6b	Normal Turbulence Model (NTM) $u_{in} < u < u_{out}$		Codirectional in one direction	Normal Current Model (NCM)	Normal Water Level Range (NWLR)	ULS	N

APPENDIX B

CYCLE COUNTING AND CUMULATIVE DAMAGE ESTIMATION

The estimation of the cumulated damage due to a stress time history requires several processing steps which can be described as:

- the decomposition of the stress time history into fatigue cycles
- the quantification of the mechanical damage for each extracted cycles
- the estimation of the cumulated damage

This appendix proposes a brief presentation of these steps. The rainflow cycle counting method is first introduced. The use of S-N curves to estimate the individual contribution of fatigue cycle in terms of damage is then desribed and the linear Palmgren-Miner cumulative law is presented.

B.1 The rainflow cycle counting

From the time signal of a local stress $\sigma(t)$ engineers are interested in (*e.g.* generalized Von Mises stress), the rainflow cycle counting method allows to extract the stress variations $\Delta\sigma$ that potentially participate to the fatigue accumulation at a given structural location. A pre-treatment of the time signal is performed by transforming it into a peak-valley signal. From the reduced time signal σ^* of size n_{tot}, a 4-points forward rainflow algorithm is executed to extract the cycles. This algorithm is presented as follows:

1. The algorithm and the residue index n_R are initialized: $i = 1$, n_R=0. The mean $\boldsymbol{\sigma}_m$ and amplitude $\boldsymbol{\sigma}_a$ vectors of the extracted cycles are initialized to empty vectors.
2. Four consecutive points of the reduced stress time signal σ^* are considered:

$$\{\sigma_i^*, \sigma_{i+1}^*, \sigma_{i+2}^*, \sigma_{i+3}^*\}$$

Their relative stress variations are computed as:

$$\Delta\sigma^*_{12} = |\sigma^*_{i+1} - \sigma^*_i|$$
$$\Delta\sigma^*_{23} = |\sigma^*_{i+2} - \sigma^*_{i+1}|$$
$$\Delta\sigma^*_{34} = |\sigma^*_{i+3} - \sigma^*_{i+2}|$$

3. If $\Delta\sigma^*_{23} \leq \Delta\sigma^*_{12}$ and $\Delta\sigma^*_{23} \leq \Delta\sigma^*_{34}$, the stress variation $\Delta\sigma^*_{23}$ is extracted. In this case, the amplitude σ_a and the mean σ_m of the related cycle are computed and stored:

$$\boldsymbol{\sigma}_a := \{\boldsymbol{\sigma}_a; \frac{\Delta\sigma^*_{23}}{2}\}$$
$$\boldsymbol{\sigma}_m := \{\boldsymbol{\sigma}_m; \frac{\sigma^*_{i+1} + \sigma^*_{i+2}}{2}\}$$

   The indices $i+1$ and $i+2$ are erased of the sequence σ^*.
4. The algorithm goes two steps backward $i = i - 2$ (or $i = 1$ if $i < 3$) and returns to step 2.
5. If the sequence is fully analyzed ($i = n_{tot}$) and n_R=0, the residue $\{R\}$ composed of the non extracted stress variations is obtained. The residue index is incremented:

$$n_R = 1 \tag{B.1}$$

   An additional treatment is required to extract extreme cycles. The algorithm goes back to step 2 with:

$$\sigma^* = \{R; R\} \text{ and } i = 1 \tag{B.2}$$

6. If $n_R = 1$, the algorithm stops.

The proposed rainflow procedure outputs an ensemble of extracted stress variations that may contribute to the fatigue damage accumulation at the given structural location of interest. These variations are stored as a series of equivalent stress cycles which means and amplitudes contained in the vectors $\boldsymbol{\sigma}_m$ and $\boldsymbol{\sigma}_a$.

B.2 S-N curves and cycle damage estimations

For each of the extracted stress cycles, the potential contribution in terms of damage is computed by means of S-N curves. These curves represent the material behavior under constant amplitude loading. From a given amplitude stress level σ, one can know the number of cycles the given material can resist, *i.e.* the number of cycles to failure for this particular constant amplitude fatigue loading. In the context of the structural certification of the wind turbine, DNV-GL proposes a general S-N equation to be adapted to the study case:

$$\log_{10}(N) = \log_{10}(a) - m \times \log_{10}\left(S \times \left(\frac{t}{t_{ref}}\right)^k\right) \tag{B.3}$$

where:

- $-m$ is the slope of the $\log(S)$-$\log(N)$ curve
- $\log_{10}(a)$ is the interception of the $\log(N)$ axis
- t is the thickness in which fatigue cracks can propagate (t_{ref} is a reference to set)
- k is a scale exponent

Each of the above-mentioned parameters are referenced in guidelines to correspond to the considered geometry and the environmental situation (air, sea water with or without cathodic protection). As a result, the equivalent number of cycles to failure N_i ($i \in \{1, \ldots, n_{RF}\}$) is computed for each of the n_{RF} extracted cycles. Haigh diagrams should first be used. A Goodman linear model is selected in the certification process for that purpose.

B.3 Miner's cumulative damage

Once the n_{RF} damage effective loading cycles are extracted and their respective effects in terms of damage estimated, a global estimation of the cumulated damage induced by the time signal $\sigma(t)$ can be computed by the use of the Palmgren-Miner law presented as:

$$d = \sum_{i=1}^{n_{RF}} \frac{1}{N_i} \tag{B.4}$$

By definition, this quantity is assumed to be equal to 1 when failure occurs.

APPENDIX C

THESIS EXTENDED SUMMARY IN FRENCH

Ce manuscrit de thèse présente l'ensemble des développements proposés au cours d'un projet réalisé avec l'Université Clermont Auvergne, l'Institut Pascal, SIGMA Clermont et EDF R&D (financement CIFRE #2015/0692). Le résumé étendu présenté ci-dessous reprend de manière concise le contexte industriel, les problématiques scientifiques liées et les propositions faites dans le cadre de ce projet. Le contexte industriel de l'étude et les problématiques scientifiques déduites sont présentées en Section C.1. Dans un second temps, la méthode de prédiction des réponses de codes numériques coûteux par métamodèle de Krigeage est brièvement présentée en Section C.2. La méthode AK-DA ("Adaptive Kriging for Damage Assessment") est ensuite synthétisée en Section C.3, avant d'exposer les résultats de l'extension de cet algorithme à l'analyse de fiabilité (couplage AK-MCS/AK-DA) en Section C.4.

C.1 Contexte industriel et problématiques scientifiques de l'étude

C.1.1 Contexte industriel du projet

La production d'électricité est aujourd'hui un enjeu majeur et indispensable au développement de notre société. EDF (*i.e.* Éléctricité De France) se positionne aujourd'hui comme un acteur majeur de cette industrie et se doit d'étayer ses technologies de production afin de fiabiliser son offre tout en minimisant son impact environnemental. Bien que majoritairement décarbonnée grâce au nucléaire, la production française se tourne progressivement vers des technologies vertes afin de répondre aux attentes politiques et sociales. Parmi l'ensemble des sources d'énergie renouvelables, le développement de la production éoliennes concentre aujourd'hui une part importante des investissements du groupe. L'évolution progressive de cette technologie a permis une réduction importante de son coût de revient et de nouveaux challenges industriels s'ouvrent avec les projets futurs de développement de la production éolienne en mer.

De part les dimensions des structures proposées et des risques liés à leur utilisation, la certification des conceptions est une étape indispensable à l'industrialisation des projets en mer.

Afin de tenir compte de la complexité des états de sollicitation induits par l'environnement marin et de garantir une sécurité maximale des installations, les organismes certificateurs (*i.e.* tiers de confiance) proposent un processus détaillé de vérification des performances physiques de chaque conception reposant sur l'application directe des exigences développées dans les documents normatifs [DNV-GL, 2014; IEC, 2005, 2009]. Ainsi, l'ensemble des caractéristiques de tenue et de production sont vérifiées afin de valider les performances attendues. D'un point de vue mécanique, différentes réponses structurelles relatives aux états de sollicitation estimées sur la durée de vie de la conception doivent être réalisées. Cette thèse se focalise uniquement sur les problématiques de vérification de la tenue mécanique vis-à-vis du cumul d'endommagement. Plus particulièrement, l'estimation rapide et fiable des quantités liées et l'ouverture à l'analyse de fiabilité tenant compte des incertitudes de conception sont ici traitées. L'ensemble des propositions contenues dans ce document ont été faites dans le souci de correspondre au mieux aux attentes des organismes certificateurs afin de faciliter l'industrialisation des méthodes proposées.

Dans le cadre industriel présenté ici, le processus de certification propose aux ingénieurs un découpage précis de la durée de vie en un ensemble de *situations conceptuels*, toutes présentées en Figure C.1. Pour chacune, un ensemble d'analyses mécaniques doit être réalisé afin de prendre en compte la totalité des états de sollicitation potentiels. Pour ce faire, la norme défini des cas de charges ("Design Load Cases" abrégées "DLC" dans la suite) définissant toutes les configurations de chargement possibles pour chacune des situations conceptuelles définies. Parmi ces cas de charge, plusieurs requièrent de quantifier l'endommagement mécanique cumulé. A partir de la combinaisons de ces estimations pour chacune des situations conceptuelles, un endommagement à durée de vie peut être défini.

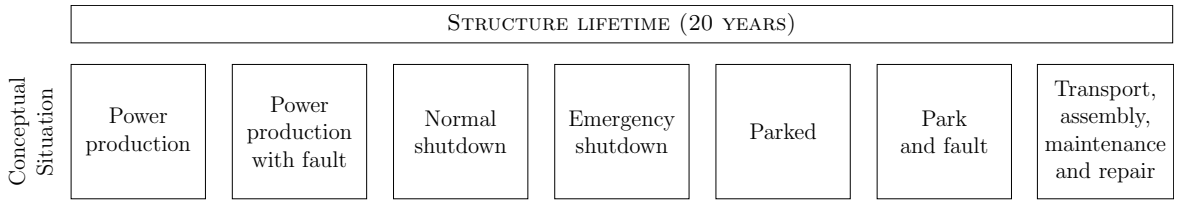

Figure C.1: Présentation des différentes situations conceptuelles à prendre en compte lors de la validation de la tenue mécanique des unités offshores [IEC, 2009]

L'ensemble des exemples traités dans cette thèse porte sur l'estimation de l'endommagement cumulé sur les cycles de vie relatifs à la situation conceptuelle "Power Production". Plus particulièrement, le cas de charge décrit par le DLC 1.2 s'orientant sur la production dite "normale" où l'éolienne produit de l'énergie et où les sollicitations environnementales sont modérées. Deux problématiques industrielles sont définies et présentées dans la suite afin d'introduire les problématiques scientifiques du projet.

C.1.2 Formalisation scientifique du processus de certification

La formalisation du calcul d'endommagement introduit ici est réalisée comme suit. L'état de sollicitation est défini d'une manière globale à partir d'un vecteur $\boldsymbol{x}$, regroupant n paramètres environnementaux supposés décrire l'état environnemental lié à chaque DLC. Quatre paramètres environnementaux sont définis et utilisés dans ce manuscrit ($n = 4$) : la vitesse moyenne du

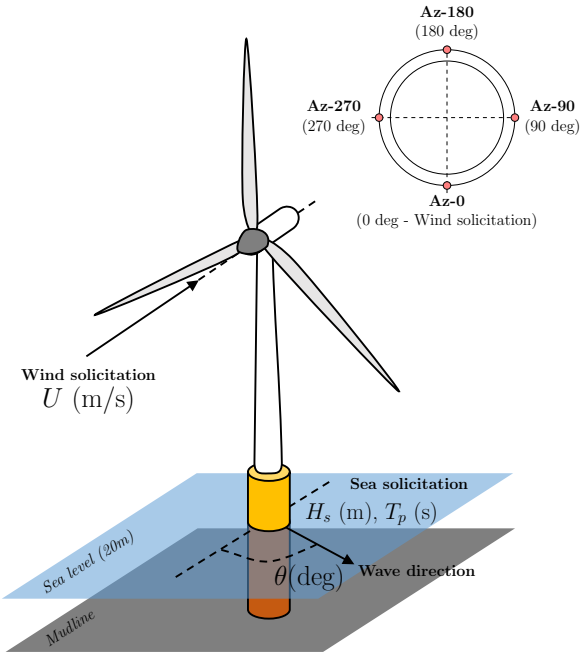

Figure C.2: Schéma de la structure d'intérêt de la thèse, basée sur la modélisation NREL 5MW OC3 Monopile [Jonkman et al., 2009]

vent au niveau du rotor U estimée sur 10 minutes, le désalignement entre le vent et les vagues θ, la période de pic spectral T_p et la hauteur significative des vagues H_s. L'ensemble des paramètres est reporté sur la Figure C.2 représentant l'exemple industriel, servant d'illustration industrielle tout au long de cette thèse.

Chacun de ces paramètres admet un domaine de variation qui regroupés, donnent le domaine global de variation $\mathcal{D}_{\boldsymbol{x}}$ du vecteur de paramètres environnementaux $\boldsymbol{x}$. A partir de ce paramétrage, l'endommagement estimé pour une situation conceptuelle et en un point défini de la structure est manipulé grâce à la quantité d'intérêt appelée dans la suite "endommagement moyen" D et définie comme suit :

$$D = \int_{\boldsymbol{x}\in\mathcal{D}_{\boldsymbol{x}}} d(\boldsymbol{x})\, p(\boldsymbol{x})\, \mathrm{d}\boldsymbol{x} \approx \sum_{i=1}^{n_c} d(\boldsymbol{x}_i)\, p(\boldsymbol{x}_i)\, \Delta \tag{C.1}$$

où d est l'endommagement estimé sur une période de temps définie (en général égale à 600 secondes), p est la probabilité d'occurrence du paramètre environnemental $\boldsymbol{x}$, Δ le pas de discrétisation et n_c le nombre de combinaisons de paramètres environnementaux à prendre en compte. La discrétisation du domaine de variation $\mathcal{D}_{\boldsymbol{x}}$ permettant de passer d'une formalisation continue à un problème discret est considérée comme imposée par la norme et envisagée ici comme une grille régulière. Ainsi, le pas de discrétisation Δ est défini comme :

$$\Delta = \delta_1 \times \cdots \times \delta_n \tag{C.2}$$

où δ_i représente le pas de discrétisation du paramètre environnemental $i \in \{1, \ldots, n\}$.

C.1.3 Limitations industrielles et problématiques scientifiques

Bien que facile d'accès, la formalisation présentée ci-dessus reste complexe à appliquer d'un point de vue industriel. Deux limitations industrielles découlent de la formalisation du calcul d'endommagement présentée ci-dessus : le coût du calcul de l'endommagement moyen D et l'investissement numérique nécessaire à la mise en place d'analyse de fiabilité mécanique vis-à-vis de la tenue des conceptions au cumul de fatigue.

Limitation 1 : une estimation coûteuse de l'endommagement moyen D

La discrétisation du problème, permettant de passer d'une formulation continue à une formulation discrète est déterminée par le choix du pas de discrétisation Δ mentionné en Eq. C.1 et défini en Eq. C.2. Afin de garantir la représentativité de l'estimation de l'endommagement moyen D, le domaine de variation des paramètres environnementaux $\mathcal{D}_{\boldsymbol{x}}$ doit être approché par un ensemble discret de n_c combinaisons environnementales défini à partir de grilles régulières proposées par les organismes certificateurs. Afin d'assurer une représentativité maximale du modèle de sollicitation environnemental, plusieurs paramètres doivent être pris en compte. Pour certains cas de charge (ex : DLC 1.2 "Estimation de l'endommagement cumulé sur les cycles de production normale"), le nombre n_c de combinaisons environnementales possibles peut alors atteindre plusieurs dizaines de milliers. Dans l'exemple présenté ci-dessus ($n = 4$), l'utilisation d'une discrétisation comparable à celle présentée dans les documents de certification entraine à un nombre $n_c = 10120$ combinaisons. Pour chacune de ces combinaisons, un endommagement d doit être estimé.

Cet endommagement d est estimé par le moyen d'une chaîne numérique complexe, utilisée dans cette thèse comme présenté en Figure C.3. Pour chacune des n_c combinaisons environnementales, des trajectoires aléatoires sont générées à partir des paramètres environnementaux définis par le problème (vitesse moyenne du vent à hauteur de moyeu, hauteur significative des vagues, etc.). A partir de ces trajectoires, les réactions structurelles aux différentes localisations d'intérêt sont calculées via l'utilisation de simulateurs multiphysiques temporels afin de maximiser la représentativité des situations envisagées et la prise en compte des non-linéarités de réponse. A partir de ces dernières, plusieurs décomptes rainflow sont réalisés et les endommagements d dus à l'état de sollicitation sont évalués au sens de Miner-Palmgren grâce à l'utilisation de courbes "S-N". Par conséquent, un unique appel à cette chaîne de calcul représente un investissement numérique important allant de quelque minutes à plusieurs heures selon le degré de représentativité structurel et la conception.

Le processus de calcul des endommagements et plus particulièrement le coût général lié à l'évaluation de la quantité d'endommagement moyen D est une réelle limitation industrielle. Cette thèse s'est focalisée dans un premier temps sur la réduction de cet investissement numérique et une première problématique scientifique du projet est présentée comme :

> Comment réduire le nombre d'appels au simulateur coûteux d nécessaire à l'estimation de l'endommagement moyen D tout en quantifiant l'erreur d'approximation ?

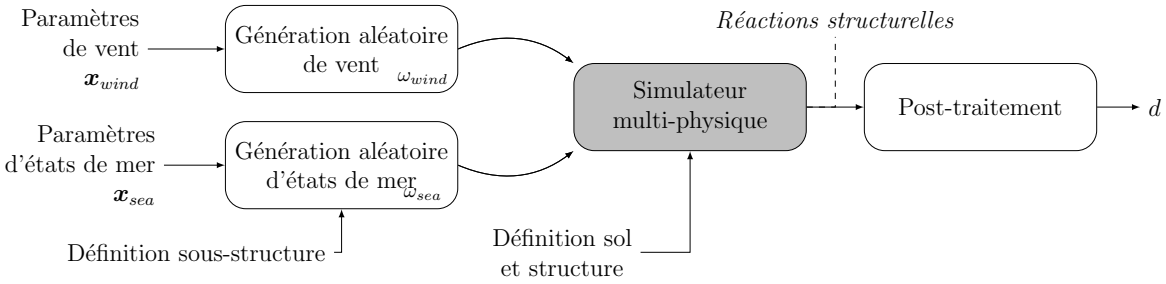

Figure C.3: Schéma général de la chaîne de calcul utilisée pour l'estimation de l'endommagement d à partir d'un état de sollicitation $\boldsymbol{x} = \{\boldsymbol{x}_{wind}, \boldsymbol{x}_{sea}\}$

Limitation 2 : des analyses de fiabilité coûteuses

Afin de maximiser la sécurité des installations, la norme et les organismes certificateurs présentent un ensemble de facteurs de sécurité à prendre en compte lors de la phase de vérification des performances structurelles présentée ci-dessus. L'ingénieur peut, suivant les situations et le degré de conservatisme recherché, augmenter l'amplitude de chargement ou réduire la résistance structurelle artificiellement via l'utilisation de ces coefficients. Ces derniers sont donnés par les normes suivant le degré de risque lié au composant étudié (choix systématique). Cette situation conduit à une difficulté réelle quant au contrôle des marges de sécurité réelles. Afin de réduire les coûts de production, la réduction des marges sous contrainte de seuil de sécurité minimal est une alternative envisagée industriellement.

Afin d'analyser les performances de fiabilité des conceptions éoliennes, un ensemble de processus et méthodes a été proposé dans les dernières décennies et appliqué à divers domaines de l'ingénierie mécanique. Concernant l'étude de fiabilité relative au cumul de fatigue des structures, ces analyses permettent de quantifier la capacité de résistance structurel compte tenu des incertitudes de conception. Dans cette logique, un dimensionnement au plus juste est alors recherché. Dans l'état de l'art actuel, l'ensemble des algorithmes proposés oblige l'ingénieur à faire appelle à un nombre important, souvent inabordable, d'estimation de l'endommagement D comme présenté ci-dessus. En considérant le coût potentiellement important de chacun de ces appels, les analyses de fiabilité représentent alors un investissement numérique impossible à mettre en place. Afin de résoudre cette limitation industrielle, une seconde problématique scientifique est proposée comme :

Comment procéder de manière efficace et représentative à une étude de fiabilité des conceptions vis-à-vis du risque de ruine en fatigue ?

☞ *Le Chapitre 1 présente précisément le contexte industriel, la formalisation du calcul d'endommagement, les limitations industrielles et problématiques scientifiques de la thèse.*

C.2 Utilisation des métamodèles de Krigeage pour la prédiction des réponses numériques de codes coûteux

L'utilisation de métamodèle, ou modèle de substitution, s'est développé de manière importante durant les dernières décennies. D'un point de vue global, ces méthodes permettent de prédire la réponse d'un code de calcul à partir d'un ensemble de réalisations préalablement observées. Parmi l'ensemble des méthodes dont l'ingénieur dispose, l'approximation par métamodèles de Krigeage (aussi appelé approximation par processus Gaussien) a permis de réduire les temps de traitement de divers problèmes. Deux domaines ont particulièrement utilisé cette approche : la fiabilité et l'optimisation numérique.

Cette approche permet de construire mathématiquement un estimateur de la réponse globale d'un modèle numérique à partir d'un ensemble fini et réduit d'observations. L'estimateur est déterminé sous contrainte de non-biais et minimisant la variance d'estimation. Considérant un modèle numérique $\mathcal{M}$ explicité comme suit :

$$\begin{aligned} \mathcal{M} : \mathcal{D}_{\boldsymbol{x}} \subset \mathbb{R}^n &\to \mathcal{D}_y \subset \mathbb{R} \\ \boldsymbol{x} &\to y(\boldsymbol{x}) \end{aligned} \tag{C.3}$$

La prédiction par métamodèle de Krigeage permet de construire un estimateur $\hat{y}$ déterminé à partir d'un set d'observations $\{\boldsymbol{\mathcal{X}}_{obs}, y_{obs}\}$. Cette estimateur présente l'avantage d'être défini comme étant linéaire, à variance minimal et sans biais ("meilleur estimateur linéaire sans biais"). A partir de la construction de ce dernier, un métamodèle $\hat{\mathcal{M}}$ du modèle $\mathcal{M}$ supposé coûteux peut être construit comme suit :

$$\begin{aligned} \hat{\mathcal{M}} : \mathcal{D}_{\boldsymbol{x}} &\to \mathcal{D}_y \\ \boldsymbol{x} &\to \hat{y}(\boldsymbol{x}) \end{aligned} \tag{C.4}$$

En plus de permettre le calcul d'une prédiction statistiquement évaluée via l'ensemble des observations du modèle coûteux, le Krigeage propose de calculer d'une manière économe une estimation de l'erreur d'approximation via la variance de Krigeage. Ainsi, pour chaque point du domaine de définition, l'ingénieur peut avoir une idée de la qualité de son approximation au sens de la construction statistique de l'estimateur et assujetti du choix de la base d'observation.

Afin d'illustrer le fonctionnement de la prédiction par métamodèles de Krigeage, un exemple d'approximation est présentée en Figure C.4. Le modèle numérique utilisé ici est la fonction $x = x\sin(x)$ définie pour $x \in [0, 10]$. Afin de calibrer la prédiction présentée, cinq observations de la fonction vraie (supposée ici coûteuse) sont utilisées. La variance de Krigeage est ici utilisée pour construire un intervalle de confiance à 95% de l'estimateur présenté.

L'une des principales difficultés de la construction du métamodèle présenté réside dans le choix de la base réduite d'observation $\{\boldsymbol{\mathcal{X}}_{obs}, y_{obs}\}$. L'information contenue par ce dernier

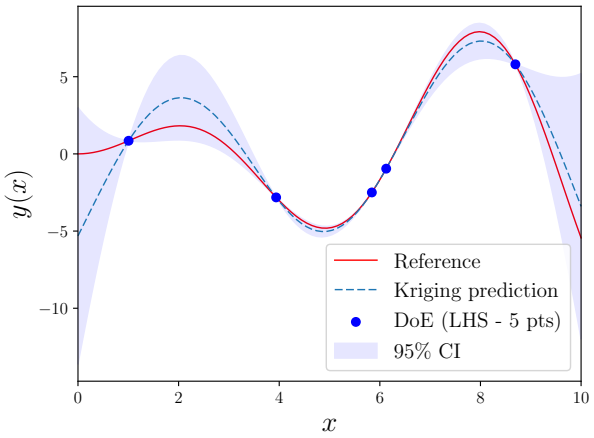

Figure C.4: Illustration de la prédiction par métamodèle de Krigeage sur la fonction $x\sin(x)$ calibrée à partir de 5 observations

est déterminante pour la qualité de l'estimateur $\hat{y}$ présenté. Afin de réduire les risques de non représentativité de l'ensemble d'observation, l'utilisation d'architectures adaptatives s'est rapidement imposée dans les développements méthodologiques basés sur les approximations par métamodèles de Krigeage. Ces dernières se basent sur la construction itérative d'un plan d'expériences informatif et de taille réduite par l'utilisation de prédictions successives de prédictions de Krigeage. Dans les domaines de la fiabilité et de l'optimisation numérique, diverses architectures ont été proposées et utilisées afin de réduire l'investissement numérique requis par les méthodes couramment utilisées.

☞ *Le Chapitre 2 présente l'ensemble des explications, la formalisation et diverses illustrations de la méthode de prédiction de réponses numériques par métamodèles de Krigeage.*

La prédiction par métamodèle de Krigeage est utilisée tout au long de cette thèse afin de proposer plusieurs approches numériques permettant de réduire l'investissement numérique relatif au calcul de l'endommagement moyen (approximation par la méthode AK-DA) et l'analyse de fiabilité (couplage AK-MCS/AK-DA).

C.3 Adaptive Kriging for Damage Assessment (AK-DA) pour l'approximation efficace de l'endommagement structurel

L'approche Adaptive Kriging for Damage Assessment (AK-DA) est proposée dans cette thèse afin de réduire l'investissement numérique requis pour l'estimation de l'endommagement moyen D. Trois algorithmes sont présentés dans ce document et résumé dans la suite de cette partie : l'approche AK-DA pour l'estimation de l'endommagement en un point structurel unique, son extension à l'utilisation dans un contexte HPC (high performance computer) par la méthode multi-enrichissements par "zone d'influence" et finalement l'utilisation de la méthode pour l'analyse structurelle multi-points.

C.3.1 Présentation de la méthode AK-DA (approche uni-localisation)

Approche théorique

L'algorithme AK-DA propose d'utiliser une méthode adaptative de Krigeage afin de déterminer efficacement l'endommagement structurel proposé en Eq. C.1. A partir d'un ensemble d'observations initiales $\{\boldsymbol{\mathcal{X}}_0, d_0\}$, obtenu par un plusieurs appels à la chaîne numérique (*c.f.* Figure C.3), un métamodèle de Krigeage $\hat{d}$ de l'endommagement d peut être calibré. La substitution du modèle coûteux d par sa prédiction $\hat{d}$ au sein de l'expression de l'endommagement moyen D (Eq. C.1) permet de déterminer un estimateur $\hat{D}$ comme :

$$\hat{D} = \sum_{i=1}^{n_c} \hat{d}(\boldsymbol{x}_i)\, p(\boldsymbol{x}_i)\, \Delta \tag{C.5}$$

Construit à partir d'une prédiction statistique de l'endommagement d, cet estimateur présente une incertitude estimée numériquement à partir de son coefficient de variation $\delta_{\hat{D}}$ explicité comme suit :

$$\delta_{\hat{D}} = \frac{\sigma_{\hat{D}}}{\hat{D}} \quad \text{avec} \quad \sigma^2_{\hat{D}} = \sum_{i=1}^{n_c}\sum_{j=1}^{n_c} p_i\, p_j\, \mathrm{Cov}(\hat{d}_i, \hat{d}_j)\, \Delta^2 \tag{C.6}$$

où Cov représente la covariance estimée grâce à la formalisation du Krigeage.

Afin de réduire les risques de non-représentativité de l'estimation $\hat{D}$ basée sur un nombre réduit d'observations du modèle réel d, une architecture itérative est utilisée. A partir d'un nombre réduit d'observations du modèle d'endommagement d, une prédiction initiale de krigeage $\hat{d}$ est calibrée afin d'obtenir une première prédiction du comportement global de la réponse d. Par conséquent, une première estimation $\hat{D}$ de l'endommagement D est alors calculable comme présenté en Eq. C.5.

Afin de structurer l'architecture itérative utilisée ici, une fonction d'apprentissage est utilisée afin de sélectionner la combinaison de paramètres environnementaux $\boldsymbol{x}^*$ réduisant le plus l'incertitude sur l'estimateur $\hat{D}$. Cette notion est ici traitée via l'utilisation de la variance d'estimation $\sigma^2_{\hat{D}}$ et basée sur la décomposition suivante :

$$\sigma^2_{\hat{D}} = \sum_{i=1}^{n_c} \mathcal{C}_i \quad \text{avec} \quad \mathcal{C}_i = p_i \sum_{j=1}^{n_c} p_j\, \mathrm{Cov}(\hat{d}_i, \hat{d}_j)\, \Delta^2 \tag{C.7}$$

où $\mathcal{C}_i$ est définie comme la "*contribution*" et représente l'impact de l'incertitude relative à l'estimation de la réponse $d(\boldsymbol{x}_i)$ sur la variance globale de l'estimateur $\hat{D}$. A chaque itération de l'algorithme, cette quantité d'apprentissage est calculée et un nouvel appel au simulateur d est réalisé pour la combinaison de paramètres environnementaux $\boldsymbol{x}^*$ vérifiant :

$$\boldsymbol{x}^* = \underset{\boldsymbol{x}\in\mathcal{D}_{\boldsymbol{x}}}{\mathrm{argmax}}\ |\mathcal{C}(\boldsymbol{x})| \tag{C.8}$$

Le plan d'expériences initial est alors complété par l'observation d'apprentissage $\{\boldsymbol{x}^*, d(\boldsymbol{x}^*)\}$ et un nouveau métamodèle de Krigeage est calibré afin d'affiner l'approximation $\hat{d}$ du modèle

d'endommagement d. Itérativement, le plan d'expériences initial est enrichi avec de nouvelles simulations jusqu'à la réduction suffisante de la variance d'estimation $\sigma^2_{\hat{D}}$ de l'estimateur $\hat{D}$. Le critère d'arrêt de la méthode est construit à partir de cette quantité et est explicité comme :

$$\delta_{\hat{D}} < \delta_t \tag{C.9}$$

où δ_t représente la valeur de précision recherchée au sens du coefficient de variation $\delta_{\hat{D}}$ de l'estimateur $\hat{D}$. L'ensemble de l'algorithme est présenté en Figure C.5.

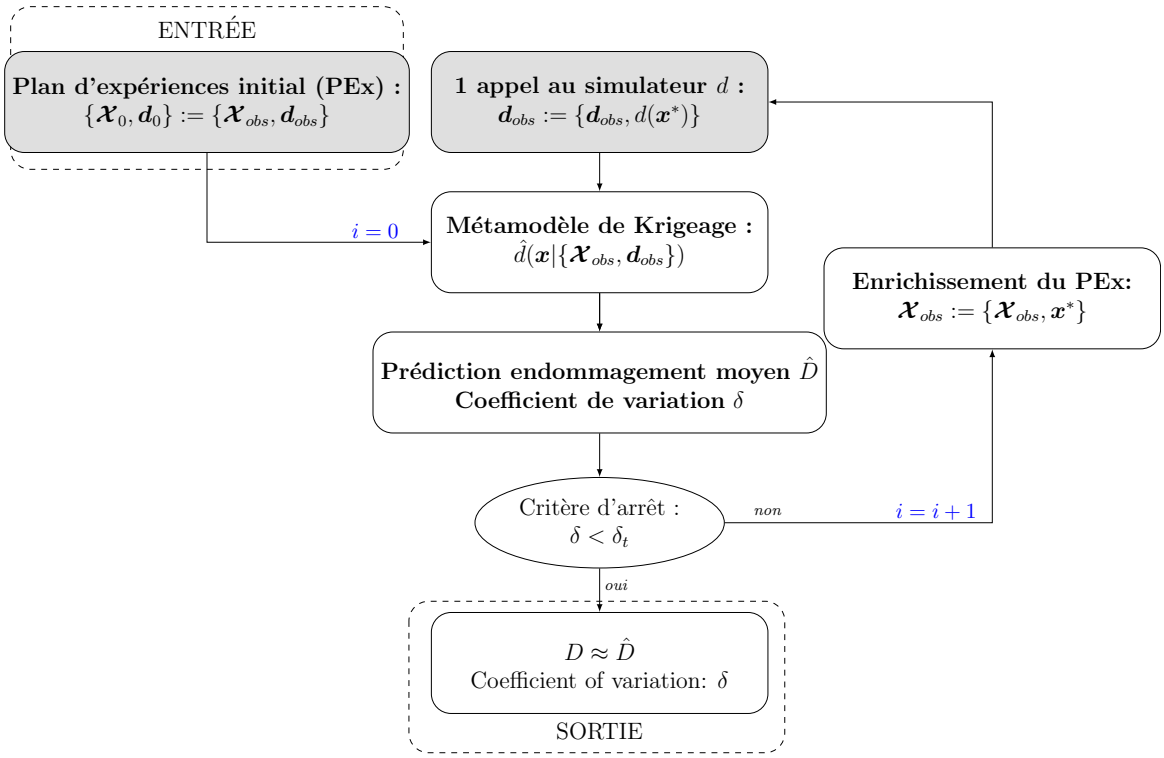

Figure C.5: Présentation de l'algorithme AK-DA

☞ *L'ensemble des explications concernant l'algorithme AK-DA ainsi que plusieurs cas de validation sont présentés Section 3.2.*

Illustration industrielle

Parmi d'autres exemples de validation, l'algorithme AK-DA est illustré industriellement avec le cas d'application présenté en Figure C.2. L'objectif de l'étude est d'estimer de façon précise l'endommagement mécanique cumulé au point *az-0* pour le cas de charge DLC 1.2. Un calcul préalable de référence est réalisé sur la base de la discrétisation complète présentant au total 10120 appels au simulateur d. L'endommagement moyen D de référence est obtenu comme :

$$D = \sum_{i=1}^{n_c=10120} d(\boldsymbol{x}_i)\ p(\boldsymbol{x}_i)\ \Delta = 8.475 \times 10^{-8} \tag{C.10}$$

L'algorithme AK-DA est initialisé grâce au calcul d'un set initial d'observations de la réponse du modèle d'endommagement d composé de 320 combinaisons de paramètres environnementaux. Le critère d'arrêt est fixé ici à $\delta_t = 5\%$. L'évolution de l'estimation $\hat{D}$ et de la valeur de son coefficient de variation $\delta_{\hat{D}}$ en fonction du nombre d'appels au simulateur d est présentée en Figure C.6.

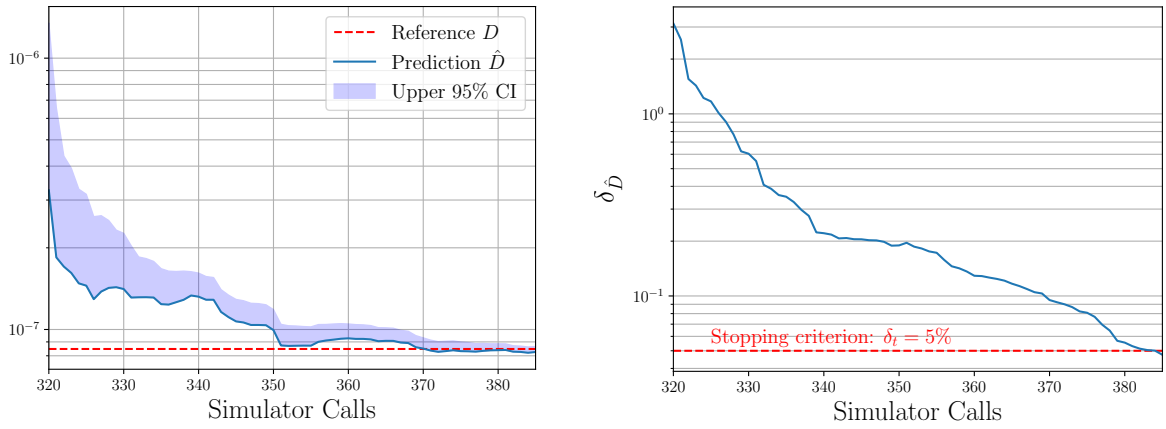

(a) Estimation $\hat{D}$ (b) Coefficient de variation $\delta_{\hat{D}}$

Figure C.6: Courbe de convergence de l'estimateur $\hat{D}$ et évolution du coefficient de variation $\delta_{\hat{D}}$ lors de l'estimation de l'endommagement du point Az-0 par utilisation de l'algorithme AK-DA

A convergence (*i.e.* $\delta_{\hat{D}} < 5\%$), l'estimation $\hat{D}$ de l'endommagement D est calculée comme :

$$\hat{D} = \sum_{i=1}^{n_c=10120} \hat{d}(\boldsymbol{x}_i)\ p(\boldsymbol{x}_i)\ \Delta = 8.260 \times 10^{-8} \tag{C.11}$$

Cette approximation présente une erreur relative de -2.54% au regard du calcul de référence présenté en Eq. C.10. Au total, 385 appels au simulateur d ont été nécessaires afin de réduire suffisamment l'incertitude relative à l'estimateur $\hat{D}$, composés de 320 appels initiaux (plan d'expérience initial) et 65 enrichissements automatiques proposés par la méthode AK-DA. Cette réduction du nombre d'appels représente un gain numérique approximativement égal à 26.

C.3.2 Utilisation de la méthode d'enrichissement multi-points par "zone d'influence"

Approche théorique

Afin de réduire le temps nécessaire à la convergence de l'algorithme AK-DA, une méthode complémentaire d'enrichissement multi-points est proposée dans ce manuscrit. A la différence de l'algorithme AK-DA initialement présenté, cette extension permet de sélectionner simultanément n_e simulations à chaque itération de la méthode. Cette stratégie permet de réduire le nombre d'itérations de l'algorithme nécessaire à l'atteinte du critère de convergence et donc de diminuer le nombre de métamodèle de Krigeage potentiellement coûteux à calibrer.

Plusieurs méthodes ont été proposées afin d'automatiser la sélection de sets d'enrichissement multi-points lors de l'utilisation de méthodes adaptatives de Krigeage (*ex.* Lelièvre et al. [2018]). Cette thèse propose une méthode basée sur la construction itérative de sets d'enrichissement minimisant les corrélations croisées des différents points d'apprentissage sélectionnés à chaque itérations de l'algorithme. L'hypothèse de cette construction réside dans l'idée que l'apport d'information d'un set d'enrichissement multi-points est maximal lorsque l'ensemble des combinaisons environnementales présente des corrélations croisées faibles vis-à-vis de la réponse du modèle coûteux (ici l'endommagement d). Cette stratégie est appelée méthode d'enrichissement multi-points par "zone d'influence".

A partir du calcul de la contribution présenté en Eq. C.7, une première combinaison de paramètres environnementaux notée x_1^* est sélectionnée sur l'ensemble du domaine de définition $\mathcal{D}_1 = \mathcal{D}$. Cette sélection est réalisée par l'optimisation présentée en (Eq. C.8). Une zone d'influence est déduite de cette sélection regroupant l'ensemble des points non observés du domaine $\mathcal{D}_1$ dont l'estimateur de la réponse d présente une corrélation supérieure à un paramètre $r_0 \in [0, 1]$ défini par l'utilisateur et formalisé comme :

$$\Big\{|r(\boldsymbol{x}_1^*, \boldsymbol{x})| \geq r_0)\Big\} \tag{C.12}$$

Un nouveau domaine de recherche, noté $\mathcal{D}_2$ est alors défini par l'exclusion de ce domaine influencé du domaine initial de recherche $\mathcal{D}_1$:

$$\mathcal{D}_2 = \Big\{\boldsymbol{x} \in \mathcal{D}_1 \text{ such as } |r(\boldsymbol{x}_1^*, \boldsymbol{x})| \leq r_0)\Big\} \tag{C.13}$$

Un second point d'apprentissage x_2^* peut alors être déduit via l'utilisation de la fonction d'apprentissage de la méthode AK-DA sur le domaine $\mathcal{D}_2$. Itérativement, un ensemble de points d'apprentissage peut être construit minimisant les corrélations croisées de ces derniers vis-à-vis des prédictions de la réponse en endommagement d.

Cette construction est poursuivie jusqu'à l'atteinte de la taille maximale du set d'enrichissement ou le recouvrement d'influence total du domaine initial. Une fois l'un de ces critères d'arrêt atteint, n_e simulations peuvent être réalisées en parallèle afin d'enrichir le plan d'expériences.

☞ *L'ensemble des explications et illustrations de l'approche multi-enrichissements par "zone d'influence" est proposé dans la Section 3.3.*

Illustration industrielle

L'exemple industriel présenté plus haut est réutilisé afin de montrer les performances de la méthode multi-enrichissements par "zone d'influence". L'endommagement moyen cumulé D est estimé par la méthode AK-DA au niveau de la localisation structurelle Az-0. Le tableau C.1 présente les résultats obtenus où n_{iter} et n_{obs} représentent respectivement le nombre d'itérations de l'algorithme AK-DA et le nombre d'observations total de la réponse d. Ainsi,

le cas $n_e = 1$ représente l'application de l'algorithme AK-DA dans sa forme simple présentée en C.3.1.

Taille des sets d'enrichissement n_e	n_{iter}	n_{obs}	$\hat{D}$	Erreur relative
1	65	$320 + 65 = 385$	8.260×10^{-8}	-2.54%
2	34	388	8.283×10^{-8}	-2.27%
3	22	386	8.362×10^{-8}	-2.54%
4	17	388	8.535×10^{-8}	0.71%
5	14	390	8.356×10^{-8}	-1.41%
6	12	392	8.298×10^{-8}	-2.09%
7	11	397	8.269×10^{-8}	-2.43%
8	9	392	8.515×10^{-8}	-0.70%

Table C.1: Performance de la stratégie multi-enrichissements par "zone d'influence" sur l'exemple industriel à quatre dimensions.

Cet exemple montre l'intêret de l'utilisation de cette méthode dans un contexte de parallélisation des simulations (contexte HPC). Plus la taille de l'enrichissement augmente, plus le nombre d'itérations de la méthode AK-DA est réduit. Ceci permet de réduire l'effort numérique lié à la calibration du métamodèle de Krigeage $\hat{d}$ nécessaire à chaque itération de l'algorithme et potentiellement coûteux. L'utilisation de sets d'enrichissement composés de 8 simulations ($n_e = 8$) permet de diviser le nombre d'itérations de l'algorithme AK-DA par environs 8 passant de 65 itérations pour $n_e = 1$ à seulement 9. Le nombre d'observations du modèle d reste quant à lui sensiblement égal variant de 385 observations ($n_e = 1$) à 397 ($n_e = 7$).

C.3.3 Utilisation de la méthode AK-DA pour l'estimation multi-localisations de l'endommagement

Approche théorique

Les deux approches AK-DA présentées précédemment permettent à l'ingénieur d'estimer seulement l'endommagement global cumulé D pour une unique localisation d'intérêt (ici *Az-0*). Cette formalisation ne permet pas en l'état l'applicabilité industrielle de cette approche. En effet, lors de la phase de conception/certification, un ensemble de localisations doit être pris en compte. Pour chacune d'elles, l'endommagement global moyen D doit être déterminé. L'approche AK-DA multi-localisations permet d'étendre la stratégie d'estimation de cette quantité d'intérêt à un ensemble fini de n_s points structuraux. La stratégie AK-DA initiale présentée en Figure C.5 est modifiée afin de permettre l'estimation simultanée de n_s estimateurs $\hat{D}_i$ où $i \in \{1, n_s\}$. Les modifications sont présentées ci-après :

- *Calibration parallèle de n_s métamodèles de Krigeage :* pour l'ensemble des n_s points d'intérêt, n_s métamodèles de Krigeage sont calibrés indépendamment sur la base commune d'observation notée ici $\{\boldsymbol{\mathcal{X}}_{obs}, \boldsymbol{d}_{i,obs}\}$ où $i \in \{1, n_s\}$.
- *Stratégie d'enrichissement par point pilote :* Afin de déterminer le ou les points d'apprentissage à chaque itérations de l'algorithme AK-DA, p localisations sont déterminées comme

étant *point pilotes* de l'enrichissement. Cette sélection est réalisée vis-à-vis de l'incertitude relative aux estimateurs $\hat{D}_k$ considérée ici par les coefficients de variations liés $\delta_{\hat{D},k}$. Ainsi, l'ensemble des indices pilotes sont regroupés dans le vecteur $\boldsymbol{k}_p$ défini comme :

$$\boldsymbol{k}_p = \left\{ k \in \{1, \dots, n_s\} \text{ tel que } \delta_{\hat{D},k} \geq \delta_t \right\} \tag{C.14}$$

La sélection du ou des points d'apprentissage se base alors sur la détermination de la contribution normalisée absolue $|\bar{\mathcal{C}}_k|$ définie pour chacune des combinaisons environnementales non observées et pour chaque point pilote comme :

$$\sum_{i=1}^{n_c} |\bar{\mathcal{C}}_k(\boldsymbol{x}_i)| = 1 \text{ avec } k \in \boldsymbol{k}_p \tag{C.15}$$

La fonction d'apprentissage est modifiée afin de tenir compte de l'apport global d'information et la réduction des variances de prédiction sur l'ensemble des localisations pilotes. Cette dernière est alors formalisée comme suit :

$$\boldsymbol{x}^* = \underset{\boldsymbol{x} \in \mathcal{D}_{\boldsymbol{x}}}{\operatorname{argmax}} \sum_{k=1}^{n_s} \mathbb{1}_{\boldsymbol{k}_p} |\bar{\mathcal{C}}_k(\boldsymbol{x})| \tag{C.16}$$

- *Critère d'arrêt :* l'enrichissement est stoppé lorsque l'ensemble des estimateurs $\hat{D}_i$ des endommagements moyens D_i présente un coefficient de variation $\delta_{\hat{D},k}$ inférieur à une valeur limite choisie par l'utilisateur :

$$\delta_{\hat{D},k} < \delta_t \text{ quelque soit } k \in \{1, \dots, n_s\} \tag{C.17}$$

La prise en compte de ces modifications mènent à la présentation générale de l'algorithme AK-DA pour l'approche multi-localisations présenté en Figure C.7.

☞ *L'ensemble des explications et illustrations de l'approche AK-DA multi-localisations est proposé dans la Section 3.4.*

Application industrielle

L'exemple présenté en Figure C.2 est utilisé pour illustrer la méthode d'estimation multi-localisations proposée dans cette thèse. Les quatre localisations définies au niveau de la transition monopile-sol sont pris en compte (*i.e.* Az-0,Az-90,Az-180 et Az-270). Les performances de l'algorithme proposées sont comparées à celles obtenues avec la mise en place de quatre lancements AK-DA indépendants. Les résultats de cette illustration sont proposés dans le tableau Table C.2.

Le lancement de quatre analyses indépendantes AK-DA sur les quatre localisations structurelles d'intérêt mène à un nombre de simulations total de $n_{obs} = 1624$ composé de 563 simulations uniques. La convergence de cette approche est obtenue ici après un nombre total

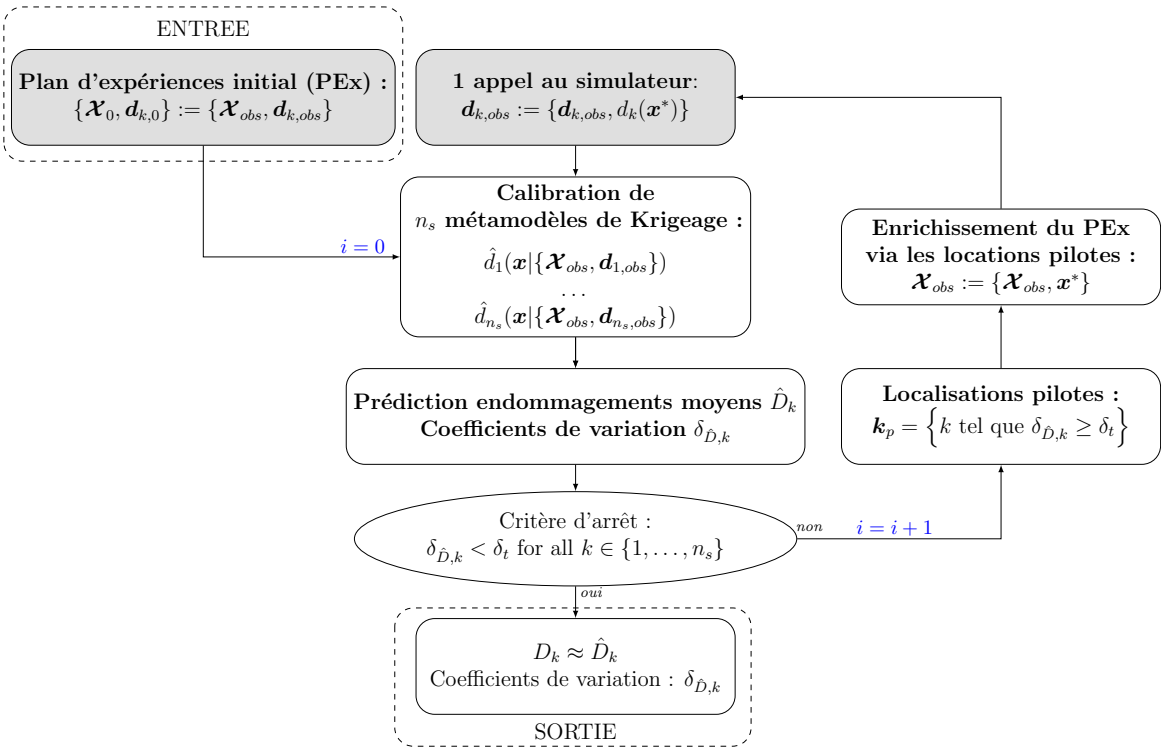

Figure C.7: Presentation of the multi-localisations extension of the AK-DA algorithm.

Localisation	n_{obs}	n_{iter}	$\hat{D}$	D	Erreur relative
Lancements AK-DA indépendants					
Mud-line Az-0	388	17	8.55×10^{-8}	8.48×10^{-8}	0.83%
Mud-line Az-90	408	22	1.38×10^{-9}	1.39×10^{-9}	−0.72%
Mud-line Az-180	428	27	3.57×10^{-8}	3.41×10^{-8}	4.7%
Mud-line Az-270	400	20	1.39×10^{-9}	1.39×10^{-9}	0%
Total	1624 563 distincts	86			
AK-DA multi-localisations					
Mud-line Az-0	444	31	8.40×10^{-8}	8.48×10^{-8}	−0.94%
Mud-line Az-90			1.34×10^{-9}	1.39×10^{-8}	−3.60%
Mud-line Az-180			3.42×10^{-8}	3.41×10^{-8}	0.29%
Mud-line Az-270			1.38×10^{-8}	1.39×10^{-8}	−0.72%

Table C.2: Performance de la stratégie multi-localisations pour l'approximation efficace des endommagements sur l'exemple industriel à quatre dimensions.

d'enrichissements de 86. L'utilisation de la formalisation multi-localisations réduit le nombre total de simulations à convergence avec un nombre total $n_{obs} = 444$. De plus, le nombre d'itérations de l'algorithme AK-DA est réduit de manière significative par l'utilisation de l'approche ici présentée avec un nombre total d'itérations $n_{iter} = 31$ à convergence. La précision des estimations de l'endommagement moyen aux quatre localisations structurelles d'intérêt reste comparables dans les deux cas et industriellement acceptables (erreur relative inférieure à 5%).

C.4 Vers le calcul de fiabilité de la tenue en fatigue des conceptions

L'ensemble des développements présenté dans le Chapitre 3 et résumé ci-dessus s'intéresse à la détermination de la quantité d'endommagement D pour un cycle de vie défini dans l'hypothèse que les paramètres environnementaux décrivent parfaitement la situation à modéliser. Dans l'exemple industriel traité, les paramètres du modèle numérique sont considérés comme parfaitement représentatifs de la structure étudiée. Dans la réalité, un ensemble d'incertitudes entache la modélisation comme, par exemple, les caractéristiques mécaniques du sol (rigidité, amortissement, etc.). Afin de garantir une sécurité maximale des installations, la détermination des quantités d'endommagement est réalisée via l'utilisation de modèles déterministes dont les performances sont réévaluées par la mise en place d'un ensemble de coefficients de sécurité. Cette pratique, bien qu'étant conservative, mène à un sur-dimensionnement des structures et augmente le coût de fabrication et d'installation des unités éoliennes posées en mer. Afin de réduire les marges, l'une des possibilités est de faire appel à l'analyse de fiabilité des conceptions vis-à-vis de leur risque de ruine en fatigue.

Le Chapitre 4 propose une ouverture à l'analyse de fiabilité des conceptions tenant compte du processus de calcul des quantités d'endommagement comme présenté précédemment. Cette approche est proposée ici sous le point de vue probabiliste par la définition de la probabilité de défaillance P_f définie comme suit [Lemaire, 2013] :

$$P_f = \text{prob}\Big(D_t - D(\boldsymbol{\zeta}) \leq 0\Big) = \int_{D_t - D(\boldsymbol{\zeta}) \leq 0} f_{\boldsymbol{\zeta}}(\boldsymbol{\zeta}) \mathrm{d}\boldsymbol{\zeta} \tag{C.18}$$

où $\boldsymbol{\zeta}$ représente un vecteur de réalisations des paramètres incertains pris en compte dans la modélisation, supposé suivre une loi de distribution $f_{\boldsymbol{\zeta}}$ et D_t, l'endommagement global moyen minimal requis (seuil de performance admissible).

Dans ce manuscrit, trois méthodes numériques d'approximation de la probabilité de défaillance sont présentées et comparées : l'approche Crude Monte Carlo (CMC), l'approche Adaptive Kriging for Monte Carlo Simulation (AK-MCS [Echard et al., 2011]) et son couplage avec la méthode AK-DA (AK-MCS/AK-DA) présentée ci-dessous et regroupant l'apport du Chapitre. Afin de tester ces méthodes, un cas d'illustration est présenté reprenant l'ensemble des contraintes industrielles. Ce dernier défini une situation où l'endommagement d est défini comme fonction d'un paramètre déterministe $x \in \mathcal{D}_x = [10, 20]$ (discrétisé sur $n_c = 11$ combinaisons) et d'un paramètre incertain $\zeta \in \mathcal{D}_\zeta$ étant considéré comme la réalisation

d'une loi normale $\mathcal{N}(12, 1)$ assimilable à un paramètre incertain de modélisation. L'évolution de l'endommagement $d(x, \zeta)$ ainsi que l'endommagement global moyen $D(\zeta)$ fonction du paramètre incertain sont présentés en Figure C.8. Dans cet exemple, le seuil de performance admissible est fixé à $D_t = 0.26$ (représenté en Figure C.8b).

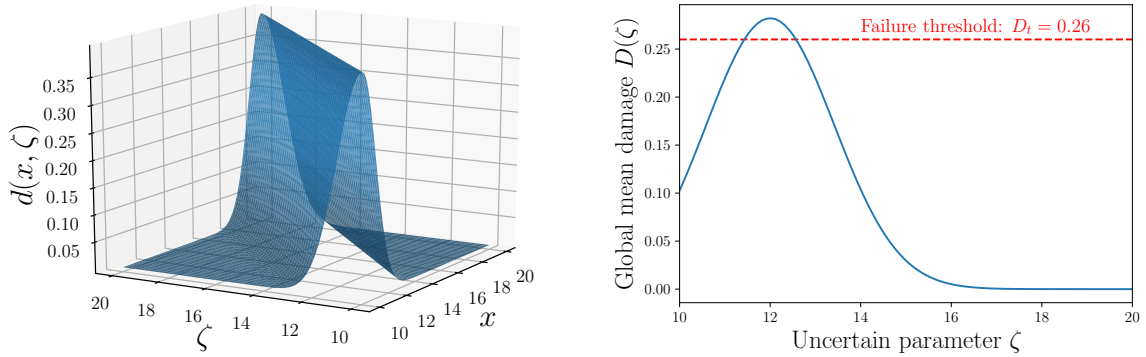

(a) Short-term damage d

(b) Global mean damage D

Figure C.8: Illustration of the short term damage d considered in the illustrative example and the related evolution of the global mean damage $D(\zeta)$ with $\zeta \in [10, 20]$.

C.4.1 Approximation par CMC

La méthode d'approximation par Crude Monte Carlo (CMC) est utilisée afin d'obtenir une valeur approchée de la probabilité de défaillance relative au problème présenté. Cette méthode, bien que présentant l'avantage d'être aisée à implémenter, nécessite un investissement numérique important. Pour l'exemple d'illustration, le nombre n_D de calculs de l'endommagement global moyen D atteint 51345 pour obtenir un estimateur de la probabilité de défaillance présentant un coefficient de variation de 10%. Pour chacun de ces appels, $n_c = 11$ appels au simulateur d sont nécessaires ce qui représente, au total, $51345 \times 11 = 594795$ calcul de l'endommagement d. La valeur approchée de la probabilité de défaillance est alors donnée par :

$$\hat{P}_f \underset{\text{CMC}}{=} 7.73 \times 10^{-3} \tag{C.19}$$

Cet exemple montre l'impossible applicabilité industrielle de cette approche numérique. Dans les cas industriels complets, chaque estimation de l'endommagement global moyen repose sur un nombre n_c d'appels au simulateur d atteignant généralement plusieurs milliers selon la complexité du problème (cf. exemple numérique présenté ci-dessus). Afin de palier à cette limitation, l'application de la méthode numérique AK-MCS pour l'approximation de la probabilité de défaillance est présentée.

C.4.2 Approximation par AK-MCS

L'algorithme AK-MCS utilise la prédiction par métamodèles de Krigeage. Afin d'accélérer la convergence de l'estimation de la probabilité de défaillance, un métamodèle est calibré afin d'approximer la fonction de performance, notée G est définie comme :

$$G(\boldsymbol{\zeta}) = D_t - D(\boldsymbol{\zeta}) \tag{C.20}$$

A partir d'un nombre réduit d'observations de la réponse $D(\boldsymbol{\zeta})$ obtenues à partir de réalisation aléatoires du vecteur de paramètres incertains $\boldsymbol{\zeta}$, la fonction de performance est approximée par son métamodèle de Krigeage, noté $\hat{G}$ et un estimateur de la probabilité de défaillance P_f est obtenu comme suit :

$$P_f \approx \hat{P}_f = \text{prob}\Big(\hat{G}(\boldsymbol{\zeta}) \leq 0\Big) = \int_{\hat{G}(\boldsymbol{\zeta})\leq 0} f_{\boldsymbol{\zeta}}(\boldsymbol{\zeta})\mathrm{d}\boldsymbol{\zeta} \tag{C.21}$$

Afin de garantir la représentativité de l'approximation de la fonction de performance G au voisinage des zones de défaillance, la méthode AK-MCS intègre une architecture d'apprentissage visant à enrichir le set d'observations initial. Afin de se concentrer sur les points proches des zones de défaillance, la fonction d'apprentissage utilisée repose la quantification du risque de mauvais classement des approximations du métamodèle vis-à-vis de la fonction de l'état limite de la fonction de performance ($G = 0$). La fonction U est alors utilisée afin de sélectionner le point d'apprentissage $\boldsymbol{\zeta}^*$ utilisé pour enrichir le set d'observations initial :

$$\boldsymbol{\zeta}^* = \underset{\boldsymbol{\zeta}\in\mathcal{P}}{\text{argmin}}\ U(\boldsymbol{\zeta}) = \underset{\boldsymbol{\zeta}\in\mathcal{P}}{\text{argmin}}\ \frac{|\hat{G}(\boldsymbol{\zeta})|}{\sigma_{\hat{G}}(\boldsymbol{\zeta})} \tag{C.22}$$

où $\sigma^2_{\hat{G}}(\boldsymbol{\zeta})$ représente la variance d'estimation lié à l'incertitude du métamodèle $\hat{G}$ au point $\boldsymbol{\zeta}$.

Ainsi, le métamodèle de Krigeage est itérativement enrichi afin d'assurer la représentativité de l'approximation $\hat{G}$ de la fonction de performance G. Cet enrichissement est poursuivi jusqu'à atteindre la condition d'arrêt présentée ici comme :

$$\min_{\boldsymbol{\zeta}\in\mathcal{P}} U(\boldsymbol{\zeta}) > 2 \tag{C.23}$$

L'application de cette méthode d'approximation permet, pour l'exemple d'illustration, de réduire de manière significative l'investissement numérique lié à l'approximation de la probabilité de défaillance. La mise en place de ce dernier permet de converger après seulement $n_D = 8$ calculs d'endommagements globaux moyen D, représentant un total de $n_D \times n_c = 88$ appels au simulateur coûteux d. La probabilité de défaillance P_f est alors approchée par :

$$\hat{P}_f \underset{\text{AK-MCS}}{=} 7.73 \times 10^{-3} \tag{C.24}$$

Bien que permettant une réduction importante du nombre d'appels au simulateur coûteux d, cette méthode nécessite le calcul complet des endommagement globaux moyen D pour chaque observation. Ainsi, ce dernier développement propose de coupler cette méthode avec l'approche AK-DA présentée précédemment dans ce résumé.

C.4.3 Couplage AK-DA/AK-MCS

L'un des apports de cette thèse est le couplage de l'algorithme d'approximation de la probabilité de défaillance AK-MCS avec la méthode d'approximation de l'endommagement AK-DA. Ainsi, ce travail a permis d'étendre la formalisation de l'algorithme AK-MCS à la prise en compte d'approximations des réponses observées obtenues par l'algorithme AK-DA. Globalement, trois modifications ont été apportées à la formalisation initiale de l'algorithme AK-MCS :

- *Utilisation d'un espace augmenté :* un métamodèle de Krigeage $\hat{d}$ est calibré sur un domaine augmenté $\mathcal{D}_{\boldsymbol{x},\boldsymbol{\zeta}}$ composé du domaine de définition des paramètres environnementaux déterministes $\mathcal{D}_{\boldsymbol{x}}$ et de celui des paramètres incertains $\mathcal{D}_{\boldsymbol{\zeta}}$. Ainsi, pour chaque point de la population de Monte Carlo, un estimateur de l'endommagement moyen est donné par :

$$\hat{D}(\boldsymbol{\zeta}) = \sum_{i=1}^{n_c} p(\boldsymbol{x}_i)\ \hat{d}(\boldsymbol{x}_i, \boldsymbol{\zeta})\ \Delta \tag{C.25}$$

  L'approximation de la fonction de performance est alors déduite de l'Eq. C.25 comme :

$$\hat{G}(\boldsymbol{\zeta}) = D_t - \hat{D}(\boldsymbol{\zeta}) \tag{C.26}$$

- *Adaptation de la méthode d'apprentissage :* cette étape est dès lors réalisée en deux temps. Dans un premier temps, le point de la population de Monte Carlo $\boldsymbol{\zeta}^*$ est sélectionné par la minimisation de la fonction U (application de l'algorithme AK-MCS). Une fois ce point sélectionné, le paramètre environnemental est choisi selon la méthode AK-DA afin d'affiner l'approximation de l'endommagement global moyen $\hat{D}(\boldsymbol{\zeta}^*)$.
- *Adaptation du critère d'arrêt :* la convergence de l'algorithme est considérée si l'estimateur de l'endommagement global présente un risque faible de mauvais classement vis-à-vis de l'état limite. Ce risque prend en considération la variance d'estimation des endommagements moyens globaux, via l'évaluation de leurs coefficients de variation $\delta_{\hat{D}(\boldsymbol{\zeta})}$. Ainsi, le critère d'arrêt modifié est formalisé comme suit :

$$\min_{\substack{\boldsymbol{\zeta}\in\mathcal{P} \\ \delta_{\hat{D}(\boldsymbol{\zeta})}>\delta_t}} U(\boldsymbol{\zeta}) > 2 \tag{C.27}$$

L'application de cette méthode sur le cas d'application présenté dans ce Chapitre permet une approximation rapide de la probabilité de défaillance. Cette dernière converge pour le cas d'application présenté après seulement 63 appels au simulateur d. La probabilité de défaillance est alors approximée par :

$$\hat{P}_f \underset{\text{AK-MCS/AK-DA}}{=} 8.70 \times 10^{-3} \tag{C.28}$$

Bien que présentant une erreur d'approximation de l'ordre de 12%, cette méthode permet un approximation rapide des quantités de probabilité de défaillance.

☞ *L'ensemble de la formalisation du problème de fiabilité, les explications relatives ainsi que les illustrations complètes des méthodes présentée ici sont présentées dans le Chapitre 4.*

Bibliographie synthétique

DNV-GL. *DNV-OS-J101: Design Of Offshore Wind Turbine Structures*, 2014.

B. Echard, N. Gayton, and M. Lemaire. AK-MCS: An active learning reliability method combining kriging and monte carlo simulation. *Structural Safety*, 33(2):145 – 154, 2011.

IEC. *IEC 61400-1: Wind turbines - Part 1: Design Requirements (Third Edition)*, 2005.

IEC. *IEC 61400-3: Wind turbines - Part 3: Design requirements for offshore wind turbines*, 2009.

J. Jonkman, S. Butterfield, W. Musial, and G. Scott. Definition of a 5-mw reference wind turbine for offshore system development. Technical report, National Renewable Energy Laboratory, 2009.

N. Lelièvre, P. Beaurepaire, C. Mattrand, and N. Gayton. AK-MCSi: A kriging-based method to deal with small failure probabilities and time-consuming models. *Structural Safety*, 73: 1–11, 2018.

Maurice Lemaire. *Structural reliability.* John Wiley & Sons, 2013.